CHEMICAL AND ELECTROCHEMICAL STUDIES OF LECLANCHE CELLS

José LARCIN

A Thesis submitted to the Council for National Academic Awards in partial fulfilment of the requirements for the degree of Doctor of Philosophy

September 1991

The work was carried out in the Energy Technology Centre at Middlesex Polytechnic, School of Mechanical Engineering, Bounds Green Road, London N11 2NQ
and was funded by the NAB Research Initiative 3 and Sedema SA.

to Maria

PAGE

NUMBERING

AS ORIGINAL

Abstract

The densities of NH_4Cl-$ZnCl_2$ solutions were measured at 25 °C over a wide range of concentrations and a calculation procedure was derived assuming ideal mixing of solutions of NH_4Cl, $ZnCl_2$ and the complex $(NH_4)ZnCl_3$ which accurately predicted the measured densities within ± 0.7 %. The question of the NH_4Cl concentration at which the precipitate formed on discharge changes from $Zn(NH_3)_2Cl_2$ to $ZnCl_2.4Zn(OH)_2.H_2O$ has been clarified and the free energies of formation of both products have been determined, for the first time for $ZnCl_2.4Zn(OH)_2.H_2O$. The zinc electrode potential was measured in solutions of $ZnCl_2$ (0 to 17 molal) and of NH_4Cl (zero to saturation). The concentrations of the different species were calculated; $ZnCl_3^-$ appeared to be predominant in all solutions except those with a large excess of NH_4Cl. The solubility diagram of the NH_4Cl-$ZnCl_2$-H_2O system was determined for the first time at 25 °C.

The three stages of the intermittent discharge of a Leclanché cell previously predicted by Tye have been observed and the duration of each stage explained on a theoretical basis. Hetaerolite was formed during intermittent discharge of cells containing the chemically prepared manganese dioxide (CMD) Faradiser M, as a chemical step following the normal reduction of the MnO_2. This formation increased the positive electrode potential and regenerated the NH_4Cl by dissolving the $Zn(NH_3)_2Cl_2$ formed earlier in the discharge. This is the first reported observation of the regeneration of NH_4Cl caused by hetaerolite formation. In zinc chloride electrolyte, the discharge product appeared to be $2ZnCl_2.5Zn(OH)_2.H_2O$ and not $ZnCl_2.4Zn(OH)_2.H_2O$ as previously reported.

An interruption technique has been used to study cells undergoing continuous discharges. The reverse reaction rate was negligible during the anodic zinc dissolution and no significant activation overpotential was observed for the manganese dioxide electrode. During these discharges in Leclanché electrolyte, the NH_4Cl concentration decreased at the zinc electrode interface reducing the activation overpotential and increasing the concentration overpotential. When the NH_4Cl concentration reached zero at the interface, the concentration profile (moving boundary) moved toward the cathode. In the zinc chloride electrolyte, the $ZnCl_2$ concentration at the negative electrode increased proportionally with the square root of the time on load until the diffusion layer intercepted the positive electrode. The MnO_2 electrode potentials measured against a reference electrode, the Luggin capillary of which was inserted inside the cathode, were very similar for electrodeposited manganese dioxide (EMD) and CMDs throughout the discharge in $ZnCl_2$ but higher for EMD than for a CMD in the Leclanché electrolyte. Towards the end of the discharge in both electrolytes, a large (70-100 mV) diffusion potential was generated in the separator region causing the cell voltage to decrease rapidly. This is the first time that this phenomenon has been reported. The main difference between the various cells in $ZnCl_2$ electrolyte was in the magnitude of this diffusion potential which was significantly decreased by increase of volume of electrolyte in the cell. Although the cells containing EMD lasted longer than those containing CMD on continuous discharges, the specific performances (F mol^{-1}) were very similar for all the materials. The non-uniform reduction rate distribution in the positive electrode has been calculated on the basis of measured potential differences within the mix using a new model of the electrode.

The MnO_2 potential-composition relationship conformed to the equation derived by Tye for all the dioxides at low degrees of reduction. Beyond about $MnOOH_{0.4}$, the potential of EMD followed the equation derived assuming independent mobility of inserted protons and electrons while the potential of CMDs suggested permanent association of the inserted species. This difference, which was observed after both chemical and electrochemical reduction, is a new finding.

Acknowledgements

This work would have been impossible without the collaboration of many people.

I am particularly indebted to Professor F.L. Tye for having arranged and directed this study. He has also curbed my flights of fancy, pronounced the magic words to make me work more or better, given advice and encouragements when I was depressed, and given me a lot of his time whenever needed, for very interesting and fruitful discussions.

I wish to express my gratitude to my second supervisor, Dr. W.C. Maskell, for his always pertinent remarks and useful suggestions. Both of my supervisors have helped to transform my somewhat broken English text into a readable thesis.

Thanks are due to my advisors, Mr. S. Davis for his recommendations and the time he spent to study and comment on my reports, and Mr. M. Bloyce for his help in the choice of the electronic instrumentation and the wiring of the experimental set-up.

I am grateful to my colleagues at the Middlesex Polytechnic's Energy Centre for their help and the very many interesting, mostly lunch-time, discussions or chats. I am pleased to mention especially Dr. M. Benammar for his help in the design and the construction of the electronic circuits used in my thesis, L. MacLean and E. Gehain for their assistance in the X-ray diffraction work and their efforts to make clearer to me the structure of manganese dioxide and J. Jones, A. Ioannou and R. Copcutt for the stimulating conversations and ideas they gave me.

I am thankful to the staff of Middlesex Polytechnic's Machine Tool Laboratory for their collaboration and their help in making a template used in this work.

Finally, I thank the Société Européenne des Dérivés du Manganèse (SEDEMA S.A.) for their technical support and the manufacture of all the cells used in this study.

Content

Main symbols used

a,b,c...	coefficients of an algebraic equation
a_i	activity of the species i
A	specific electrochemically active surface area
C	electrode double layer capacitance
C_i	molarity of the species i
CCV	closed circuit voltage
CMD	chemically prepared manganese dioxide
D	diffusion coefficient
D_i	density of phase i
E_i	potential of the electrode i
E_0	standard electrode potential
EMD	electrodeposited manganese dioxide
f	adjustable parameter in an algebraic equation
F	faraday
I	current density
J	charge transfer current density
K	equilibrium constant
m_i	molality of the species i
M_i	molecular mass of the species i
n	number of electrons transferred during an electrochemical reaction
n_i	number of mole of the species i
OCV	open circuit voltage
r	degree of H insertion (in $MnOOH_r$)
R	gas constant
R_i	radius of the item i
SCE	saturated KCl calomel electrode
T	absolute temperature
U	potential difference across a resistive material
V	volume
W_i	mass of the item i
x	oxidation degree of manganese dioxide, in MnO_x
X_i	mole fraction of the species i

Greek

α	transfer coefficient
η	electrode overpotential
κ	conductivity
ρ	resistivity
Φ	apparent molar volume

Chapter 1. Introduction

1.1. Objective of the study

The nature of the products formed in the electrolyte during the discharge of a Leclanché cell is known, but there remain some doubts about the point at which the precipitate changes from $Zn(NH_3)_2Cl_2$ to $ZnCl_2.4Zn(OH)_2.H_2O$. The influence of the electrolyte composition, and specially of the ammonium chloride concentration, on the negative electrode potential has received little attention and no systematic experimental investigation has been reported.

The active material of high performance Leclanché cells is synthetic manganese dioxide which may be prepared by an electrolytic or by a chemical process. The discharge behaviour of the batteries depends on the type of material, electrodeposited or chemically prepared, used in their manufacture. This influence appears in both continuous and intermittent discharge tests and may favour either material. Electrodeposited manganese dioxide is generally better on continuous discharge at heavy drain, while, for example, chemical manganese dioxide performs better on intermittent discharge in Leclanché electrolyte.

The objectives of this study were therefore

- To investigate the chemistry of the Leclanché electrolyte and its influence on the zinc electrode potential.
- To examine the discharge behaviour of Leclanché cells containing either electrodeposited or chemical manganese dioxide in either standard NH_4Cl - $ZnCl_2$ or pure zinc chloride electrolyte, mostly on continuous heavy drain, in order to understand better the reasons for their different behaviour.

1.2. Historical introduction

All Leclanché cells have a negative zinc electrode, a positive electrode of manganese dioxide mixed with an electronic conductor and an electrolyte which is a slightly acidic aqueous solution of ammonium and zinc chlorides.

In its original form [1], the Leclanché cell was made of a rod of zinc and of some natural manganese dioxide powder packed around a piece of carbon (acting as current collector) in a porous earthenware vessel. The electrolyte was a concentrated solution of ammonium chloride and the container was a glass jar. Although the electrolyte was immobilised by an absorbent material ("...sand, sawdust, papier mâché reduced to powder or any other pulverized substance of the same nature ..." [2]), the cell could only be used in an upright position. The first main improvement to the initial design was the incorporation of carbon powder into the cathode [3] in order to increase its electrical conductivity. The development of the Leclanché cell was essentially empirical [4]. The use of the zinc electrode as the cell container came into use at the end of the nineteenth century [5] and its amalgamation to reduce the zinc corrosion, although known to Leclanché [6] appeared in commercial cells around 1910 [7]. Zinc chloride became a component of the electrolyte in 1886 [5]. The sand or the sawdust used to immobilise the electrolyte in the first designs, was replaced by a starch or an agar paste and the earthenware separator by a cloth wrapping (1890) [8]. Later (1919), due to the improvement of the manufacturing processes, the cloth wrapping around the bobbin (manganese dioxide electrode) was eliminated [9]. This kind of cell, known as the "pasted cell" is still manufactured. The starch coated paper separator patented in 1893 [10], was not generally adopted until 1915 [7]. These "paper lined cells" allowed more manganese dioxide to be packed into the cell and therefore improved the battery performance.

Another increase in performance occurred in the nineteen thirties [11] when acetylene black began to replace graphite as the electronic conductor in the manganese dioxide electrode mix. Acetylene black has a low resistivity [12] and its structure confers to the mix the porosity required to accommodate the electrolyte and the discharge products [13].

Synthetic manganese dioxide made by electrolysis of a manganous sulphate solution [14] appeared in Leclanché cells during the Second World War [15]. Along with chemically prepared manganese dioxide [16,17], these synthetic materials are necessary in high performance batteries for appliances requiring moderate daily energy demands.

Although the pasted cells are still commercially available, using manganese dioxide ore as the active material for cheap standard Leclanché batteries, the modern premium Leclanché cell is of the paper lined type and contains synthetic manganese dioxide. The electrolyte of the standard cell is a zinc chloride solution saturated with ammonium chloride; its cathode mix contains some solid NH_4Cl. They give their best output if they are discharged intermittently over periods longer than one month [18]. The "zinc chloride" cells, have an electrolyte which is a $ZnCl_2$ solution usually containing some ammonium chloride well below the saturation level. They are better than conventional Leclanché cells on discharges lasting a few days or less [13].

The present study is concerned with these paper lined cells containing either electrodeposited (EMD) or chemically prepared manganese dioxide (CMD) in standard Leclanché electrolyte and in pure zinc chloride electrolyte.

1.3. The Leclanché electrolyte.

In an undischarged dry cell, the electrolyte consists mainly of zinc chloride, ammonium chloride and water [19]. Its composition affects the zinc electrode potential E_{Zn} through the Nernst equation

$$E_{Zn} = E_0 + \frac{RT}{2F} \ln a_{Zn} \qquad (1.1)$$

where E_0 is the standard zinc potential, R the gas constant, T the absolute temperature and F the Faraday. The electrolyte composition also affects the manganese dioxide electrode potential through dependence of the latter upon the electrolyte pH [13].

1.3.1 Behaviour of zinc chloride in aqueous solutions

Due to its small size (0.074 nm [20]) and its double charge, the bare Zn^{2+} ion exerts a very strong electrostatic attraction on the surrounding water molecules. The electric field the ion exerts on the solvent has the same effect as very high effective pressures thus reducing the space between the water molecules and increasing the solvent density [21], an effect known as electrostriction. In 1 molar $Zn(NO_3)_2$ solutions, X-ray investigation has shown that the first hydration shell of the Zn^{2+} contains six water molecules firmly bound to the central ion and forming an octahedron [22]. The acidic character of the zinc solutions is due to hydrolysis according to the reaction [23]

$$Zn^{2+} + H_2O \rightleftharpoons ZnOH^+ + H^+ \qquad (1.2).$$

In solutions containing chloride ions, zinc forms chloro-complexes [13]. From the result of a vapour pressure study, Stokes [24] concluded that a $ZnCl_4^{2-}$ complex was formed and ruled out the possible formation of $ZnCl_3^-$ or the neutral $ZnCl_2$. With Robinson [25], he considered concentrated $ZnCl_2$ solutions to be in fact solutions of $Zn.ZnCl_4$. In more dilute solutions, zinc chloride begins to form self complexes ($ZnCl^+$) above 0.1 molar $ZnCl_2$ [26,27]. In the presence of chloride ions, the general complexation reaction may be written [13]

$$Zn^{2+} + n\ Cl^- \rightleftharpoons ZnCl_n^{(2-n)+} \qquad (1.3)$$

with n = 1, 2, 3 or 4. The equilibrium constants of this reaction (one constant for each complex) have the general form

$$K_n = \frac{a_{ZnCl_n^{(2-n)+}}}{a_{Zn^{2+}}\ a_{Cl^-}^n} \qquad (1.4)$$

where a_i is the activity of the subscript species and K_n the stability constant.

The zinc complexation has been studied by many workers but without general agreement. Weingartner *et al.* [27] measured the conductivity of $ZnCl_2$ solutions and concluded that $ZnCl^+$ or $ZnCl_3^-$ were present while Irish *et al.* [28], using Raman spectroscopy, found evidence for the presence of $Zn(H_2O)_6^{2+}$, $ZnCl^+$ and

$ZnCl_4(H_2O)_2^{2-}$. Also by Raman spectroscopy, Marley and Gaffney [29] found the predominant species to be the neutral $ZnCl_2$ with $ZnCl_3^-$ and $ZnCl_4^{2-}$ in lower concentrations (in 1 molar $Zn(ClO_4)_2$ + 5 molar NaCl). Using a solvent extraction technique (on about 10^{-2} M $ZnCl_2$ in solutions from 0 to 6 M in LiCl), Sato and Nakamura [30] found that $ZnCl^+$ was predominant up to 2 molar total chloride and that $ZnCl_4^{2-}$ became predominant above 6 molar total chloride. From ultrasonic velocity measurements in $ZnCl_2$ + LiCl solutions, Boch and Goc [31], deduced that no $ZnCl_4^{2-}$ was present in pure $ZnCl_2$ solutions (up to 5.5 molal) but that this complex was formed on addition of LiCl. The presence of the tetra chloro-complex in Leclanché electrolyte was also the conclusion of Sasaki and Takahashi [32]. Skou *et al.* [33] calculated the stability constants of the different complexes from the results of cell emf measurements and deduced that the neutral $ZnCl_2$ complex was virtually non-existent. Atlung *et al.* [34] using these stability constants, calculated that the predominant species in a typical Leclanché electrolyte was the $ZnCl_3^-$ complex. The results of all these experiments appear to be very difficult to interpret, and if there is no doubt about the existence of different chloro-zinc complexes, there is no general agreement about their relative concentrations.

The zinc complexation phenomenon is of great importance in Leclanché electrolyte due to its effects on the electrolyte density and on the zinc electrode potential [32].

1.3.2 The electrolyte density

The conversion of concentration units, e.g. from mass percentage (common in battery literature) to molarities (as used in diffusion calculations), requires knowledge of the solution density. The density data are available for pure NH_4Cl solutions [35-37] or pure zinc chloride solutions [37-41] over a wide range of concentrations. The only set of experimental results for the system NH_4Cl - $ZnCl_2$ - H_2O is due to Takahashi and Sasaki who presented the data both as specific volume [42] and density [32].

In the calculation of the density of solutions it is convenient to use the solute apparent molar volume Φ_s defined by [43]

$$\Phi_s = \frac{V_s - n_w \Phi_w}{n_s} \tag{1.5}$$

where Φ_w is the pure water molar volume, n_s and n_w are the number of moles of solute and of water in the solution and V_s is the volume of the solution. This definition of the solute apparent molar volume assumes that the water maintains an unchanged density on addition of a salt. Although this assumption is not realistic in most cases (due to the electrostriction phenomenon), it provides a useful method of carrying out calculations of the density of mixed electrolyte solutions. Equation (1.5) may be rearranged as

$$V_s = n_s \Phi_s + n_w \Phi_w \tag{1.6}$$

which states that the solution volume is the sum of the water volume and of the solute apparent volume. The solute apparent molar volume is related to the solution density D_s and the water density D_w by [44,45]

$$\Phi_s = \frac{1000}{C_s D_w} (D_w - D_s) + \frac{\bar{M}_s}{D_w} \tag{1.7}$$

where C_s and $\bar{M}_s$ are the solute molarity and molecular mass, respectively. Masson [46] found that for most electrolytes, the apparent molar volume could be expressed by

$$\Phi_s = \Phi_0 + K \sqrt{C_s} \tag{1.8}$$

where K is a constant and Φ_0 is the apparent molar volume at infinite dilution. Combining (1.7) and (1.8) gives [45]

$$D_s = D_w + a\,C + b\,C^{\frac{3}{2}} \qquad (1.9)$$

where a and b are constants. Root [45] found that these constants were additive for alkali halides i.e. that it was possible to calculate the density of ternary solutions from the corresponding binary solutions data. This was confirmed by Young and Smith [43] for alkaline earth halides. Equation (1.9) may be generalised for n salts and becomes

$$D_s = D_w + \sum_{i=1}^{n} (a_i\,C_i + b_i\,C_i^{\frac{3}{2}}) \qquad (1.10)$$

for the n salts. The values of the constants a and b have been compiled by Novotny and Sohnel [37] for more than three hundred inorganic salts. Their values are a = 17.368 10^{-3} and b = -1.4561 10^{-3} for NH_4Cl and a = 113.14 10^{-3} and b = -5.7917 10^{-3} for $ZnCl_2$ at 25 °C for the densities in g ml^{-1} and the concentrations in mol l^{-1}. Atlung *et al.* [34] have used an equation of the form of equation (1.6) to fit the data of Sasaki and Takahashi [32] and proposed

$$V_s = 17.7\,n_w + 44.4\,n_n + 43.5\,n_z \qquad (1.11)$$

where V_s is the volume of a solution containing n_w, n_n and n_z moles of water, NH_4Cl and $ZnCl_2$ respectively. In equation (1.11), the water apparent molar volume was also used as a fitting parameter. When Novotny and Sohnel data are applied to the more concentrated solutions used by Sasaki and Takahashi, the calculated density is found to be about 8 % too high [47].

Due to the complexation phenomenon (section 1.3.1), the addition of ammonium chloride to a zinc chloride solution cannot be considered as a simple mixing but rather as a reaction. Sasaki and Takahashi [32] proposed

$$[Zn(H_2O)_4]^{2+} + x\,Cl^- \rightleftharpoons [Zn(H_2O)_{4-x}Cl_x]^{(2-x)+} + x\,H_2O \qquad (1.12)$$

and therefore both equations (1.10) and (1.11) must be corrected to take into account this complexation.

The study of Sasaki and Takahashi [32] was limited to the range 0 - 25 w/w % NH_4Cl and 0 - 45 w/w % $ZnCl_2$. The ranges have been extended in this work up to saturated solutions for NH_4Cl and up to 70 w/w % $ZnCl_2$.

1.3.3 Reactions in the Leclanché electrolyte

For each zinc ion produced during the discharge of a Leclanché cell, two protons are extracted from the electrolyte [13]. This has been approximately simulated by addition of NH_3 [19,48,49] or ZnO [49,50] to the electrolyte. The product that precipitates on addition of these reagents depends on the ammonium chloride concentration of the starting solution. At high NH_4Cl concentrations, $Zn(NH_3)_2.Cl_2$ precipitates while in less concentrated NH_4Cl, $ZnCl_2.4Zn(OH)_2.H_2O$ is formed [13]. There is no agreement in the reported data about the NH_4Cl concentration at which the transition from one reaction product to the other occurs. Cahoon [17] found the transition almost independent of the zinc chloride concentration and at about 7 w/w % NH_4Cl. Friess [48] showed a transition at about 14 w/w % NH_4Cl while McMurdie *et al.* [50] gave a value which increased from about 18 w/w % to about 25 w/w % when the initial $ZnCl_2$ concentration increased from 10 to about 40 w/w % respectively. More recently, Bredland and Hull [49] found that the zinc diamine precipitated first on addition of NH_4OH or ZnO if the NH_4^+/Zn^{2+} molar ratio was larger than about 2.4 in the solution at the precipitation point. If this ratio was lower than about 2.4, the zinc hydroxychloride precipitated. This result shows much greater sensitivity of the transition point to zinc chloride concentration than would be expected from the data of earlier investigators. From thermodynamic considerations, Tye [13] calculated the transition level as 16 w/w % NH_4Cl in a typical Leclanché electrolyte.

A knowledge of the transition concentration of NH_4Cl is necessary to model behaviour during cell discharge. A study to resolve the above differences and to determine the free energy of formation of $Zn(NH_3)_2Cl_2$ and of

$ZnCl_2.4Zn(OH)_2.H_2O$ is included in this work. The results have been compared with the reported values [18,51].

1.3.4 Zinc potential in Leclanché electrolyte

Thermodynamically, zinc is not stable in water: it corrodes and evolves hydrogen [52]; amalgamation of the zinc electrode is almost universally adopted to reduce that corrosion [53]. Amalgamated zinc electrodes have been used in the present work.

Mercury deposition onto the zinc surface may be carried out by electrodeposition [53] or by contact with a mercury salt. In batteries a paper coated with calomel may be pressed against the zinc electrode, and the amalgamation occurs when the electrolyte is added to the system [54], or the mercury is deposited by immersion of the electrode into a $HgCl_2$ solution [55]. In Leclanché electrolyte, the zinc electrode potential is about 30 - 50 mV more negative for the amalgamated electrode than for the non-amalgamated zinc [54]. The level of amalgamation does not affect the zinc potential in the range 0.01 - 1 mg Hg cm^{-2} [56] and the electrode behaviour is independent of the method of amalgamation [54].

The effect of zinc complexation on the zinc electrode potential may be obtained by combining the Nernst equation (equation 1.1) with the complex stability constants (equation 1.4) as follows

$$E_{Zn} = E_0 + \frac{RT}{2F} \ln\left(\frac{a_{ZnCl_n^{(2-n)-}}}{K_n\, a_{Cl^-}^{n}}\right) \qquad (1.13)$$

In this equation which shows the influence of the chloride ion activity on the zinc potential, the term in brackets must be simultaneously the same for the four possible chloro-complexes.

The only experimental study of the zinc electrode potential in the system $ZnCl_2$ - NH_4Cl - H_2O is due to Takahashi *et al.* [32,57] who reported the electrode potential in 15, 20 and 25 w/w % NH_4Cl in the range 5 to 45 w/w % $ZnCl_2$. The

value of the electrode potential in pure $ZnCl_2$ and in zinc chloride saturated by NH_4Cl was also reported by Cahoon [4] for concentrations up to 13 molal $ZnCl_2$. The effect of the electrolyte composition on the electrode potential is shown in figure (1.1) from the results of Takahashi *et al.* [32,57].

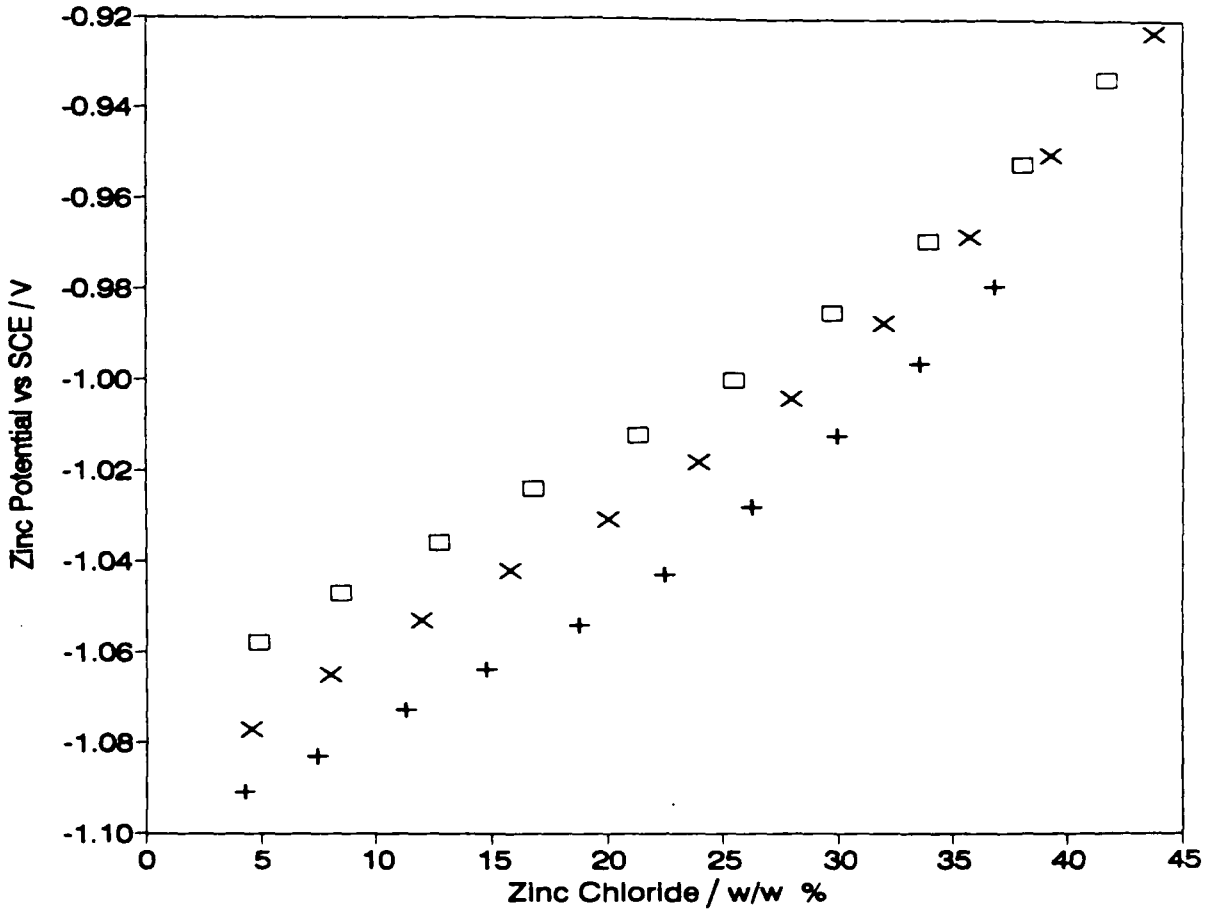

Figure 1.1 : Zinc electrode potential in the system $ZnCl_2$ - NH_4Cl - H_2O, from [32,57]. □ 15 w/w % NH_4Cl, x 20 w/w % NH_4Cl and + 25 w/w % NH_4Cl.

In water, the zinc ion forms hydrates [20,21] and the potential-determining reaction must be written [34]

$$Zn(H_2O)_n^{2+} + 2e \rightleftharpoons Zn + n\ H_2O \qquad (1.14)$$

The electrode potential therefore depends on the water activity in the solution and equation (1.1) is modified to

$$E_{Zn} = E_0 + \frac{RT}{2F}\ln(a_{Zn(H_2O)_n^{2+}}) - n\frac{RT}{2F}\ln(a_{H_2O}) \qquad (1.15)$$

As n is in the range 12 - 18 [34] and as the water activity in concentrated $ZnCl_2$ solutions may become low (about 0.2 in 14 molal $ZnCl_2$ [25]), the effect of hydration on the zinc potential is likely to be significant. In their calculations of the zinc electrode potential, Atlung *et al.* [34] used equation (1.15) with n=16.

No data are available for the zinc electrode potential in the ternary $ZnCl_2$ - NH_4Cl - H_2O system in the range 0 to 15 w/w % NH_4Cl and only four points (15, 20, 25 w/w % and saturation) have been reported in the presence of NH_4Cl. In the present work, the potential of a zinc electrode (with respect to a saturated KCl calomel electrode) has been measured in solutions 0.2 to 17 molal $ZnCl_2$, from pure zinc chloride to solutions saturated by NH_4Cl additions.

1.3.5 The NH_4Cl - $ZnCl_2$ - H_2O solubility diagram

The conventional Leclanché electrolyte is a zinc chloride solution saturated with NH_4Cl. Meerburg [58] studied this system at 0, 20 and 30 °C and found that the solid phase in equilibrium with a saturated solution was NH_4Cl, $ZnCl_2.3NH_4Cl$, $ZnCl_2.2NH_4Cl$ or a mixture of $ZnCl_2.2NH_4Cl$ and $ZnCl_2$ depending on the soluble $ZnCl_2$ concentration. The transition, at 20°C, between the different solid phase products occurred at 26.3, 43.8 and 66 w/w % soluble $ZnCl_2$ respectively. The line representing the NH_4Cl solubility was driven toward higher values with increasing temperature. Meerburg's results at 20 °C are shown in figure (1.2). Cahoon [19] found at 21 °C results in good agreement with Meerburg's data and confirmed the composition of the solid phase components.

This solubility diagram has not been reported at 25 °C. In this work, the NH_4Cl solubility has been calculated from the results of the zinc potential measurements.

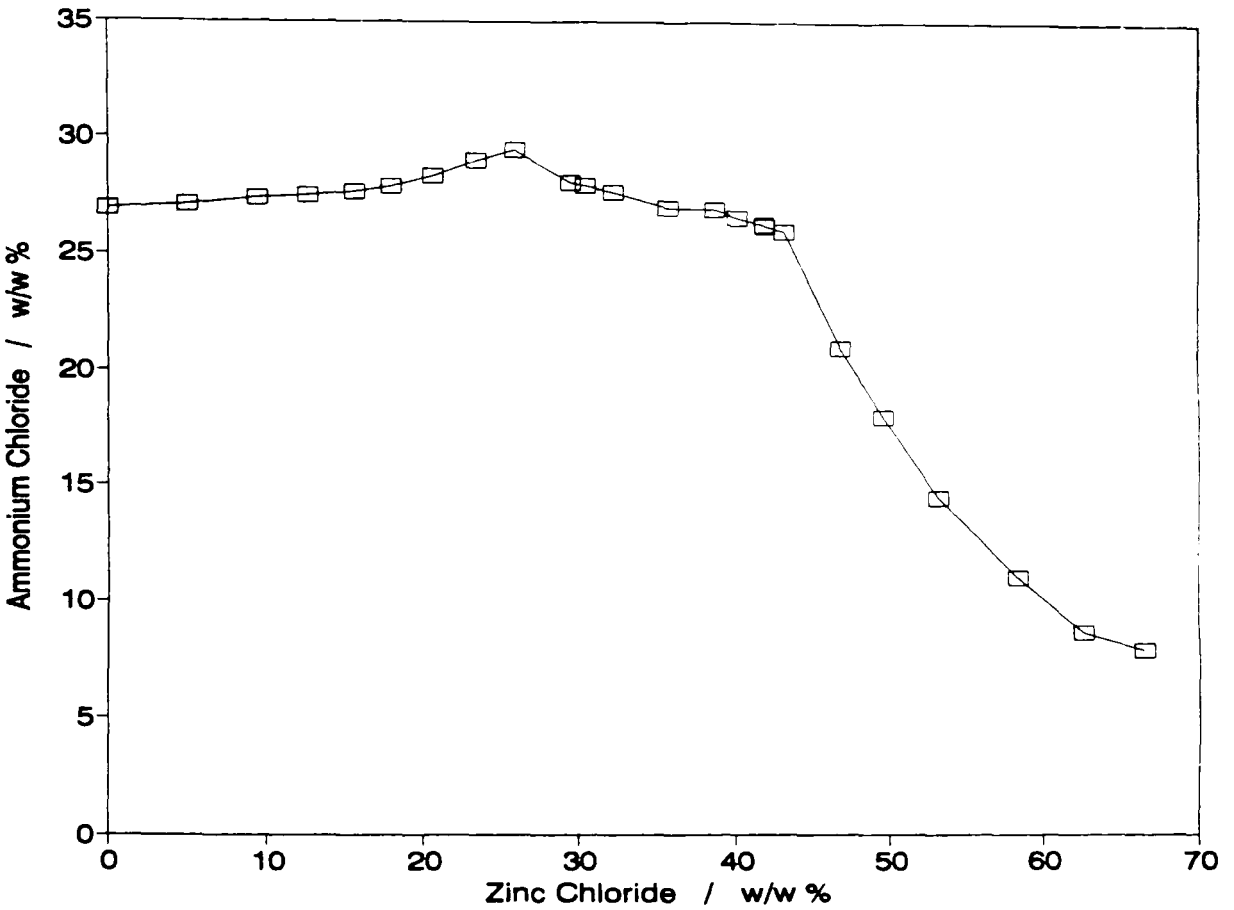

Figure 1.2 : Ammonium chloride solubility at 20 °C after Meerburg [58]

1.4. The zinc electrode

The negative electrode of the Leclanché cell is a zinc can used as the negative active material and cell container. The material is an alloy of high purity zinc with less than 1 % lead and about 0.1 % cadmium [59]. Lead and cadmium improve the strength of the can. Lead is necessary for the can manufacture as it acts as an internal lubricant during the extrusion process [59]. Both act as corrosion inhibitors [59]. In the following, the term 'zinc' refers to the zinc battery alloy.

1.4.1 The negative electrode overpotential

The zinc potential as treated in section 1.3.4 is the electrode equilibrium potential at which the rates of the forward and back reactions in, for example, equation (1.14) are equal.

$$Zn(H_2O)_n^{2+} + 2e \rightleftharpoons Zn + n\ H_2O \qquad (1.14)$$

The common value of these reaction rates, expressed as current density is the exchange current density, I_0.

When a net current crosses the electrode-electrolyte interface, equilibrium (1.14) is disturbed and the electrode potential departs from its equilibrium value by an amount called electrode overpotential , overvoltage or polarisation. That part of the overpotential which is necessary to maintain the net electrode current at constant interfacial electrolyte composition is the charge transfer or activation overpotential. Its magnitude is related to the net current density I by the Butler-Volmer equation [60]

$$I = I_0[\exp(\frac{-\alpha nF\ \eta}{RT}) - \exp(\frac{(1-\alpha)nF\ \eta}{RT})] \qquad (1.16)$$

where n is the number of electrons involved in the reaction (here, n=2), F is the faraday, η is the overpotential, R and T have their usual significance and α is termed the transfer coefficient.

At low overpotentials ($\eta << RT/nF$), equation (1.16) may be simplified to

$$I = \frac{I_0 nF\ \eta}{RT} \qquad (1.17)$$

showing that current density is a linear function of the overpotential.

At high electrode overpotential ($\eta > 0.1$ V), equation (1.16) may be simplified to

$$\eta = a + b \log I \qquad (1.18)$$

Equation (1.18) is the Tafel equation. The intercept of a Tafel line is $a = -b \log I_0$, and the magnitude of the slope is

$$b = \frac{2.303\ RT}{\alpha nF}$$

for a cathodic process and

$$b = \frac{2.303\ RT}{(1-\alpha)\ nF}$$

for an anodic process [60].

If the solution is not very strongly stirred, the net electrode reaction also induces a modification of the electrolyte composition at the interface with the electrode. The equilibrium electrode potential then changes in accordance with the Nernst equation (1.1) due to the modified interfacial electrolyte composition. The change in the electrode potential due to this phenomenon is called concentration overpotential or concentration polarisation.

1.4.2 The zinc electrode activation overpotential

In a study where the concentration overpotential was minimised, Baugh and White [61] found that the presence of NH_4Cl in a zinc chloride solution caused the zinc activation overpotential to be substantially larger than in pure $ZnCl_2$ solution. They also found that the presence of a separator increased dramatically the activation overpotential, especially in the NH_4Cl - $ZnCl_2$ electrolyte. In another study [62], they found that the separator inhibited the zinc dissolution more than expected from the blocking effect. The blocking effect of the separator was assumed to operate by preventing the contact between zinc and electrolyte. This effect increased the effective current density and the activation overpotential changed accordingly. The slope of the anodic Tafel line was also modified by the presence of the separator. They explained these results by considering that the separator slowed down the second step of the zinc oxidation, the dissolution being considered as two successive one-electron charge transfers.

Baugh and Higginson [63] found that amalgamation increased the anodic current by decreasing the dissolution activation energy. Brouillet and Jolas [64] showed that the reverse reaction rate is negligible (high activation energy) during zinc dissolution. Baugh *et al.* [53] concluded that the dissolution of an amalgamated zinc electrode was irreversible.

1.4.3 The zinc electrode concentration overpotential

When the discharge of a Leclanché cell is started, ionic zinc species are produced at the zinc electrode (anode) and a potential gradient appears in the electrolyte. In a battery, negligible convection of electrolyte may be assumed and therefore mass transport occurs only by diffusion and migration. Diffusion is the result of concentrations profiles, while migration results from the effect of the electric field upon the ions present in solution.

A model taking into account both diffusion and migration effects was proposed by Dewhurst [65] to describe the changes in concentration at an electrode - electrolyte interface. This model considers plane electrodes and semi-infinite electrolyte medium and predicts that the concentration of a given species at the electrode interface, c, changes linearly with the square root of the electrolysis time, t, according to :

$$c = c_0 \, (1 - Mt^{1/2}) \tag{1.19}$$

where c_0 is the concentration of the bulk solution (mol cm^{-3}), and

$$M = \frac{2 \, (1-a) \, I}{c_0 z F \, (\pi D)^{1/2}} \tag{1.20}$$

where a is the ion transport number, z its electric charge, F is the faraday, I the current density (A cm^{-2}) and D the diffusion coefficient (cm^2 s^{-1}). The transport number of an ion is the fraction of the total current carried by that ion [60]. Equation (1.20), which is equivalent to the Sand's equation [66] (Sand's equation was written using the gram equivalent scale), shows that the transport number and the diffusion coefficient are the two parameters influencing the interfacial concentration.

Zinc is the negative active material of many electrochemical systems and its electrochemical properties have therefore been studied by many workers. Harris and Parton [67] reported that the zinc transport number in $ZnCl_2$ solutions is positive at low concentration but becomes negative above 2 molal. This result was confirmed by Agnew and Paterson [39] who also reported the $ZnCl_2$ diffusion

coefficient in pure zinc chloride solutions as ranging from 1.05 10^{-5} to 1.27 10^{-5} cm^2s^{-1} for concentrations between 0.05 and 3.9 molal. Surprisingly, the diffusion coefficient is higher at 25 °C in agar gelled solution (1.23 10^{-5} cm^2s^{-1}) than in free aqueous solution (0.90 10^{-5} cm^2s^{-1}) in 0.05 M solution [68]. The addition of a chloride salt supporting electrolyte to a $ZnCl_2$ solution influences the zinc transport properties by increasing the proportion of anionic zinc species [69]. Moreover, the addition of another cation into the solution decreases the relative contribution of the zinc to the overall ionic transport so that its transport number decreases [70]. The $ZnCl_2$ diffusion coefficient is also slightly lowered by the addition of KCl to the solution [70]. In 3.5 M KCl, the zinc diffusion coefficient was found to be almost independent of the zinc chloride concentration (about 0.9 10^{-5} cm^2 s^{-1}) [71,72].

The presence of a separator also affects the anodic concentration polarisation. In addition to the blocking effect [62], the separator reduces drastically the zinc diffusion [56]. Its effect on the electrical conductivity and on the diffusive flux of the electrolyte is due to physical obstacle effects [73]. If the separator tortuosity θ is defined by [73]

$$\theta = \frac{mean\ path\ length}{separator\ thickness} \tag{1.21}$$

and the porosity V by

$$V = \frac{pore\ volume}{total\ separator\ volume} \tag{1.22}$$

then the effect on the conductivity κ and the diffusion coefficient D is [73]

$$\frac{\kappa'}{\kappa} = \frac{D'}{D} = \frac{\theta^2}{V} \tag{1.23}$$

where κ', D', κ and D are the conductivity and the diffusion coefficient in the separator and in free solution, respectively.

Although equation (1.23) has been derived for a separator in which all the pores have the same tortuosity [73], it also holds when this is not the case if θ is

an averaged value of the different pore tortuosities [74]. Tye [74] showed that at given porosity, the separator averaged tortuosity is strongly dependent on the pore tortuosity distribution, the pores of high tortuosity having a relatively small influence on the separator properties.

The precipitation of $Zn(NH_3)_2Cl_2$ and/or $ZnCl_2.4Zn(OH)_2.H_2O$ that occurs during the cell discharge decreases the separator porosity [75,76]. It may also build up a low porosity layer in the outermost part of the positive electrode [77-79]. Both phenomena increase the anodic concentration overpotential.

Agopsowicz *et al.* [80] studied composition changes in a simulated separator of a Leclanché cell; they reported these changes in the form of concentration profiles. In pure $ZnCl_2$ electrolyte, the application of Dewhurst's theory [65] was found to be satisfactory and gave a zinc transport number $t_{Zn} = 0.13$. The presence of NH_4Cl in the electrolyte changed this transport number to $t_{Zn} = -0.14$ (corresponding to a transport of zinc towards the zinc electrode) due to the existence of negative zinc species. The ammonium chloride concentration at the electrode interface was found to decrease rapidly with discharge time and, after it had reached zero, a constant NH_4Cl concentration profile (moving boundary) started to move away from the zinc electrode. The zinc concentration overpotential was much higher in NH_4Cl - $ZnCl_2$ electrolyte than in pure zinc chloride electrolyte.

Another approach was used by Atlung *et al.* [34]. They developed a model for the separator of a pasted cell and solved the equations numerically. In spite of the many assumptions necessary in this approach, e.g. zinc complex stability constants, activity coefficients and ionic mobilities, their theoretical results were in good agreement with Agopsowicz *et al.* [80] except for the identification of the moving boundary phenomenon. They ascribed this difference to a lower current density and the absence of a separator. They also found a zinc transport number changing from a positive value in pure $ZnCl_2$ electrolyte to a negative value (-0.12) in mixed electrolyte.

Coleman [81] connected a small zinc electrode via a capillary to the electrolyte of a pasted cell to monitor the anodic overpotential during a continuous discharge. He found that the zinc electrode overpotential was small compared to the cell polarisation, particularly at low drain. An anodic concentration overpotential of about 0.16 V was also reported by Cahoon [19], but the experimental technique was not clearly described. In both cases, the electrolyte composition was not given but it certainly contained NH_4Cl and probably some $ZnCl_2$. Huber and Bauer [82], using a calomel electrode connected to the paste by a Luggin capillary, found a roughly linear increase of the zinc electrode closed circuit potential with the current delivered by the cell during a constant resistance continuous discharge.

A more recent study was carried out by Uetani *et al.* [75] on paper lined cells. They inserted a Luggin capillary connected to a calomel reference electrode through a hole drilled into the zinc can. They expressed the overpotential as the difference between the open circuit potential just after the end of a 600 mA continuous discharge and the value after a 48 hour recovery. Anodic overpotential, so defined, was found to be much higher for cells using mixed $ZnCl_2$ + NH_4Cl electrolyte than for the cells with almost pure zinc chloride electrolyte. This overvoltage also increased continuously with increasing initial NH_4Cl electrolyte concentration after a 4 hour discharge.

The present work was concerned with the study of the zinc electrode concentration and activation overpotential in pure zinc chloride solution and in mixed Leclanché electrolyte. The batteries (paper lined type), were tested on continuous discharge at constant resistance load. They contained either electrodeposited or chemical manganese dioxide.

Some intermittent discharges were also performed to study the chemistry of Leclanché cells.

1.5. The manganese dioxide electrode

1.5.1 General

Although the general formula is usually written as MnO_2, active manganese dioxides are non-stoichiometric compounds with an O to Mn ratio less than 2 [83]. They also have a significant water content (about 5-8 %) [84,85]. The water evolution rate on heating exhibits three maxima [86,87] corresponding to different types of bonding to the manganese dioxide structure. However, the water has been divided into hydration and structural water [88]; the content in the latter type was found [88] to increase linearly with the reduction level of the oxide. If the content of hydration water is neglected, manganese dioxides may be represented by the formula $MnOOH_r$. For the synthetic manganese dioxides used in batteries, either electrodeposited or chemically prepared manganese dioxides, r is about 0.1 in the unreduced material [83,89,90] and increases towards 1 during the reduction process [13]. Another common notation that only takes into account the non-stoichiometry of the oxide is MnO_x, where x may vary from about 1.95 (in the unreduced material) to 1.5 at the completion of the discharge. The relationship between r and x is $r = 4 - 2x$.

In electrolyte solution, manganese dioxide adsorbs cations from the solution and releases an equivalent amount of protons [91,92]. The ion exchange mechanism probably involves hydration water molecules which exchange protons with cations from the solution [92,93]. If ≡ Mn-OH groups are formed at the manganese dioxide surface [94], the ion exchange may be written, for example with zinc as

$$m \equiv Mn\text{-}OH \;+\; Zn^{2+} \rightleftharpoons [(\equiv Mn\text{-}O)_m Zn]^{(2-m)+} \;+\; m\,H^{+} \qquad (1.24)$$

Tamura and Nagayama [94] found that the quantity of zinc removed from the solution was higher than the amount of released protons and concluded that there was a simultaneous adsorption of zinc and its associated anion. From similar observations, Gabano *et al.* [92] concluded that the adsorbed species was $Zn(OH)^+$.

In addition, the water content affects the electronic conductivity of MnO_2 [85,95], its battery activity [96,97] and is also strongly correlated with its electrode potential [85,87,98-100]. In the latter case, it is not clear whether this dependence is due to an influence of the water content on the properties of the bulk of the MnO_2 material [85,98,100] or due to a surface effect [83,99].

1.5.2 MnO_2 reduction

In Leclanché cells, the general reduction reaction may be written [101,102]

$$MnOOH_r + \Delta H^+ + \Delta e \longrightarrow MnOOH_{r+\Delta} \qquad (1.25)$$

where the value of r is about 0.1 in the starting material and the end product is MnOOH [13].

Although equation (1.25) represents the main reduction path in the limited electrolyte volume of the Leclanché cell [18], the discharge also produces Mn^{2+} ions [76,103-106]. This fact lead Cahoon and coworkers [103,104] to believe that the main reaction was

$$MnO_2 + 4 H^+ + 2 e \longrightarrow Mn^{2+} + 2 H_2O \qquad (1.26)$$

followed by the recovery according to

$$MnO_2 + Mn^{2+} \rightleftharpoons MnOOH + 2 H^+ \qquad (1.27)$$

Reaction (1.27) occurs in any neutral or alkaline solution in absence of species complexing Mn(III) [107].

Whatever the discharge reaction, the electrons are provided by the external cell circuit and the protons are taken from the electrolyte [83]. It is now generally agreed [13,105,108-110] that MnOOH is the product of the reduction of MnO_2 and that Mn^{2+} is formed by the disproportionation reaction (1.27) [13]. The disproportionation in NH_4Cl solutions of oxide intermediate between MnO and MnO_2 was already reported by Divers [111] in 1882, "... a little manganese dissolving and the remaining oxide approaching more and more the dioxide in

composition. ". He also reported "hydrogen manganite" ($Mn_2O_4H_2$ - or MnOOH) as the main reduction product [111]. Divers' findings have remained unnoticed by other workers.

Later, Coleman [81] proposed that the reduction of manganese dioxide produced an oxide of lower oxidation degree than MnO_2 and that this oxide diffused away from the surface where it was formed. This was supported by McMurdie [112] who found by X-ray diffraction of a discharged cell that the manganese dioxide had been reduced to a Mn(III) oxide. Ferrell and Vosburgh [113] proposed that the insertion of protons and electrons into the manganese dioxide by reaction (1.25) produced a solid solution of oxyhydroxide of lower manganese valency. The concept of solid solution between the different manganese oxides, had already been mentioned in 1916 [114], but it remained unnoticed by battery technologists for more than thirty years.

The amount of Mn^{2+} formed during the reduction of the manganese dioxide is very dependent on the reaction conditions, particularly the volume ratio of solution to solid. Chreitzberg *et al.* [115] found a dependence on the electrolyte pH and an increase with the discharge depth. They also showed that the recovery was related to the presence at the electrode surface of a Mn(III) oxide and to the changes in its concentration. Mendzhertskii [116] suggested that the interfacial pH of the manganese dioxide during the discharge was the factor determining the reaction path (equation 1.25 or 1.26). According to this assumption, the reduction mechanism depends not only on the bulk electrolyte pH but also on the discharge current through its influence on the electrolyte pH. The quantity of Mn^{2+} formed during the reduction also depends on the amount of electrolyte [117]. The effect of the electrolyte quantity, pH, and the discharge level on the Mn^{2+} formation may be understood by considering the equilibrium (1.27) along with the Mn^{2+} equilibrium concentration as given by Shaw who reported [118,13] that the concentration of Mn^{2+} in the solution increased with increasing reduction of the manganese dioxide phase.

When zinc ions are present, the reduction of manganese dioxide may also form $Mn_2O_3.ZnO$ (hetaerolite) [111,119] according to the overall reaction [13]

$$2\ MnO_2 + Zn \longrightarrow Mn_2O_3.ZnO \qquad (1.28)$$

McMurdie [112] found that hetaerolite was the main reduction product while Gabano *et al.* [76] reported its formation only at the end of the discharge. Cahoon *et al.* [103] reported that the proportion of hetaerolite increased with increasing discharge depth. Electrodeposited manganese dioxide does not form hetaerolite in the normal discharge conditions except at the very end of the discharge [13]. However, some synthetic manganese dioxides [83,119] and particularly chemical manganese dioxides [13,106,120] form hetaerolite at much lower reduction levels. The mechanism of hetaerolite formation probably involves Mn^{2+} ions as proposed by McMurdie *et al.* [50]

$$MnO_2 + Mn^{2+} + Zn^{2+} + 2\ H_2O \longrightarrow Mn_2O_3.ZnO + 4\ H^+ \qquad (1.29)$$

Even when hetaerolite is formed, the main current producing reaction is given by equation (1.25), hetaerolite formation occurring as a subsequent chemical step [13,108].

1.5.3 Potential - pH relationship

The manganese dioxide electrode potential, E, varies with the solution pH according to

$$E = E' - 2.303\ \frac{RT}{F}\ pH \qquad (1.30)$$

where E' depends on the composition of the manganese oxide phase. At 25 °C, the theoretical slope is 0.059 V pH^{-1}.

Many studies have been aimed at the determination of this slope. Holler and Ritchie [121] found a slope of 0.067 and 0.080 V pH^{-1} in NH_4Cl solutions for two different ores. Cahoon [122] found 0.061 V pH^{-1} at 27.5 °C in NH_4Cl / $ZnCl_2$ solutions in the range $1 \leq pH \leq 12$ for an African ore. Sasaki [123] found linear potential - pH relations but the slopes were different for different materials. He

emphasised the role of ion exchange and the need of sample equilibration before the potential measurement. The accent was also put on the ion exchange phenomenon by Benson *et al.* [124] who found a 0.059 V pH^{-1} slope in hydrochloric acid. They worked on a manganese dioxide from which ion-exchanged cations were removed by prior HCl washing. The same slope was found by Caudle *et al.* [125] who studied acid-washed electrodeposited and natural manganese dioxides. The replacement of HCl by H_2SO_4 had no effect on the potential - pH curve.

When Mn^{2+} ions are added to the solution, reaction (1.27) occurs and the manganese dioxide is reduced. Such a reduction was taken into consideration by Caudle *et al.* [126] who corrected their measurements in order to draw the potential - pH curve at constant manganese dioxide composition and found the theoretical slope for a one electron reduction. Equation (1.25) is therefore the potential-determining reaction, even in presence of Mn^{2+} ions. An identical slope of the potential - pH dependence was also reported by Shaw [118] for a manganese dioxide reduced to $MnOOH_{0.74}$.

Although protons are extracted from the electrolyte during the discharge of a Leclanché cell [13], the electrolyte pH is buffered by the $Zn(NH_3)_2Cl_2$ or $ZnCl_2.4Zn(OH)_2.H_2O$ precipitation and the pH change, after recovery, is limited to about 1 unit during the exhaustion of the cell capacity [13]. Consequently, the effect of pH change on the equilibrium manganese dioxide electrode potential is limited to about 60 mV during the discharge [13].

1.5.4 Potential - composition relationship

The influence of the composition on the manganese dioxide electrode was implicit in Coleman's model [81] of the cathode recovery when he suggested that the recovery was due to the diffusion of the reaction products away from the reduction site. Johnson and Vosburgh [127] prepared some electrodes by mixing MnO_2 and MnOOH and found that the potential after long equilibration could be expressed by :

$$E = E_0 + 0.073 \log \frac{[MnO_2]}{[MnOOH]} \qquad (1.31)$$

Chreitzberg *et al.* [115] showed that the electrode potential was influenced by the surface composition of the oxide. The dependence of the electrode potential on its composition was explained by Vetter [128]. His theory predicts that the electrode potential is independent of the oxide composition when the oxidised and reduced forms of the oxide belong to separate phases but that the potential varies continuously with composition if the non-stoichiometric oxide consists of one single phase, as in solid solutions. This criterion has been used by many workers [110,118,129-134] to determine the limits of the homogeneous reduction of manganese dioxide. The reduction was either electrochemical [110,118,129-132] or chemical [110,118,133,134] with equivalent results [130,135]. The nature of the material and the conditions of the reaction have an influence on the range of the homogeneous reduction. Gabano *et al.* [129] and Kozawa and Powers [131] reported that the electrochemical reduction of electrodeposited manganese dioxide was homogeneous up to the formation of MnOOH. This finding was confirmed by Shaw [110,118] for both electrochemical and chemical reduction and by Bode and Schmier [133] for chemical reduction. However, Desai *et al.* [132] found that homogeneous electrochemical reduction occurred only up to about $MnOOH_{0.8}$ for EMD and to up to about $MnOOH_{0.5}$ for CMD. Even when the reduction proceeded homogeneously over the whole range of compositions, the potential versus oxide composition curve showed a change of its slope at about mid-reduction [110,118]. Maskell *et al.* [110,136-140] developed a model incorporating this feature which showed good agreement with the experimental data. It involved independent mobilities for inserted protons and electrons, the existence in the starting material of some Mn(III) inactive in the potential-determining process and two different insertion sites for the first and the second half of the reduction. The equations for the electrode potential derived from this model were rather complicated [140]. Tye [141] obtained simpler equations by considering that the reduction produces a solid solution of $MnOOH_{0.5}$ in the

starting material during the first half of the reduction and a solid solution of MnOOH in the starting material during the second half of the reaction. This model which also requires the presence of an amount of inactive Mn(III) equivalent to the Mn(III) that was not removed by acid-washing of the starting material, gives a very good agreement with the experimental data. Xi *et al.* [142] found a concentration of Mn(III) resistant to $HClO_4$ oxidation equivalent to the inactive Mn(III) content of the latter models. Two different reduction mechanisms for the first and the second half of the discharge had already been suggested by Laurent and Morignat [130], and more recently, Chabre [143] brought new evidence to support this suggestion.

1.5.5 MnO_2 electrode overpotential

Synthetic manganese dioxides, either electrodeposited or chemically prepared, have high surface area, 40 - 60 m^2g^{-1} and 70 - 80 m^2g^{-1} (BET method) respectively [144]. Although the electrochemically active surface area is much smaller than the total surface area (3 to 10 times [145] or 400 to 800 times [146]), the effective current density across the MnO_2 interface is very small (less than 1.5 10^{-5} mA cm^{-2} active surface area for a R20 cell containing 23 g MnO_2 on a 4 Ω discharge [47]) and therefore, the charge transfer overpotential,η

$$\eta = \frac{I}{I_0}\,\frac{RT}{F} \qquad (1.32)$$

is generally considered to be negligible. Equation (1.32) is derived from equation (1.17) for a one electron charge transfer.

The insertion of protons and electrons generates a concentration gradient in the solid manganese dioxide phase [147] and the electrode potential will be controlled by the diffusion of the inserted species, protons and electrons, from the external surface towards the bulk of the electrode as suggested by Coleman [81]. Scott [148] and later Brouillet *et al.* [147] developed a polarisation model in which the electrode was considered as semi-infinite and the potential was related to the

composition by an empirical relationship. A discharge at constant current gave an equation of the form [147]

$$E = E_i - k \frac{i\,(\sqrt{t} - \sqrt{t-T})}{\sqrt{A\,D}} \qquad (1.33)$$

where E and E_i are the potential at time t and initially respectively, i is the current, A the active surface area, D is the diffusion coefficient for the H^+/e couple, t is the time from the start of the discharge, T is the time at which the discharge is stopped and k is a constant. When $t < T$, the terms containing $(t\text{-}T)$ are taken as zero [147].

Scott [148] reported good agreement of the model with experimental curves except at long recovery times when the semi-infinite diffusion model was not adequate. Brouillet *et al.* [147] found a difference between their observations and the values predicted by equation (1.33) and explained them by invoking charging of the electrode double layer. Kornfeil [149] reported some discrepancies between Scott's equation and experimental results and attributed them to the limitations of the semi-infinite diffusion model. Era *et al.* [150] introduced an extra term into Scott's equation to take into account the limited volume of the MnO_2 electrode. Their equation reads [150]

$$E = E_i + k_1 \log\left(\frac{\sqrt{\pi\,D}}{2\phi\,[\sqrt{t' + \tau} - \sqrt{t'} + \sqrt{t_0}]} - 1\right) \qquad (1.34)$$

where E is the electrode potential, E_i is its initial value, τ, t' and t_0 are respectively the discharge time, the recovery time and a constant, k_1 is another constant, ϕ is the amount of MnOOH produced by unit surface area (g equivalent $cm^{-2}s^{-1}$) and D is the (H^+,e) diffusion coefficient. This equation is only valid when the rate of disproportionation of MnOOH is negligible, i.e. in alkaline solutions [150]. Valand [101] considered the electrode to be composed of spheres to derive the current - time relationship in response to a potential step imposed upon an MnO_2 electrode. He claimed a good agreement of his model with these

transients. The spherical diffusion model has also been used in some attempts to determine the proton diffusion coefficient, e.g. by Laragne and Brenet [145].

More recently, Hong *et al.* [151] proposed a "double plane" model and applied it to the study of the MnO_2 electrode response to a potential step. In this case, the diffusion was assumed to occur between two parallel planes at which (H^+,e) concentrations were kept constant by the applied potential. The authors claimed a better agreement with the experimental data than was obtained with the previously proposed models. Chabre [143] denied that the transients he observed in very similar experiments were controlled by a diffusion phenomenon.

1.5.6 MnO_2 electrode discharge in Leclanché electrolyte

The positive electrode of the Leclanché cell is a mixture of manganese dioxide and carbon black, the latter acting as electronic conductor. In the case of standard Leclanché formulations, it also contains some solid NH_4Cl. Some ZnO is also added to control the electrolyte pH [13]. The mix, wetted with the electrolyte, is introduced into the cell with interposition of the separator to prevent any electronic contact with the can.

When such a porous electrode is discharged, the current enters the cathode from the separator as an ionic current, flows through some of the interstitial electrolyte, becomes an electronic current when it crosses the MnO_2 - electrolyte interface, enters the web of carbon black, flows through it and eventually is collected by the carbon rod and goes into the external circuit. The main resistances to this current flow are due to the electrolyte and the carbon black resistivities and also to the charge transfer resistance. The contact resistance between the carbon web and the current collector as well as the current collector resistance are usually neglected. The passage of the current through the electrolyte and the web of black produces an ohmic drop across these media, while a charge transfer overpotential occurs at the sites of the electrochemical reaction. The electrode overpotential is the sum of these three potential differences and the decrease of the electrode potential due to the reduction of the

material (higher at the dioxide surface than within the material during the discharge and the recovery) and of the change in electrolyte pH.

The first model to describe the discharge of a cylindrical MnO_2 electrode was due to Coleman [81] who applied Kirchoff's law to the flow of current. He deduced that the MnO_2 reduction current could not be uniform all over the cathode volume and that the reduction rate was a maximum close to the carbon rod with another maximum close to the external cathode surface. He also calculated the influence of the relative proportions of electrolyte and solid phase resistances on the current distribution. Using specially designed cells [152], he showed the influence of these resistances on the change in position and in magnitude of the maximum reduction current. Daniel-Bek's model [153,154] predicted a charge transfer current density at a distance x from the current collector proportional to the second derivative of the electrode potential, E, measured with respect to a reference electrode located at this point, (d^2E/dx^2), and a minimum in the overvoltage curve at a position depending on the ratio between the electrolyte and the solid phase conductivities [154], but not depending on the total current if the electrode was operated in the region of linear overvoltage. He also reported [153] an experimental investigation of the potential distribution into an electrode by using Luggin capillaries positioned at different locations in the MnO_2 electrode.

The literature dedicated to the theory of charge transfer current distribution within porous electrodes is abundant [78,81,152-171] but the reports of experimental investigations are scarce. Cahoon and Heise [78] analyzed concentric layers of the mix taken at different moments during a 4 Ω continuous discharge. They found that the utilisation rate of the manganese dioxide increased with the distance from the carbon rod. A similar method was used by Tsuruoka *et al.* [155] who reported a change in the distribution of MnO_2 utilisation according to the discharge regime. The inner part of the cathode was most reduced at light drains while at heavy drains, the maximum reduction was in the outer part of the electrode. In both cases, the reduction was a minimum in the middle of the cathode. Simonsson [156] used electron microprobe analysis to

measure the $PbSO_4$ formed by the discharge of a lead dioxide plate. He found a maximum reduction at the electrode-electrolyte boundary and explained it on the basis of the conductivity of the solid phase being much higher than the electrolyte conductivity. A maximum charge transfer current density at the outside of a porous zinc electrode in alkaline electrolyte was also reported by Yamazaki and Yao [157] who used a specially built sectioned electrode to measure the current distribution. A segmented silver electrode was used by Szpak and Katan [158] to measure the current flowing in the different slices of the electrode. They also found a maximum charge transfer current density in the outside region of the electrode. All these results were explained by the electronic conductivity of the electrode being much higher than the ionic electrolyte conductivity. Brodd [159] built an MnO_2 electrode in a tube containing regularly-spaced reference electrodes and platinum electronic probes. He found that the charge transfer current was minimum in the central region of the electrode where he often observed a charging current (increase in the electrode potential) during a reduction experiment.

Newman and Tobias [160] developed a pseudo-homogeneous model of a porous electrode in which both solid and electrolyte phases were considered as macroscopically continuous media, disregarding the actual geometry of the pores. Average properties were used for both the solid and electrolyte phases. Their theoretical analysis revealed the influence of the relative resistivities of the two phases but also showed the effect of the total current, of the electrode thickness and of the activation overpotential on the charge transfer current distribution. The charge transfer current density was found most often at a maximum close to the current collector, but another less pronounced maximum was possible close to the electrode edge. Brodd [161] put the accent on the effect of the activation overpotential which tends to reduce the non-uniformity of the charge transfer current distribution. The solid phase resistance was considered to be negligible in the model proposed by Grens and Tobias [162]. In this case, the non uniformity of the charge transfer current distribution increased with the current drain, the electrode specific surface area and the exchange current density of the

electrochemical reaction. A single maximum at the outer surface of the electrode was also reported. The effect of the reaction exchange current density on the current distribution was in agreement with Brodd's report [161]. Negligible matrix resistance was also assumed in many other studies [164-168] and the system of equations was most often solved by a numerical method [165-168]. Except for Marshall's work [163] which concerned cylindrical electrodes, these studies concerned planar electrodes. They all confirmed the crucial influence of the electrolyte and solid phase conductivities on the charge transfer current distribution as predicted by Newman and Tobias [160], both in planar and cylindrical electrodes. Similar results were obtained by Euler and coworkers [169-171] who advocated analog solutions (most often made of resistor networks) to the problem of the current distribution in porous electrodes.

The coulombic yield of a discharge will be maximum if the whole electrode mass participates in the reduction process, that is to say if the charge transfer current distribution is uniform.

The charge transfer current distribution in the manganese dioxide electrode of cells undergoing heavy continuous discharge has been investigated in the present work. Small carbon electrodes were inserted into the positive electrode mass as suggested by Coleman [81] and the measured potential differences were interpreted to deduce the electrochemical current distribution. In some discharges, these electronic probes were replaced by salt bridges connected to references electrodes as used by Daniel-Bek [153] in order to distinguish clearly the different ohmic losses within the electrolyte phase.

1.6. Discharge tests

The continuous discharge test was used by Leclanché [172] to demonstrate the superiority of his cell over the other available systems. To do so, he recorded the electromotive force of the different cells as a function of the discharge time on a constant resistance load. He claimed superiority of his system on the basis of a higher electromotive force at any discharge time. The discharge tests presently in use to measure battery performance are still based on this idea.

A summary of the tests in common use was given by Tye [18] who also showed the influence of the discharge regime on the actual capacity of the battery. A test simulating the use of an R20 cell in a radio may last more than 2 months [89] and therefore much more rapid continuous tests (about 15 hours on 4 Ω [89]) are commonly used in the battery industry to judge battery performance [173].

The decrease in the voltage of a cell undergoing a discharge results from the summation of the voltage losses in the negative and positive compartments (modification of the equilibrium potentials and concentration overpotentials) and in the separator region. The negative electrode activation and concentration overpotentials have been described in sections 1.4.2 and 1.4.3 respectively, and the MnO_2 electrode overpotential in section 1.5. The voltage loss in the separator region results from an ohmic drop across the electrolyte with the effect of the separator being given by equation (1.23) and probably also from a diffusion potential due to the presence of concentration gradients. The Henderson equation [174] which is most often used to estimate the magnitude of diffusion potentials requires the knowledge of transport numbers and activities of the various species [175,176]. As this information is not available, its application is very uncertain in Leclanché electrolyte.

A reference electrode inserted into the cell enables the zinc electrode overpotential to be separated from the total polarisation [18,75,81,82]. The ohmic drop across the cell is usually measured by an interruption technique [75,82,177-179]. It is determined by the magnitude of the very fast change in the cell voltage that occurs when the discharge circuit is broken. The analysis of the potential decay after current interruption may be carried out by consideration of the electrode equivalent circuit as proposed by Randles [180] and the overpotential equations (1.16) and (1.17). At low overpotential, the decay corresponds to the discharge of a capacitance across a constant resistance which results in the logarithm of the potential (corrected for the ohmic drop) being a linear function of the time [181]. At higher overpotentials, or when the electrode reaction may be considered to be unidirectional, the ohmic-free overpotential E is of the form

$$E = a + b \ln(t + c) \qquad (1.35)$$

where a,b and c are constants and t is the time [182-184].

A concentration overpotential is diffusion controlled and its slower decay [185] is most often a function of $t^{1/2}$ as for example in equation (1.33).

1.7. Overall cell reactions.

In the absence of hetaerolite formation, three stages may be distinguished during the intermittent discharge of a standard Leclanché cell [13]. During the first stage, the solid NH_4Cl contained in the positive electrode mass is consumed by the precipitation of $Zn(NH_3)_2Cl_2$. The overall cell reaction is

$$Zn + 2\ NH_4Cl_{solid} + 2\ MnO_2 \longrightarrow Zn(NH_3)_2Cl_2 + 2\ MnOOH \qquad (1.36)$$

The electrolyte is invariant and the zinc electrode potential on open circuit and after recuperation remains constant [13]. The $Zn(NH_3)_2Cl_2$ precipitation continues during the second stage causing a decrease in the soluble NH_4Cl concentration and an increase of the equilibrium zinc electrode potential. The overall cell reaction may be written

$$Zn + 2\ NH_4^+ + 2\ Cl^- + 2\ MnO_2 \longrightarrow Zn(NH_3)_2Cl_2 + 2\ MnOOH \qquad (1.37)$$

The third stage begins with the precipitation of the $ZnCl_2.4Zn(OH)_2.H_2O$ which is accompanied by a decrease of the negative electrode potential. The cell overall reaction is

$$4Zn + Zn^{2+} + 2Cl^- + 9H_2O + 8MnO_2 \longrightarrow ZnCl_2.4Zn(OH)_2.H_2O + 8MnOOH \qquad (1.38)$$

In equations (1.36) to (1.38), MnO_2 and MnOOH are components of the manganese dioxide solid solution.

During the last two stages, the electrolyte pH increases slightly [13] decreasing the MnO_2 electrode potential by up to about 0.05 V by the end of the discharge. Although the zinc electrode potential is the best indicator to identify the different

discharge stages, the beginning of stage 3 should also be apparent from the cell open-circuit voltage after recuperation curve as a decrease of the slope against the time on discharge. For zinc chloride cells, the same product (zinc hydroxychloride) is formed throughout the discharge which therefore corresponds to the stage 3 (equation 1.38) of the standard Leclanché discharge.

The discharge behaviour of a Leclanché cell depends strongly on the origin, electrodeposited (EMD) or chemical (CMD), of the manganese dioxide used [75,106,186-188]. During intermittent discharges, CMDs tend to form hetaerolite [13,75,106]. In 1882, Divers [111] reported that this formation occurred by a reaction which involved dissolution of previously formed $Zn(NH_3)_2Cl_2$

$$Mn_2O_4H_2 + Zn(NH_3Cl)_2 \longrightarrow Mn_2O_4Zn + 2\ NH_4Cl \qquad (1.39)$$

which with the modern notation reads

$$2\ MnOOH + Zn(NH_3)_2Cl_2 \longrightarrow Mn_2O_3.ZnO + 2\ NH_4Cl \qquad (1.40)$$

In pure zinc chloride electrolyte, hetaerolite formation may also cause the dissolution of the $ZnCl_2.4Zn(OH)_2.H_2O$ produced in an earlier stage of the discharge [13]. In both cases, the dissolution of the precipitate that hinders the mobility of the dissolved species improves the cell performance during subsequent discharge. It also regenerates NH_4Cl or $ZnCl_2$.

Intermittent discharges have been carried out in both Leclanché and zinc chloride electrolytes in order to identify these different discharge stages and to study the cell chemistry.

1.8. Discharge performance of Leclanché cells.

Relative performances of electrodeposited and chemically prepared manganese dioxides vary according to the discharge regime of the cells. EMDs perform better than CMDs on continuous discharge at heavy drain in both Leclanché [186] and $ZnCl_2$ electrolytes [186-188]. On intermittent discharge, EMDs are better

than CMDs in zinc chloride electrolyte [186] but the performances are equivalent in Leclanché electrolyte [106,186]. However, performances per unit weight of MnO_2 are similar on heavy continuous discharge for both materials in pure zinc chloride [106,188] and in Leclanché electrolyte [186]. On intermittent discharge tests, the performance per unit weight of MnO_2 are similar in $ZnCl_2$ electrolyte [106,186] and better for CMDs than EMDs in Leclanché electrolyte [186]. The discharge performance of cells containing CMD is improved by increasing the electrolyte content of the cell [106,187,188] except for intermittent discharges at low drain [188]. In pure zinc chloride electrolyte, the improved performance of CMDs on intermittent discharge tests is attributed to the fact that discharge with hetaerolite formation does not consume any water or $ZnCl_2$ [106].

Faradiser M and Faradiser WSZ are chemically prepared manganese dioxides which are optimised for Leclanché and zinc chloride cells, respectively [89,120]. The reasons for the different behaviour of EMD and CMDs, especially under continuous heavy discharge, are not clear and have been investigated in this study.

Cells containing either EMD or CMD have been discharged continuously on constant 4 ohm resistance. The possible origin of the different performances has been studied by monitoring the separate contributions of the zinc electrode, the manganese dioxide electrode and the separator region to the overall cell polarisation.

Chapter 2. Experimental

2.1. General

The calibrated laboratory glassware was of the class A type. Analytical reagent grade chemicals (from Merck-BDH) and singly distilled water were used throughout this study.

An analytical balance Stanton type CL41 was used for weighing to the closest 0.1 mg and a balance Sartorius model 1203 MP was used for weighing to the closest 0.1 g.

The experiments requiring a constant temperature were carried out in an air box maintained at (25 ± 0.5)°C by an Accuron type X120 control unit. The voltage and current measurements were made with a Solartron model 7150 digital multimeter from Schlumberger. Electrode potentials were measured against saturated calomel electrodes (SCE) provided by Gallenkamp who also provided the combination pH electrodes used with a Philips PW9420 pH meter calibrated with standard pH solutions from Tacussel.

The electronic equipment included a Tektronix model 2211 digital storage oscilloscope which could be connected to an IBM compatible personal computer for permanent storage of the data.

The X-ray powder diffraction measurements were carried out with a Philips PW 1710 diffractometer using Cu K_α radiation.

2.2. Chemical analyses

Most of the methods used for the analyses were taken or adapted from ref [189].

2.2.1 NH_4Cl concentration

Principle [189, p312]

The samples containing the ammonium chloride were treated by a solution of concentrated NaOH and distilled. The ammonia was expelled with the steam and absorbed in an excess of standard acid. The excess of acid was back titrated in the presence of methyl red. Each mole of acid consumed corresponded to 53.49 g (1 mole) of NH_4Cl.

Reagents

- solution of NaOH approximately 10 molal (about 30 w/w %)
- standard 0.1 M HCl solution (volumetric standard solution from Merck-BDH verified against dried anhydrous Na_2CO_3 in the presence of methyl orange)
- approximately 0.1 M NaOH solution (4 g of NaOH dissolved in 1 litre of H_2O) titrated against the standard HCl solution in the presence of methyl red
- methyl red indicator solution (1 g l^{-1} in water)
- pH indicator paper

Method

The apparatus used for this determination is shown in figure (2.1). All the parts were from the Quickfit range with ground glass connections.

The sample containing about 0.1 g of NH_4Cl in V_s ml was transferred into the three-neck flask containing 2 or 3 anti bumping granules (4 mm glass balls) and diluted to about 200 ml with water. A conical 500 ml flask containing V_1 ml of 0.1 M acid (diluted to about 50 ml with water) was placed as in figure (2.1) with

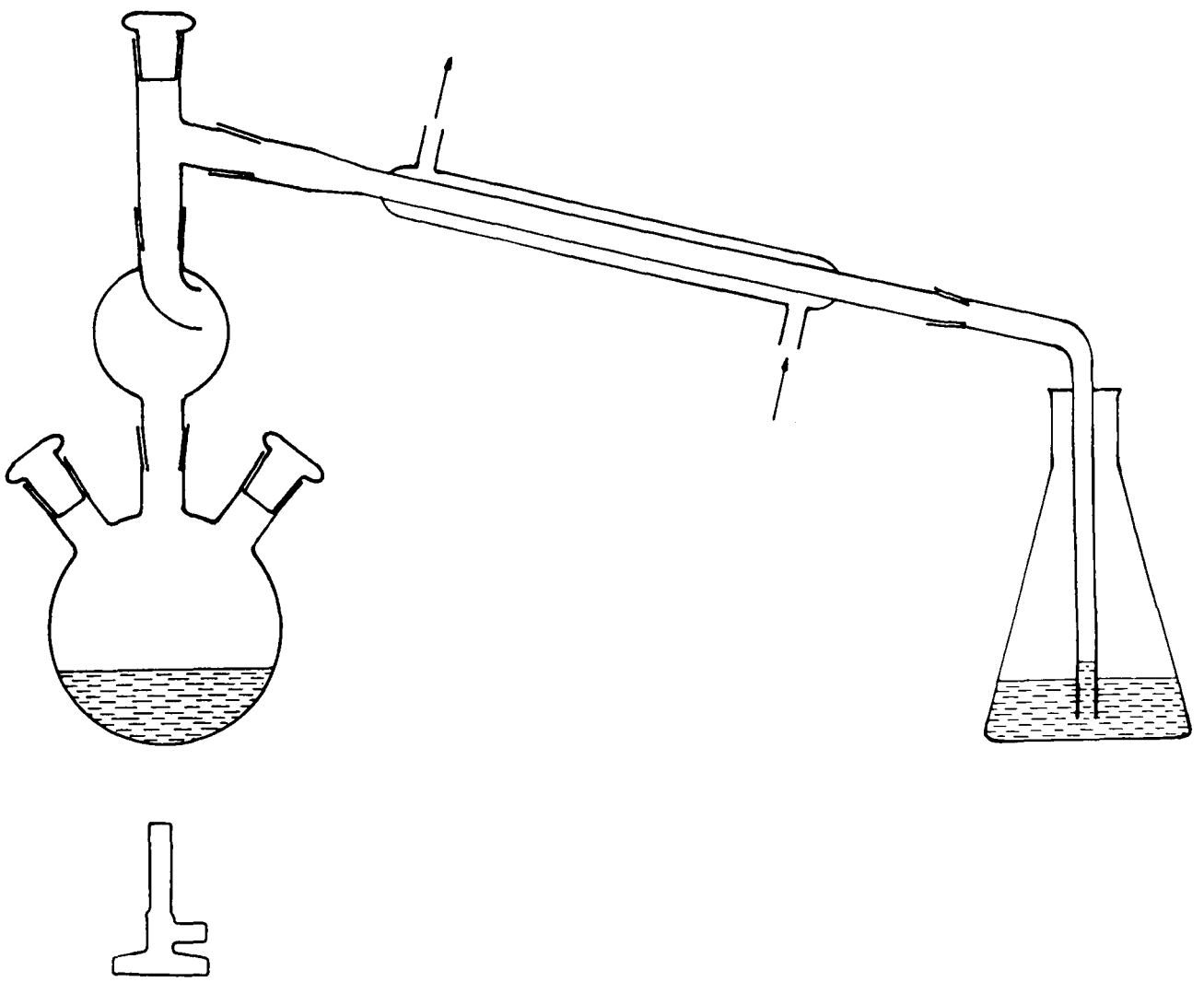

Figure 2.1 : Apparatus for NH_4Cl analysis

the condenser end immersed into the acid solution. About 20 ml of the 10 molal NaOH solution was rapidly poured into the three neck flask which was closed immediately. The distillation was carried out using a Bunsen burner. When about 100 ml of the sample solution had been distilled, the receiving flask was lowered in order that the condenser end was no longer immersed into the acid solution. The distillation was continued with this arrangement until the pH of the distillate (controlled with a pH indicator paper strip) was lower than 7. The condenser was rinsed with distilled water. The rinser was added to the solution which was then back-titrated by the 0.1 M NaOH solution in the presence of methyl red indicator. V_2 ml of NaOH were required to reach the titration end point. This solution had been standardized by titration of 20 ml of the 0.1 M HCl solution in the presence of methyl red indicator. V_3 ml of NaOH were used for this standardisation.

Calculations

- the NaOH concentration f, relative to the HCl concentration was

$$f = 20 / V_3$$

- the NH_4Cl concentration in the sample was

$$C_s = [\ 0.1\ (V_1 - fV_2)] / V_s$$

- for the sample solution made up by dissolving Q g of sample in 1 litre of solution, the NH_4Cl weight percentage was

$$NH_4Cl = (\ 100 \times 53.49 \times C_s\ ) / Q$$

or

$$NH_4Cl = 534.9\ (V_1 - fV_2) / (V_s\ Q)$$

2.2.2 $ZnCl_2$ concentration

Principle [189, p330]

Zinc was titrated by EDTA solution at pH 10 using solochrome black as indicator. When manganese was present, ascorbic acid was added to prevent its oxidation and sodium tartrate to prevent the precipitation of $Mn(OH)_2$. In this case, the sum zinc + manganese was measured. One mole of EDTA reacted with one mole of zinc or manganese ion.

Reagents

- pH 10 buffer (solution containing 70 g NH_4Cl and 560 ml of 35% NH_3 solution per litre of buffer solution)
- 0.1 M EDTA solution (37 g of the sodium salt in 1 litre)
- solochrome black (0.5 g of solochrome black ground with 100 g NaCl)
- standard solution of zinc (an exactly known quantity, about 0.1 mole - Z g, of complexometric standard zinc dissolved in HCl and diluted to 1 litre with

distilled water)

- Ascorbic acid
- Sodium tartrate

Method

The sample (V_s ml) was transferred into a 300 ml conical flask and diluted to about 100 ml with water. About 5 ml of the pH 10 buffer solution and 25 -30 mg of solochrome black indicator were added. The solution was then titrated by the EDTA solution (V_1 ml) until the colour changed from violet to pure blue.

When the sample also contained manganese, about 0.1 g of ascorbic acid and 1-2 g of sodium tartrate were added to the diluted sample and the solution was heated at about 70 °C (to dissolve the sodium tartrate). The titration was then carried out as above. The manganese content of the sample was measured by atomic absorption spectrophotometry (see below). C_{Mn} is the manganese molarity in the sample solution.

The EDTA solution was standardised against the standard zinc solution (V_2 ml of the zinc solution titrated by V_3 ml of the EDTA solution).

Calculations

- the standard zinc solution molarity was

$$C_{Zn} = Z / 136.28$$

- the EDTA molarity was

$$C_{EDTA} = (V_2 C_{Zn}) / V_3$$

- the sample concentration (when no Mn was present) was

$$C_s = (C_{EDTA} V_1) / V_s$$

or (in the presence of Mn)

$$C_s = [(C_{EDTA} V_1) / V_s] - C_{Mn}$$

For the analyzed solution made by dissolving Q g of sample in 1 litre of solution, the $ZnCl_2$ weight percentage was

$$ZnCl_2 = 13628\ C_s / Q$$

2.2.3 Manganese concentration

The samples were diluted with water until their manganese contents fell in the range 0.1 - 3 mg Mn l^{-1} and then they were analyzed by atomic absorption spectrophotometry. The instrument was calibrated using standard manganese solutions made by dilution of 1.000 g Mn l^{-1} Spectrosol solution.

An SP9 Pye Unicam spectrophotometer with an acetylene/air flame and a 10 cm wide burner was used. The wavelength was adjusted to 279.5 nm with a band pass of 0.5 nm. The hollow cathode lamp (from SJ Electronics) current was 10 mA.

2.2.4 Chloride concentration

Principle [189, p337]

Chloride ions were titrated by an $AgNO_3$ solution of known concentration using potassium chromate as indicator (Mohr titration). When acidic, the solution was neutralised by addition of $CaCO_3$.

Reagents

- 0.1 M $AgNO_3$ (17 g $AgNO_3$ in 1 litre of water)
- 0.1 M KCl (7.455 g of KCl dried for 2 hours at 110 °C in 1 litre of water)
- 5 % potassium chromate solution (5 g K_2CrO_4 in 100 ml of water)
- $CaCO_3$

Method

The sample (V_s ml) was transferred into a 300 ml conical flask and diluted to 100 ml with water. 1 ml of potassium chromate solution was added and the sample titrated with the $AgNO_3$ solution (V_1 ml). In the case of an acidic sample, about 1 g of $CaCO_3$ was added to the solution before the addition of the indicator solution.

The $AgNO_3$ was standardised against the 0.1 M KCl solution or against 0.1 M HCl solution as used for the NH_4Cl determination.

Calculations

- $AgNO_3$ concentration C_{Ag}

  V_2 ml of the 0.1 M Cl^- solution were titrated by V_3 ml of the $AgNO_3$ solution, thus its concentration in mol l^{-1} was

  $$C_{Ag} = 0.1\ V_2 / V_3$$

- the chloride concentration C_s (in mol l^{-1}) in the sample was

  $$C_s = C_{Ag}\ V_1 / V_s$$

2.2.5 Analysis of manganese dioxide

These analyses were performed according to the method of Vetter and Jaeger [190].

Principle

The samples were reductively dissolved in an excess of $FeSO_4$ according to the reaction

$$MnOOH_r + (4-r)H^+ + (2-r)Fe^{2+} \longrightarrow Mn^{2+} + (2-r)Fe^{3+} + 2H_2O \qquad (2.1)$$

The excess of ferrous sulphate was potentiometrically back-titrated by $KMnO_4$ according to the reaction

$$MnO_4^- + 8H^+ + 5Fe^{2+} \longrightarrow Mn^{2+} + 5Fe^{3+} + 4H_2O \qquad (2.2)$$

The manganese contents of the samples were measured by $KMnO_4$ titration in sodium pyrophosphate solution according to the reaction

$$4Mn^{2+} + MnO_4^- + 8H^+ + 15H_2P_2O_7^{2-} \longrightarrow 5Mn(H_2P_2O_7)_3^{3-} + 4H_2O \qquad (2.3)$$

The degree of oxidation was calculated from the amount of ferrous sulphate consumed by reaction (2.1) and from the manganese content of the sample given by reaction (2.3).

Reagents

- approximately 0.1 M acidic ferrous sulphate solution (40 g of $FeSO_4.(NH_4)_2SO_4.6H_2O$ + 20 ml concentrated H_2SO_4 in 1 litre of solution)
- approximately 0.02 M $KMnO_4$ in water (3.3 g $KMnO_4$ in 1 litre of solution)
- standard solution of $Na_2C_2O_4$ approximately 0.05 M (an exactly known quantity, about 6.7 g, N g - of $Na_2C_2O_4$ dried at 110 °C for 2 hours in 1 litre)
- $Na_4P_2O_7.10H_2O$
- concentrated H_2SO_4

Method

The sample (about 0.16 g) was transferred into a 250 ml beaker. The acidic ferrous sulphate solution (25 to 40 ml depending on the oxidation state of the sample) was added, the solution was diluted to 50 ml with water and the dissolution carried out with a magnetic stirrer (15 to 40 minutes depending on the nature of the material - electrolytic or chemical manganese dioxide - and on the

value of the ferrous sulphate excess). A platinum electrode and a saturated KCl calomel reference electrode (SCE) were then placed into the solution and the excess ferrous sulphate potentiometrically titrated by the $KMnO_4$ solution using the digital multimeter to monitor the Pt electrode potential. The $KMnO_4$ solution volume at the equivalence point (about +0.9 V versus the SCE) was recorded as V_1 ml.

The pH of the solution was then adjusted to 6.5 - 7.5 by addition of sodium pyrophosphate and the second titration by $KMnO_4$ was carried out potentiometrically. The permanganate solution volume at the end of this titration was recorded as V_2 ml.

The $KMnO_4$ concentration relative to the $FeSO_4$ concentration was measured by potentiometric titration of the same volume of $FeSO_4$ as used for the dissolution of the manganese dioxide. The volume of $KMnO_4$ corresponding to the end point was recorded as V_0 ml.

When the manganese content of the sample was also required, the $KMnO_4$ solution was standardised against the $Na_2C_2O_4$ solution. 20 ml (V_N ml) of this solution were transferred into a 300 ml conical flask, diluted to 100 ml and acidified by addition 5 ml of concentrated H_2SO_4. The solution was heated to 70-80 °C and titrated by the $KMnO_4$ solution (V_3 ml) until a pink coloration persisted. In this case, it was also necessary to know the exact amount - Q g - of sample used for the analysis.

The reaction with sodium oxalate was

$$2MnO_4^- + 5C_2O_4^{2-} + 16H^+ \longrightarrow 2Mn^{2+} + 5CO_2 + 8H_2O \qquad (2.4)$$

Calculations

- the concentration of the $Na_2C_2O_4$ solution was

$C_N = N / 134.0$ in mol l^{-1}

- the concentration of the $KMnO_4$ solution was

$$C_K = 2/5\ (\ V_N\ C_N\ /\ V_3\ )\ \text{ in mol } l^{-1}$$

- the amount of $FeSO_4$ consumed during the sample dissolution corresponded to $(V_0 - V_1)$ ml of $KMnO_4$ or (introducing the stoichiometry of equation 2.2) $5C_K(V_0-V_1)\ 10^{-3}$ moles of $FeSO_4$ consumed.

During the second titration, the sum of the manganese from the sample and from the first titration was measured. From the stoichiometry of reaction (2.3), the volume of $KMnO_4$ corresponding to the manganese content of the sample was therefore $(V_2 - V_1/4)$ ml or $4C_K\ (V_2 - V_1/4)\ 10^{-3}$ moles of Mn in the sample. From equation (2.1), each mole $MnOOH_r$ dissolved by consuming (2-r) moles $FeSO_4$ produced 1 mole Mn^{2+}, therefore

$$2 - r = \frac{5\ C_K\ (V_0 - V_1)\ 10^{-3}}{4\ C_K\ (V_2 - \frac{V_1}{4})\ 10^{-3}} \qquad (2.5)$$

and

$$r = 2 - \frac{5\ (V_0 - V_1)}{4\ V_2 - V_1} \qquad (2.6)$$

The knowledge of the $KMnO_4$ concentration was thus unnecessary for the calculation of the oxidation degree of the samples.

- the total manganese content (in w/w % Mn) of the sample was

$$Mn = 54.94 \text{ x } 4\ C_K(V_2-V_1/4)\ 10^{-3} \text{ x } 100/Q$$

or $$Mn = (21.976/Q)\ C_K(V_2-V_1/4)$$

2.3. The Leclanché electrolyte study

2.3.1 The density of the electrolyte

The density of the electrolyte solutions were measured at 25 °C in 25 ml density bottles calibrated with distilled water.

Preparation of the solutions

A stock solution of concentrated (about 70 w/w %) $ZnCl_2$ was prepared by dissolving the anhydrous salt in water. The zinc content was analyzed (section 2.2.2).

Dilute solutions (5, 10, 15, ..., 65, 70 w/w %) of pure $ZnCl_2$ were prepared by weighing various amounts of the stock solution and water in tared 50 ml conical flasks fitted with rubber stoppers. After overnight equilibration at 25 °C, the densities of these solutions were measured. The solutions were poured back into their respective flask which were weighed again.

Pure NH_4Cl (less than 0.1 w/w % water as measured by weight loss after 2 hours at 110 °C) was added into each flask. The quantities added were measured by weight difference of the solutions flasks. After dissolution, the samples were returned to the temperature controlled air box and their densities were measured after overnight equilibration. This procedure was repeated until the solutions were saturated.

Various solutions (5, 10, ..., 25, 28.5 w/w %) of NH_4Cl in water were also prepared by careful weighing of NH_4Cl and water and their densities measured.

For the pure $ZnCl_2$ or NH_4Cl solutions, the solution concentrations C_0 were given by

$$C_0 = C_s \frac{(W_0 - W_w)}{(W_0 - W_t)} \qquad (2.7)$$

where C_s is the stock solution concentration and W_0, W_w and W_t are the masses of the flask containing the water and the solute ($ZnCl_2$ or NH_4Cl), the water only,

and of the empty flask respectively. C_0 and C_s are in w/w % (g of solute in 100 g of solution).

In the case of the $ZnCl_2$ + NH_4Cl solutions, the NH_4Cl contents subsequent to the first NH_4Cl addition were

$$C_{N\,i} = \frac{C_{N\,i-1}\,(W_{i-1} - W_t) + 100\,(W_i - W_{i-1})}{100\,(W_i - W_t)} \qquad (2.8)$$

where $C_{N\,i}$ and $C_{N\,i-1}$ are the NH_4Cl concentrations and W_i and W_{i-1} are the masses of the flask after and before the ammonium chloride addition respectively. In equation (2.8), the first term in the numerator is the NH_4Cl content of the flask before the addition. The $ZnCl_2$ content was

$$C_{Z\,i} = C_{Z\,0}\,(1 - \frac{C_{N\,i}}{100}) \qquad (2.9)$$

where $C_{Z\,0}$ and $C_{Z\,i}$ are the $ZnCl_2$ contents in the binary solution and in the solution after the NH_4Cl had been added respectively.

Bottle calibration

The empty density bottles were weighed (to the closest 0.1 mg), equilibrated at 25 °C in the air box (more than 3 hours), filled with distilled water (stored at 25 °C), dried with absorbent paper and weighed again.

The volume V of the bottle was given by

$$V = \frac{W_f - W_e}{D_w} \qquad (2.10)$$

where W_e and W_f are the masses of the bottle empty and filled with distilled water respectively and D_w is the water density (0.99705 g ml^{-1} [191]).

This procedure was repeated 3 times and the average volumes were used in the subsequent calculations.

Density measurements

After overnight equilibration in the air box, the calibrated density bottles were filled with the solutions, dried with absorbent paper and weighed. Subsequently, the solutions were poured back into their respective flasks while the bottles were washed with water, rinsed with acetone, dried with compressed air and replaced into the air box.

The solution densities D_s were calculated by

$$D_s = \frac{W_f - W_e}{V} \qquad (2.11)$$

2.3.2 The Leclanché electrolyte chemistry

This chemistry was investigated by adding ZnO to $ZnCl_2$ + NH_4Cl solutions and measuring either the solution pH or the potential of a zinc electrode immersed in these solutions.

Preparation of the solutions

The solutions were prepared as for the density measurements by dilution of a concentrated $ZnCl_2$ stock solution. This solution was analyzed for its zinc and chloride contents (sections 2.2.2 and 2.2.4) to determine its initial ZnO concentration by considering that the analytical grade zinc chloride was in fact a mixture of $ZnCl_2$ and ZnO [40]. Binary solutions were prepared by mixing weighed amounts of the $ZnCl_2$ stock solution, water and solid NH_4Cl. The solutions compositions were calculated by equation (2.8) with $C_{Ni-1} = 0$, and equation (2.9).

For the study of the NH_4Cl influence on the zinc electrode potential, stoichiometric $ZnCl_2$ was prepared by adding to the stock solution an amount of concentrated HCl (titrated against a standard NaOH solution) calculated to

neutralize the ZnO initially present [193]. Such a stoichiometric solution did not form any precipitate on dilution [40].

Influence of ZnO on the zinc electrode potential

The experimental set-up used for these experiments is shown figure (2.2).

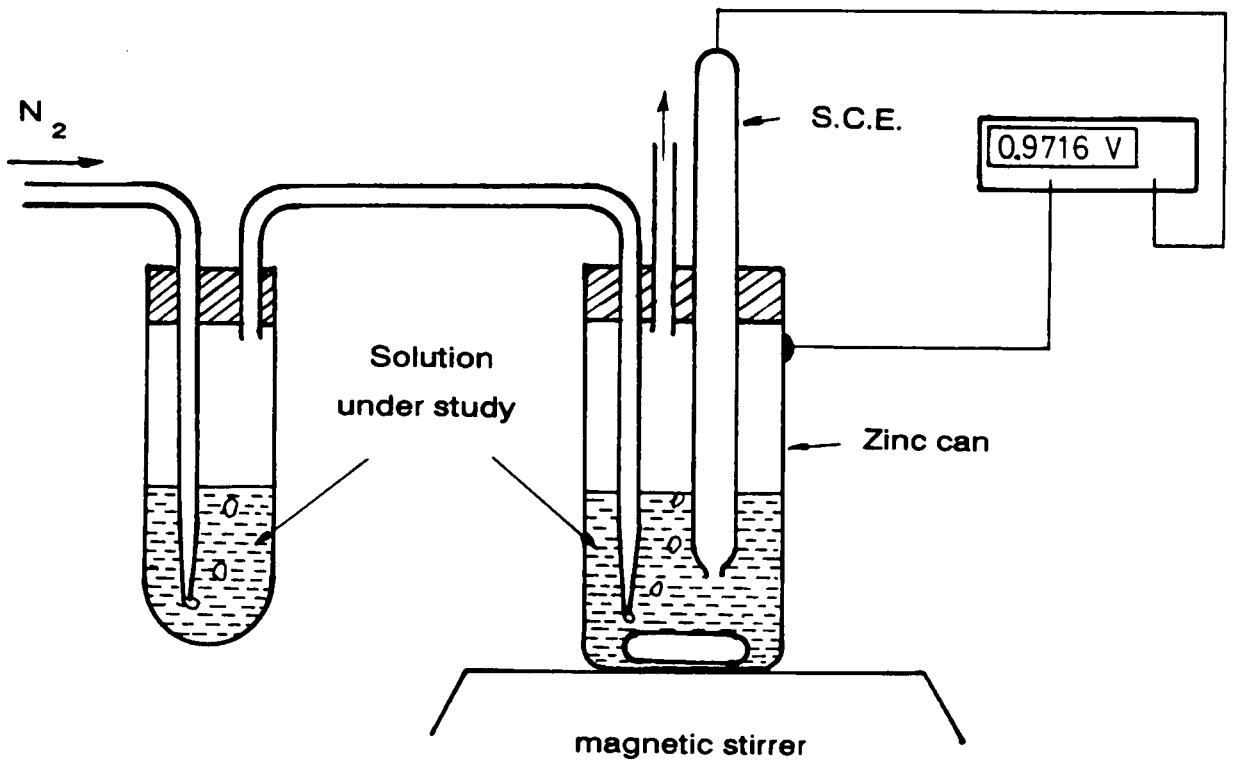

Figure 2.2 : Experimental set up for the zinc potential measurements

This apparatus was kept at 25 °C in the temperature-controlled air box. The zinc cans used in this work were standard R20 cell cans amalgamated [55,192] by overnight contact with a solution containing 35 mg $HgCl_2$ (giving about 0.5 mg Hg cm^{-2}). After the residual solution was discarded, the cans were rinsed with acetone and dried by compressed air. They were stored in plastic bags filled with nitrogen.

After equilibration at 25 °C (minimum 8 hours), the solutions were deoxygenated by nitrogen bubbling (oxygen-free nitrogen from BOC) for about half an hour (in the left hand side flask in figure 2.2). Part of it (about 15 g) was transferred to the zinc can and accurately measured by weight difference of the can, another portion being kept for subsequent pH experiments. An aliquot

of this solution was also taken for the determination of its total zinc ($ZnCl_2$ + ZnO) and NH_4Cl contents (sections 2.2.2 and 2.2.1). By taking the sample for analysis after the deoxygenation, any possible change in concentration of the solution due to the nitrogen bubbling was taken into account. The reference electrode was positioned and the potential of the zinc electrode in the starting solution was recorded.

Small quantities of ZnO (50 to 100 mg, weighed by difference from a small glass tube containing the ZnO, before and following the addition) were added to the solution at chosen intervals and the zinc potential was recorded. The ZnO was either added to the solution at regular intervals (3, 5 or 10 minutes) or after the potential had reached a stable value (less than 0.05 mV shift min^{-1}).
The added ZnO was calculated for 100 g of the starting solution.

pH titrations by ZnO

For these titrations, the zinc can (in figure 2.2) was replaced by an 18 ml flat bottom glass tube and the calomel electrode by a pH electrode. No nitrogen bubbling was used. ZnO was added by portions increasing from about 2 mg (at the beginning of the titration) to about 100 mg (towards the end of the experiment) to the solution (10 - 12 g) using the same procedure as in the previous section. The additions were performed after the solution pH had reached a stable value (less than 0.01 pH unit shift in 2 minutes). The portions of solution set aside before the zinc potential experiments described in the previous section, were examined by this procedure.

During one experiment carried out on a $ZnCl_2$ solution containing a large excess of NH_4Cl, the pH and the zinc electrode potential were measured simultaneously while ZnO was added to the mixture.

Effect of NH_4Cl on the zinc electrode potential.

The stoichiometric $ZnCl_2$ stock solution was diluted to prepare pure zinc chloride solutions in the range 3-70 w/w %.

The set-up was the same as for the study of the ZnO influence on the zinc electrode potential (fig. 2.2). The procedure was also identical except for the replacement of ZnO by NH_4Cl additions. The zinc concentration in the starting solution was measured by analysis of an aliquot of the solution poured into the zinc can (section 2.2.2).

Following the first addition, a total NH_4Cl quantity $Q_{N\,i}$ had been introduced into a zinc can which had contained initially Q_s g of starting solution. The NH_4Cl concentration in the ternary solution $C_{N\,i}$ (in w/w %) was

$$C_{N\,i} = \frac{100\ Q_{N\,i}}{Q_{N\,i} + Q_s} \qquad (2.12)$$

The NH_4Cl additions were continued until a break was found in the zinc potential - NH_4Cl concentration curve or until a permanent solid phase was formed in the solution.

To complement the results of these experiments, 6 samples were prepared by saturating stoichiometric $ZnCl_2$ solutions with an excess of NH_4Cl (the estimated values of the NH_4Cl solubilities were taken from the work of Meerburg [58]). All the added NH_4Cl was dissolved by heating the solutions at about 70 °C. The samples were then allowed to equilibrate at 25 °C for 2 weeks. They were deoxygenated by nitrogen bubbling for half an hour and part of the mixture (containing some solid particles) poured into an amalgamated zinc can for potential measurement (as in fig. 2.2). The solid particles were allowed to settle into the can and a portion of the supernatant taken for analysis ($ZnCl_2$ and NH_4Cl).

The part of the saturated mixtures not used for the potential measurement was filtered (filter paper) and the solid washed with methanol and dried at 50 °C for

about 1 hour. They were analyzed chemically for ammonium, zinc and chloride (see section 2) and by X-ray diffraction to identify the nature of the solid phase.

2.4. Intermittent discharges

2.4.1 Description of the cells

The cells (schematically represented in figure 2.3) were of the paper lined type and were prepared by SEDEMA in their research laboratory.

Two chemical manganese dioxides (Faradiser M and Faradiser WSZ from SEDEMA) and an electrolytic manganese dioxide (EMD, produced in Ireland by Mitsui) were used with either NH_4Cl-$ZnCl_2$ or pure $ZnCl_2$ electrolyte.

The content of the cells are given in tables (2.1) for the mixed electrolyte and (2.2) for pure $ZnCl_2$ electrolyte. The ratio MnO_2/acetylene black was 10.7 and 5.0 in Leclanché and zinc chloride cells, respectively. The volume of the manganese dioxide electrode was the same for all the cells.

The electrolyte compositions are given in table (2.3).

The main characteristics of the manganese dioxides are summarized in table (2.4) [194,195].

The carbon black was Knapsack UV acetylene black, the separator was a typical Leclanché cell separator (starch-coated paper) and the zinc cans made of 0.24 % Pb, 0.054 % Cd [47] zinc alloy. The alloy composition was determined by atomic absorption spectrophotometry.

Table 2.1 Composition of the cells - Leclanché electrolyte

Quantities, in g	Faradiser M	EMD
Manganese dioxide	31.00	36.04
Carbon black	2.89	3.36
ZnO	0.51	0.59
NH_4Cl	7.73	8.07
$ZnCl_2$	2.71	2.33
$HgCl_2$	0.03	0.02
H_2O	11.13	9.58

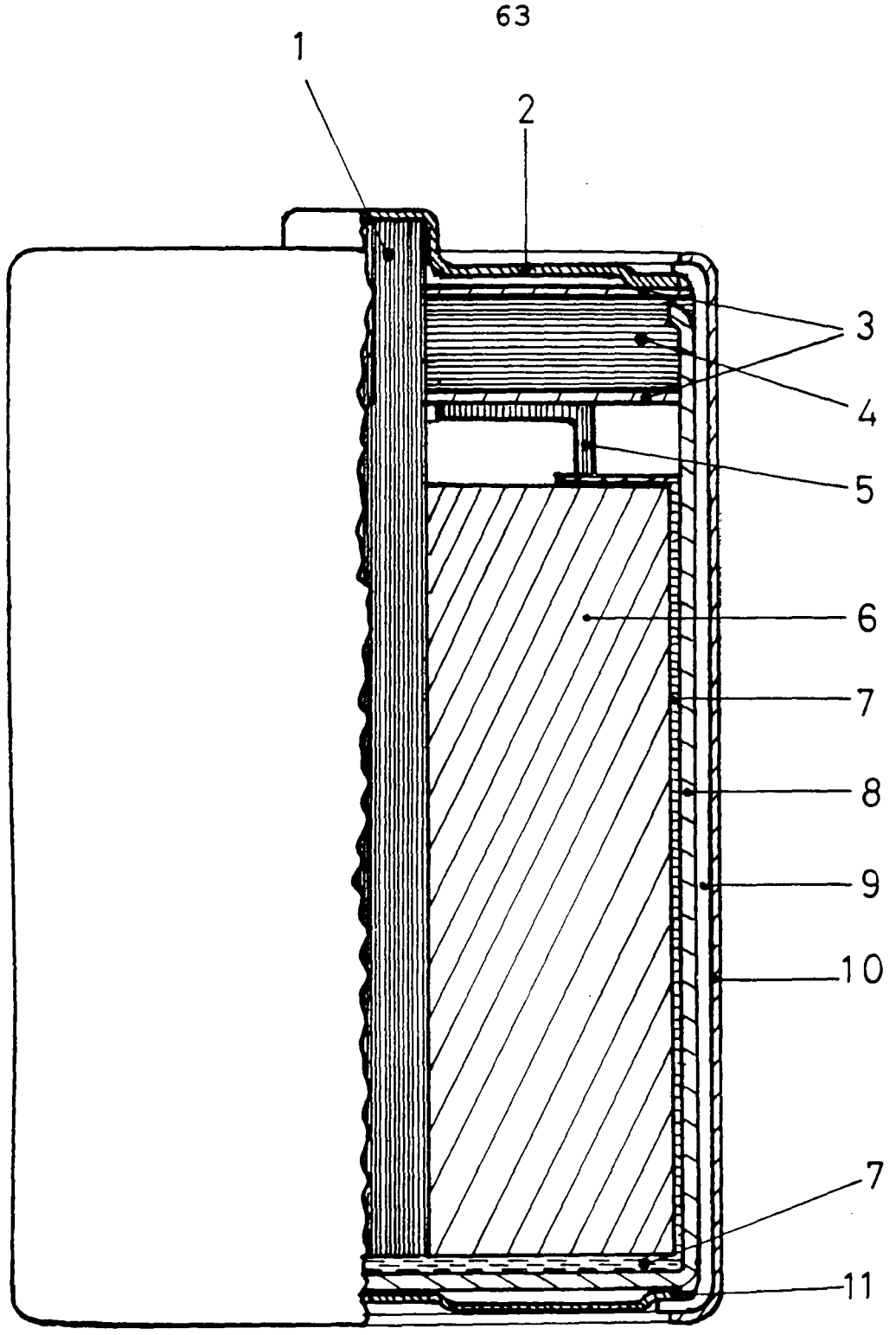

Figure 2.3 : R20 cell. (1) carbon rod, (2) metal top cap, (3) cardboard disks, (4) bitumen seal, (5) plastic spacer, (6) electrode mix, (7) separator, (8) zinc can, (9) cardboard container, (10) metal jacket, (11) metal plate

Table 2.2 Composition of the cells - $ZnCl_2$ electrolyte

Quantities, in g	EMD	Far.M	Far.WSZ-1	Far.WSZ-2
Manganese dioxide	24.84	21.79	23.45	23.45
Carbon black	4.95	4.34	4.67	4.67
ZnO	0.39	0.34	0.37	0.37
$ZnCl_2$	6.14	6.47	6.06	6.33
$HgCl_2$	0.02	0.02	0.02	0.02
H_2O	16.66	17.54	16.43	17.16

The cells labelled Far.WSZ-1 and Far.WSZ-2 were prepared in parallel but 1 ml of electrolyte was added into the zinc cans of the latter series before inserting the positive electrode mass.

Table 2.3 Electrolyte composition

Concentrations / w/w %	Leclanché	$ZnCl_2$
NH_4Cl	18.0	0.0
$ZnCl_2$	16.0	26.92
$HgCl_2$	0.16	0.08
H_2O	65.84	73.0

Table 2.4 Main characteristics of the manganese dioxides

	EMD	Far.M	Far.WSZ
O/Mn ratio [47]	1.952	1.948	1.948
MnO_x / % [47]	94.4	95.3	95.7
H_2O at 110 °C / %	1.5	3.5	2.5
Tap density / gml^{-1}	2.38	1.79	1.70
Specific surface area / m^2g^{-1}	38	95	65

The set-up used for the intermittent discharges is given schematically in figure (2.4).

2.4.2 The load

The discharge regime was chosen in order to be not too time consuming (low resistance load) with the requirement that the recovery could be considered as completed at the end of the rest period. Discharges on 4Ω satisfy these conditions for on-load times up to 2 hours a day [13].

The load was made by connecting in parallel four 16 ohm resistors (0.5 W from RS components), R, and one 1 kΩ adjustable resistor, P. The total load on discharge was constituted by the serial connection of this group of resistors with the necessary leads. The resistance of the ensemble was adjusted to 4.00 Ω using the set-up given in figure (2.5).

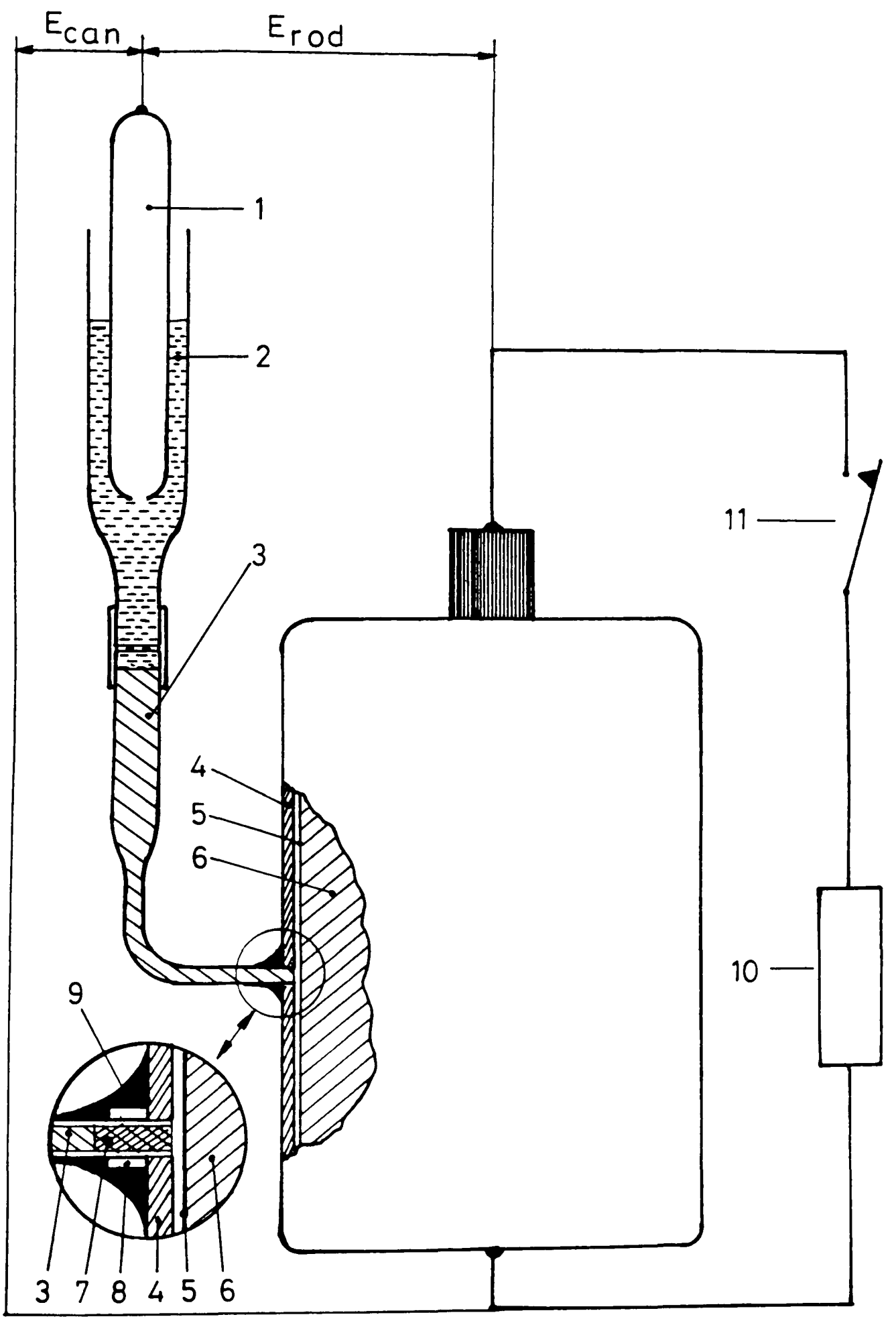

Figure 2.4 : Set-up for intermittent discharge. (1) SCE, (2) saturated KCl, (3) gelled KCl, (4) zinc can, (5) separator, (6) electrode mix, (7) porous plug, (8) shrinkable tube, (9) glue, (10) load, (11) switch.

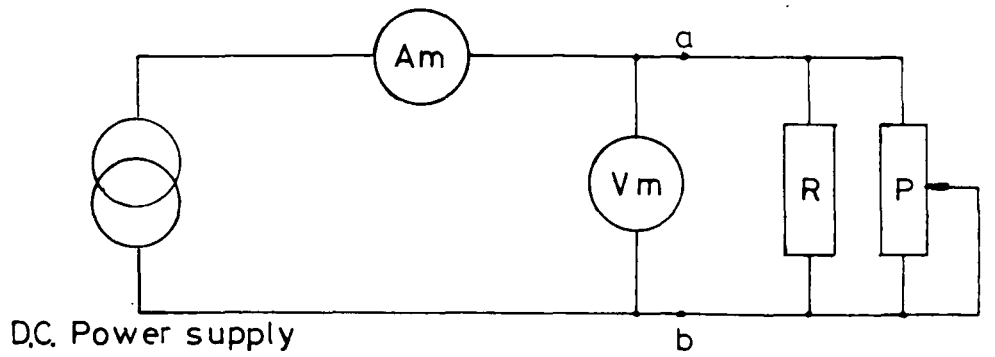

Figure 2.5 : Adjustment of the load to a given resistance. (a) and (b) are the connection points to the cell.

2.4.3 Preparation of the cells

The salt bridges

Glass Pasteur pipettes were bent as in figure (2.4). The capillary end of the bent pipettes were cut where their diameter was about 1.8 - 1.9 mm and a small piece (2-3 mm long) of shrinkable plastic tubing (from RS components) was placed around it and fixed in position by heating (in the flame of a gas lighter). The tip of each pipette was then ground (wet abrasive paper, 3M grade P600) until the exposed part corresponded to the thickness of the zinc cans (see fig 2.4). A small plug of quartz wool was then inserted and pushed to the tip by compressed air.

Saturated KCl (the supernatant of a 4 M solution) was gelled by boiling with 1% agar and used to fill the bent pipettes by sucking in the molten gel until the solution exuded through the quartz plug. These gelled KCl salt bridges were stored in saturated KCl solution.

Cell assembly

After the metal jacket had been removed, the cardboard container was cut at about 1 cm from the metal cover and discarded. This operation uncovered a 2 mm diameter hole that had been drilled into the zinc can, before cell manufacture,

at about 2 cm from the bottom. A piece of adhesive tape sealing the hole was removed. The load (with the switch open) was soldered to the cell. A drop of the same electrolyte as in the cell (squeezed out of another cell of the same type as described below) was poured into the hole and the capillary end of the salt bridge glued to the cell with epoxy resin. Care was taken to avoid any air bubbles at the join between the salt bridge and the cell. The whole system, clamped on a stand was transferred into the temperature-controlled air box. The cell assembly was made at least 12 hours before the first discharge.

2.4.4 Discharge procedure

The cells were discharged through a 4 ohm load for 30 (or exceptionally 15 or 60) minutes a day, five days a week.

The potential of the zinc electrode and of the manganese dioxide electrode were measured on open circuit just before the beginning of a discharge period. During the discharge, potentials were measured every minute for the first 10 minutes and then every two minutes until the end of the discharge period. The cells were then allowed to recover until the next discharge. The test was started every day at the same time in order to have a 24 hour 'discharge + recovery' cycle. The test was terminated when the on-load cell voltage reached 0.9 V. In one case, a discharge started at the '30 minutes a day' regime was continued on a '15 minutes a day' regime after the cell on-load voltage had reached the 0.9 V cut-off value for a first time.

The open circuit potentials were measured again one day after the last discharge period.

Calculations

At any moment, the cell voltage E_c was

$$E_c = E_{Mn} - E_{Zn} \tag{2.13}$$

where E_{Mn} and E_{Zn} are the manganese dioxide electrode and the zinc electrode potentials respectively, both potentials being expressed with respect to the saturated KCl calomel reference electrode.

If at the beginning of a discharge period the cell had delivered (during the previous discharges) a current quantity $Q_{0\,i}$, at a time t_j during the discharge on a load R (Ω) the current $Q_{t\,i}$ delivered by the cell was calculated by

$$Q_{t\,i} = Q_{0\,i} + \sum_{n=1}^{j} 60\ (t_j - t_{j-1})\ \frac{E_j + E_{j-1}}{2\ R} \tag{2.14}$$

where the times are in minutes, the cell voltages in volts (V) and the current delivered in coulombs (C).

2.4.5 Electrolyte analyses

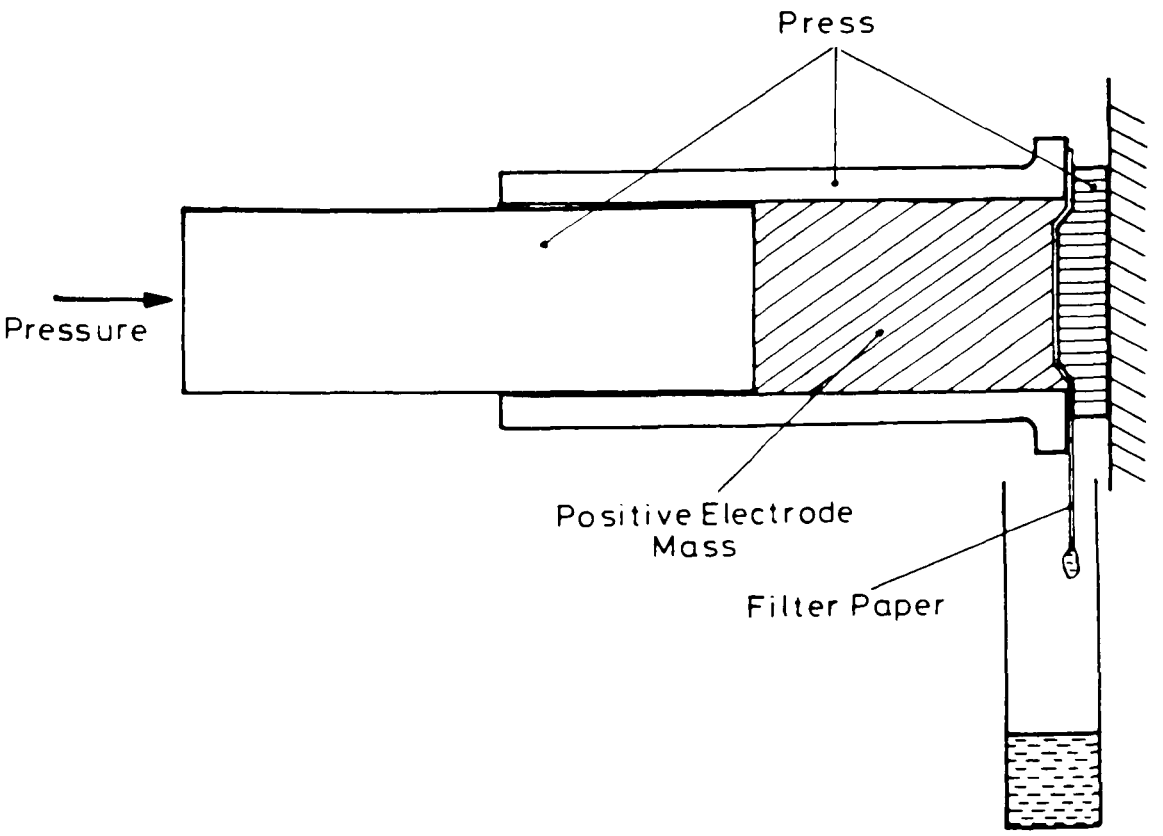

Figure 2.6 : Extraction of the electrolyte out of the positive electrode mass.

The electrolyte was extracted from the manganese dioxide electrode mass using a procedure developed by Maskell *et al.* [110]. After opening of the cell, the positive electrode mix was transferred into the press schematically shown in figure (2.6). The system was compressed with a vice and the electrolyte collected in a tared glass tube.

After weighing of the tube, the electrolyte pH was measured. The electrolyte was acidified by 2-3 drops of concentrated HNO_3 to avoid precipitation of zinc compounds and filtered on a tared dry sintered glass crucible (pore aperture 10-16 µm). The crucible was dried for 1 hour at 110 °C and weighed. The electrolyte weight was corrected for the quantity of deposit (carbon black and manganese oxide particles). The filtrate was quantitatively transferred into a 250 ml calibrated flask and analyzed for zinc, manganese and, in the case of $ZnCl_2$-NH_4Cl electrolyte for NH_4Cl (see section 2.2).

2.5. Continuous discharges

2.5.1 Experiments with zinc probes

Probe preparation

Pieces, 6 cm long, were cut from 1mm diameter high purity zinc wire (99.99+ % from Goodfellow). They were coated with a thin layer of epoxy resin and covered with 5 cm of 1.6 mm internal diameter shrinkable tube (from RS components). The tube was shrunk and the epoxy resin was hardened by placing them in an oven at 130 °C for 10 - 15 minutes. Another short piece of shrinkable tube was placed on the protected zinc wire (fig. 2.7) and shrunk in the flame of a gas lighter. The end of the probe was then ground in a way similar to that described for the salt

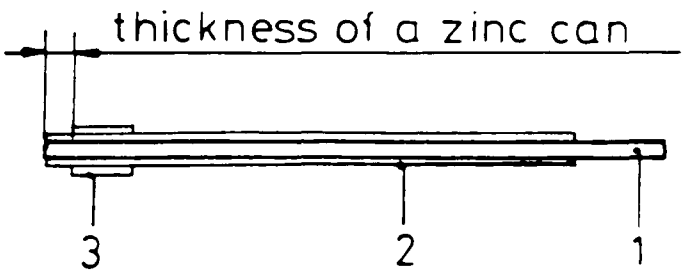

Figure 2.7 : Zinc probe.
(1) zinc wire, (2) and (3) shrinkable tubes.

bridges (section 2.4.3) until a length of probe corresponding to the thickness of the zinc cans could be inserted into a 2 mm diameter hole.

For one experiment, two probes were sheathed with thicker shrinkable tube (from RS components) to give them an external diameter of 3.4 mm instead of the usual 1.8 mm. In this case 3.5 mm holes were drilled into the zinc can.

The probes were amalgamated by immersion in a 10 g l^{-1} $HgCl_2$ solution for about 10 - 15 seconds, the drop of solution remaining on the probe was discarded by shaking and the sheath was dried with absorbent paper. The amalgamation was done just before the cell assembly.

Cell assembly

The metal jacket and the cardboard container were removed as in section 2.4.3. If the holes necessary for the salt bridge (all the potentials were measured against a saturated KCl reference electrode connected to the electrolyte through the zinc electrode) and for the probe insertion had not been drilled into the can before the cell manufacture, or if they were of a too small diameter, the holes were drilled (or enlarged) using a slot drill. In this case, the zinc can was slightly distorted and most times, a small zinc disk formed during the drilling had to be left in the cell. In a typical experiment, 3 probes were used. A fourth hole was necessary for the salt bridge. They were regularly spaced around the can on a circle at about 2 cm from the bottom.

The probes and the salt bridge were carefully glued (epoxy resin) onto the cell as described in section 2.4.3, the battery was connected to the load (switch open) and the whole set-up (fig. 2.8) transferred into the air box. The cell was allowed to equilibrate overnight before discharge.

Discharge procedure

After overnight equilibration, the potential (against the reference electrode) of at least one of the probes was very different from the negative electrode (zinc

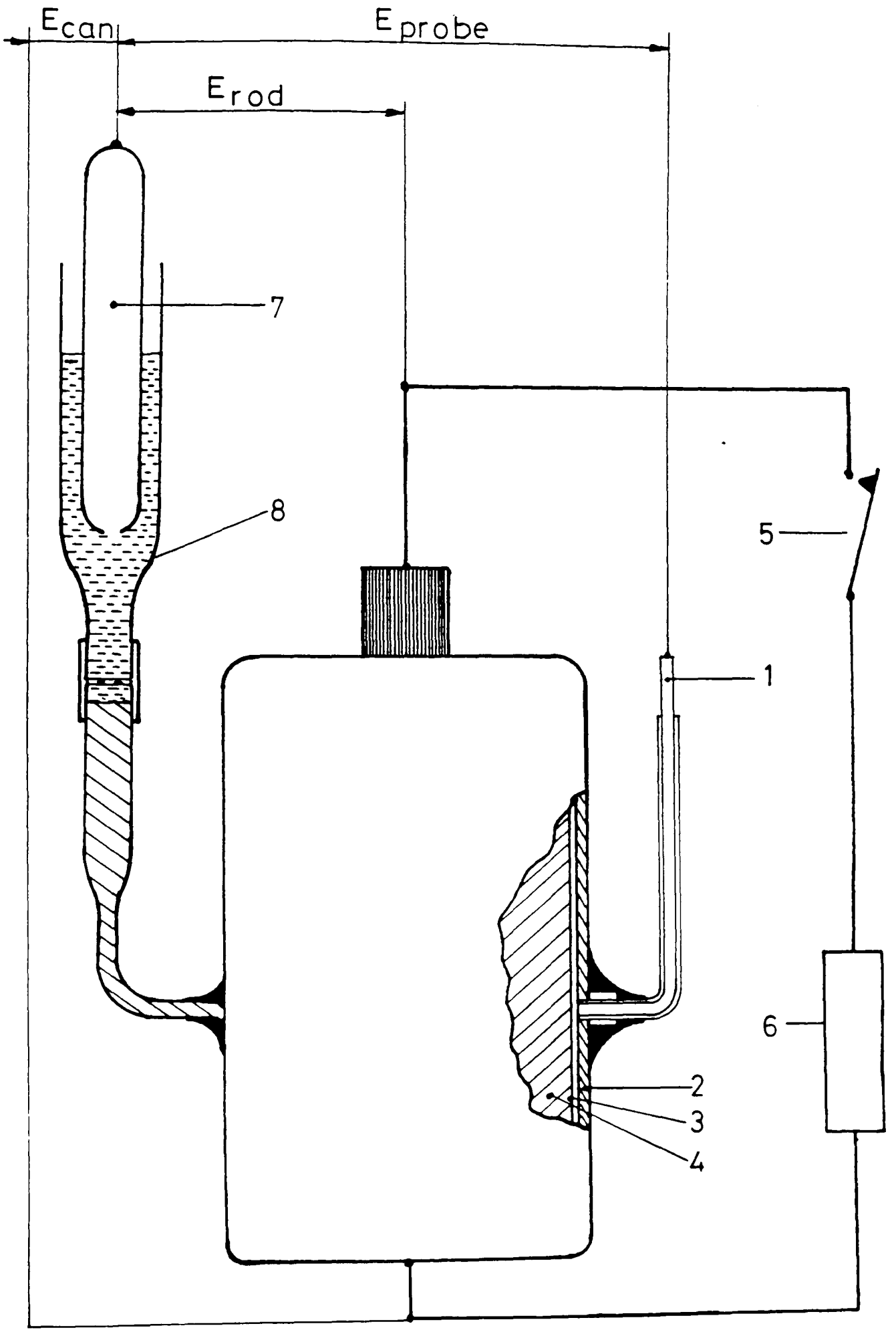

Figure 2.8 : Set-up for discharge using zinc probes. (1) zinc probe, (2) zinc can, (3) separator, (4) MnO_2 electrode, (5) switch, (6) load, (7) reference electrode, (8) salt bridge.

can) potential. A difference of more than 100 mV was not exceptional. It was found that after a first continuous discharge of the cell (for one hour) and overnight recuperation, the probes had almost the same potential as the zinc can. Therefore, each cell was discharged twice (on constant 4 ohms load). The first continuous discharge lasted for one hour and the second discharge (after overnight recovery) was carried out down to a close circuit voltage of 0.9 V. The different potentials with respect to the calomel electrode (manganese dioxide electrode, zinc electrode and probe potentials) were measured at regular intervals. The current delivered by the cells was calculated as for intermittent discharge by equation (2.14).

The electrolyte analysis was carried out as described in section 2.4.5.

2.5.2 Carbon probes inserted in the positive electrode

Cell preparation

The metal jacket was cut at about 5 mm from the top cap; the metal cap and the upper part of the jacket were removed. The cardboard disk covering the bitumen seal was also discarded. The top of the zinc can is curved inwards during the cell manufacture (see fig. 2.3) and this could cause a short circuit of the cell if this part of the can came into contact with the outermost carbon probe. To avoid the problem, the edge of the can was straightened in the region where it might come in contact with the probe. A template (fig. 2.9) was positioned on the cell and three holes (2.4 mm or 3/32") drilled through the bitumen seal and the plastic spacer down to the positive electrode top surface. Without moving the template, three carbon probes (3/32" carbon rods provided by Dr. Barnard of British Ever Ready) were inserted into the mix . They were pushed down with a drill bit, until the distance between their tops and the can bottom was 6.5 cm (contact length with the mix about 2.5 cm). The template was then carefully removed. Molten bitumen was poured around each probe (with special care for the probe close to the can) to restore the good seal. A brass cap was placed with pressure on the top of the central carbon rod and the connections to the load soldered to the cell. A salt bridge was glued to the cell as described in section 2.4.3.

The cell with inserted probes is shown schematically in figure (2.10).

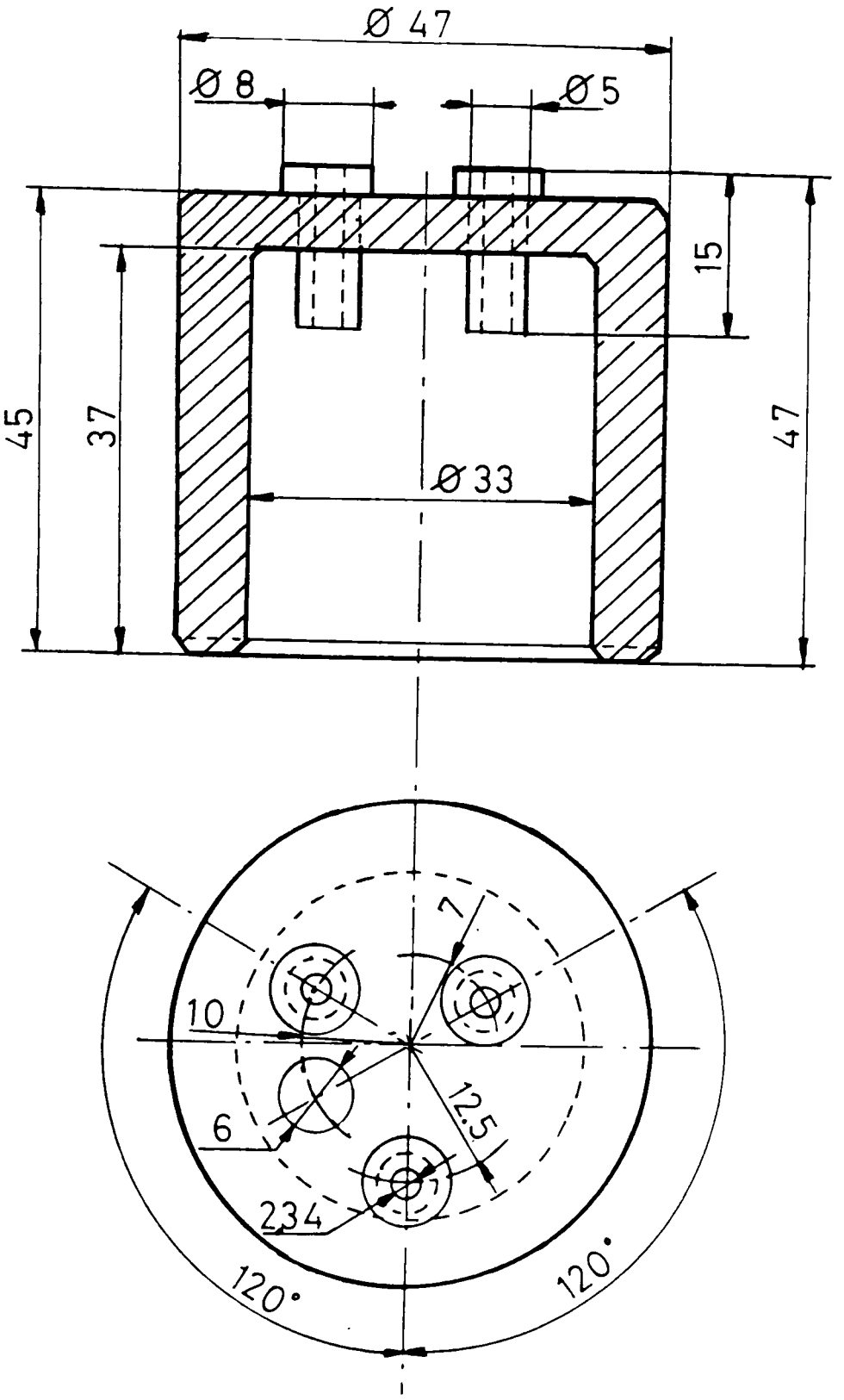

Figure 2.9 : Template used for carbon probe insertion.

2.5.3 Salt bridges inserted in the positive electrode

The salt bridges

Glass pasteur pipettes with a quartz wool plug pushed into the tip were filled with the molten gelled KCl as described in section 2.4.3. They were stored in saturated KCl solution. When used, they were connected to an adaptor (with a piece of rubber tube) to accommodate the reference electrode.

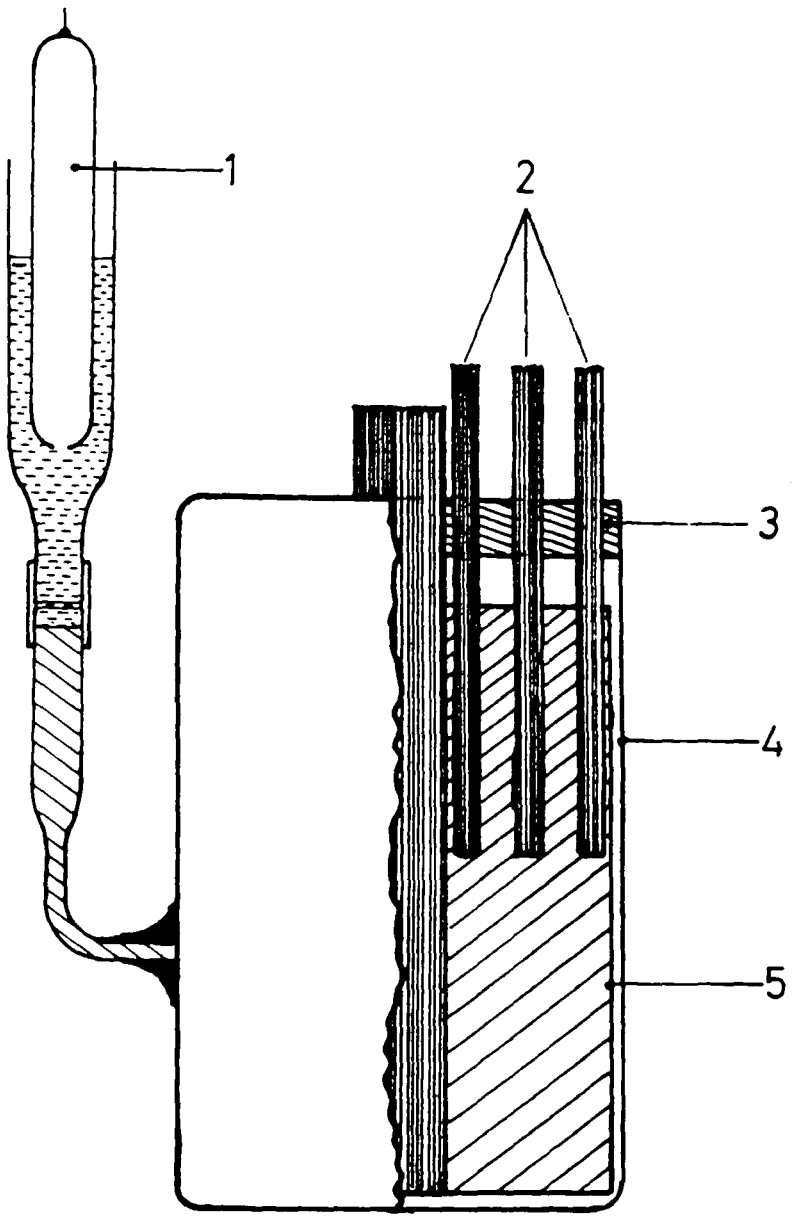

Figure 2.10 : Cell with carbon probes inserted into the positive electrode mix. (1) reference electrode, (2) carbon probes, (3) bitumen seal, (4) zinc can , (5) MnO_2 electrode mass.

Cell preparation

The cells were prepared as described in section 2.5.2 (with carbon probes). The template was removed after the bitumen seal had been drilled, a brass cap placed at the top of the carbon rod and the connections of the load soldered to the cell. The cell was then clamped to a stand and the three salt bridges inserted vertically into the positive electrode mix, as close as possible to the same location as the carbon probes. They were sealed to the bitumen by a ring of Bostik solvent-free glue. A thick piece of wood with three appropriately sized holes was used to hold the salt bridges in the correct position. A fourth salt bridge was

connected to the cell electrolyte through a hole drilled into the can (as in section 2.4.3).

2.5.4 Interruption method

The cells were prepared as in sections 2.5.2 and 2.5.3. An additional switch (mercury wetted relay [179,196,197]) was inserted in the discharge circuit. The voltage transients were monitored on the screen of a storage oscilloscope [197-199] that was triggered by the change in one of its input values.

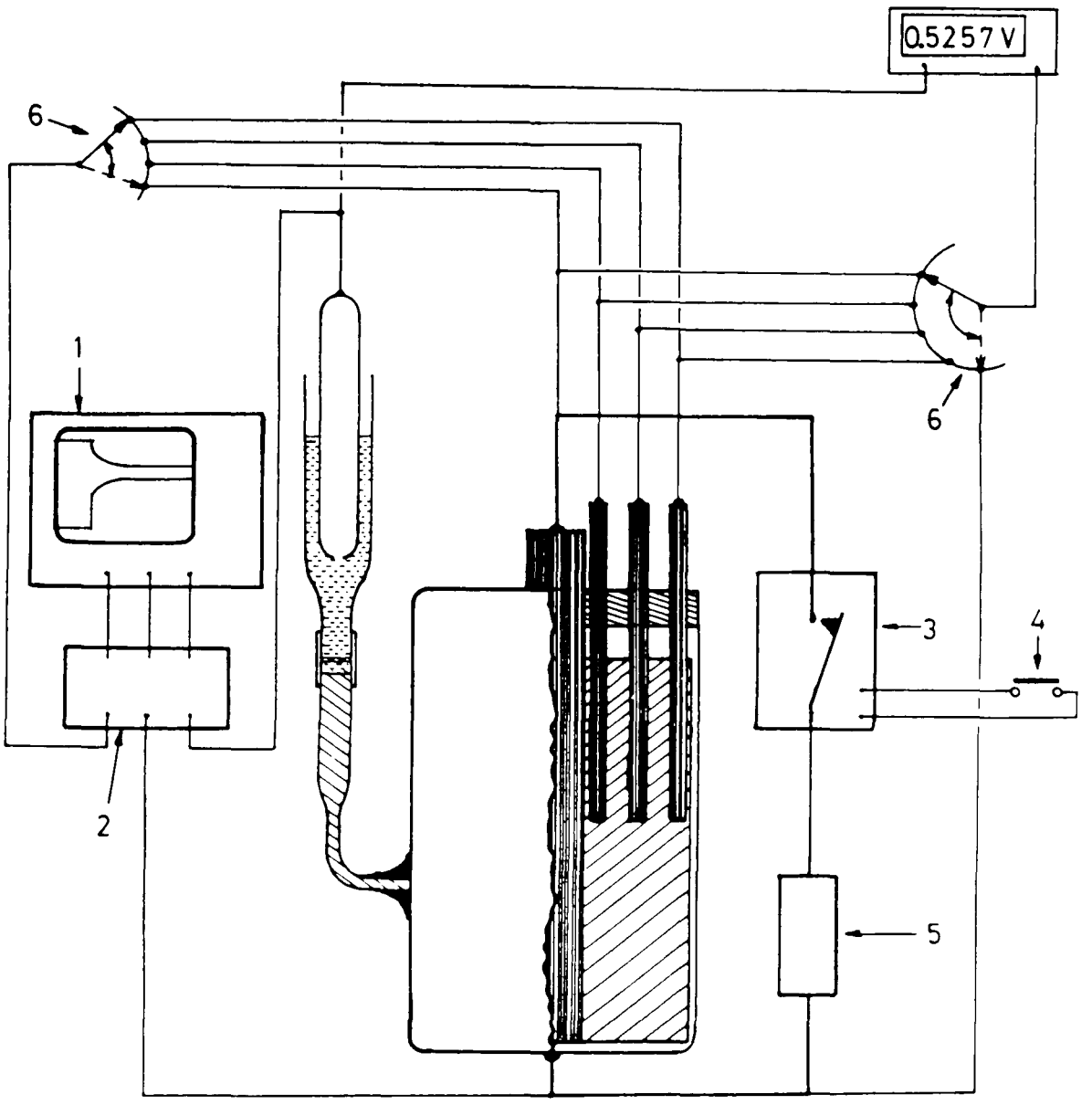

Figure 2.11 : Set-up for discharges using the interruption procedure. (1) Storage oscilloscope, (2) voltage shifter, (3) mercury relay, (4) mercury switch, (5) load, (6) rotary switches.

The set-up used for these experiments is given in figure (2.11). The relay was driven by the circuit given in figure (2.12), in which the mercury switch was operated manually. The mercury relay and mercury switch were used to ensure bounce-free switching.

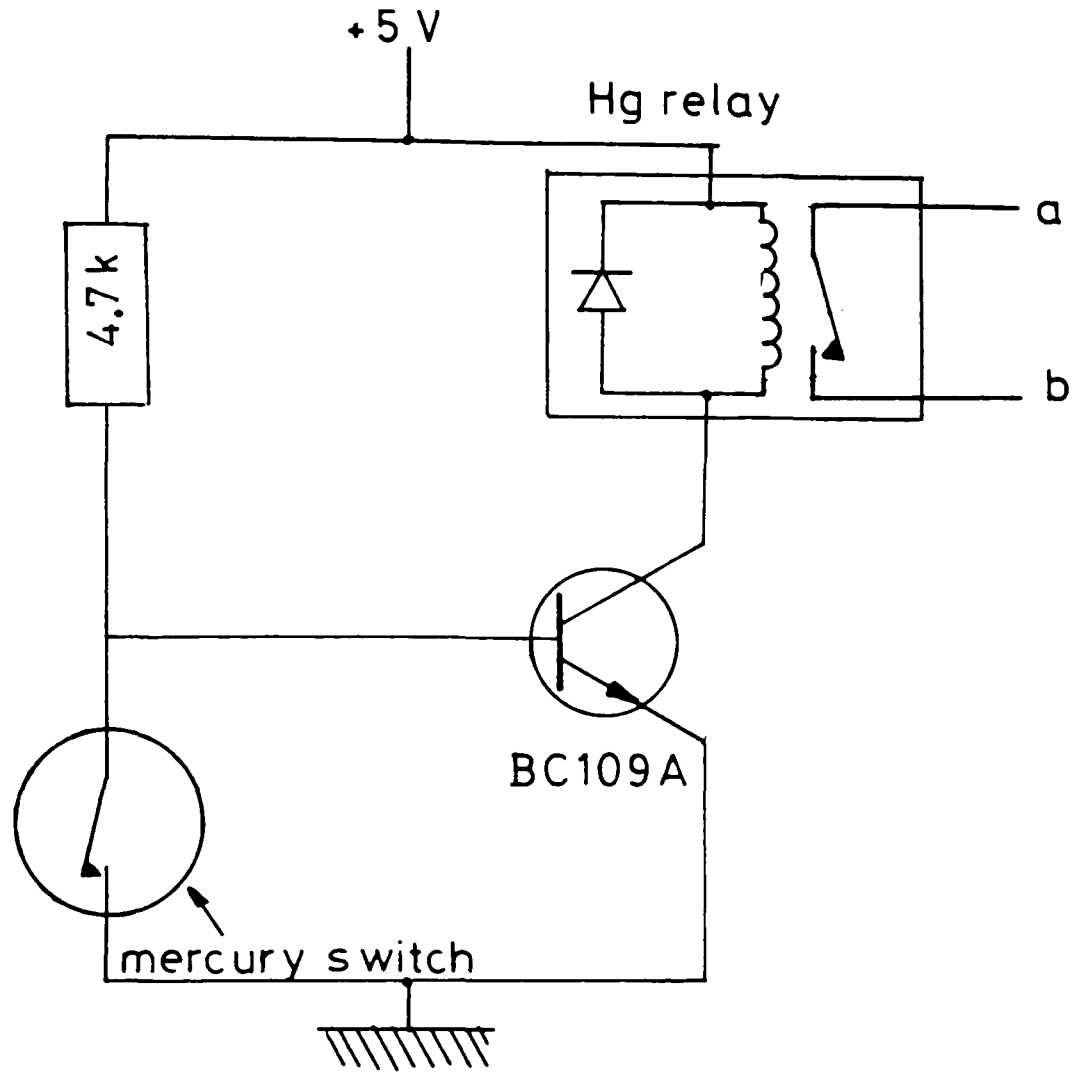

Figure 2.12 : Mercury relay circuitry. (a) and (b) connections to the cell circuit.

The changes in the electrode/probe potentials on interruption were usually small differences between large values. The achievement of a good sensitivity required that the different potentials were shifted by a constant adjustable amount to small values that permitted the use of the high sensitivity ranges of the oscilloscope. This was accomplished using the circuit in figure (2.13) with the output transmitted to the oscilloscope.

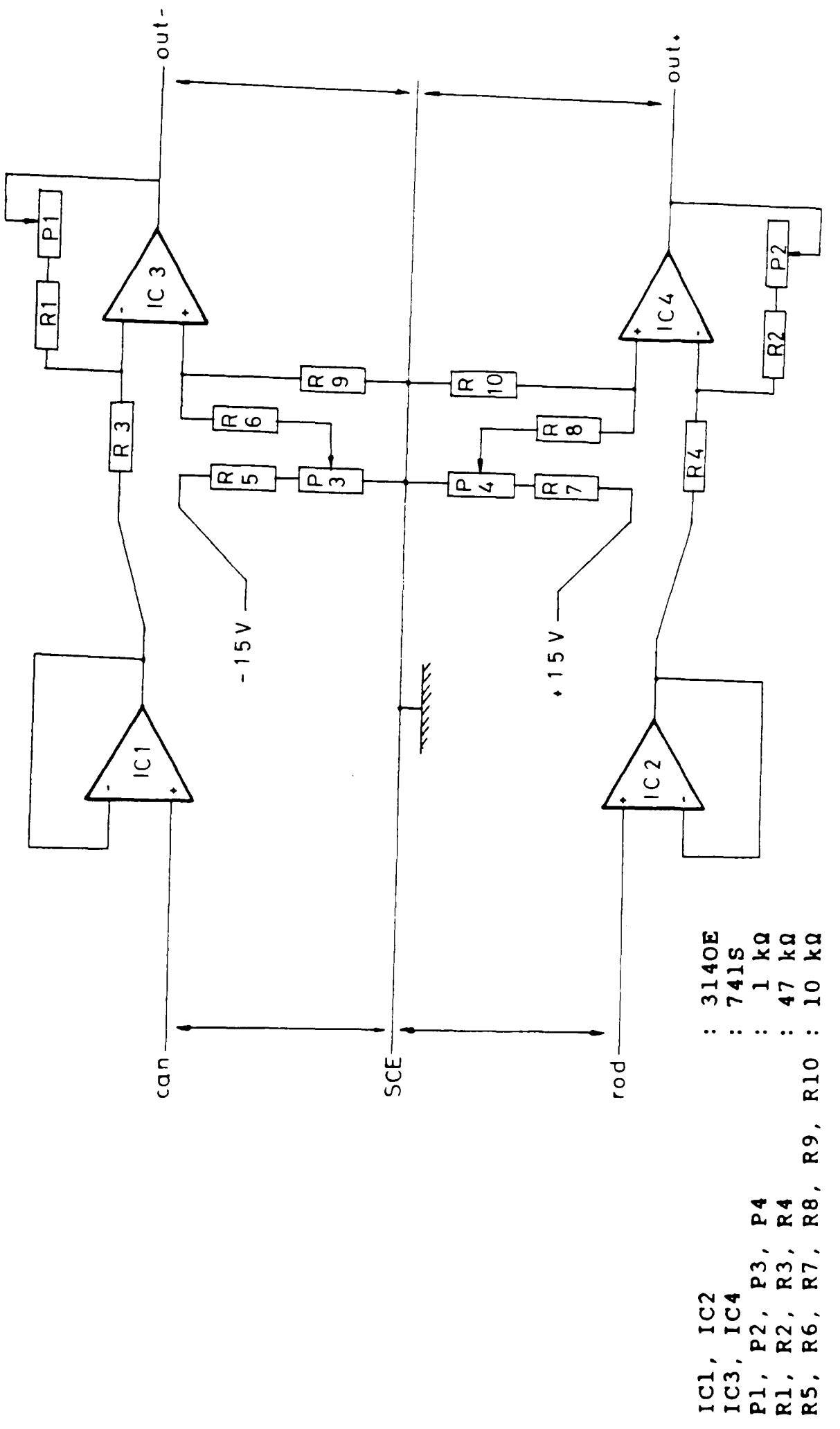

Figure 2.13 : Voltage shifter.

The ohmic overpotential was measured 12 μs after the interruption and the ohmic + charge transfer overpotential 35 ms after the interruption. The interruptions usually lasted 0.2 to 0.4 seconds.

Shielded cables were used for all the connections in figure (2.10), the shield being earthed via the oscilloscope earth point.

2.6. Chemical reduction of manganese dioxide

2.6.1 Acetone reduction

This reduction was carried out at room temperature by suspending 30 g samples in 40 ml acetone. At the completion of the contact time, the sample was filtered on sintered glass (grade P16), dried as a thin layer (2-3 mm) at 50 °C for about 15 minutes and then outgassed (residual relative pressure about 20 mm Hg) for 15 minutes. The contact time was varied from 30 seconds to 2 weeks (4 weeks for the electrodeposited manganese dioxide sample).

2.6.2 Acetone and hydrazine hydrate reduction

About 1 kg of MnO_2 was reduced by a two week contact with 1 litre of acetone, filtered, dried and outgassed in small portions as described above. 30 g aliquots were suspended in 35-40 ml hexane (AnalaR 95 % n-hexane) in 50 ml conical flasks containing a stirring bar. One ml portions of a solution of hydrazine hydrate in propan-2-ol (17.2 g $N_2H_4.H_2O$ in 100 ml of solution) were added to the vigorously stirred suspensions every 50 - 60 minutes. Each sample received a different number of reductant additions (between 1 and 26 additions). An hour after the last hydrazine addition, the sample was filtered on sintered glass, transferred to a large Petri dish, dried at 50 °C for about 15 minutes and outgassed for about 15 minutes.

Hydrazine hydrate was chosen because it reduced MnO_2 with nitrogen and water as the other reaction products; its concentration was calculated to produce a reduction of r (in $MnOOH_r$) equal to 0.04. The reaction was

$$4\ MnO_2 + N_2H_4.H_2O \longrightarrow 4\ MnOOH + N_2 + H_2O \qquad (2.15)$$

Hexane was chosen as a suspension medium as the solubility of Mn^{2+} in it was expected to be small. Such a small solubility was necessary to reduce the risk of heterogenous reduction in which the Mn^{2+} ion may play an important role [200]. Propan-2-ol was chosen because it was soluble in hexane in all proportions [191], the hydrazine hydrate solubility in it was high [191] and because its first oxidation product is acetone. After two weeks of contact, the reaction between acetone and MnO_2 had practically stopped and consequently the acetone that might have been produced by the oxidation of propan-2-ol was not expected to react further with MnO_2 (and form an acid which could increase the Mn^{2+} solubility).

2.6.3 Hydrazine hydrate reduction in water suspension

30 g samples of MnO_2 were suspended in 35-40 ml of water in conical flasks containing a stirring bar. 1 ml portions of a solution of hydrazine hydrate in water (8.6 g in 100 ml) were added to the vigorously stirred samples every 50-60 minutes. Each sample received one to six hydrazine hydrate additions. An hour after the last reductant addition, the sample was filtered on a sintered glass crucible, transferred to a large Petri dish and dried at 80 °C for about 2 hours. The sample reduction caused by one such addition was calculated to be 0.02 of the r value in $MnOOH_r$. At the low degree of reduction ($r <$ about 0.2) obtained by this procedure, the MnO_2 reduction was homogeneous [200] and the dissolved Mn^{2+} was therefore harmless.

2.6.4 Hydrazine hydrate reduction in hexane suspension

The procedure and the solutions were the same as in section 2.6.2 but the reduction was started with unreduced MnO_2 samples.

2.6.5 Analysis of the reduced samples

The reduction degree was measured by the method described in section 2.2.5. The most reduced samples were also examined by X-ray diffraction.

2.6.6 Electrode potential

The procedure used in this work was a variation of the centrifuge method described by Suzuki *et al.* [201].

25 ml of a 10^{-3} M KCl solution were pipetted into 50 ml conical flasks. The flasks were stoppered and weighed to the closest 0.1 mg. About 15 g of the samples were suspended in the KCl solutions and the flasks were shaken vigorously and reweighed to determine the size of the samples (Q grams). The samples were then allowed to equilibrate at 25 °C for 2 or 3 days. The suspensions were then transferred into polypropylene centrifuge tubes containing a spiral of platinum wire (0.2 mm diameter, 30 cm long with about 20 cm forming a spiral at the bottom of the tube). After a 5 minutes centrifugation at 4000 rpm, the tubes were placed in a water bath at 25 °C for about 10 minutes and then transferred into the air box. The potential of the platinum wire (the MnO_2 electrode) was measured with respect to a saturated KCl calomel electrode immersed in the liquid phase. After about 45-60 seconds, the potential difference reached a maximum value and then started to shift slowly (about 0.5 mv minute^{-1}) towards lower potentials. The maximum value was taken as the manganese dioxide potential. The pH of the supernatant was also measured.

In a few cases, after the potential and the pH measurements, the manganese dioxide was suspended again in the KCl solution by very vigorous shaking, centrifuged, equilibrated at 25 °C and the potential re-measured. The difference with the previous measurement was in the range 5-10 mV.

The samples were filtered on dry filter paper, 5 ml of the filtrate diluted to 100 ml (in a calibrated flask) with water and analyzed for soluble manganese by atomic absorption spectrophotometry (section 2.2.3).

Calculations

The potentials were calculated at pH 0 by

$$E_c = E_m + 0.0592\ pH \qquad (2.16)$$

where E_c and E_m are the corrected and measured potentials respectively and 0.0592 is the slope (in V pH^{-1}) of the potential pH relationship [13]. The potentials are in V.

The formation of Mn^{2+} when the reduced samples were kept in dilute KCl solution was due to the disproportionation of the reduced oxide by

$$MnOOH_r + 2\Delta H^+ \rightleftharpoons \Delta Mn^{2+} + (1-\Delta)MnOOH_{\frac{r-2\Delta}{1-\Delta}} + 2\Delta H_2O \qquad (2.17)$$

If there were N moles $MnOOH_r$ in the starting sample and n moles Mn^{2+} ($n = N\Delta$) were formed on disproportionation, the degree of reduction became r' given by

$$r' = \frac{r\,N - 2n}{N - n} \qquad (2.18)$$

Chapter 3. Study of the Leclanché electrolyte

3.1 The electrolyte density

3.1.1 Calculations using the molal scale

The experimental results are compared in figure (3.1) with equation (1.11) [34]

$$V_s = 17.7\ n_w + 44.4\ n_n + 43.5\ n_z \qquad (1.11)$$

where V_s is the volume of a solution containing n_w, n_n and n_z moles of water, NH_4Cl and $ZnCl_2$ respectively, and equation (1.10)

$$D_s = D_w + \sum_{i=1}^{n} (a_i\ C_i + b_i\ C_i^{\frac{3}{2}}) \qquad (1.10)$$

where D_s and D_w are the density of the solution and of pure water respectively, C is the molarity of the subscript species and a_i and b_i two constants the values of which were taken from the work of Novotny and Sohnel [37]. At 25°C, these values are for NH_4Cl a=17.638 10^{-3}, b=-1.4561 10^{-3} and for $ZnCl_2$ a=113.14 10^{-3} and b=-5.7917 10^{-3} for the densities in g ml^{-1} and the concentrations in mol l^{-1}. Although the results calculated from equation (1.11) agree rather well with the experimental results at $ZnCl_2$ concentrations higher than about 1 molal and NH_4Cl higher than about 2 molal, neither of the equations gives a good estimate of the density over the whole range of concentrations.

The results for the binary solutions are compared with the values given in the literature in figure (3.2) and (3.3). For the NH_4Cl solutions, the agreement is almost perfect. For the pure $ZnCl_2$ solutions, careful examination of the figures reveals that the experimental results are systematically slightly higher than the literature results. For the 6.36 molal $ZnCl_2$ solution (46 w/w %), the difference was 0.0011 g ml^{-1}. For this concentration, the temperature effect is about 0.001 g/(ml °C) (from ref [38]) while a 1 w/w % increase of the concentration increases the density by about 0.015 g ml^{-1} [37].

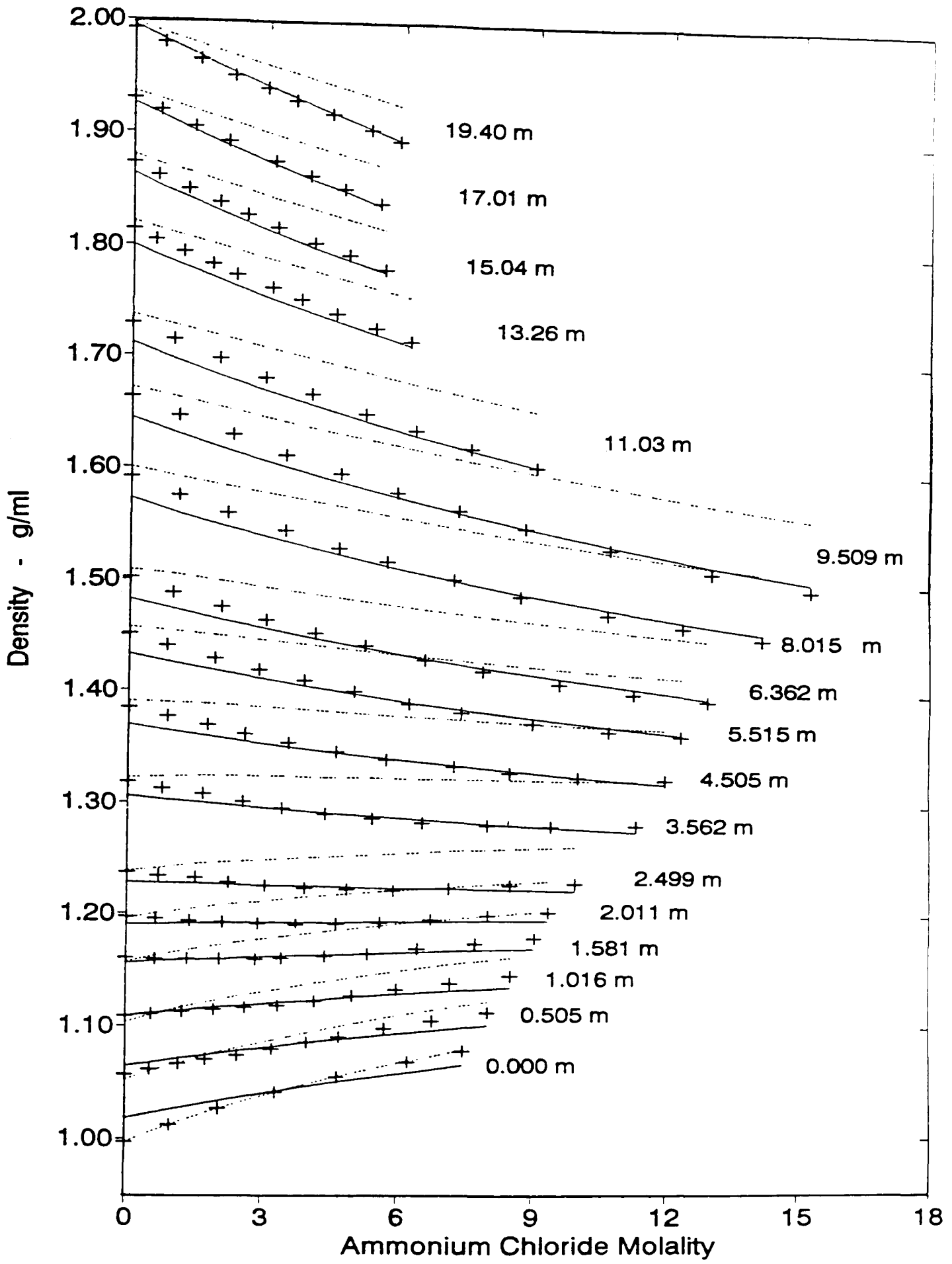

Figure 3.1 : Density of the ternary solutions for different $ZnCl_2$ molalities (parameters); • experimental results, - - - equation (1.10), —— equation (1.11).

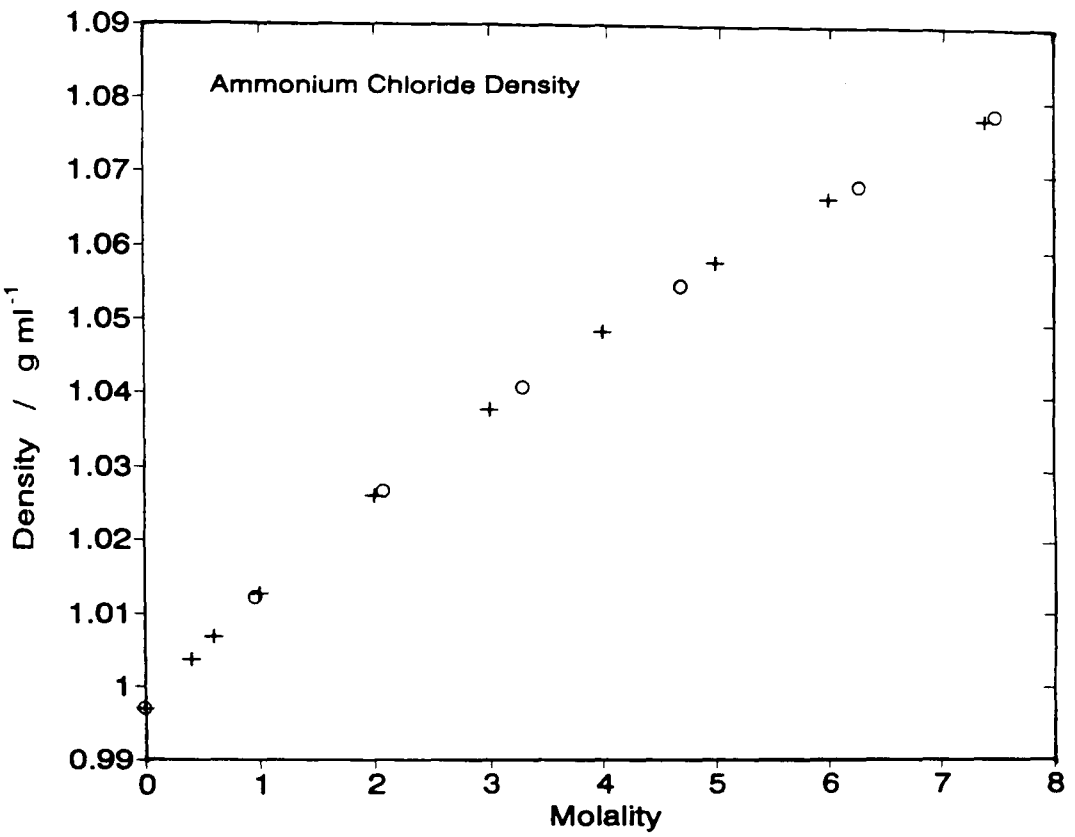

Figure 3.2 : NH_4Cl density; + from ref [35], o this work.

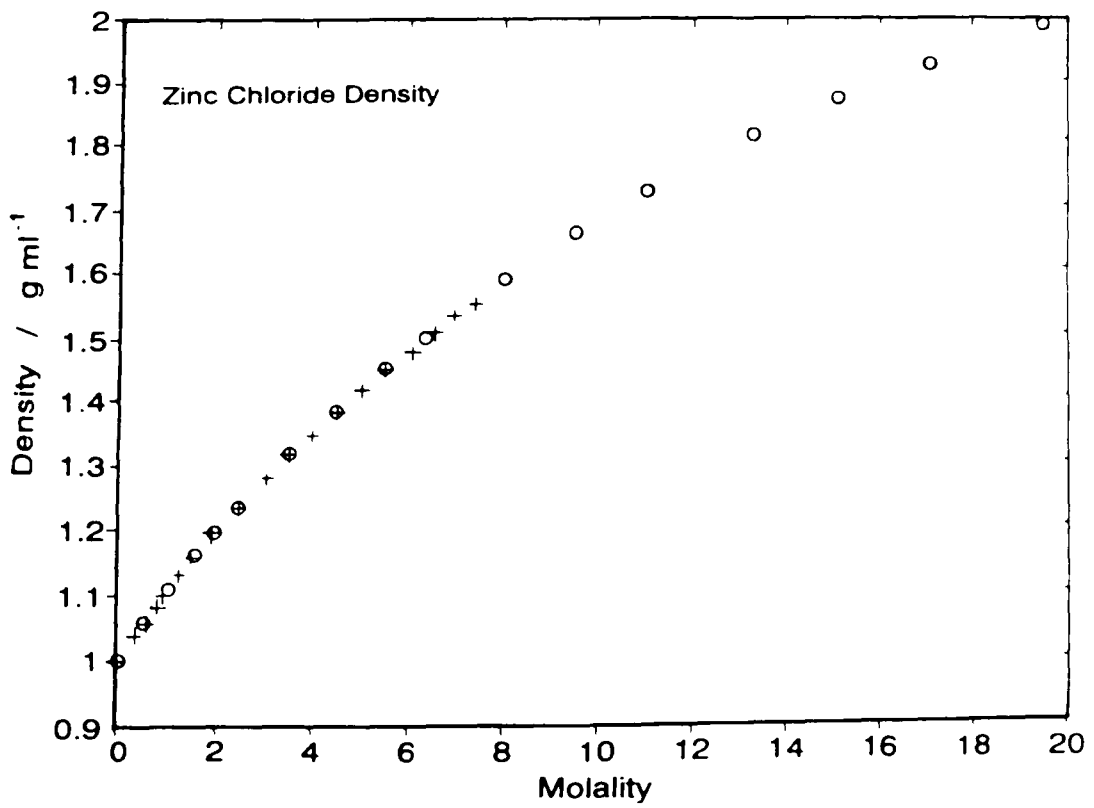

Figure 3.3 : $ZnCl_2$ density; + from ref [40], o this work.

The difference may therefore be explained by a difference of about 1 °C in the temperatures, a relative difference of about 0.2 % in the concentrations or a combination of the two factors. The presence of some ZnO (about 1 %, see section 3.2) in the analytical grade $ZnCl_2$ used in this work may also have influenced the results. The molecular weight of water is 18.015 [191] and its density at 25 °C is 0.99705 g ml^{-1} [191]; its molar volume is therefore (1000 × 0.99705)/18.015 = 18.07 ml $mole^{-1}$. The NH_4Cl and $ZnCl_2$ apparent molar volumes were calculated using equation (1.5), and are shown in figures (3.4) and (3.5). They were fitted to a polynomial equation in order to permit numerical interpolations.

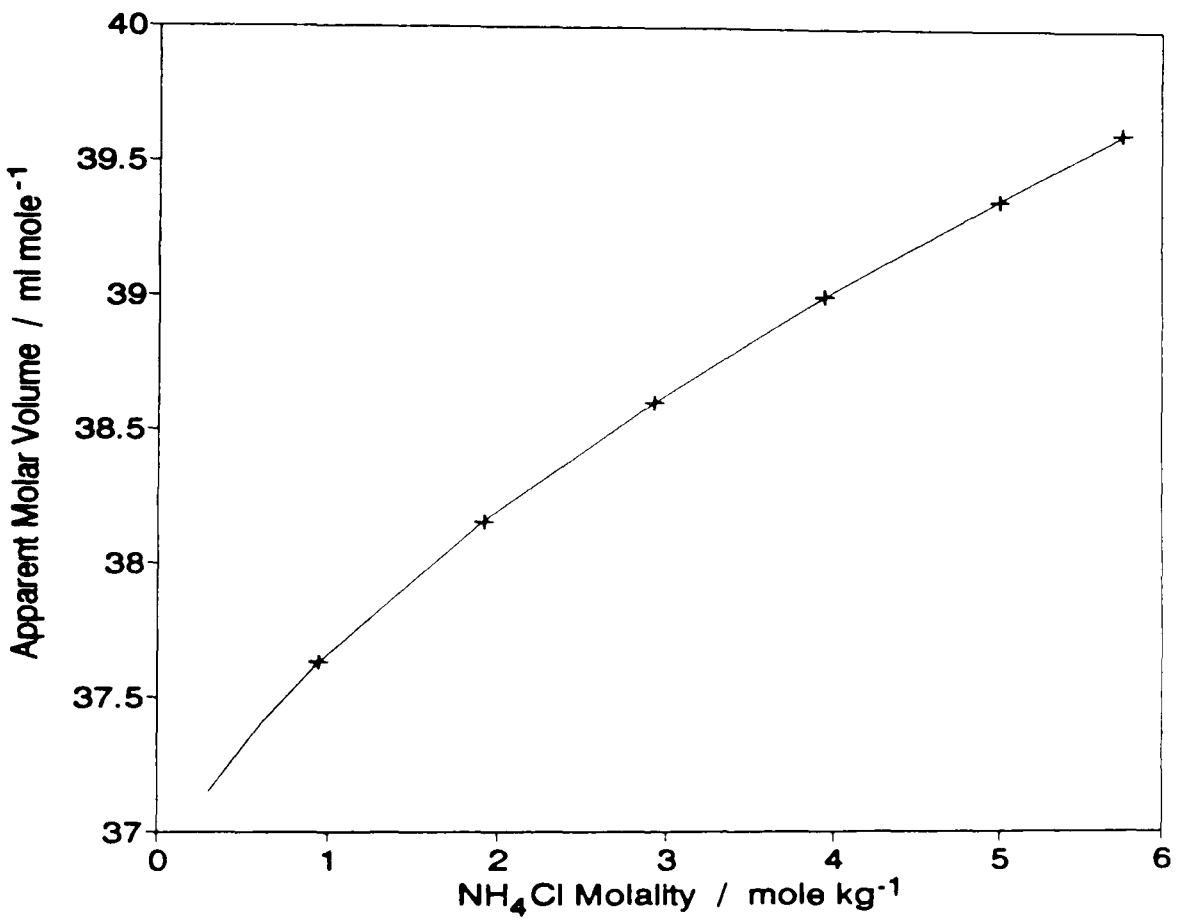

Figure 3.4 : The ammonium chloride apparent molar volume; + experimental results, —— equation (3.1)

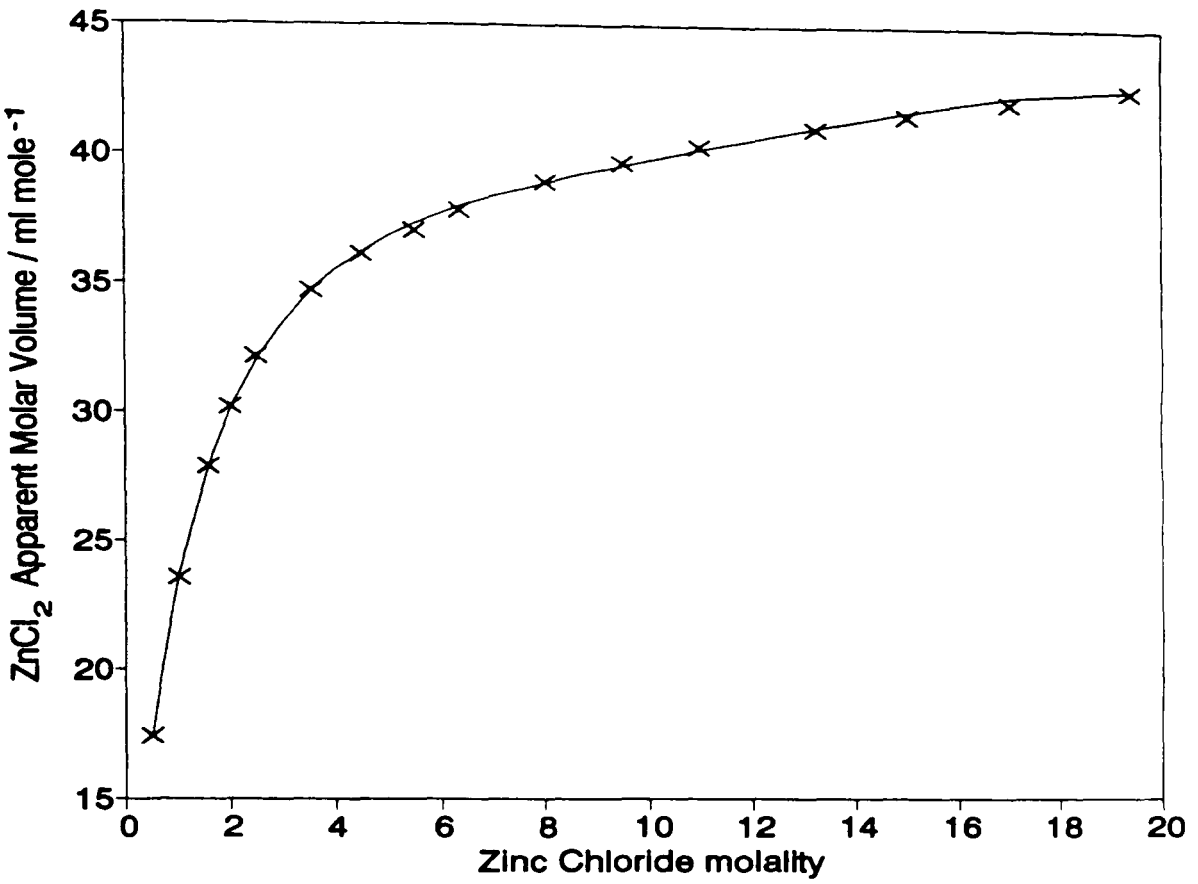

Figure 3.5 : The zinc chloride apparent molar volume; × experimental results, —— equation (3.2)

The best fits are given in equations (3.1) and (3.2) for NH_4Cl and $ZnCl_2$ respectively.

$$\Phi_n = 36.522 + 1.064\sqrt{m_n} + 0.0585\ m_n - 0.0047\ m_n^2 \qquad (3.1)$$

$$\Phi_z = -4.332 + 37.463\sqrt{m_z} - 9.88 m_z + 0.296 m_z^2 - 0.00517 m_z^3 \qquad (3.2)$$

where Φ_n and Φ_z are the apparent molar volumes and m_n and m_z the NH_4Cl and $ZnCl_2$ molalities. Even with four terms in equation (3.2), the fit is not as good for $ZnCl_2$ (average deviation 0.102 ml mol^{-1}) as it is for NH_4Cl (average deviation 0.003 ml mol^{-1}). The difficulty of fitting experimental results to a polynomial equation was also found by Rard and Miller [40] who used 11 terms in their equation to calculate the density of zinc chloride solutions.

In the case of ideal mixing, the mean apparent molar volume ${}_c\Phi_{av}$ may be calculated by [43]

$$ {}_c\Phi_{av} = \frac{n_n \Phi_n + n_z \Phi_z}{n_n + n_z} \tag{3.3} $$

where n_n and n_z, and Φ_n and Φ_z are the number of moles and the apparent molar volumes of NH_4Cl and $ZnCl_2$ respectively.

In the actual solution, the experimental mean apparent molar volume ${}_e\Phi_{av}$ is [43]

$$ {}_e\Phi_{av} = \frac{V_s - n_w \Phi_w}{n_n + n_z} \tag{3.4} $$

where V_s is the solution volume containing n_w moles of water.

The differences (${}_e\Phi_{av}$ - ${}_c\Phi_{av}$) are given in figure (3.6) as a function of the logarithm of the NH_4Cl to $ZnCl_2$ mole ratio.

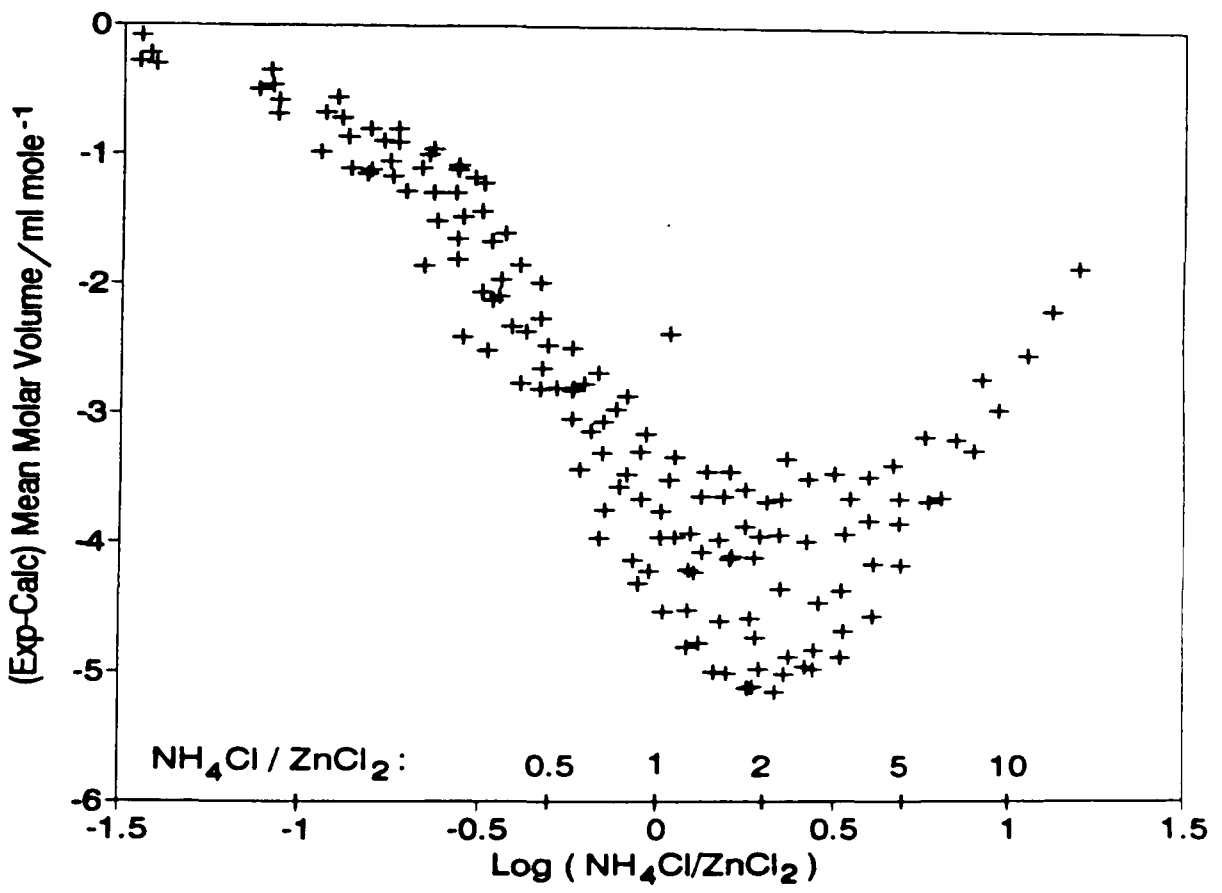

Figure 3.6 : Difference between the calculated (equation 3.3) and experimental (equation 3.4) mean apparent molar volumes.

In this figure, the maximum deviation from ideal mixing appears to correspond to a NH_4Cl to $ZnCl_2$ ratio of 2 suggesting the formation of a zinc complex according to the reaction

$$ZnCl_2 + 2\ NH_4Cl \rightleftharpoons (NH_4)_2ZnCl_4 \qquad (3.5)$$

The solution behaviour on mixing may be expected to become ideal if the complex formation is taken into account and if the solution is considered as a solution of the complex with an excess of NH_4Cl and of $ZnCl_2$. In this case the solution volume V_s becomes

$$V_s = n_w\ \Phi_w + n_c\ \Phi_c + n'_n\ \Phi_n + n'_z\ \Phi_z \qquad (3.6)$$

where n_c, n'_n and n'_z are the number of moles of complex, NH_4Cl and $ZnCl_2$ in the solution, respectively. The Φ_is are the apparent molar volumes. If the complex is assumed to be $(NH_4)_2ZnCl_4$, $n'_n = n_n - 2\ n_c$ and $n'_z = n_z - n_c$ where n_n and n_z are the overall moles numbers of NH_4Cl and $ZnCl_2$ in the solution. The dissociation constant, K_4, of the complex is

$$K_4 = \frac{m'_z\ m'^2_n}{m_c} \qquad (3.7)$$

where the m_i's are the molalities after complexation.

Assuming a value of Φ_c for the zinc complex, it was possible, using equation (3.6), to calculate the composition of the solutions that gave the same density as the measured density. The complex dissociation constant could then be calculated, for each point using equation (3.7). The procedure used for these calculations is shown schematically in figure (3.7).

Whatever the molar volume chosen for the complex, it was not possible to obtain an invariant constant. The values found using this procedure increased with the NH_4Cl molality suggesting that the NH_4Cl molality was given too much importance in the expression of the equilibrium constant.

The same procedure was repeated with the assumption of a complexation occurring according to the reaction

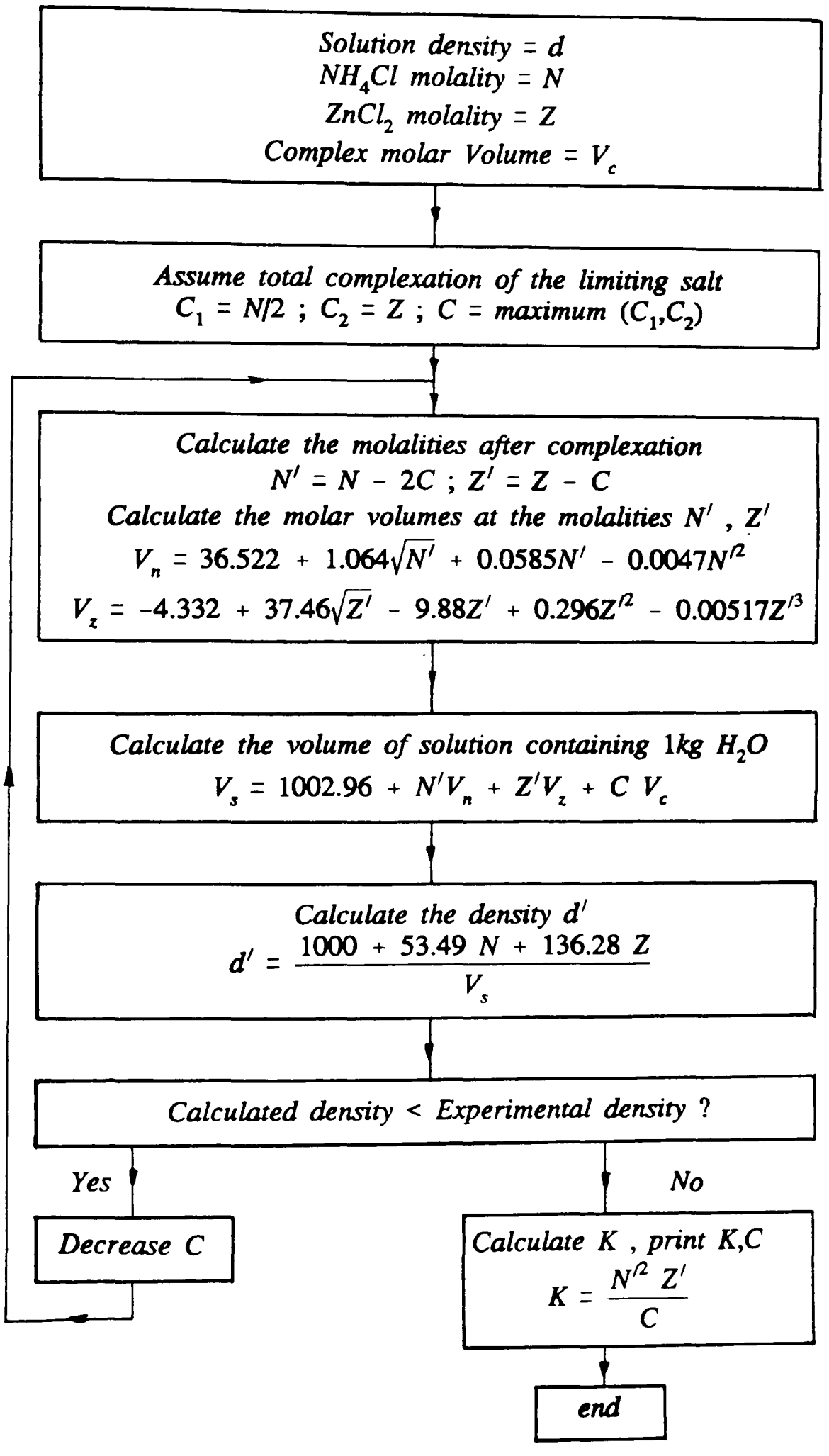

Figure 3.7 : Calculation of the complex concentration.

$$ZnCl_2 + NH_4Cl \rightleftharpoons (NH_4)ZnCl_3 \qquad (3.8)$$

In this case, the concentrations after complexation were $m'_n = m_n - m_c$ and $m'_z = m_z - m_c$ with the same notation as for equation (3.7).

On this basis, a dissociation constant K_3 corresponding to the equation

$$K_3 = \frac{m'_n \, m'_z}{m_c} \qquad (3.9)$$

could be found for a complex molar apparent volume of 105 ml. This constant was only approximately constant for a given zinc chloride molality and increased with increasing zinc concentration.

The calculation procedure was similar to the procedure shown in figure (3.7), the only change being in the calculation of the residual free NH_4Cl molality $m'_n = m_n - m_c$.

The increase of K_3 was almost a linear function of the overall zinc chloride molality and could be approximated by

$$K_3 = 1.36 + 1.12 \, m_z \qquad (3.10)$$

where K_3 and m_z are in mol kg^{-1} and m_z is the total zinc molality of the solution.

Equation (3.9) may be written as a function of the total NH_4Cl and $ZnCl_2$ molalities as

$$K_3 = \frac{(m_n - m_c)(m_z - m_c)}{m_c} \qquad (3.11)$$

and then solved for m_c. The result is

$$m_c = \frac{(m_z + m_n + K_3) - \sqrt{(m_z + m_n + K_3)^2 - 4m_z m_n}}{2} \qquad (3.12)$$

which gives m_c=0 when m_n=0.

It was then possible, with a $(NH_4)ZnCl_3$ dissociation constant of the form

$$K_3 = a + b\, m_z \qquad (3.13)$$

and a complex molar volume Φ_c to calculate the density of each of the measured solutions and use a, b and Φ_c as fitting parameters to minimize the mean absolute deviation. The results are given in figure (3.8) with Φ_c = 105 ml and $K_3 = 0.32 + 1.52\, m_z$. With these values for the parameters, the average deviation was 0.0023 g ml^{-1}. The worst fit was for the very high $ZnCl_2$ molalities with a maximum deviation of 0.0137 g ml^{-1} (about 0.7 % of the measured density).

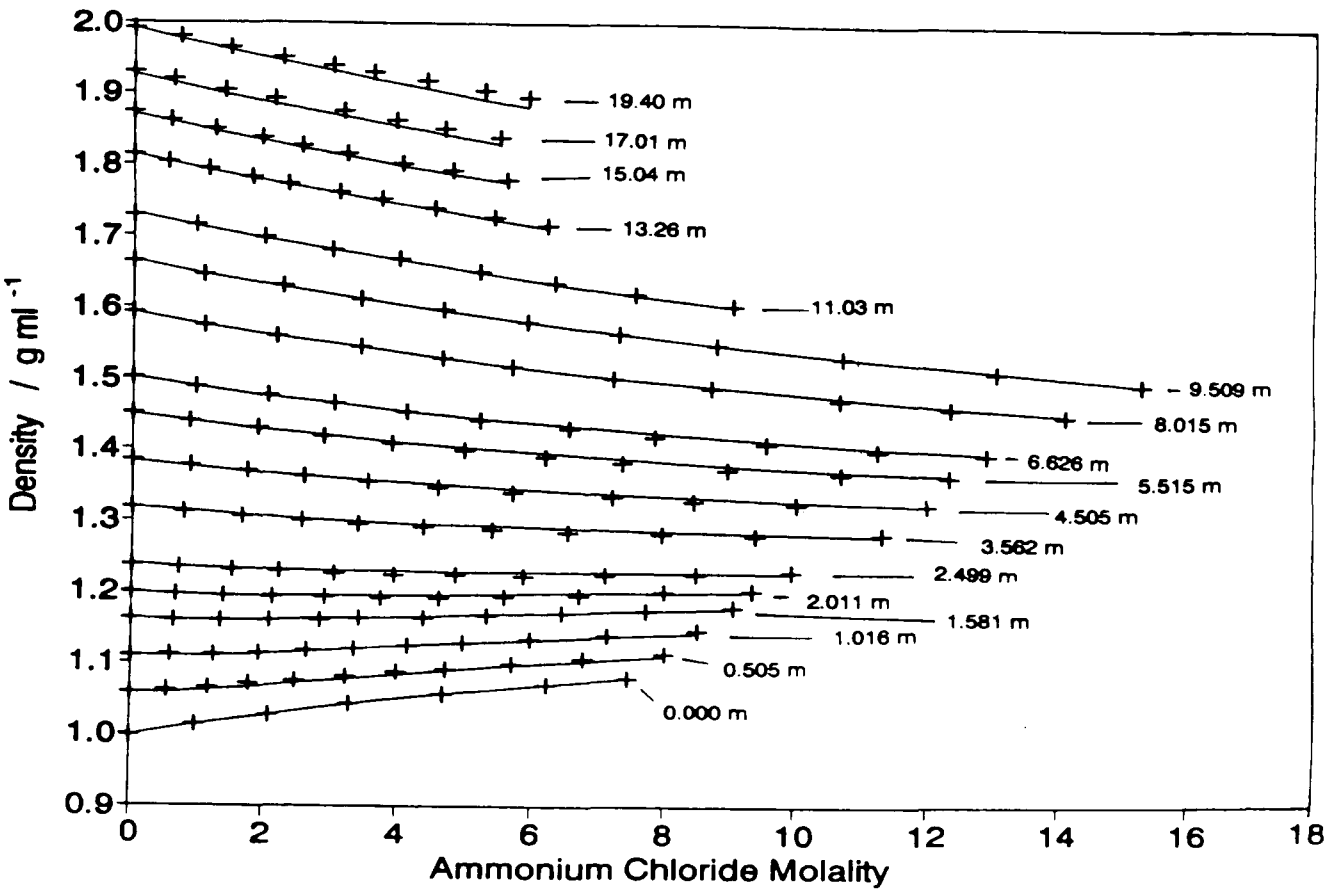

Figure 3.8 : Density of the ternary solutions; + experimental results, —— calculated by using the procedure summarized in figure (3.12); the parameters are the $ZnCl_2$ molalities

Equation (3.12) has also been solved for m_C for different values of m_n and m_z using for K_3 the values found initially and given by equation (3.10). Then equations (3.1) and (3.2) were used to calculate Φ_n and Φ_z. With Φ_C = 105, the mean apparent molar volume Φ_{av} was calculated by

$$\Phi_{av} = \frac{(m_n - m_c)\,\Phi_n + (m_z - m_c)\,\Phi_z + m_c\,\Phi_c}{m_n + m_z} \qquad (3.14)$$

where m_c is the complex molality and m_n and m_z are the NH_4Cl and $ZnCl_2$ overall molalities, respectively.

The mean apparent molar volume was also calculated by equation (3.3)

$$ {}_c\Phi_{av} = \frac{n_n \Phi_n + n_z \Phi_z}{n_n + n_z} \qquad (3.3) $$

corresponding to ideal mixing. The difference between these two sets of calculated mean molar volumes is shown in figure (3.9). Figure (3.10) shows some curves taken from figure (3.6) for similar zinc molalities. In both figures, the maximum deviation occurs for $NH_4Cl/ZnCl_2 \geq 2$ and this maximum deviation shifts towards lower NH_4Cl to $ZnCl_2$ ratios with increasing zinc chloride concentrations. Nevertheless, the magnitude of the maximum deviation from ideality is about twice as large in the calculated diagram as the experimental results. As in figure (3.8), the deviation is maximum for the highest zinc chloride concentrations.

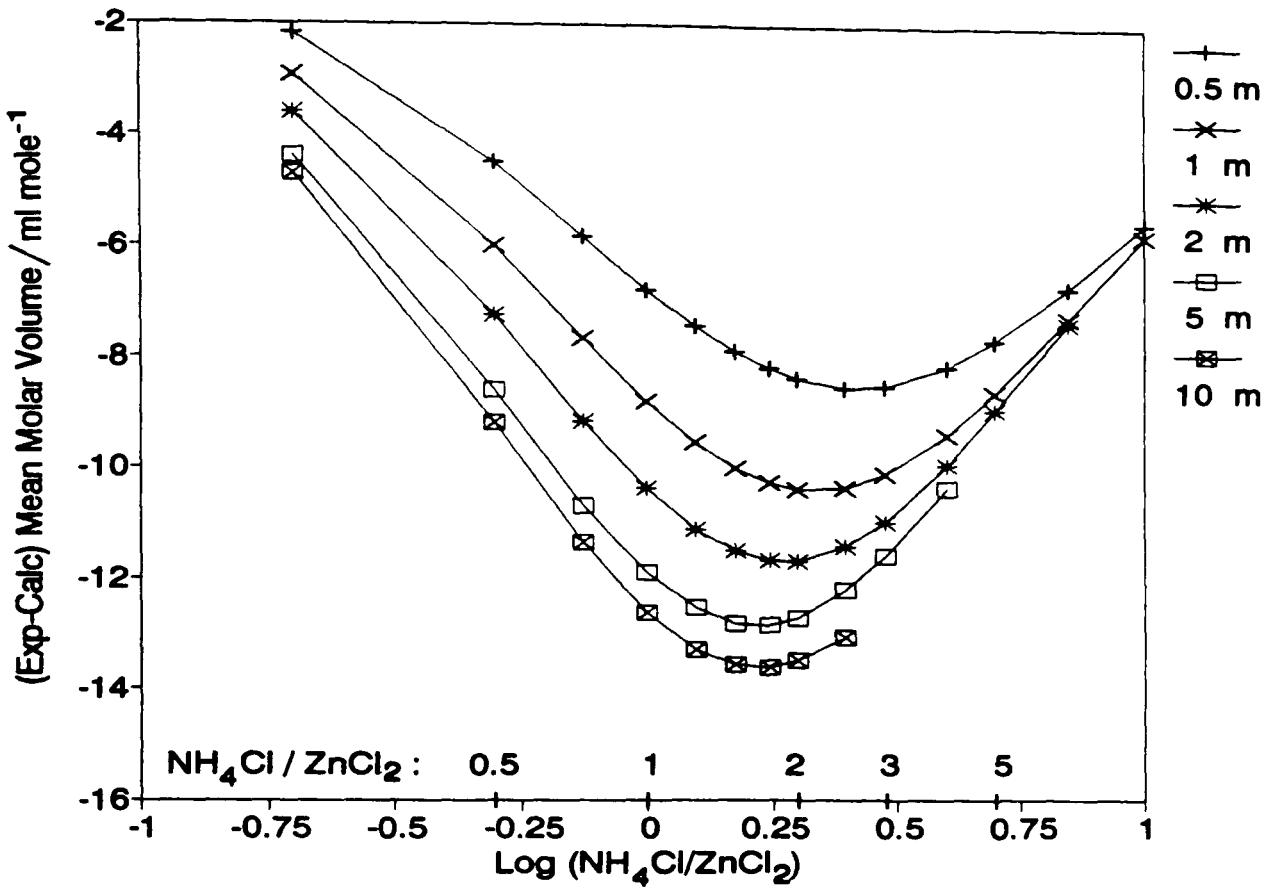

Figure 3.9 : Φ_{av} (assuming the mixture of NH_4Cl, $ZnCl_2$ and complex - equation 3.14) - ${}_c\Phi_{av}$ (assuming no complexation - equation 3.3) at different $ZnCl_2$ molalities.

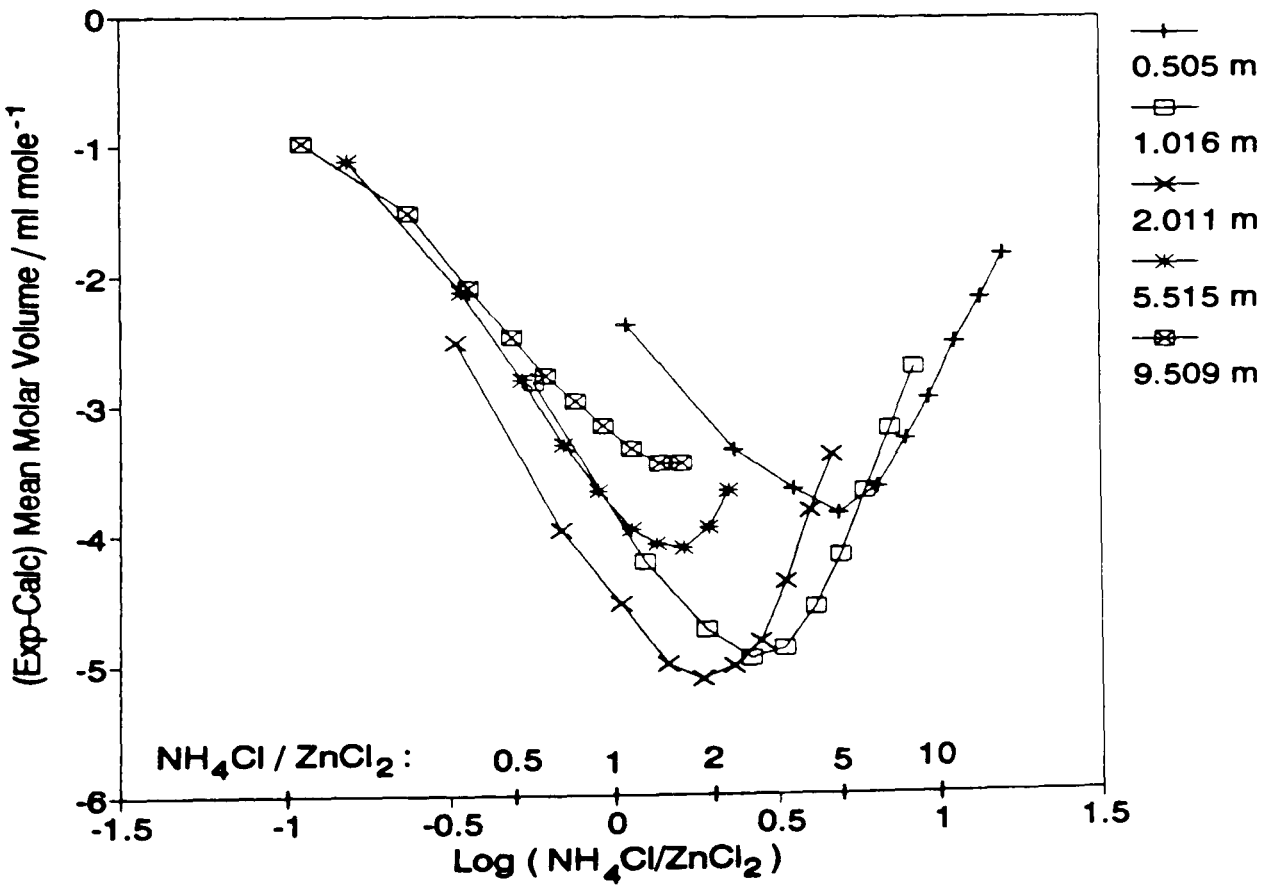

Figure 3.10 : Some (experimental - calculated) mean apparent molar volumes curves, from figure (3.6) for $ZnCl_2$ molalities similar to those in figure (3.9)

3.1.2 Calculations using the molar scale

When C_s moles of a salt, molecular weight $\bar{M}_s$ and apparent molar volume Φ_s, are introduced into one litre of water (mass = 1000 D_w), to prepare a C_s molar solution, they replace $C_s\ \Phi_s$ ml of water ($C_s\ \Phi_s\ D_w$ grams), and change the solution mass to (1000 D_w - $C_s\ \Phi_s\ D_w$ + $C_s\ \bar{M}_s$) grams. The solution density is then

$$D_s = D_w + C_s\ \frac{\bar{M}_s - \Phi_s\ D_w}{1000} \qquad (3.15)$$

In this equation, the fraction is constant for constant solute apparent molar volume or is known if the apparent molar volume is known. In case of ideal mixing, the second term of equation (3.15) is additive and for known apparent molar volumes a general form of equation (3.15), for n salts, is

$$D_s = D_w + \sum_{i=1}^{n} C_i \frac{\bar{M}_i - \Phi_i\ D_w}{1000} \qquad (3.16)$$

where the Φ_is may vary with the concentration. Introduction of Masson's expression [46] for the apparent molar volume (equation 1.8) in equation (3.16) gives equation (1.10).

The apparent molar volumes of pure NH_4Cl and pure $ZnCl_2$ solutions have been calculated as a function of the solution ionic strength IS and are approximated by

$$\Phi_n = 36.602 + 0.8945\sqrt{IS} + 0.171 IS - 0.0038 IS^2 \qquad (3.17)$$

$$\Phi_Z = -5.857 + 23.331\sqrt{IS} - 3.677 IS + 0.0410 IS^2 - 0.000235 IS^3 \qquad (3.18)$$

with the ionic strength given by

$$IS = \frac{1}{2}\sum C_i z_i^2 \qquad (3.19)$$

where the C_is are the molar concentrations of the ionic species and the z_is their charge.

In the following calculations, the ionic strength was

$$IS = 3C_z + C_n + C_c \qquad (3.20)$$

corresponding to complete ionisation of $ZnCl_2$, NH_4Cl and $(NH_4)ZnCl_3$. In equation (3.20), the concentrations are the initial concentrations corrected for the complex formation.

Using the dissociation constant and the complex molar volume as fitting parameters to minimize the average absolute deviation, the density of each of the measured solutions was calculated. The best fit was found with Φ_c = 105 ml mol^{-1} and K_3 = 1.64 + 2.59 C_z (C_z is the overall zinc molarity). The residual average deviation was 0.0007 g ml^{-1} which was much better than the value found for the calculations on a molal scale (0.0023 g ml^{-1}). The results of this curve fitting are shown in figure (3.11).

The much better fit using the molar scale than obtained with the molal scale shows that volume concentrations are better adapted to calculation of equilibrium parameters than mass concentrations which ignore the changes of the solution density.

The practical procedures to calculate the solution density are given in figures (3.12) and (3.13) for the molal and the molar scales, respectively.

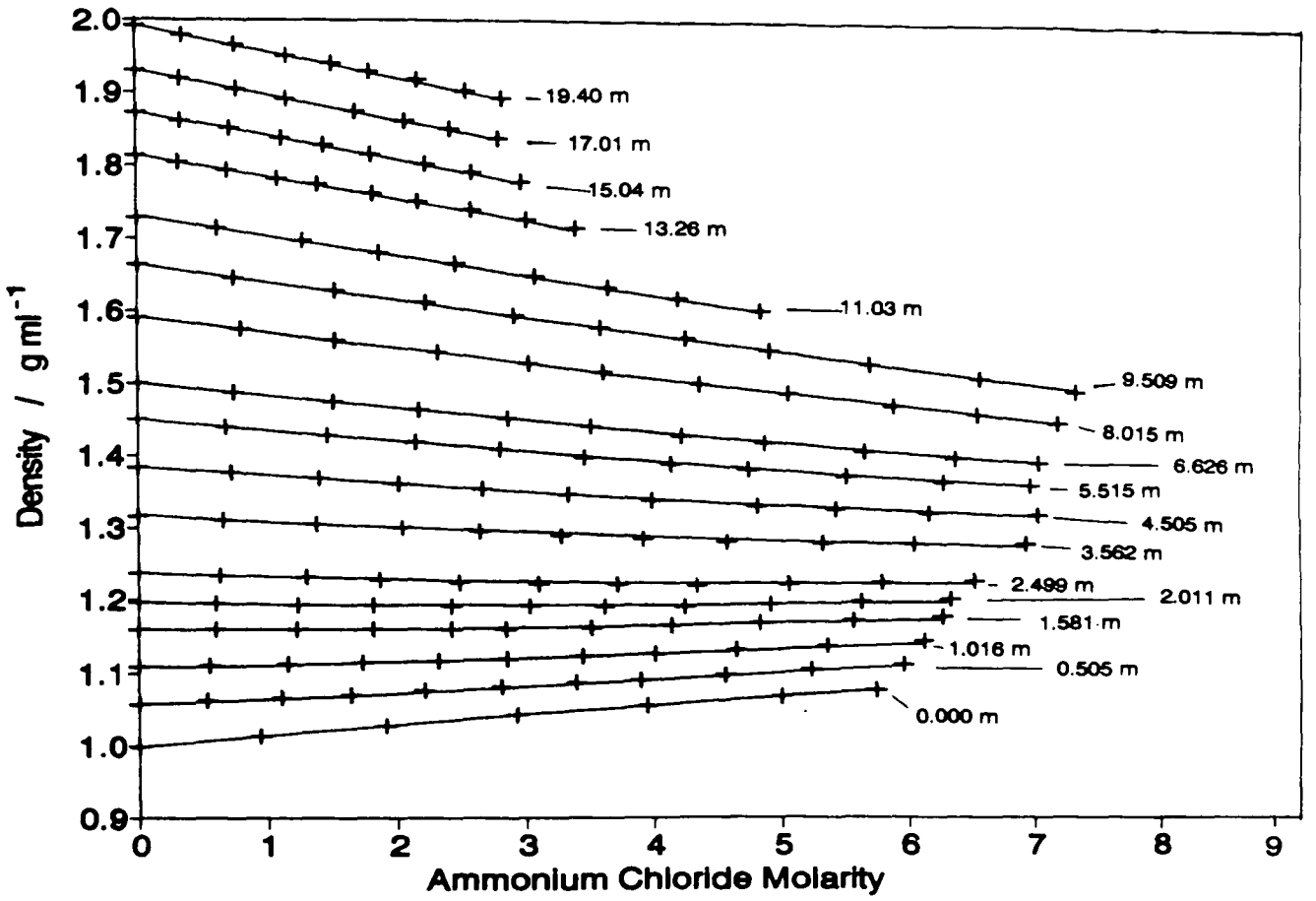

Figure 3.11 : Density of the ternary solutions; + experimental results, —— calculated by using the procedure summarized in figure (3.13); the parameters are the $ZnCl_2$ molalities.

NH_4Cl *molality* = N
$ZnCl_2$ *molality* = Z

↓

Calculate $K = 0.32 + 1.52\ Z$

↓

Calculate the complex molality C

$$C = \frac{N + Z + K - \sqrt{(N + Z + K)^2 - 4\ NZ}}{2}$$

↓

Calculate the apparent molar volumes

$$V_n = 36.522 + 1.064\sqrt{N - C} + 0.0585(N - C) - 0.0047(N - C)^2$$

$$V_z = -4.332 + 37.463\sqrt{Z - C} - 9.88(Z - C) + 0.296(Z - C)^2 - 0.00517(Z - C)^3$$

↓

Calculate the volume of solution containing 1 *kg* H_2O

$$V_s = 1002.96 + (N - C)V_n + (Z - C)V_z + 105\ C$$

↓

Calculate the solution density d

$$d = \frac{(1000 + 53.49\ N + 136.28\ Z)}{V_s}$$

Figure 3.12 : Calculation of the density - molal scale

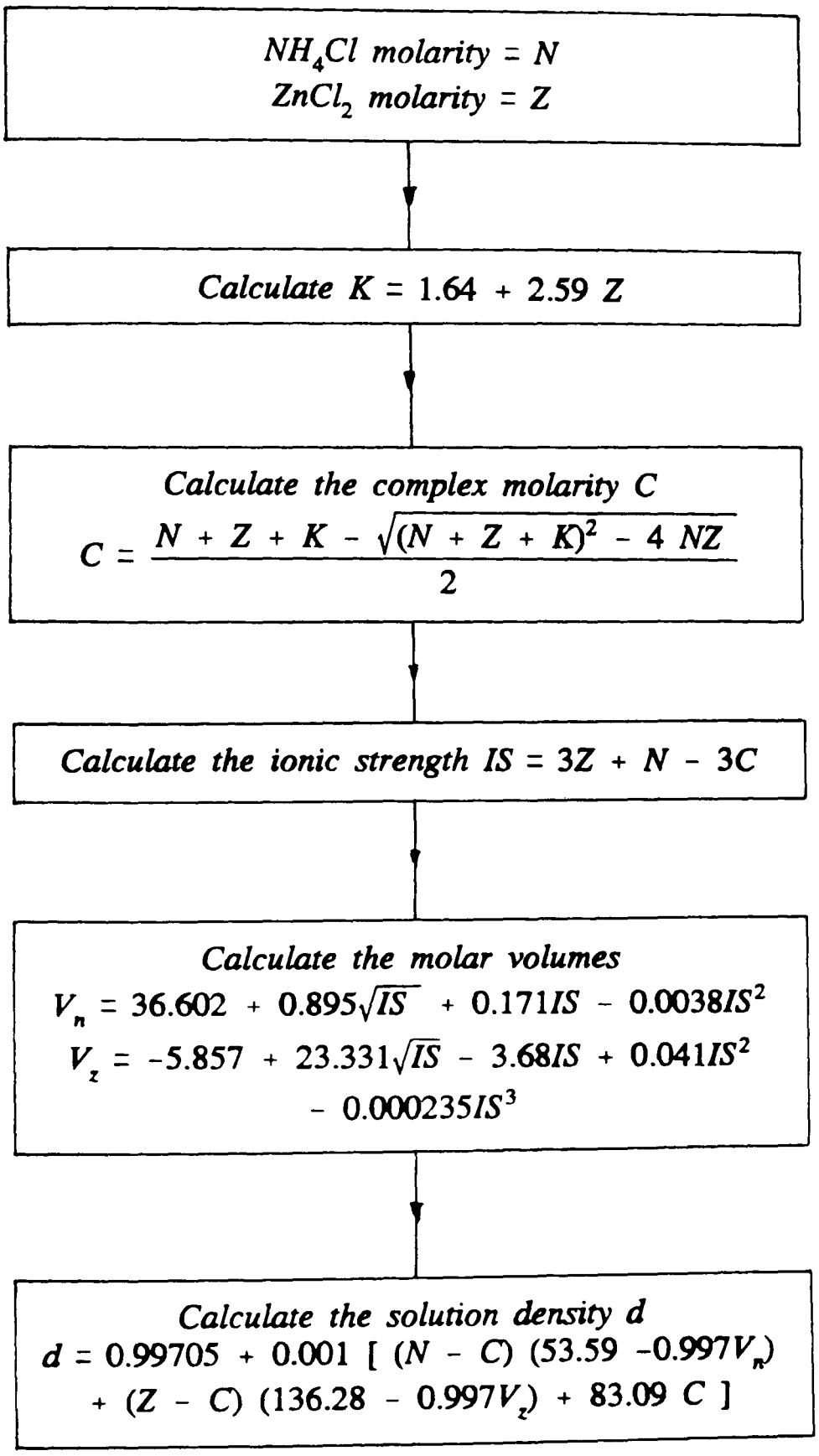

Figure 3.13 : Calculation of the density - molar scale

3.2 Products formed in the Leclanché electrolyte.

3.2.1 Results.

The curves representing the effect of ZnO addition on the potential of the zinc electrode are schematically represented in figure (3.14). From A to B, dissolution of the added ZnO increased the concentration of zinc species in the solution and drove the zinc electrode potential towards more positive values. Along the line BC, the precipitation of $Zn(NH_3)_2Cl_2$ occurred according to the reaction

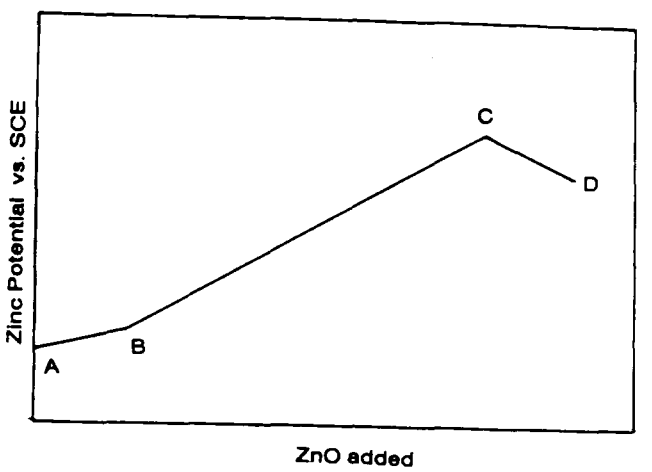

Figure 3.14 : Titration curve (schematic)

$$ZnO + 2\ NH_4Cl \longrightarrow Zn(NH_3)_2Cl_2 + H_2O \qquad (3.21)$$

and from C to D, $ZnCl_2.4Zn(OH)_2.H_2O$ was formed. An overall reaction is

$$ZnCl_2 + 4\ ZnO + 5\ H_2O \longrightarrow ZnCl_2.4Zn(OH)_2.H_2O \qquad (3.22)$$

The reaction (3.22) decreased the concentration of soluble zinc species and therefore drove the zinc electrode potential towards more negative values.

The effect of the rate of ZnO addition on the position of the transition point is shown in figure (3.15).

Despite vigorous stirring, the line corresponding to the $Zn(NH_3)_2Cl_2$ precipitation continued far beyond the true transition point (very close to C_4), with the super-saturation increasing with the ZnO addition rate. The slope of the curves after the $ZnCl_2.4Zn(OH)_2.H_2O$ precipitation had started increased with decreasing ZnO addition rate, due to the fact that the precipitation had more time to proceed between two ZnO additions at lower addition rates. This does not apply to the curve starting from C_4 since for this curve, the over-saturation was minimum. The slowness of the potential equilibration in the region CD was due to the slow dissolution of the $Zn(NH_3)_2Cl_2$ formed on ZnO addition to precipitate the zinc hydroxychloride. The reaction was

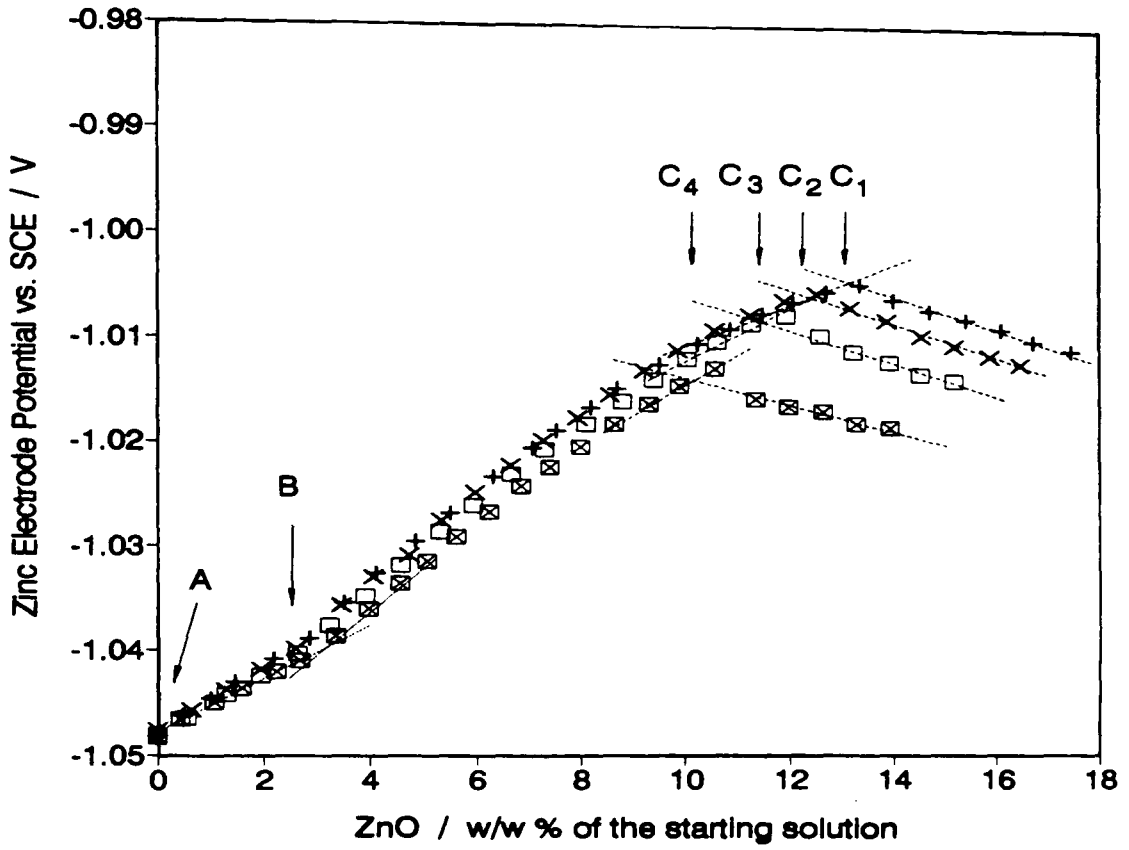

Figure 3.15 : Effect of the addition rate on the transition point in solutions containing initially 20 w/w % $ZnCl_2$ and 25 w/w % NH_4Cl; ZnO added + every 3 min., × every 5 min., □ every 10 min., ⊠ after stabilization of the potential

$$Zn(NH_3)_2Cl_2 + 4Zn^{2+} + 9H_2O \longrightarrow ZnCl_2.4Zn(OH)_2.H_2O + 2NH_4^+ + 6H^+ \qquad (3.23)$$

The super-saturation phenomenon is a likely cause of the early discrepant results [19,48-50] noted in section 1.3.3.

The results of the titration experiments in the range 10 to 35 w/w % $ZnCl_2$ (0.81 - 3.95 molal) and 25 w/w % NH_4Cl are shown in figure (3.16). The determination of the beginning of the $Zn(NH_3)_2Cl_2$ precipitation from the zinc electrode potential curve became very uncertain with increasing $ZnCl_2$ concentration and could be better determined from the pH titration curves shown in figure (3.17). The initial parts of all the curves in figure (3.17) are nearly parallel with a slope of 0.8 pH per decade of added ZnO. This suggests that the pH controlling reaction was the same for all the curves and that each mole of added ZnO consumed one mole of protons from the solution. This could be explained by the reaction

$$ZnO + H^+ \longrightarrow ZnOH^+ \qquad (3.24)$$

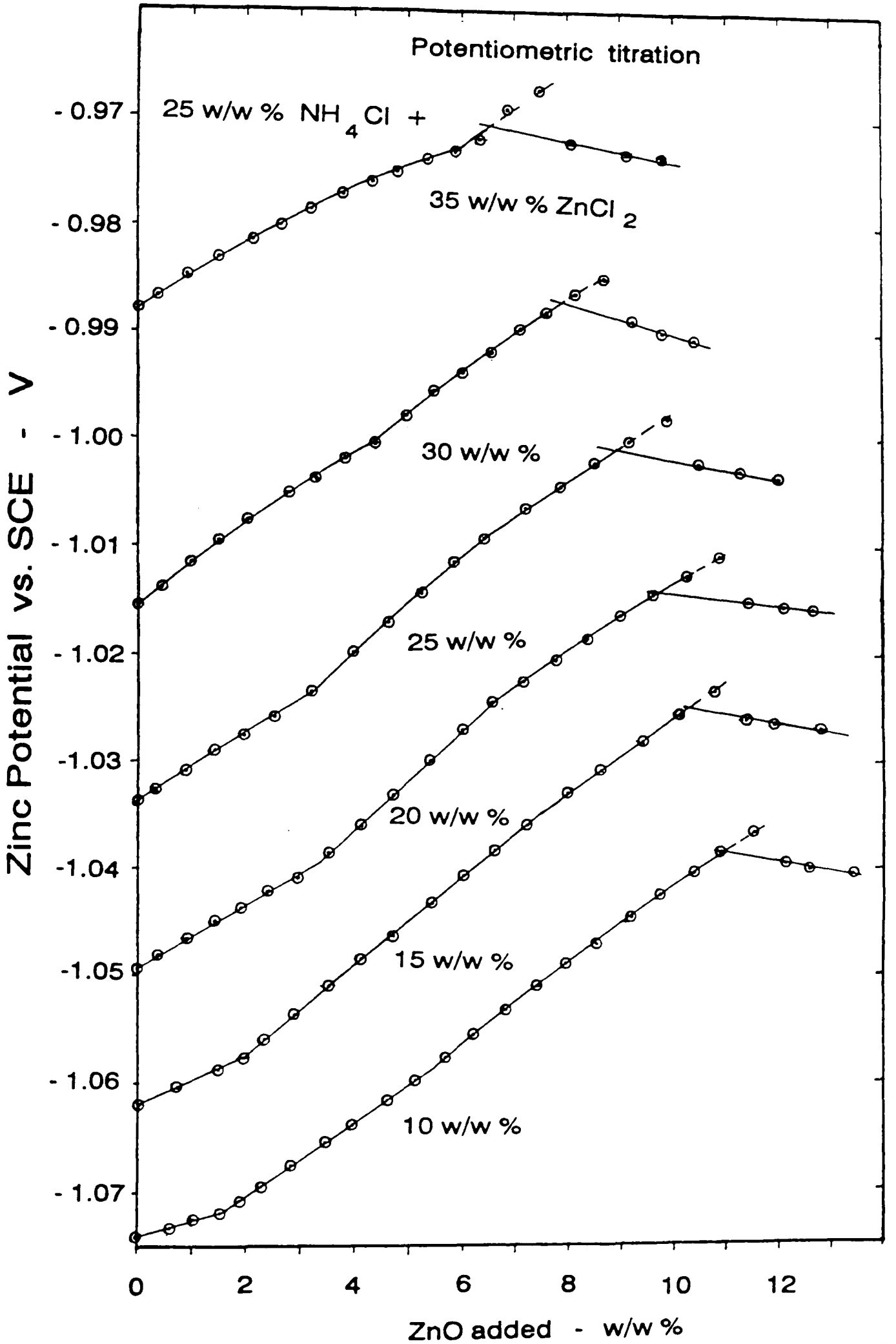

Figure 3.16 : Potentiometric titration by ZnO of solutions containing initially 25 w/w % NH_4Cl

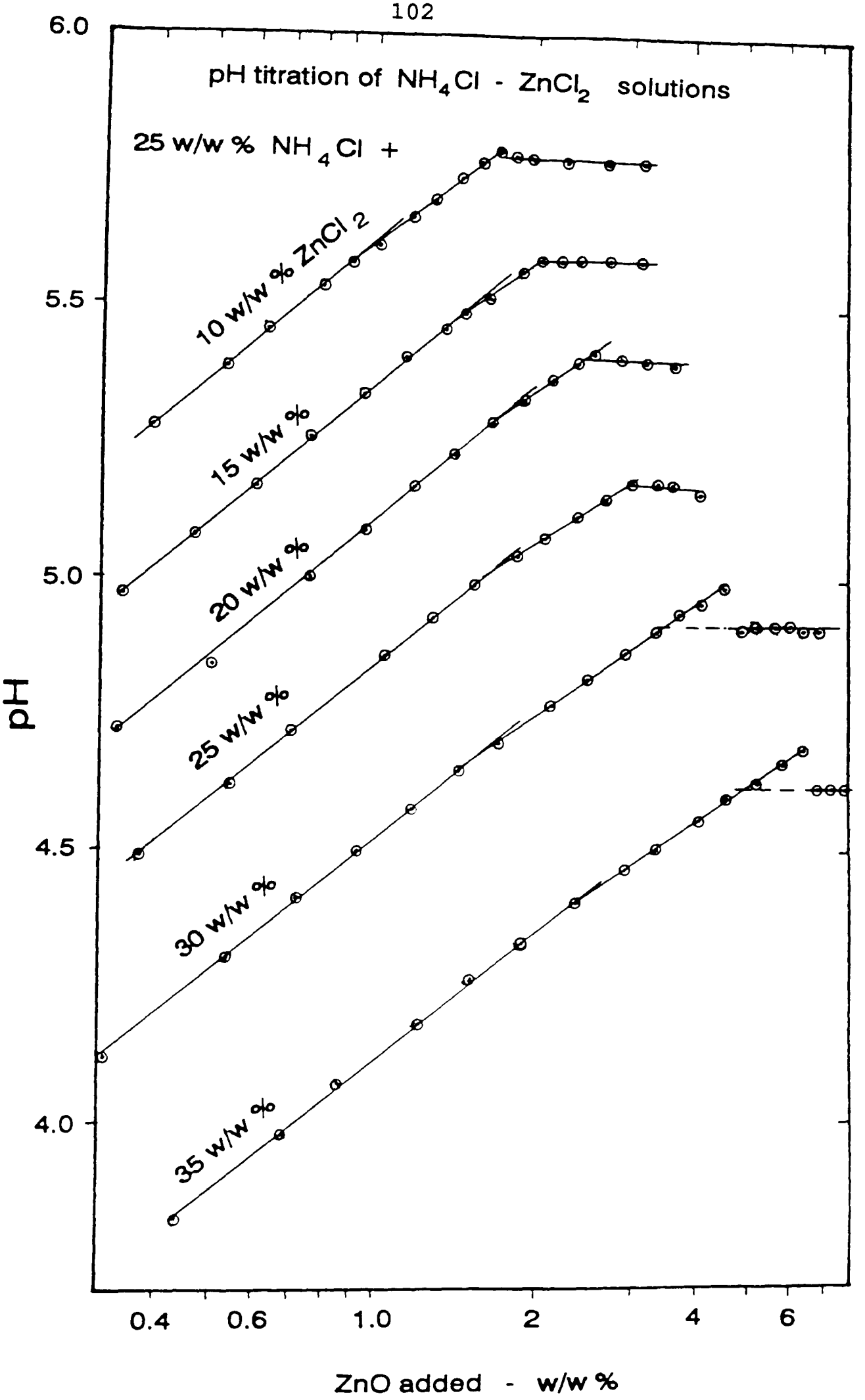

Figure 3.17 : pH titration by ZnO of solutions containing initially 25 w/w % NH_4Cl

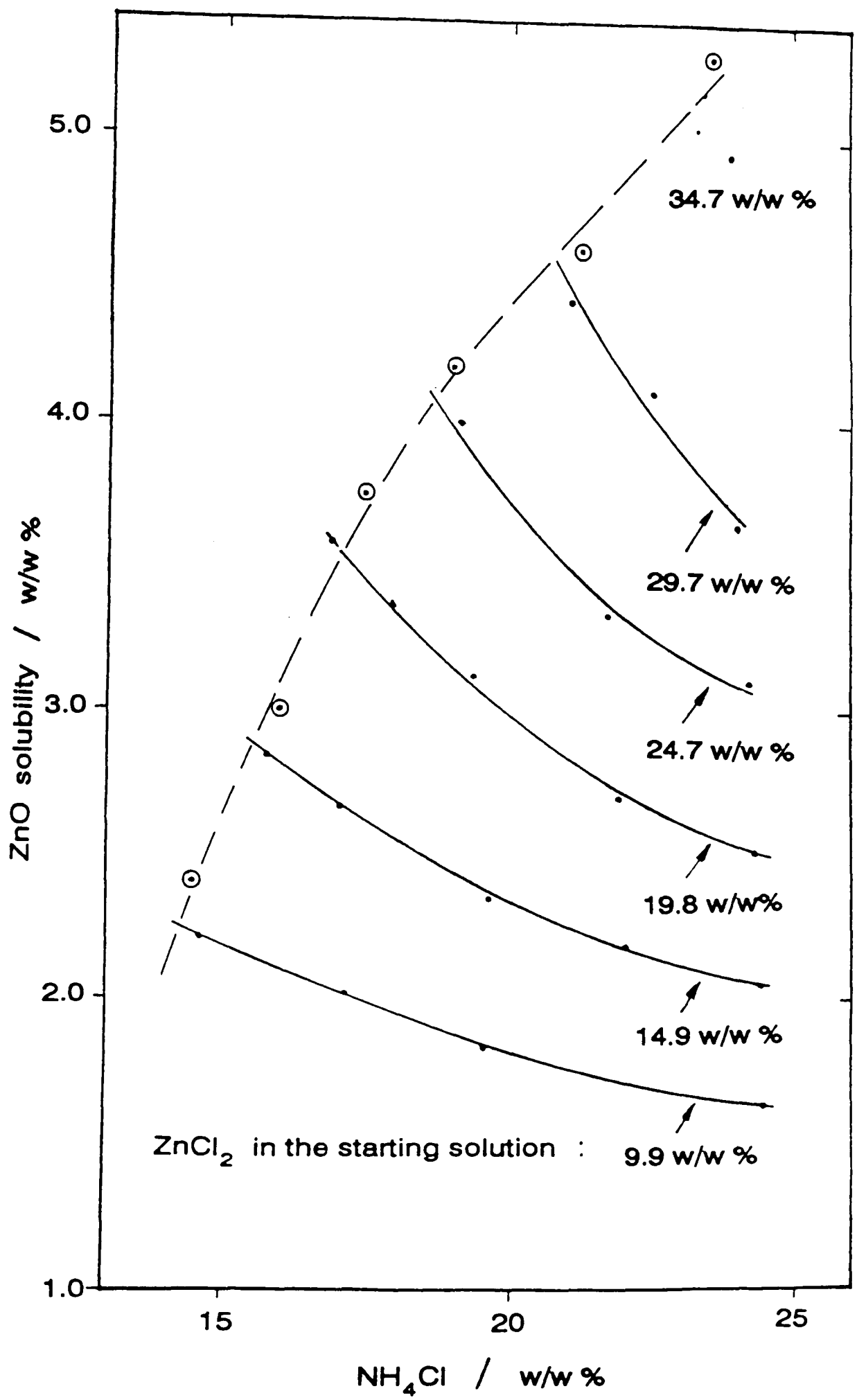

Figure 3.18 : ZnO solubility versus NH_4Cl concentration; ⊙ calculated, • from titration curve

The change of the slope in the second part of the curves shows a different overall reaction and equation (3.24) may be accompanied by a reaction such as

$$Zn(OH)^+ + NH_4^+ \longrightarrow Zn(OH)(NH_3)^+ + H^+ \qquad (3.25)$$

The calculation of the solution composition at the transition point (C in figure 3.14) requires the knowledge of the solution composition at the onset of the $Zn(NH_3)_2Cl_2$ precipitation (point B in figure 3.14) and of the proportion of the added ZnO which was precipitated as $Zn(NH_3)_2Cl_2$. At B, the solution composition could be calculated by using the mass balances of the different solution components, but at C the quantity of ZnO dissolved in the solution was required. The ZnO solubility has been measured by the same pH titrations as in figure (3.17) and the results are shown in figure (3.18). Each curve corresponds to a common $ZnCl_2$ initial concentration (10, 15, 20...35 w/w %). By chemical analyses, the starting zinc chloride was found to correspond to the formula $ZnCl_{1.98}$ i.e., 1 % of the initial total zinc could be considered as ZnO. Robinson and Stokes [193] and Lutfullah *et al.* [26] also found an excess of zinc in their analytical grade $ZnCl_2$ the main impurity being ZnO (maximum 1.2 % in this case [202]). The ZnO solubility shown in figure (3.18) includes this initial ZnO concentration and the zinc chloride concentrations (curve labels) are corrected for it. Consequently, they represent stoichiometric $ZnCl_2$ concentrations. The abscissa is the NH_4Cl content of the solution saturated by ZnO (calculated from the mass balance). Figure (3.18) shows that the ZnO solubility increased very much with increasing $ZnCl_2$ and decreasing NH_4Cl concentrations in agreement with the work of Sasaki and Takahashi [32]. In figure (3.18), the circled points are the positions of the transition points (corresponding to figure 3.16) calculated as described below, and the dashed line is the $Zn(NH_3)_2Cl_2$ stability limit. If this line is extrapolated to higher $ZnCl_2$ concentrations, it appears that the NH_4Cl concentration necessary to form $Zn(NH_3)_2Cl_2$ on ZnO addition would become larger than 25 w/w % which is impossible due to the decrease in the NH_4Cl solubility at high zinc chloride concentration [19, and section 3.3]. In such conditions, $Zn(NH_3)_2Cl_2$ could not be formed.

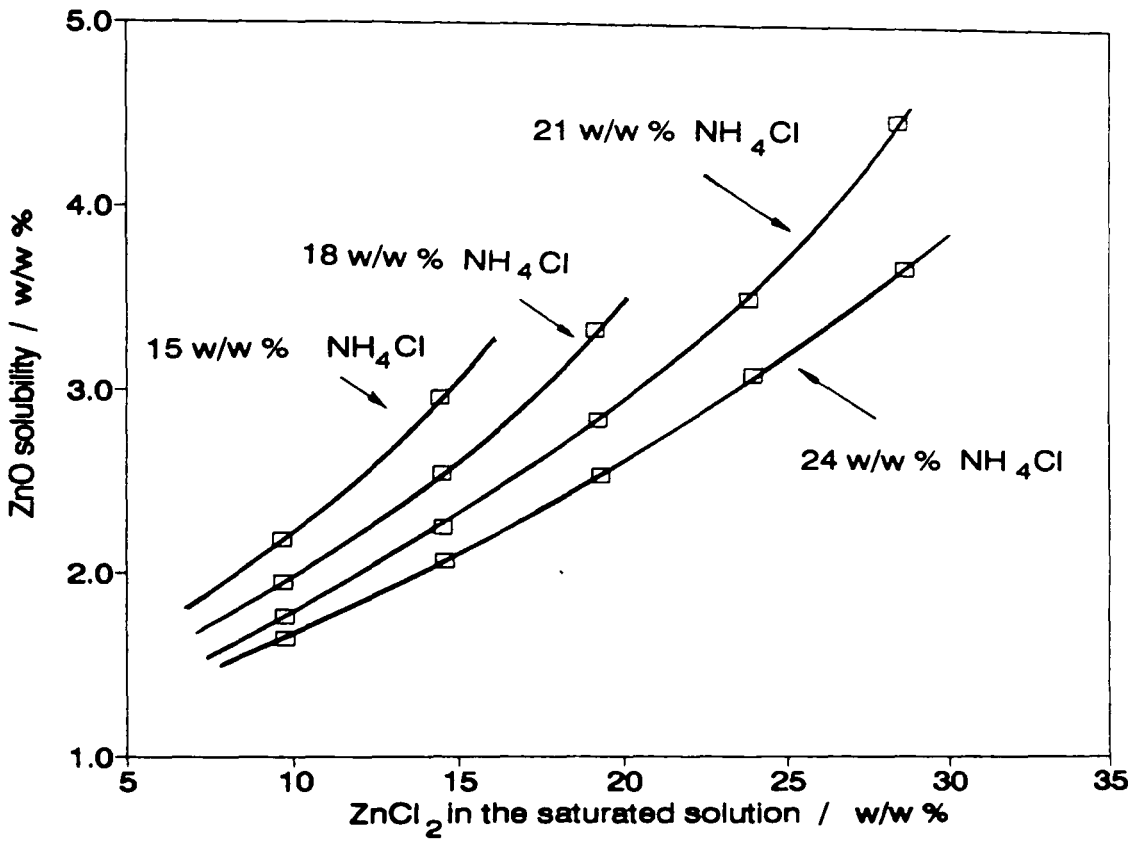

Figure 3.19 : ZnO solubility versus $ZnCl_2$ concentration

Figure (3.19) shows how the ZnO solubility changed with the $ZnCl_2$ concentration in the starting solution. These data were taken from figure (3.18) at different NH_4Cl concentrations in the solution saturated by ZnO. It shows that a good approximation of the ZnO solubility could be found from figure (3.18) by a linear interpolation - extrapolation procedure. It is therefore possible to determine graphically, from figure (3.18), the ZnO solubility in any solution at saturation and particularly in the solutions along the line BC in figure (3.14) since all these solutions were saturated with ZnO, the excess ZnO having been precipitated as $Zn(NH_3)_2Cl_2$.

3.2.2 Calculation procedure

Let Z, N and Q_1 be the "ZnO-free" $ZnCl_2$, the NH_4Cl and the initial ZnO content of the starting solution, in w/w %, (point A, see figure 3.14) and let us consider 100 g of starting solution. Let also Q_2 be the ZnO (g) added between

A and B (to saturate the solution). At the onset of the $Zn(NH_3)_3Cl_2$ precipitation (point B), the solution composition is

- total mass = $100 + Q_2$ (g)
- soluble ZnO = $Q_1 + Q_2$ (g)
- $NH_4Cl = N$ (g) and

  $ZnCl_2 = Z$ (g)

From B to C, addition of ZnO caused the precipitation of $Zn(NH_3)_2Cl_2$ according to equation (3.21) and hence a decrease in the amount of soluble NH_4Cl. This, as is evident from figure (3.18), increased the ZnO solubility. Let Q_3 (g) be the ZnO quantity added between B and C. Only a fraction f of it caused the precipitation of $2.093\, fQ_3$ g of $Zn(NH_3)_2Cl_2$. The remaining, $(1\text{-}f)Q_3$ g dissolved. The NH_4Cl consumed by reaction (3.21) was then $1.315\, fQ_3$ g (the numerical factors 2.093 and 1.315 derived from the stoichiometry of equation 3.21). At this stage, the solution mass (g) was $100 + Q_2 + (1 - 2.093\, f)Q_3$ and the concentrations (w/w %) in the solution were n, z and Q_4 for NH_4Cl, $ZnCl_2$ and ZnO respectively, with

$$n = \frac{100\,(\,N - 1.315\,f\,Q_3\,)}{100 + Q_2 + (\,1 - 2.093\,f\,)\,Q_3} \qquad (3.26)$$

$$Q_4 = \frac{100\,(\,Q_1 + Q_2 + f\,Q_3\,)}{100 + Q_2 + (\,1 - 2.093\,f\,)\,Q_3} \qquad (3.27)$$

$$z = \frac{100\,Z}{100 + Q_2 + (\,1 - 2.093\,f\,)\,Q_3} \qquad (3.28)$$

In equations (3.26),(3.27) and (3.28), the variables (n, z and Q_4) are functions of known values (N, Z, Q_1, Q_2 and Q_3) and of one unknown parameter f.

Assuming a value for f, it was possible to calculate the value of these variables and then, from figure (3.18), to find the ZnO solubility Q' at n w/w % NH_4Cl and z w/w % $ZnCl_2$. By trial and error, these calculations were repeated for different values of f until Q' and Q_4 agreed within 0.1 % (estimated uncertainty on the ZnO solubility).

Table (3.1) gives the results of the calculations in the form of the total soluble zinc ($ZnCl_2$ + soluble ZnO expressed as $ZnCl_2$) and NH_4Cl concentration along with the solution pH, the zinc electrode potential (converted to the standard hydrogen scale using E_{SCE} = 0.244 V vs.SHE [203]) and the value of f corresponding to the transitions points.

Table 3.1 : composition of the solution at the transition point.

	f	$ZnCl_2$ / w/w%	NH_4Cl / w/w%	pH	E_{Zn} / mV v.SHE
1	0.94	14.7	14.5	5.83	-794
2	0.91	20.7	15.9	5.63	-781
3	0.89	26.8	17.4	5.40	-770
4	0.80	32.9	19.0	5.15	-757
5	0.80	37.1	20.2	4.90	-743
6	0.80	42.1	22.5	4.62	-726.5

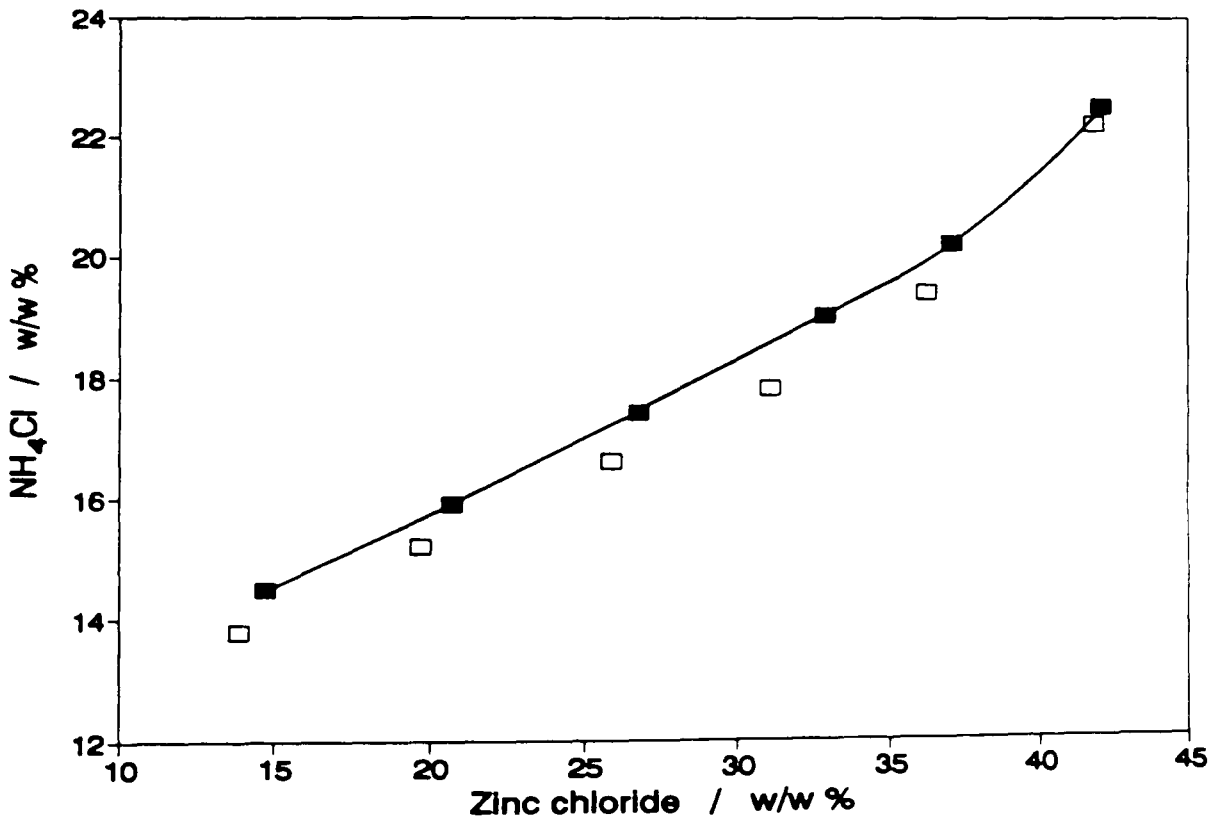

Figure 3.20 : Transition point versus $ZnCl_2$ concentration; ■ from table (3.1), □ values assuming f=1

The trend in the value of f corresponding to the transition point is parallel to the increase of slope of the ZnO solubility curves with increasing $ZnCl_2$ concentration. This reflects the increasing influence of the NH_4Cl concentration on the ZnO solubility with increasing $ZnCl_2$ concentration. The results from table (3.1) are compared in figure (3.20) to the values found assuming $f = 1$.

3.2.3 The free energies of formation of $Zn(NH_3)_2Cl_2$ and of $ZnCl_2.4Zn(OH)_2.H_2O$

The data from table (3.1) were also used to estimate the free energy of formation of $ZnCl_2.4Zn(OH)_2.H_2O$ using the method given by Tye [18]

$$\Delta G_f^0 = 10FE_{Zn} + 2(\Delta G^0_{Cl^-} + RTlna_{Cl^-}) + 9(\Delta G^0_{H_2O} + RTlna_{H_2O}) + 18.42RT\,pH \qquad (3.29)$$

In equation (3.29), the ΔG^0 are the free energies of formation of the different species and are taken from [191], E_{Zn} is the zinc electrode potential, R and T have their usual significance and the water (a_{H2O}) and chloride ion (a_{Cl-}) activities are taken from the work of Sasaki and Takahashi [32]. Equation (3.29) is derived from the equilibrium

$$5Zn^{2+} + 2Cl^- + 9H_2O \rightleftharpoons ZnCl_2.4Zn(OH)_2.H_2O_{solid} + 8H^+ \qquad (3.30)$$

Use of the values from table (3.1) in equation (3.29) gave the results shown in table (3.2). No value has been found in the literature.

Table 3.2 : The free energy of formation of $ZnCl_2.4Zn(OH)_2.H_2O$

Solution n°	free energy of formation / kJ mol^{-1}	
1	- 2898.8	
2	- 2896.9	
3	- 2898.6	average = - 2899.7 kJ mol^{-1}
4	- 2900.1	Relative Standard Deviation = 0.07 %
5	- 2901.0	
6	- 2903.0	

At the end of the titration by ZnO of a solution containing about 20 w/w % $ZnCl_2$ and a large excess of solid NH_4Cl, the pH was 5.47 and the zinc electrode potential E_{Zn} = -1.073 V vs. SCE or -0.829 V on the hydrogen scale. These conditions corresponded to the equilibrium

$$Zn^{2+} + 2NH_4Cl_{solid} \rightleftharpoons Zn(NH_3)_2Cl_{2\ solid} + 2H^+ \qquad (3.31)$$

and the $Zn(NH_3)_2Cl_2$ free energy of formation ΔG^0 is [18]

$$\Delta G^0 = 2FE_{Zn} + 2\Delta G^0_{NH_4Cl} + 4.606RT\ pH \qquad (3.32)$$

where the symbols have the same meaning as in equation (3.29). With the free energies of formation taken from [191], the result was ΔG^0 = -497.3 kJ mol^{-1} in reasonable agreement with the value given by Tye [18] (-504.8 kJ mol^{-1}) and by Takahashi and Sasaki [51] (-503.3 kJ mol^{-1}).

Application of equations (3.29) and (3.32) requires the knowledge of single electrode potential (E_{Zn}); equation (3.28) also requires the knowledge of a single ion activity (a_{Cl^-}) which are not measurable quantities.

Remembering that the pH was measured using a glass electrode and that Sasaki and Takahashi [32] measured the Cl^- activity by using a silver electrode, the results ΔG_f given in table (3.2) may be written in terms of electrode potentials as

$$\begin{aligned}\Delta G_f = {} & 10F(E_{Zn}+D_1) + 9(\Delta G^0_{H_2O} + RTlna_{H_2O}) \\ & + 2\Delta G^0_{Cl^-} + 2RT[\ \ln K_s - \frac{F}{RT}(E_{Ag^-}+D_2 - E^0_{Ag})] \\ & -8\ RT[\ \frac{F}{RT}(E_{H^+}+D_3-E^0_{H^+})]\end{aligned} \qquad (3.33)$$

where D_1, D_2 and D_3 are the diffusion potentials affecting the measured zinc, silver and glass electrode potentials, K_s is the AgCl solubility constant and the E_0s are the standard silver and glass electrode potentials.

Equation (3.29), also written in terms of electrode potentials reads

$$\Delta G_f^0 = 10FE_{Zn} + 9(\Delta G_{H_2O}^0 + RT\ lna_{H_2O}) + 2\Delta G_{Cl^-}^0 + 2RT[lnKs - \frac{F}{RT}(E_{Ag^+} - E_{Ag}^0)] - 8\ RT[\frac{F}{RT}(E_{H^+} - E_{H^+}^0)] \quad (3.34)$$

The error on the calculated free energies of formation is given by (3.33) - (3.34) or

$$\Delta G_f - \Delta G_f^0 = 10\ FD_1 - 2\ FD_2 - 8\ FD_3 \quad (3.35)$$

In this work, the zinc electrode potential was measured against a saturated calomel electrode using a saturated KCl salt bridge. The same saturated KCl salt bridge was used by Sasaki and Takahashi [32] to measure the silver electrode potential, and therefore the same diffusion potential affected both measurements and $D_1 = D_2$. In the pH measurements, the junction was between the electrolyte and a 3 molar KCl solution, i.e. very similar to the previous junctions. If we assume that both junctions behaved similarly in the same electrolyte, that is $D_3 = D_1$, the error on the calculated results (equation 3.29) becomes zero and the calculated values are insensitive to the effects of the junction potentials. The validity of this assumption is supported by the constancy of the calculated results despite the large variations of the solution composition.

The same argument applies to equation (3.32) for the measurement of the zinc electrode potential and of the pH.

3.3 The zinc electrode potential

3.3.1 The ammonium chloride solubility

The results of the titrations of the stoichiometric $ZnCl_2$ solutions by NH_4Cl are given in figure (3.21) along with the values of the zinc potential measured in specially prepared saturated solutions. The compositions of the solid phases corresponding to the latter solutions are given in table (3.3). They were measured by chemical analysis and identified by powder X-ray diffraction.

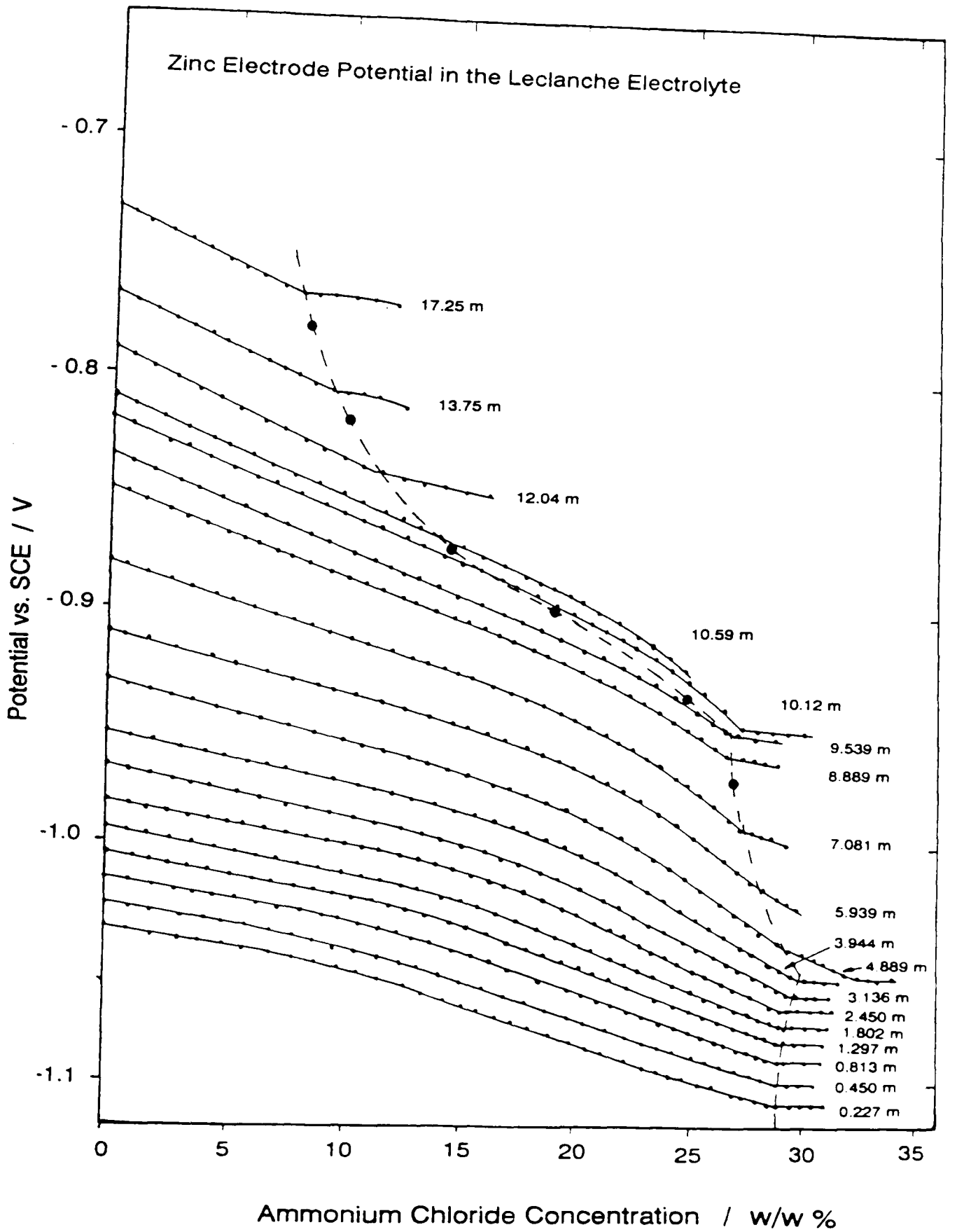

Figure 3.21 : Zinc electrode potential in $ZnCl_2$-NH_4Cl solutions. • results from titration measurements, ● measurements in saturated solutions, - - - saturation limit

Table 3.3 : Solid found in solutions saturated by NH_4Cl

	Potential mV	N/Zn ratio	Cl/Zn ratio	Composition (analysis and X-ray)
1.	- 972.6	2.96	4.97	$ZnCl_2.3NH_4Cl$
2.	- 936.6	2.07	4.25	$ZnCl_2.2NH_4Cl$+$ZnCl_2.3NH_4Cl$
3.	- 899.3	no analysis		
4.	- 873.4	2.58	4.56	$ZnCl_2.2NH_4Cl$+$ZnCl_2.3NH_4Cl$
5.	- 818.4	1.92	3.88	$ZnCl_2.2NH_4Cl$
6.	- 778.8	1.78	3.75	$ZnCl_2.2NH_4Cl$ + $ZnCl_2$?

The ratio Cl/Zn was found to be practically equal to (2 + N/Zn) indicating compounds with the general formula $ZnCl_2.nNH_4Cl$ with n = N/Zn. For sample 1 and sample 5, the X-ray diffractograms showed no other important peaks than those corresponding to $ZnCl_2.3NH_4Cl$ [204] and $ZnCl_2.2NH_4Cl$ [205] respectively. For samples 2 and 4, the peaks of both $ZnCl_2.3NH_4Cl$ and $ZnCl_2.2NH_4Cl$ appeared clearly, supporting the results of the chemical analyses which indicated a mixture of the two products. The simultaneous presence of both compounds in the solid phase may be due to the preparation procedure of the samples (dissolution of an excess NH_4Cl at about 70 °C and cooling in the air box at 25 °C). Sample 6 was probably contaminated by some $ZnCl_2$ as a result of an imperfect washing of the precipitate. None of these results contradict significantly the findings of Meerburg [58] and Cahoon [19]. As the $ZnCl_2$ concentration increased, on addition of NH_4Cl the solid phase was successively NH_4Cl, $ZnCl_2.3NH_4Cl$ and $ZnCl_2.2NH_4Cl$.

The composition of the saturated solution is given in table (3.4) and compared with Cahoon's data [19] at 21 °C in figure (3.22). The values were calculated at the break of the titration curves (fig.3.21) or given by the chemical analysis of the specially prepared solutions.

Table 3.4 : Composition of the saturated solutions

$ZnCl_2$ w/w %	NH_4Cl w/w %
2.1	28.95
4.1	29.0
7.1	29.05
10.7	29.1
14.0	29.2
17.7	29.35
21.1	29.6
24.5	29.9
28.4	29.1
32.3	27.9
35.6	27.4
38.6 *	27.1
40.0	26.9
41.4	26.8
42.3 *	25.0
47.3 *	19.3
51.2 *	14.4
55.0	11.5
57.3 *	10.1
59.0	9.6
63.1 *	8.4
64.6	8.0

* from chemical analysis of specially prepared saturated solutions.

The nature of the solid phase which was formed by NH_4Cl addition to the solution explains the shape of the titration curves (in figure 3.21) after the appearance of the solid phase. When the precipitate was NH_4Cl (solutions less than 4 molal $ZnCl_2$), any ammonium chloride added in excess of its solubility did not dissolve, the solution composition was not changed and the zinc potential remained constant. When the NH_4Cl addition induced the precipitation of $ZnCl_2.3NH_4Cl$ or $ZnCl_2.2NH_4Cl$, this addition decreased the zinc concentration in the solution driving the zinc potential towards more negative values; the plateaus were not horizontal. The curve corresponding to 4.89 molal $ZnCl_2$ shows three different parts. From 0 to 29 w/w % NH_4Cl, there was no solid phase in the solution: from 29 to 32 w/w %, the $ZnCl_2.3NH_4Cl$ precipitation decreased the soluble zinc

concentration until above 32 w/w % total added NH_4Cl, the new solid phase became NH_4Cl and the zinc electrode potential remained constant.

3.3.2 The zinc electrode potential

In pure zinc chloride solutions, the Nernst equation (e.g. equation 1.1) predicts an increase of the electrode potential of 2.303 RT/2F (29.6 mV) for a tenfold increase of the zinc activity. The results given in figure (3.21) show an increase by about 200 mV when the concentration increased from about 1 molal to about 10 molal. This corresponded to an increase of the zinc activity of more than 6 orders of magnitude which could not be explained by a similar change of the activity coefficient. The decrease of water activity in concentrated solution leads to a change of the electrode potential towards more positive values [206]. This influence is illustrated in figure (3.23) where the difference between the measured electrode potential and its value calculated from the Nernst equation is plotted versus minus logarithm of water activity (equation 1.15) [206,207]. The water activity data were taken from the works of Sasaki and Takahashi [32] and Stokes and Robinson [25].

The slope of the initial part of the curve suggests a hydration number of 18 in dilute solutions; this is of the same order of magnitude (12 to 18) as that used by Atlung *et al.* [34] and Jacobsen and Skou [208].

The decrease of the slope at low water activity was probably due to the decrease of the hydration number with increasing zinc chloride concentration [34,208].

The treatment proposed by Jacobsen and Skou [208] and used by Atlung *et al.* for their model of the separator region of a Leclanché cell [34] has been used to interpret the measured zinc electrode potentials. In this treatment, the different activity coefficients are considered as unity if the concentrations are expressed in the mole fraction scale of hydrated species.

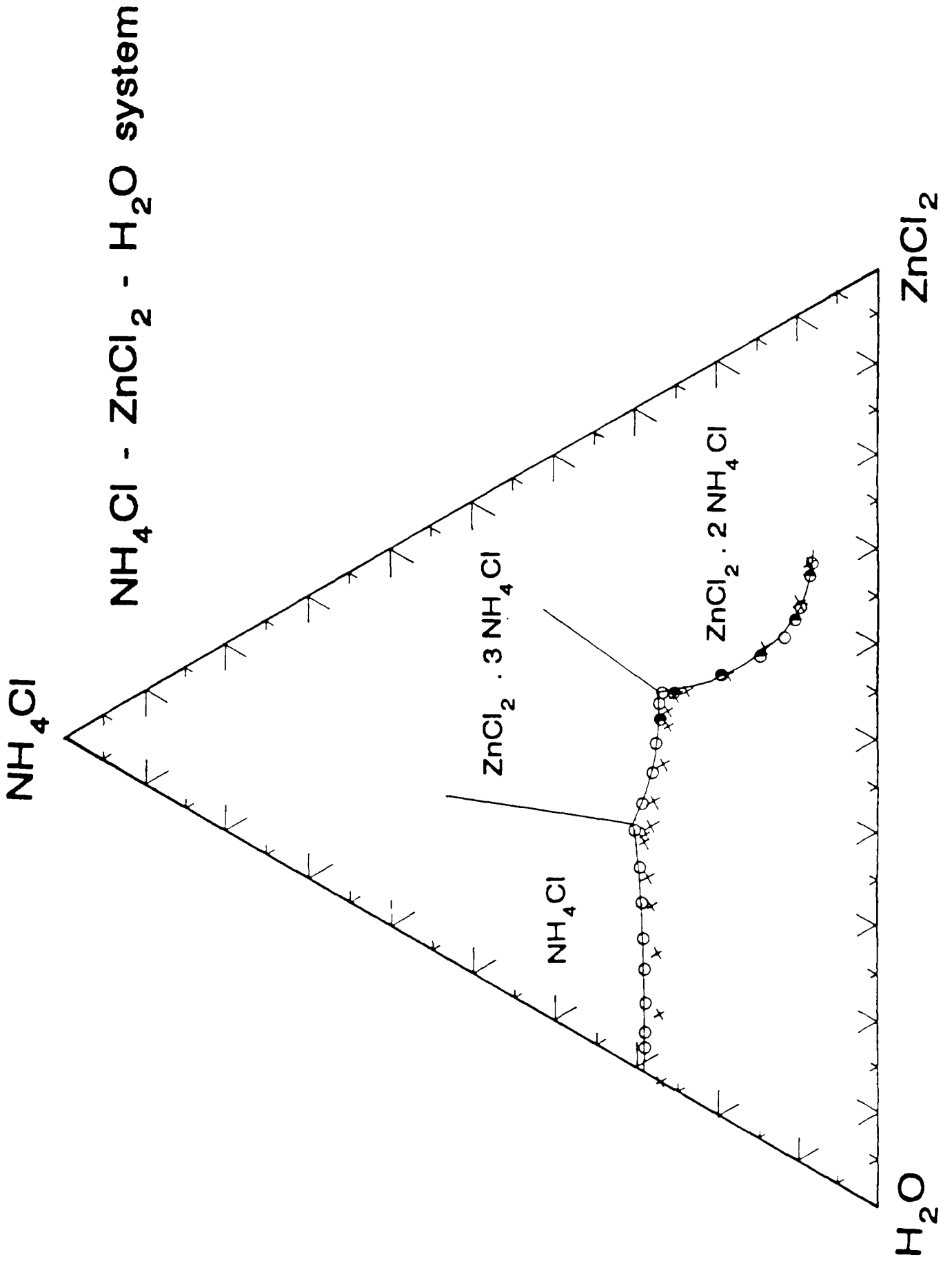

Figure 3.22 : Solubiiity diagram in NH_4Cl - $ZnCl_2$ solutions at 25 °C; ○ from potential measurements, ◑ analysis of saturated solutions, × from [19] at 21 °C

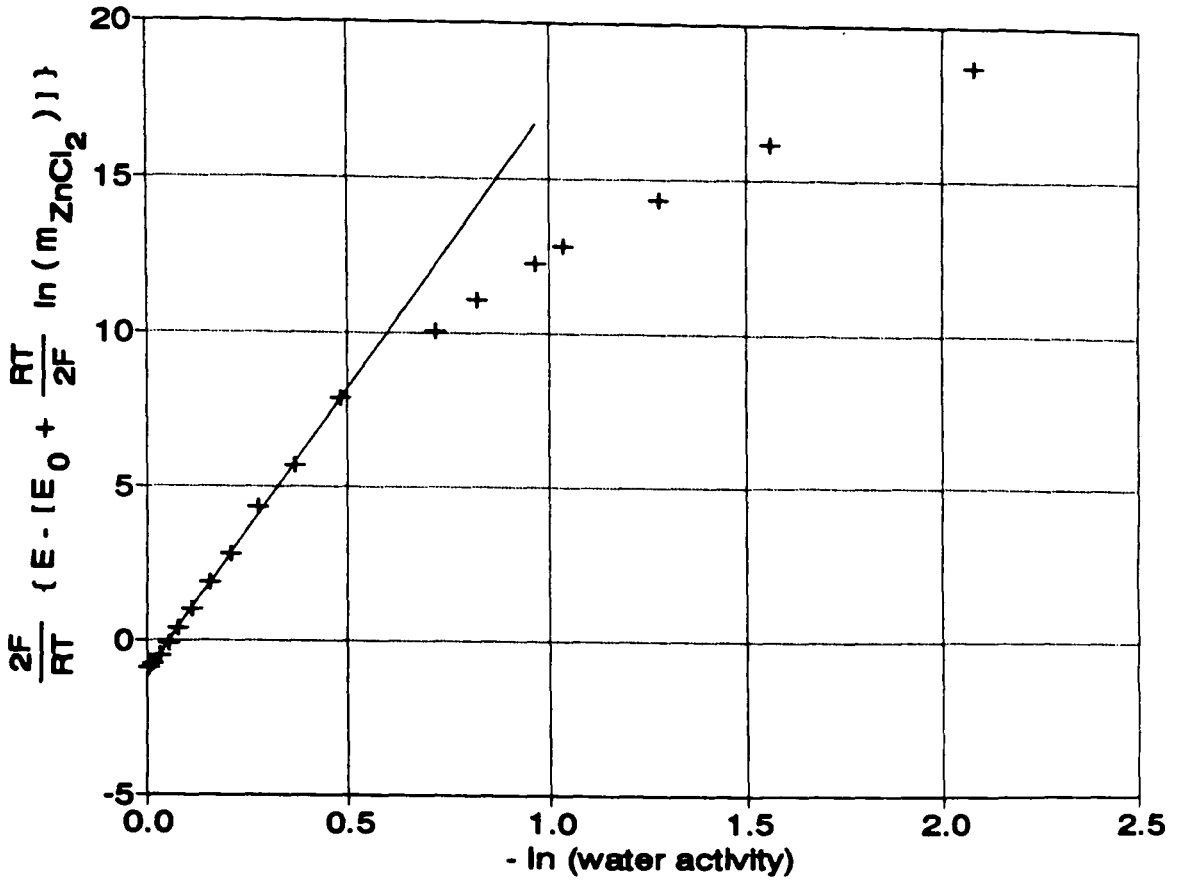

Figure 3.23 : Determination of the zinc hydration number; slope of the least square straight line = 18.4

The mole fraction X_i of the species i is given by

$$X_i = \frac{m_i}{N_t} \tag{3.36}$$

where m_i is the molality and N_t the total number of moles in the quantity of solution containing 1 kg of water. In this case, if N_w is the moles of free water (not bound in the hydration shell of a species), then

$$N_t = N_w + \sum_{i=1}^{n} m_i \tag{3.37}$$

where n is the number of species in addition to free water. The activities are replaced by the mole fractions [208] i.e.

$$a_i = X_i \tag{3.38}$$

The hydration of the non-complexed zinc is governed by the equilibrium

$$Zn\ (H_2O)_{N1}^{2+} \rightleftharpoons Zn\ (H_2O)_{N2}^{2+} + (N1 - N2)\ H_2O \qquad (3.39)$$

which equilibrium constant is

$$K = \frac{X_{Zn(H_2O)_{N2}^{2+}}\ X_w^{(N1-N2)}}{X_{Zn(H_2O)_{N1}^{2+}}} \qquad (3.40)$$

Jacobsen and Skou [208] proposed $N1 = 18$, $N2 = 12$ and $K = 0.0572$. The average zinc hydration number is [208]

$$h_0 = \frac{N1\ X_w^{(N1-N2)} + K\ N2}{X_w^{(N1-N2)} + K} \qquad (3.41)$$

The complexation reaction is written [34]

$$Zn(H_2O)_{h_0}^{2+} + i\ Cl^- \rightleftharpoons ZnCl_i(H_2O)_{h_0-\Delta h}^{(2-i)+} + \Delta h_i\ H_2O \qquad (3.42)$$

where Δh is the number of water molecules released by the complexation from the zinc hydration shell. The stability constant K_i of the complex containing i Cl^- is [33]

$$K_i = \frac{X_i\ X_w^{\Delta h}}{X_0\ X_{Cl}^i} \qquad (3.42)$$

where X_0, X_{Cl} and X_i are the mole fractions of the non-complexed zinc, free chloride and of the complex containing i Cl^-, respectively.

Skou *et al.* [33] proposed $K_1 = 45$, $K_2 = 0$, $K_3 = 45000$ and $K_4 = 450000$. They also proposed that each chloride replaced 4 water molecules in the zinc hydration shell, that is to say $\Delta h_1 = 4$, $\Delta h_2 = 8$, $\Delta h_3 = 12$ and $\Delta h_4 = 16$ for the mono-, di-, tri- and tetra-chloro complexes, respectively. When Δh_4 was negative, i.e. when the zinc hydration number, h_0, was lower than 16, they took $\Delta h_4 = h_0$ and considered the $ZnCl_4^{2-}$ complex as non-hydrated. NH_4^+ and Cl^- were regarded as non-hydrated [34]. In this work, the zinc hydration number was allowed to

become lower than 12 and in this case negative values of Δh_3 were also replaced by zero.

When the different equilibria are satisfied in a solution m_z and m_n, the molality of $ZnCl_2$ and NH_4Cl respectively, three mass balances must also be satisfied (see appendix 1 for the details of the calculations).

For water, the balance, Bal_w, is

$$Bal_w = 55.51 - (N_w + \sum_{i=1}^{n} h_i\, m_i) = 0 \qquad (3.44)$$

where h_i is the hydration number of the specie i.

For $ZnCl_2$, the balance, Bal_Z, is

$$Bal_z = m_z - m_0\,(1 + \sum_{i=1}^{4} K_i\, m_{Cl}^{i}\, N_t^{-i}\, X_w^{-\Delta h_i}) = 0 \qquad (3.45)$$

where m_i is the molality of the complex containing i Cl^-.

For chloride, the balance, Bal_C, is

$$Bal_c = (2m_z + m_n) - (m_{Cl} + m_0 \sum_{i=1}^{4} iK_i\, m_{Cl}^{i}\, N_t^{-i}\, X_w^{-\Delta h_i}) = 0 \qquad (3.46)$$

These equations are functions of N_w, m_0 and m_{Cl} only (see appendix 1 for details) and can be solved numerically for X_0, h_0 and X_w.

The zinc electrode potential was then calculated by [34]

$$E_{Zn} = E_0 + \frac{RT}{2F}\ln(X_0) - h_0\,\frac{RT}{2F}\ln(X_w) \qquad (3.47)$$

Atlung *et al.* [34] did not give the value they used for E_0 and expressed all the potentials relative to the zinc electrode potential in 1 molal $ZnCl_2$ solution.

The 8 constants of the model, namely the 5 equilibrium constants (K for the zinc hydration and K_1, K_2, K_3 and K_4 for the complexation), $N1$ and $N2$ (for the hydration equilibrium) and E_0 (the standard zinc electrode potential) have been used as fitting parameters in an iterative curve fitting to the measured zinc

potentials. A Pascal program based on the Nedler and Mead's optimisation algorithm [209] was used to minimise the goal function, G, given by

$$G = \sum_{i=1}^{n} f_i \, (E_{c,i} - E_{m,i})^2 \qquad (3.48)$$

where n is the number of points, $E_{c,i}$ and $E_{m,i}$ are the calculated and measured zinc electrode potentials, respectively, and f a factor used to give more importance to some points e.g. the potentials in pure zinc chloride solutions. A reduced set of 115 points (one point out of 3 measured points for some $ZnCl_2$ molalities mainly in the range 0.2 to 5 molal $ZnCl_2$) was used for this curve fitting in order to keep the computing time within acceptable limits.

The results are given in figure (3.24) where the calculated potentials are compared to the experimental values. The set of constants giving the minimum value to the goal function (equation 3.48) is compared in table (3.5) with the values from Atlung *et al.* [34].

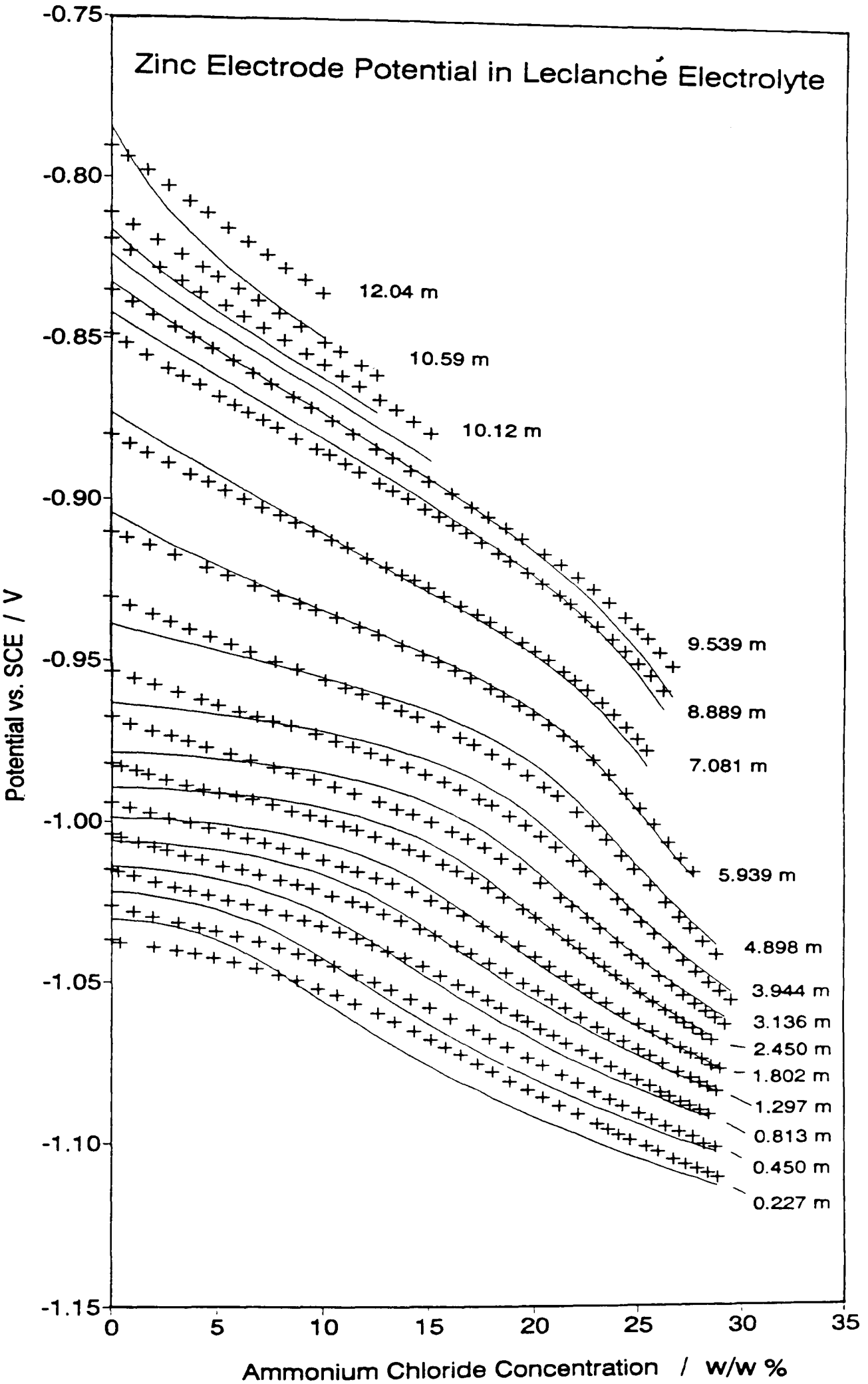

Figure 3.24 : + experimental and —— calculated zinc electrode potentials

Table 3.5 : constants used in the model of the solutions.

	This work	Atlung et al. [34]
Complexation constants:		
K_1	0.89	45
K_2	1.44	0
K_3	117000	45000
K_4	3056000	450000
Hydration constants:		
K	0.0518	0.0572
$N1$	16.48	18
$N2$	11.92	12
Standard Zinc potential:		
E_0	-961.8 mV	-955 mV (*)
Average deviation : 3.6 mV		-
Standard deviation : 4.6 mV		-
Maximum deviation : 14.0 mV		-

(*) estimated from the adjustment of the results to the measured potentials in pure zinc chloride solutions [47]

The electrode potentials measured before addition of NH_4Cl are shown in figure (3.25). The agreement between the calculated and the measured potentials is fairly good (better than 0.01 V), but the calculated values are systematically too negative in the range 2 to 6 molal and too positive above 6 molal $ZnCl_2$. The model completely fails above 12 molal $ZnCl_2$ where it gives far too high potentials. Atlung *et al.* [34] gave 10 molal $ZnCl_2$ as the upper limit of applicability of their model.

The calculated water mole fractions (X_w) are compared to the measured values of water activity in pure $ZnCl_2$ solutions [25,32] (figure 3.26) and in $ZnCl_2$ - NH_4Cl solutions [32] (figure 3.27).

Although the different constants of the model have been adjusted to fit the measured electrode potentials, figures (3.26) and (3.27) show that they also permit

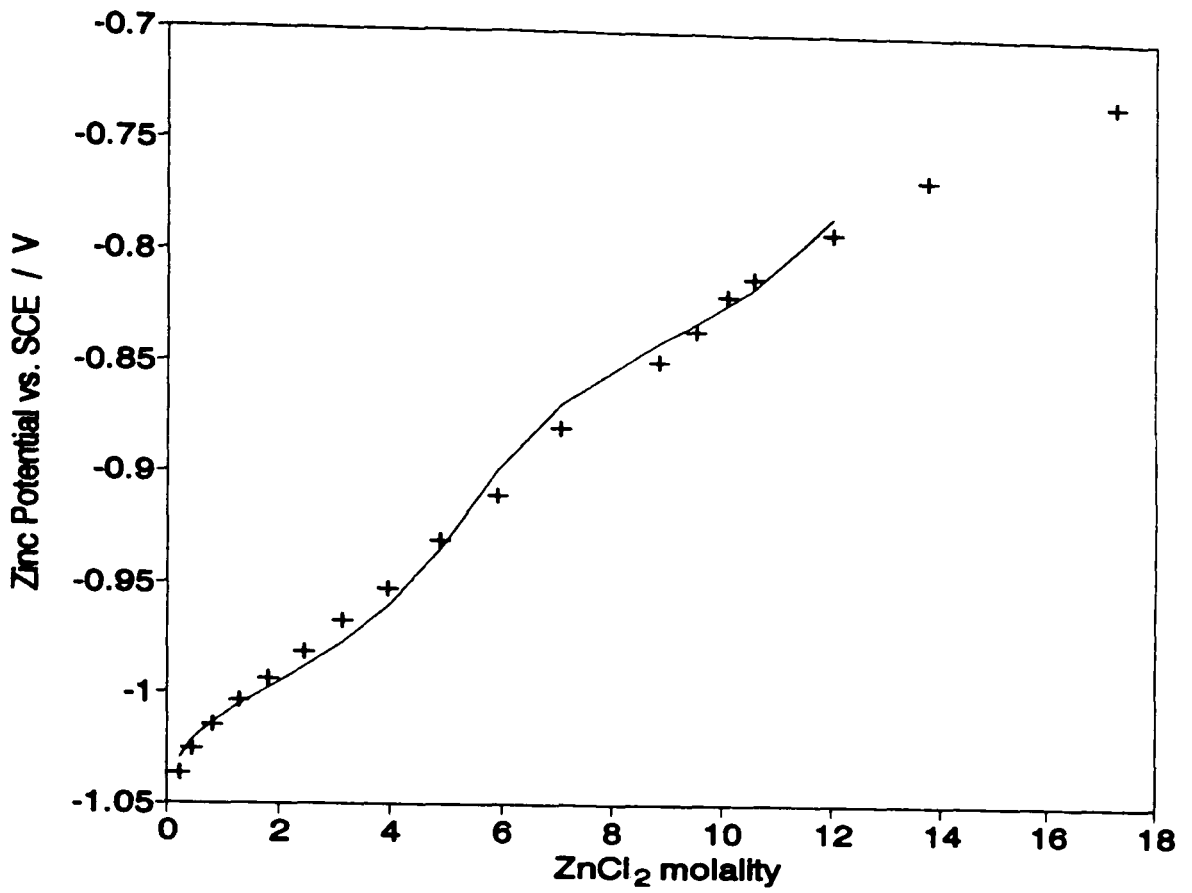

Figure 3.25 : —— calculated and + measured zinc electrode potentials (vs. SCE) in pure $ZnCl_2$ solutions

a fair prediction of the water activity in pure zinc chloride solutions and also in mixed NH_4Cl-$ZnCl_2$ solutions. Above 12 molal $ZnCl_2$ the model predicts a decrease of the free water mole fraction much steeper than was actually observed.

Figures (3.28) and (3.29) show the distribution of the different zinc complexes in 5 molal NH_4Cl solutions calculated with the parameters used by Atlung *et al.* [34] (figure 3.28) and with the parameters derived in this work from the fitting of calculated data with the experimental potentials (figure 3.29). Figure (3.29) shows that the concentration of the neutral complex $ZnCl_2$ was very low, that the predominant species above about 3 molal zinc chloride was the tri-chloro complex $ZnCl_3^-$ and the concentration of free chloride rapidly decreased with increasing zinc molality in agreement with the findings of Atlung *et al.*[34]. However, the calculated concentration of the $ZnCl^+$ complex was much lower in this work than previously reported [34], even in pure zinc chloride solution (figure 3.30), due to the very low value of its stability constant. The sevenfold increase of the $ZnCl_4^{2-}$

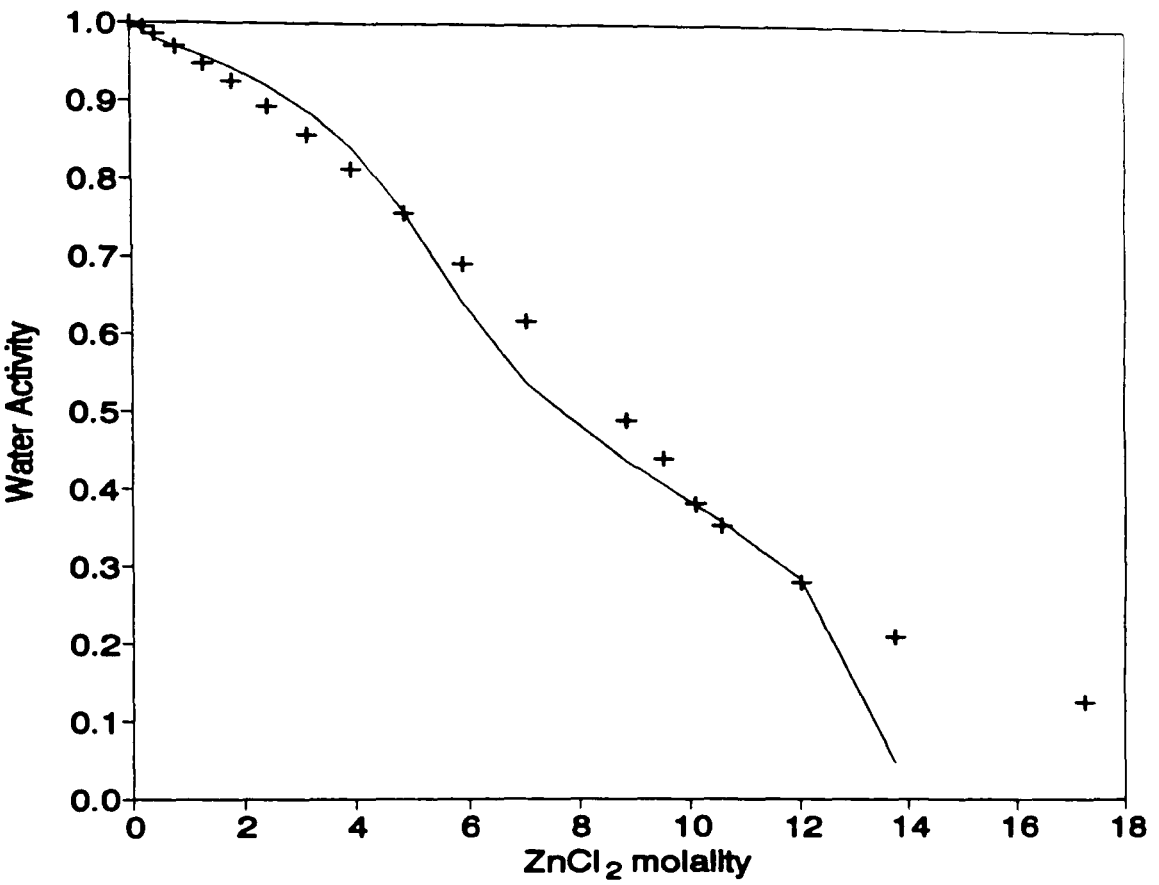

Figure 3.26 : —— calculated and + measured water activity [25,31] in pure $ZnCl_2$ solutions

stability constant (see table 3.5) does not affect significantly the species distribution. The decrease in the concentration of the latter complex at high zinc molality, in both sets of calculations, is in conflict with the figure 4 of Atlung *et al.* [34] which shows a monotonous increase of this concentration with increasing zinc chloride molality. This decay is most probably related to the practically total disappearance of the free Cl^- ion from the solution. In the pure zinc chloride solutions, chloro-complex concentrations became significant even at zinc molality as low as 0.5 molal, confirming earlier reports [26,27].

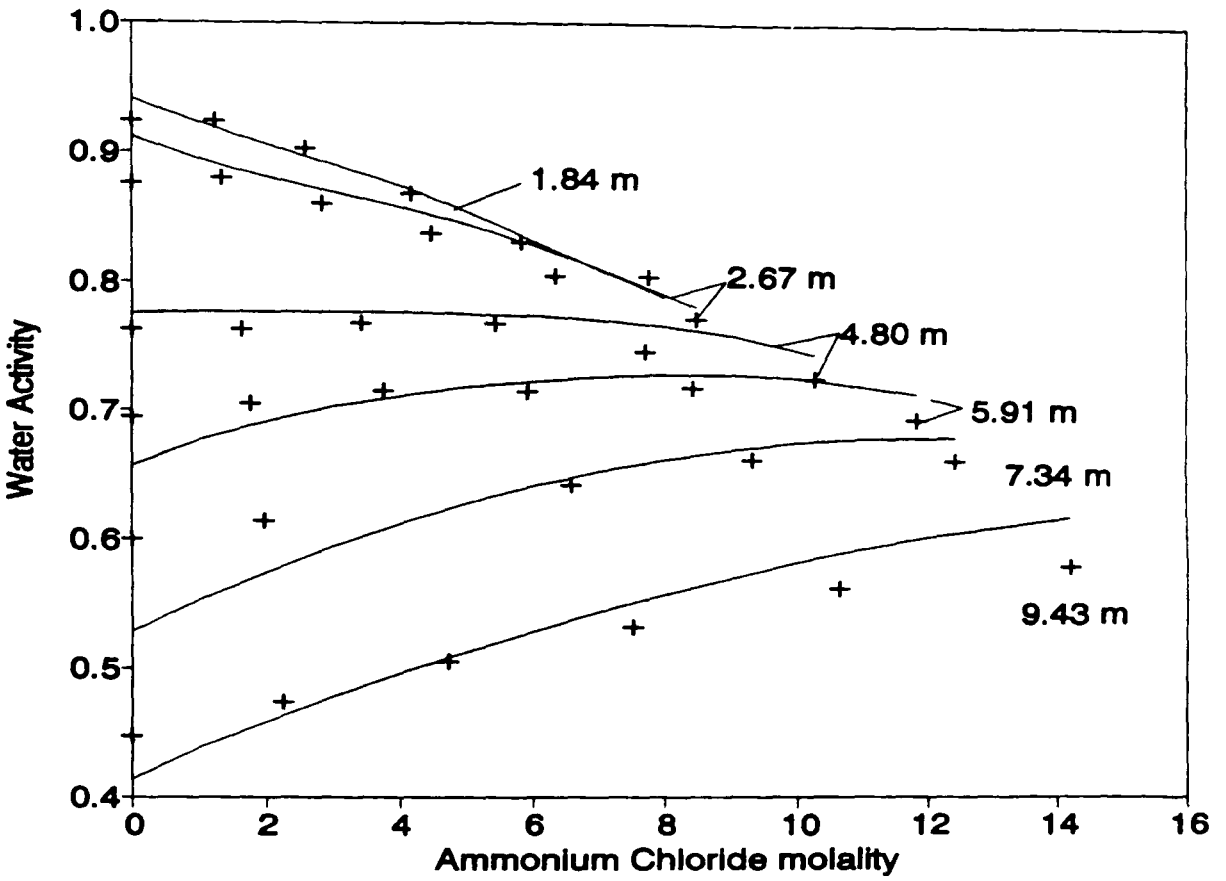

Figure 3.27 : —— calculated and + measured water activity [32] in NH_4Cl-$ZnCl_2$ solutions; the $ZnCl_2$ molalities are shown as parameters

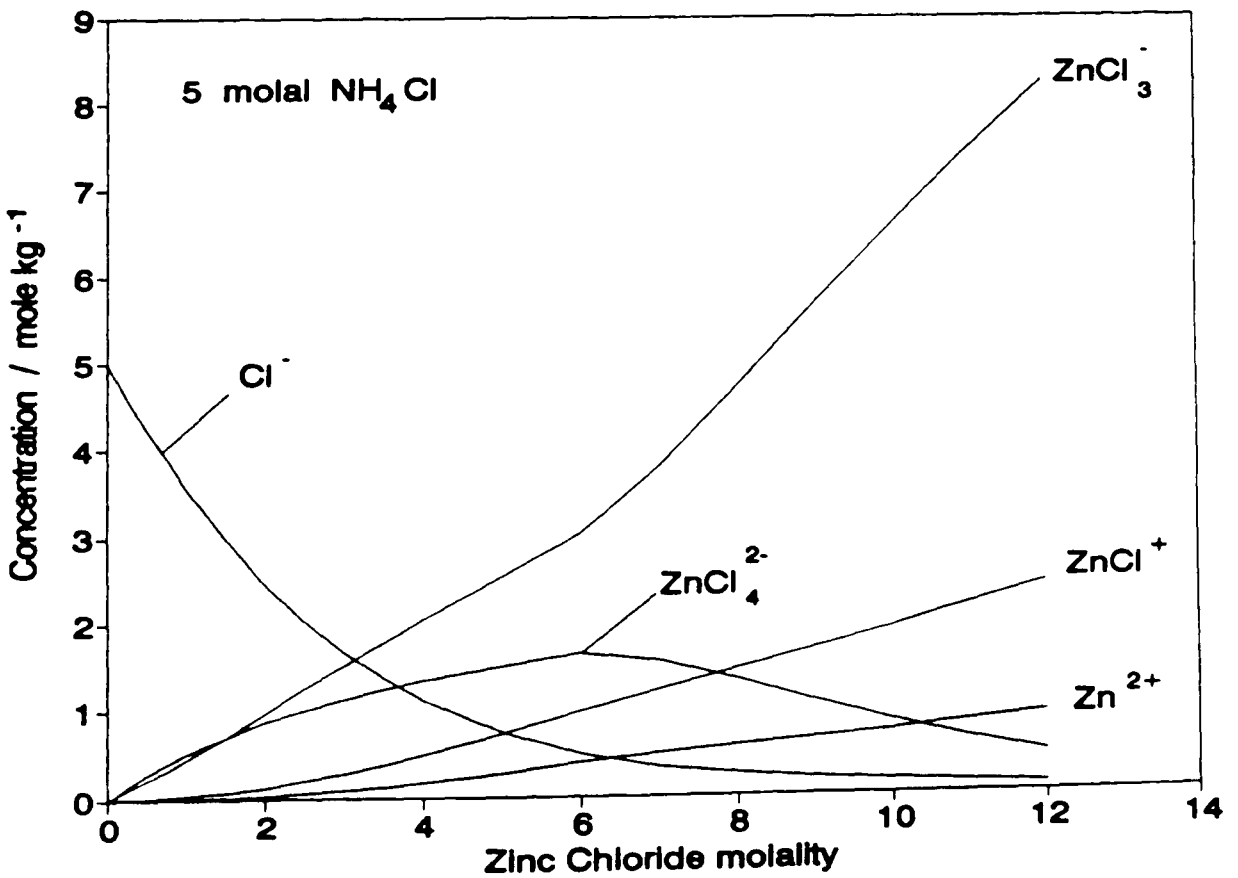

Figure 3.28 : Molalities of the different zinc species and chloride ion in 5 molal NH_4Cl solutions, model parameters taken from [34]

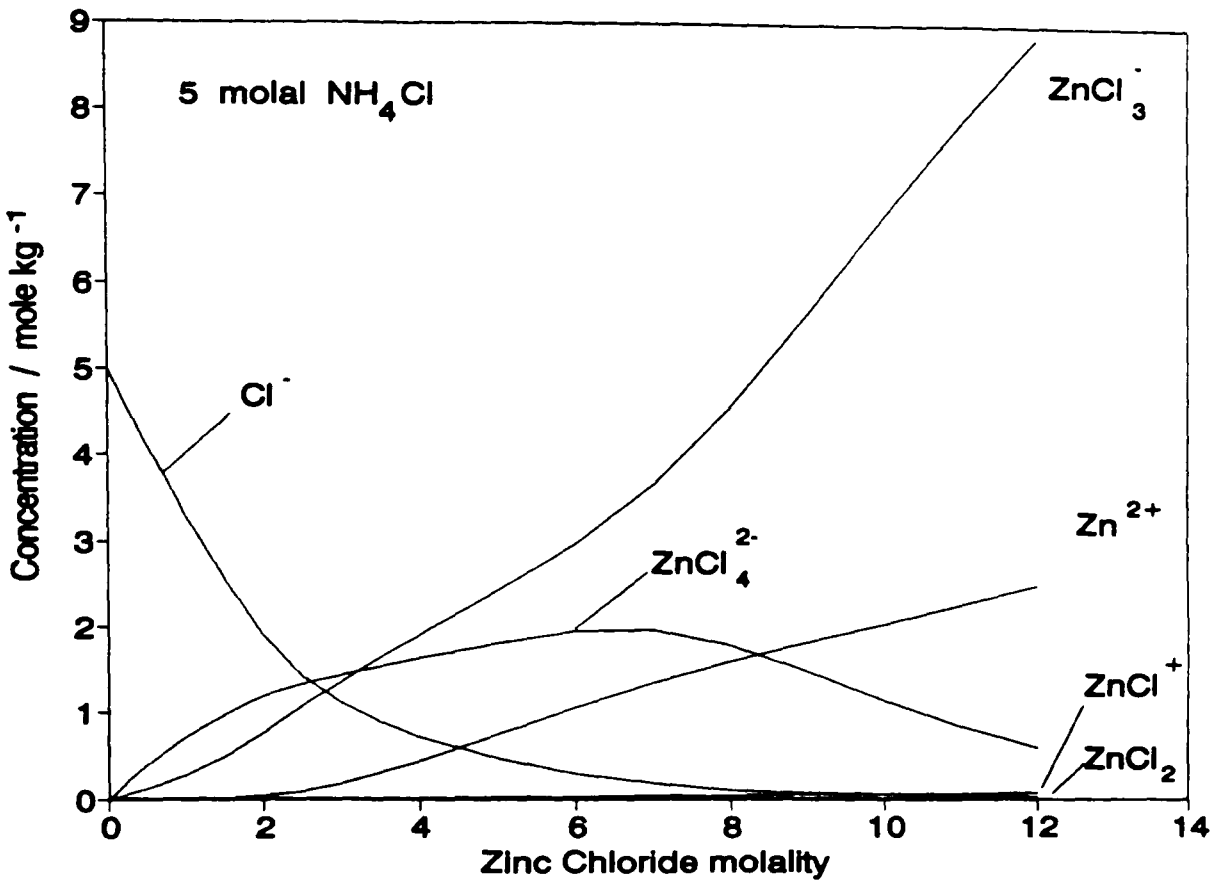

Figure 3.29 : Molalities of the different zinc species and chloride ion in 5 molal NH_4Cl solutions, model parameters obtained in this work.

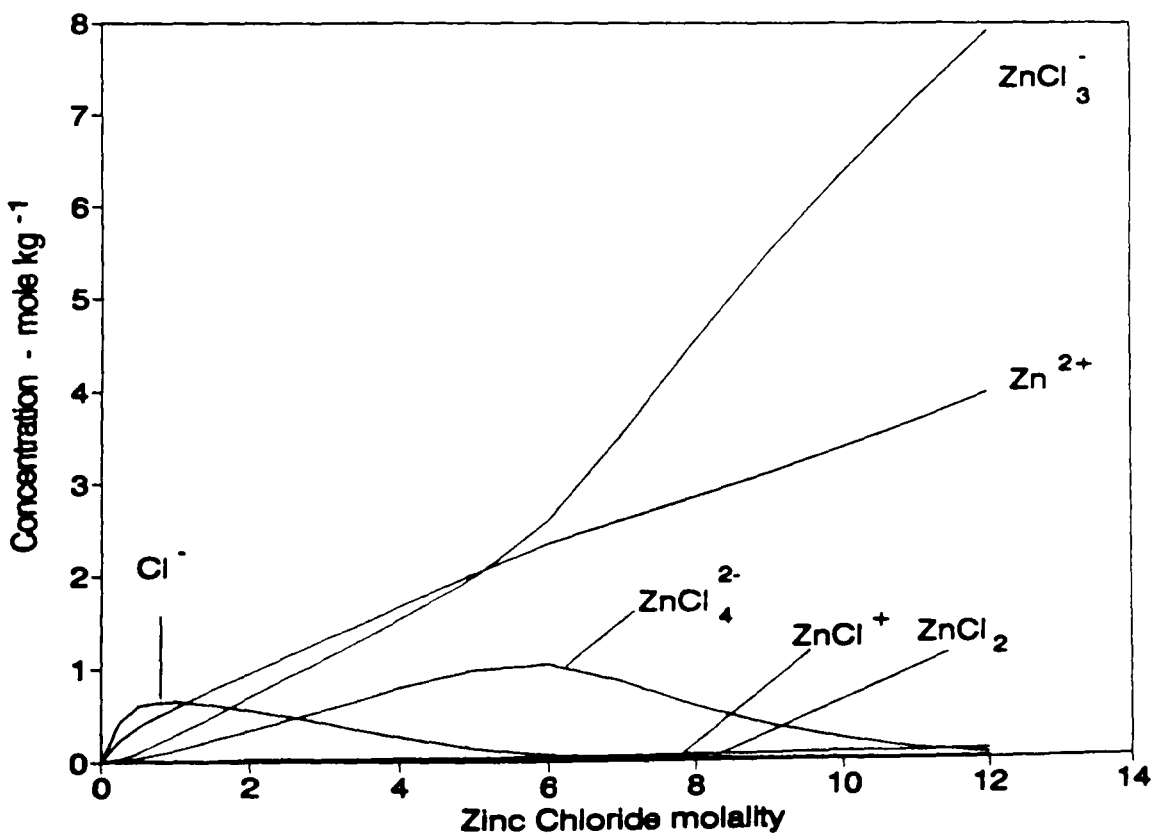

Figure 3.30 : Molalities of the different zinc species and chloride ion in pure $ZnCl_2$ solutions, model parameters obtained in this work.

3.4. Conclusions

The assumption of the formation of a weak $(NH_4)ZnCl_3$ complex permits the calculation of the densities of the ternary solutions with a good accuracy and explains semi-quantitatively the mixing behaviour of the solutions. Although the complexation equilibria were written using molecular concentrations, the agreement between the calculated and the measured densities was very good, showing that the assumption, implicit in the treatment used in this work, of associated species in the pure zinc chloride solutions was a reasonable assumption. The strong ionic association in pure zinc chloride solutions was confirmed by the analysis of the zinc electrode potential measurements.

The NH_4Cl concentration corresponding to the transition from the precipitation of $Zn(NH_3)_2Cl_2$ to the formation of $ZnCl_2.4Zn(OH)_2.H_2O$ increased with increasing $ZnCl_2$ concentration, as suggested by McMurdie *et al.* [50] but in contradiction with the results of Cahoon [19] and Friess [48]. This has two major consequences. At high zinc chloride concentration (above about 45 w/w %), the NH_4Cl solubility is too low to reach the transition level and the only stable precipitate is $ZnCl_2.4Zn(OH)_2.H_2O$. At lower zinc chloride concentrations, the formation of the zinc hydroxychloride decreases the $ZnCl_2$ concentration in the solution and also the concentration of NH_4Cl required to stabilize $Zn(NH_3)_2Cl_2$. As a consequence, both precipitates are simultaneously formed.

The potential of a zinc electrode in Leclanché electrolyte may be calculated fairly accurately by using a model of the solution initially proposed by Atlung *et al.* [34] and optimised by fitting to a large set of measured electrode potentials. The model accounts for the increase of the zinc potential with increasing zinc chloride concentration, for its decrease on NH_4Cl addition and also gives a fairly good estimate of the water vapour pressure above the different solutions. The accuracy of the calculated potentials decreases at concentrations higher than 10 molal zinc chloride and the model completely fails above about 12 molal $ZnCl_2$. The calculations appeared to be very sensitive to the parameters related to the zinc

species hydration and much less sensitive to the actual value of the different $ZnCl_i^{(2-i)+}$ stability constants. The failure of the model at high zinc chloride concentration is most probably related to its inability to predict the water activity in that range of concentrations.

The analysis of the zinc electrode potential measurements confirms the interpretation of density measurements that the tri-chloro complex is the predominant zinc species, except in solutions of low zinc chloride molality containing a large amount of NH_4Cl where the predominant complex is the $ZnCl_4^{2-}$ complex, and in pure zinc chloride solutions where the Zn^{2+} ions forms a significant fraction of the zinc species.

Although the average difference between the calculated and the experimental potentials is small (3.6 mV in the range 0.2 to 12 molal zinc chloride), the largest deviations are concentrated in particular regions, e.g. very low NH_4Cl concentration, showing that the model does not represent exactly the behaviour of the solution on NH_4Cl addition and requires refinement to lead to more reliable predictions in this region.

In its present stage of development, this model constitutes a useful tool for calculation of zinc electrode potential.

Chapter 4. Intermittent discharges

4.1. Electrodeposited manganese dioxide in Leclanché electrolyte

Figure (4.1) shows the results of a discharge through 4 ohms for 30 minute per day down to 0.9 V closed circuit voltage (CCV). From that point, the cell was further discharged for 15 minutes a day down to the same cut-off voltage. In figure (4.1) the potentials (versus a saturated KCl calomel electrode) are shown as a function of the coulombs delivered by the cell.

4.1.1 The zinc electrode potential

The three stages of the discharge predicted by Tye [13] are clearly apparent. From 0 to 3,500 coulombs, the electrolyte composition and the zinc electrode potential remained constant while the solid ammonium chloride was consumed. The overall cell reaction was [13]

$$Zn + 2NH_4Cl_{solid} + 2MnO_2 \longrightarrow Zn(NH_3)_2Cl_2 + 2MnOOH \qquad (1.36)$$

From 3,500 to 10,700 coulombs delivered by the cell the $Zn(NH_3)_2Cl_2$ precipitation continued following the overall equation

$$Zn + 2NH_4^+ + 2Cl^- + 2MnO_2 \longrightarrow Zn(NH_3)_2Cl_2 + 2MnOOH \qquad (1.37)$$

and the soluble NH_4Cl concentration decreased driving the zinc electrode potential towards more positive values (see section 3.3). This part of the curve is analogous to the line BC in figure (3.14).

When the cell had delivered more than 10,700 coulombs, the zinc electrode potential became more negative due to the precipitation of $ZnCl_2.4Zn(OH)_2.H_2O$, the main overall cell reaction became

$$4Zn + Zn^{2+} + 2Cl^- + 8MnO_2 + 9H_2O \longrightarrow ZnCl_2.4Zn(OH)_2.H_2O + 8MnOOH \qquad (1.38)$$

with the continuation, to some extent, of reaction (1.37) as showed in section (3.2).

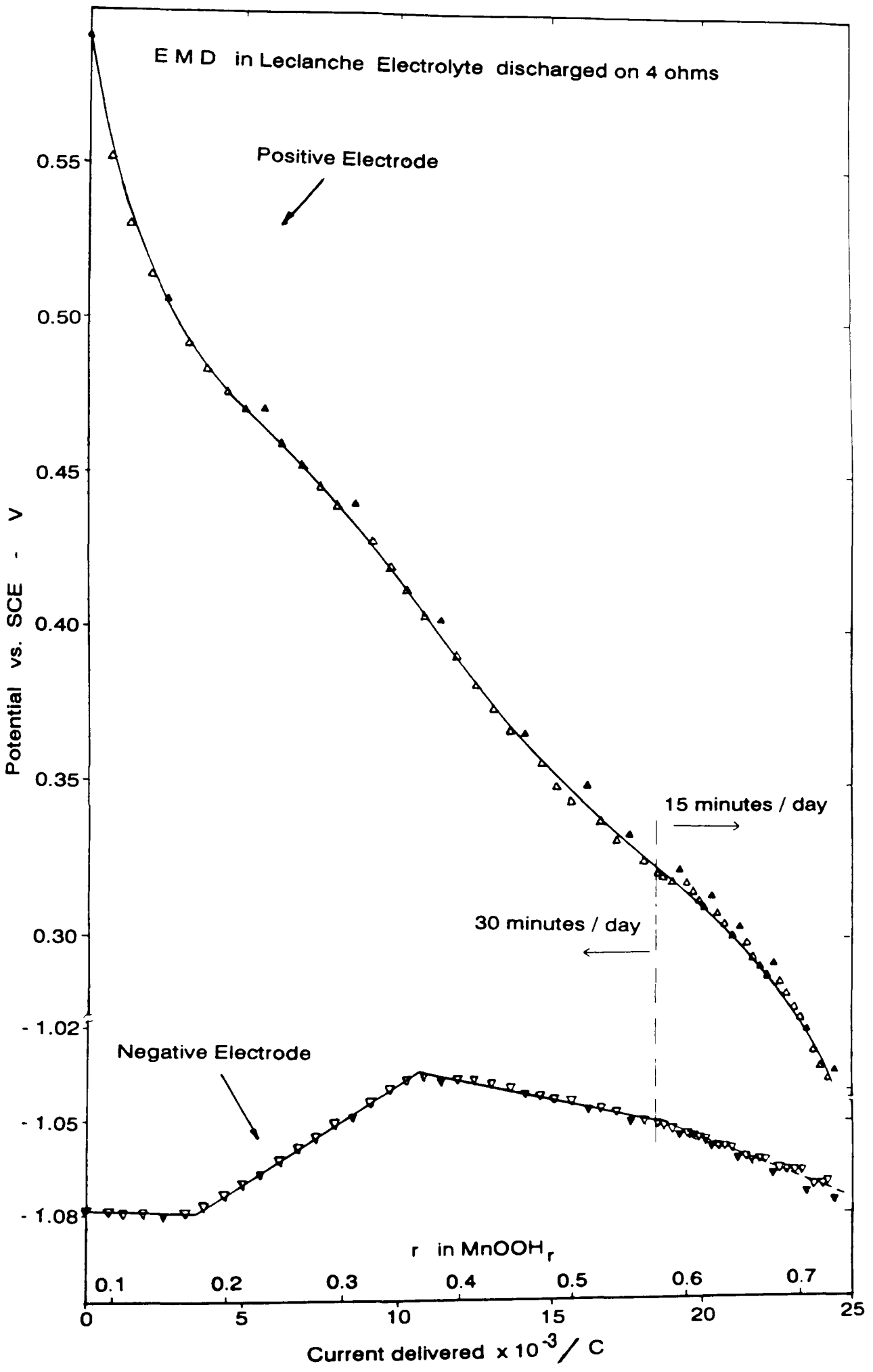

Figure 4.1 : Intermittent discharge of a cell containing EMD in Leclanché electrolyte; △,▽ 23.5 hour recovery; ▲,▼ 71.5 hour recovery

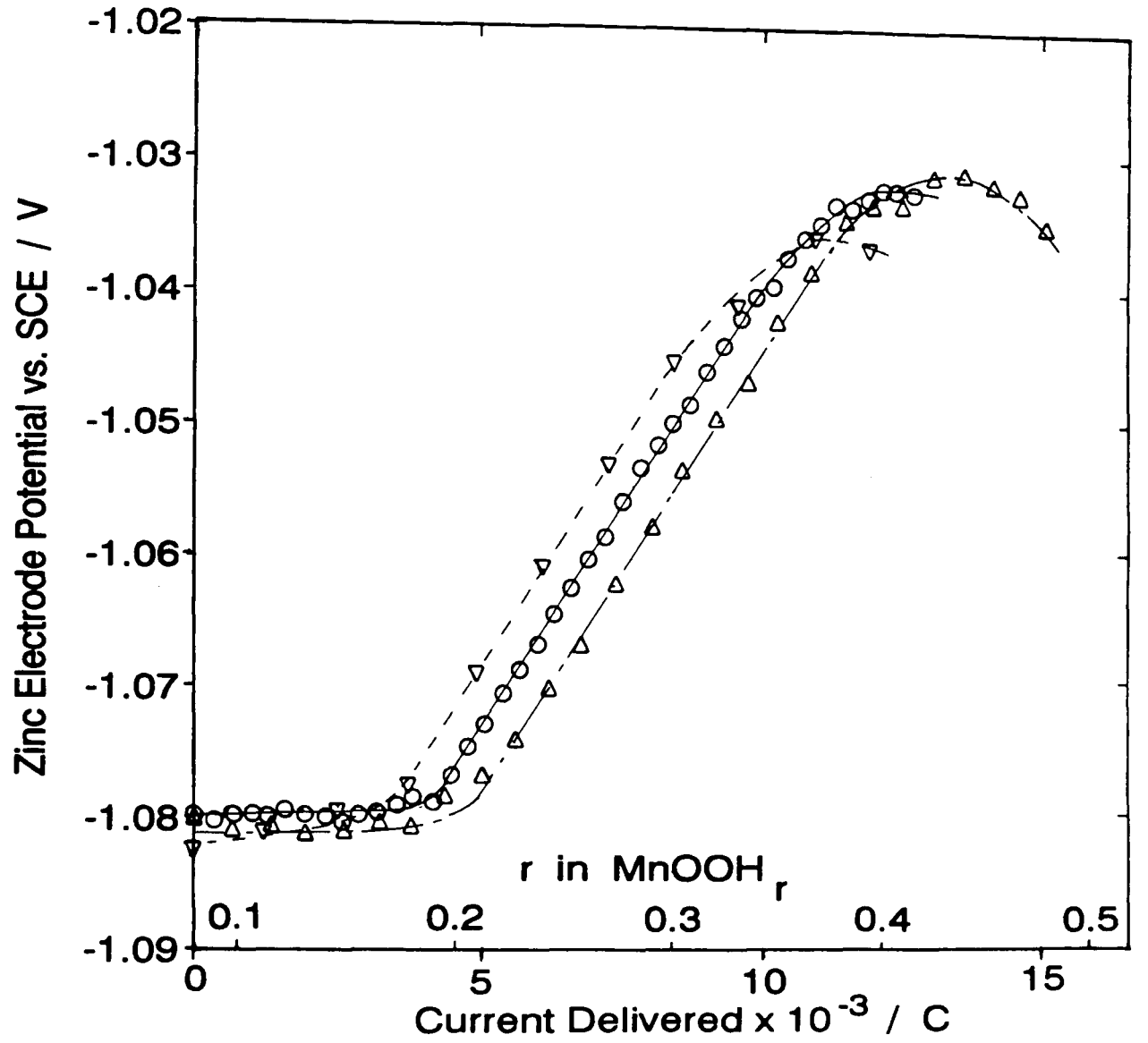

Figure 4.2 : Zinc electrode potential in cells containing EMD during intermittent discharge through 4 Ω; ○ 15 min d^{-1}, △ 30 min d^{-1}, ▽ 60 min d^{-1}

Figure (4.2) shows the zinc electrode potential for 3 cells discharged through 4 ohms for 15, 30 and 60 minutes a day. No trend can be seen in the position of the end of the initial plateaus which occurred between 3,500 and 4,500 coulombs.

The results of the chemical analyses of the electrolyte at different discharge levels are shown in table (4.1).

The electrolyte pH exhibited very little change from the undischarged cell to the end of the second discharge stage, suggesting that the electrolyte of the undischarged cells was fully buffered. The total increase of the pH for the most discharged cell corresponded to the value (about 1 pH unit) predicted by Tye [18].

The slight increase of the pH during the second stage of the discharge [18] was also apparent.

The same NH_4Cl concentration in cells 1 and 2 confirms the invariance of this concentration in the first stage of the battery discharge.

Table 4.1 : chemical analysis of the electrolyte

Current Delivered / C		pH	NH_4Cl w/w%	$ZnCl_2$ w/w%	Mn^{2+} ppm
1- 0		5.64	29.2	17.2	30
2- 1900	(a,d)	5.71	29.2	16.7	40
3- 11968	(b)	-	14.3	16.9	250
4- 12673	(c)	5.79	14.1	18.2	180
5- 15177	(d)	5.80	14.6	17.4	560
6- 24400	(e)	6.68	7.8	5.7	1180

(a) results used for the calculations of the free energy of formation of the $Zn(NH_3)_2Cl_2$ in section 3.2.3

(b) discharged 60 minutes a day
(c) discharged 15 minutes a day
(d) discharged 30 minutes a day
(e) discharged 30 min. a day down to 0.9 V CCV and then 15 min. a day

---

The zinc chloride concentration remained relatively unchanged throughout the first two stages of the discharge, in agreement with equations (1.36) and (1.37) which show that the zinc dissolved by the anodic reaction was precipitated as $Zn(NH_3)_2Cl_2$, and with the results of section (3.2) which showed large increase of the $Zn(NH_3)_2Cl_2$ solubility with decreasing NH_4Cl concentration only at high $ZnCl_2$ concentrations.

The results for the most discharged cell confirm the decrease of the zinc chloride concentration predicted by equation (1.38) and that the NH_4Cl concentration also decreased during the third stage of the discharge due to the continuation of the $Zn(NH_3)_2Cl_2$ precipitation, in agreement with the conclusion of section (3.2). The electrolyte composition at the end of the discharge corresponds to the precipitation of about 20 % of the zinc formed by anodic dissolution as $Zn(NH_3)_2Cl_2$, the rest having precipitated as $ZnCl_2.4Zn(OH)_2.H_2O$.

The concentration of Mn^{2+} in the electrolyte increased with increasing discharge degree. This is in qualitative agreement with the results reported by Shaw [118] but the Mn^{2+} concentrations found in this work at the end of the discharge were about twenty times lower than Shaw's results [118]. No explanation has been found for this difference.

At the end of the discharge only a very small quantity of Mn^{2+} (about 0.02 g) had been formed and therefore the correction (equation 2.18) of the manganese dioxide oxidation degree for the MnOOH disproportionation was negligible (about 0.001 for r in $MnOOH_r$) and was not used in the calculation of the scales of r in the figures shown in this section.

The duration of the first stage of the discharge and the composition of the electrolyte (see calculations in appendix 2) lead to the conclusion that some NH_4^+, and possibly some Zn^{2+} have been ion-exchanged onto the manganese dioxide surface. The limited zinc adsorption is in agreement with the findings of Katayama *et al.* [211] who reported that this adsorption was inhibited by NH_4Cl due to the formation of anionic species (chloro-complexes) which are not ion-exchanged on manganese dioxide.

The electrolyte composition calculated at the end of the second stage of the discharge on the basis of the cell formulation and the overall cell reactions (see appendix 2) is in good agreement with the results of the chemical study of the Leclanché electrolyte reported in section (3.2).

In figure (4.1), the change of the curve slope when the discharge regime was changed from 30 to 15 minutes a day and the fact that all the potential values measured after a week-end recovery were lower than their neighbour values show that even at the slowest discharge rate, the potentials measured at the end of the recovery periods did not correspond to equilibrium conditions, due to the slowness of the $ZnCl_2.4Zn(OH)_2.H_2O$ precipitation.

4.1.2 The manganese dioxide electrode potential

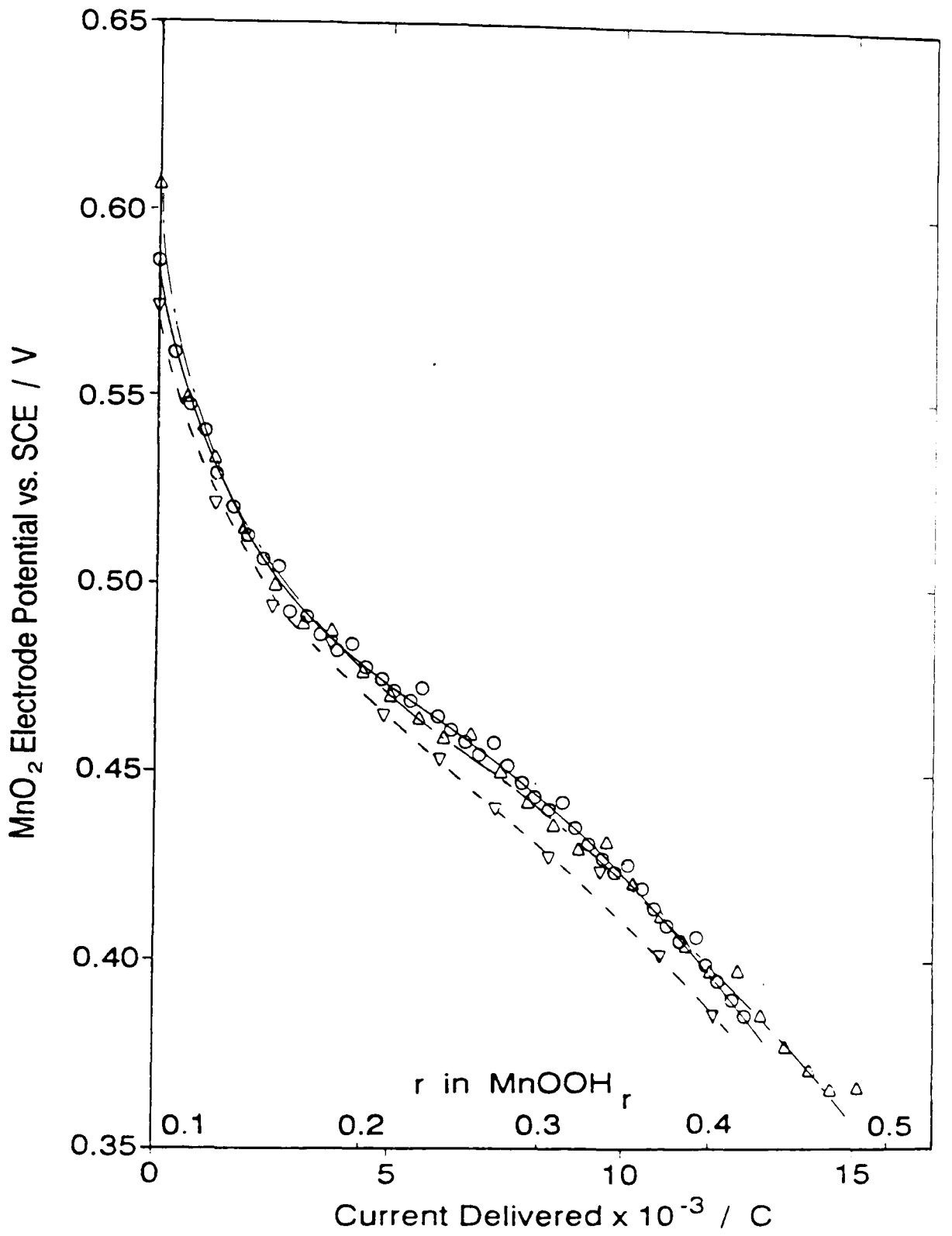

Figure 4.3 MnO_2 electrode potential on intermittent discharge through 4 ohms; ○ 15 min d^{-1}, △ 30 min d^{-1}, ▽ 60 min d^{-1}

Figure (4.3) shows the values of the manganese dioxide electrode potentials for the same cells as in figure (4.2), namely for 15, 30 and 60 minute a day discharges. Together with the equivalent curve presented in figure (4.1), these curves show the continuous decrease of the manganese dioxide electrode with the reduction depth.

There is practically no difference between the curves for the 15 and 30 minute a day discharges showing that at these discharge regimes, the recovery of the positive electrode was essentially completed at the end of the rest period. The fact that the curve corresponding to the heaviest discharge regime is slightly below the other two curves indicates that at this regime, the rest period was not quite long enough for the electrode to recover fully. Figure (4.1) shows that the change of the discharge regime at 18,500 coulombs did not affect the general trend of the curve as it did for the zinc electrode potential curve (section 4.1.1). However, the potentials measured at the end of a longer rest period are systematically above the curve showing that the recovery of the electrode was not complete at the end of the usual recuperation period (23.5 hours).

The pH of the electrolyte (from table 4.1) has been approximated by three linear relationships, pH = 5.71 from 0 to 3,500 coulombs ($0.082 \leq r \leq 0.175$); linear increase to pH = 5.80 from 3,500 to 10,700 coulombs ($0.175 \leq r \leq 0.366$) and another linear increase to pH = 6.68 from 10,700 to 24,400 coulombs ($0.366 \leq r \leq 0.729$). These estimated pH values have then been used to calculate the manganese dioxide electrode potential at pH = 0, with a correction of 0.0592 V pH^{-1} [13]. The corrected potentials have been compared to the equations given by Tye [141] from which the pH term was eliminated

$$E = E_0 + \frac{RT}{F}\ln\frac{(0.5 - r')\ (1-r')}{4r'^2} \tag{4.1}$$

for the first part of the curve and

$$E = E_0 + 2\frac{RT}{F}\ln\frac{1-r'}{r'} \tag{4.2}$$

for the second part of the reduction, with

$$r' = \frac{r-y}{1-y} \tag{4.3}$$

where the E_0s and y were considered as fitting parameters (see more details in chapter 7).

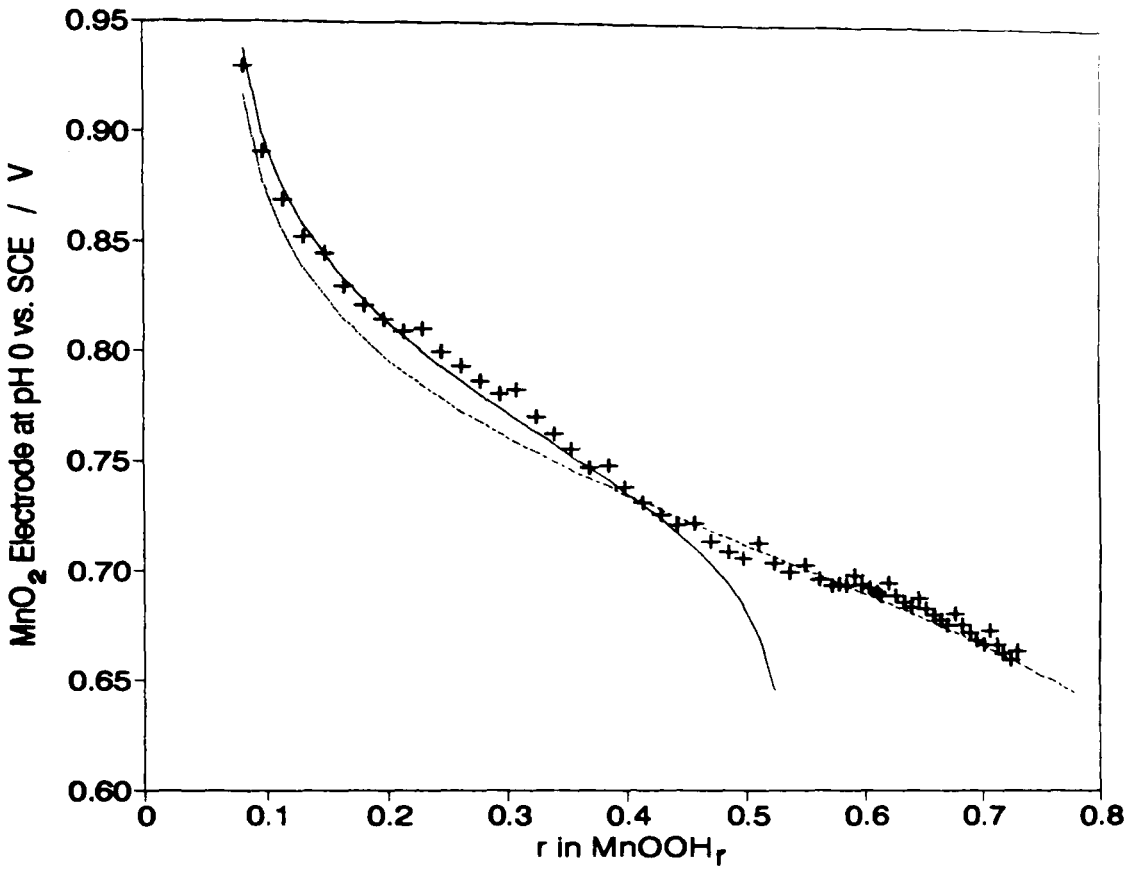

Figure 4.4 : Positive electrode potentials vs. SCE calculated at pH 0, + experimental points, —— equation (4.1) and - - - equation (4.2), with E_0 = 0.780 and 0.705 V respectively and y = 0.067

Figure (4.4) shows these results along with the lines corresponding to equations (4.1) and (4.2). The inactive Mn(III), *y*, was taken as 0.067, the E_0s as 0.780 and 0.705 V for equation (4.1) and (4.2), respectively. The agreement between the experimental points and the equations (4.1) and (4.2) confirms the validity of the assumptions underlying the model advocated by Tye [141], namely the presence of some Mn(III) inactive in the potential-determining process in the starting material and the existence of two different solids solutions in the first part and in the second part of the reduction [141]. The agreement also supports the validity of the approximations used to estimate the electrolyte pH. Although the end of the test corresponded to only 73 % of the theoretical capacity for the reduction to MnOOH, the change of the manganese dioxide electrode potential was similar to the change expected for that theoretical capacity.

The relatively low utilisation rate of the manganese dioxide was probably caused by the exhaustion of the electrolyte components at an early stage of the discharge indicating that the cell formulation was not optimum for this discharge regime.

4.1.3 The cell open circuit voltage

The open circuit voltage after recovery of the cell is shown in figure (4.5). The different discharge stages indicated in this figure were taken from the position of the breaks observed in the zinc electrode potential curve.

Due to the smoothness of the positive electrode potential curve and the relatively small changes of the negative electrode potential, these breaks are hardly visible, except the inflection at the end of the second stage of the discharge.

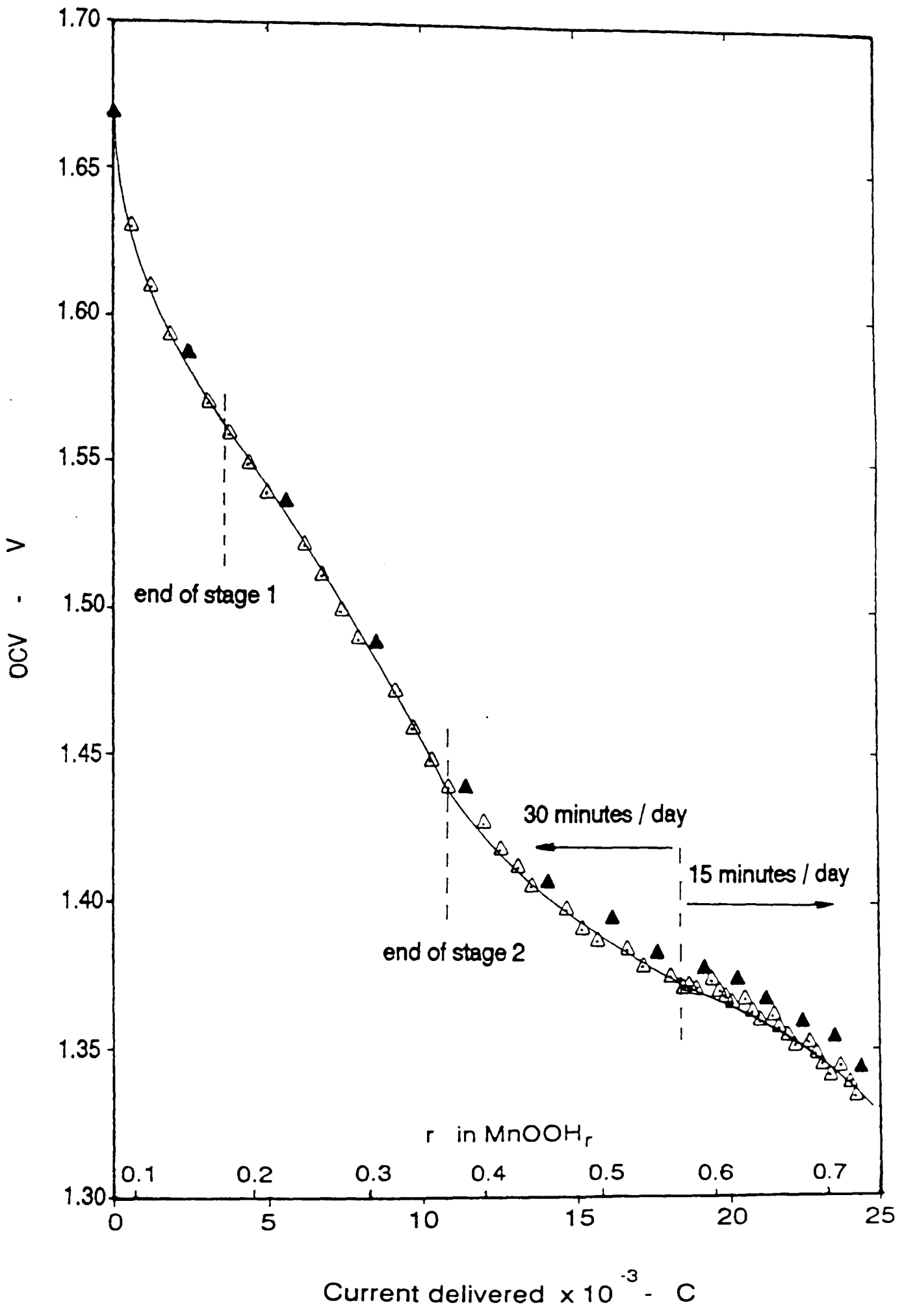

Figure 4.5 : Open circuit voltage of EMD cell as in figure (4.1). △ after 23.5 hour recovery, ▲ after 71.5 hour recovery

4.2. Faradiser M in Leclanché electrolyte

The curves recorded during the intermittent discharge of cells containing the Faradiser M on 4 ohms for 15, 30 and 60 minutes a day are shown in figure (4.6).

4.2.1 The manganese dioxide electrode potential

During the first 7,000 coulombs, the electrode potential decreased continuously with increasing discharge depth in a way similar to the cells made with the electrodeposited material described in section (4.1.2). From that stage, the cell showed typical signs of hetaerolite formation [13,213]. The increase of the positive electrode potential was due to [213]

$$2\ MnOOH\ +\ Zn^{2+}\ \longrightarrow\ Mn_2O_3.ZnO\ +\ 2\ H^{+} \qquad (4.4)$$

where MnOOH is a component of the solid solution. This reaction increased the oxidation state of the solid solution of manganese oxyhydroxide and thus increased the electrode potential. At a given discharge depth, the electrode potential was a good indicator of the amount of hetaerolite formed; the higher the potential, the larger the proportion of hetaerolite. The relative positions of the curves show that the hetaerolite formation decreased with increasing discharge regime severity. These curves also reveal two other interesting characteristics. The increase of the electrode potential due to hetaerolite formation was always greater after a longer rest period and also, even at a stage of relatively fast hetaerolite formation, the first discharge after a long rest period always produced a decrease of the electrode potential. The potential decrease on discharge shows that the current producing reaction was always the homogeneous reduction of the solid solution (reaction 1.25) and therefore that hetaerolite was formed as a subsequent step by the purely chemical reaction (4.4), in agreement with Vosburgh [108] and Tye [13]. The dependence of the amount of hetaerolite formed on the length of the rest period and on the discharge regime indicates that this formation is a slow process, probably due to the fact that it involves a recrystallisation requiring the participation of a solid phase and at least one soluble species , MnOOH and Zn^{2+} in reaction (4.4) or MnO_2, Mn^{2+} and Zn^{2+} if

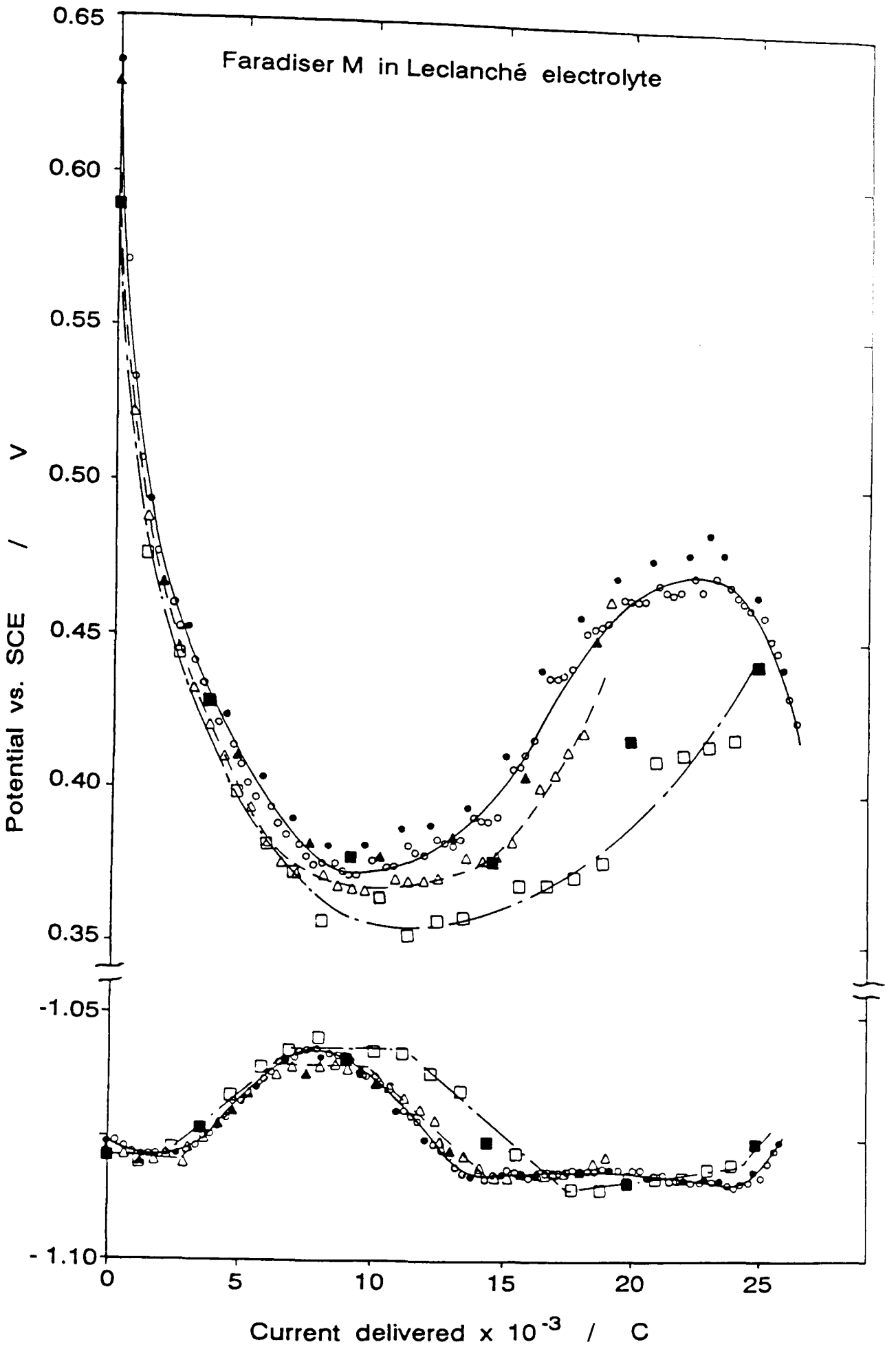

Figure 4.6 : Electrode potentials during intermittent discharge; ○● 15 min d^{-1}, △▲ 30 min d^{-1}, □■ 60 min d^{-1}; filled symbols, measured after a longer recovery.

the reaction is [50]

$$MnO_2 + Mn^{2+} + Zn^{2+} + 2\ H_2O \longrightarrow Mn_2O_3.ZnO + 4\ H^+ \qquad (1.29)$$

4.2.2 The zinc electrode potential

The curves presented in figure (4.6) are similar to the curves recorded during the discharge of cells containing EMD (figures 4.1 and 4.2) up to about 6,000 coulombs. Their interpretation is also the same, i.e. up to about 3,000 coulombs, the solid ammonium chloride was consumed according to equation (1.36)

$$Zn + 2NH_4Cl_{solid} + 2MnO_2 \longrightarrow Zn(NH_3)_2Cl_2 + 2MnOOH \qquad (1.36)$$

After about 3,000 coulombs, reaction (1.37)

$$Zn + 2NH_4^+ + 2Cl^- + 2MnO_2 \longrightarrow Zn(NH_3)_2Cl_2 + 2MnOOH \qquad (1.37)$$

decreased the soluble NH_4Cl concentration and drove the zinc electrode potential towards more positive values.

The results of the electrolyte chemical analyses are shown in table (4.2) for cells of various discharge levels.

Table 4.2 Chemical analysis of the electrolyte

	Current Delivered / C	pH	NH_4Cl w/w%	$ZnCl_2$ w/w%	Mn^{2+} ppm
1-	0	4.75	27.9	15.5	50
2-	6927	5.62	23.2	17.2	330
3-	7639	5.69	23.5	16.5	280
4-	8008	5.62	23.5	16.9	210
5-	9130	5.70	19.9	15.8	270
6-	11923	5.68	24.3	15.1	120
7-	13437	5.70	28.5	15.4	120
8-	19040 (a)	4.91	27.6	13.2	2600
9-	24875 (b)	5.40	27.8	14.0	270

(a) cell discharged for 30 minutes a day, squeezed out 10 days after the last discharge
(b) cell discharged for 60 minutes a day

The low value of the pH of the electrolyte squeezed out of the undischarged cell reveals that the cells did not contain enough ZnO to neutralise the protons released by the ion-exchange phenomenon. The important change of the pH (about 1 unit) during the early stage of the discharge caused a steeper decrease of the manganese dioxide potential on discharge than would have occurred in a fully buffered electrolyte. After the electrolyte had been buffered in the early stage of the discharge, the pH did not increase in the most discharged cells as much as it did for the cells with EMD; on the contrary, it showed a definite trend towards more acidic values.

The changes of the NH_4Cl concentrations were also very different from the variations observed in the cells with EMD. After the decrease of the ammonium chloride content during the second discharge stage, its concentration remained relatively constant and then increased again. The similarity with the zinc electrode potential is striking and shows that when the zinc electrode potential became more negative after about 9,000 coulombs, this was caused by the simultaneous increase of the NH_4Cl concentration. When this concentration reached the saturation limit, after about 14,000 coulombs, the zinc electrode potential also reached a limit very close to the value it had during the first stage of the discharge.

After the initial increase corresponding to the buffering of the electrolyte, the zinc chloride concentration remained relatively constant during the second horizontal plateau of the zinc electrode potential curve and then decreased.

Very little Mn^{2+} was formed during the discharge of these cells, with no significant increase towards the end of the discharge. The results for the cell number 8 did not correspond to the same trends as for the other cells.

Figure (4.6) shows that the beginning of the second horizontal plateau coincided with the beginning of the hetaerolite formation. At that stage of the discharge, the manganese dioxide had the composition $MnOOH_{0.318}$, i.e. hetaerolite started to form very early in the discharge. Hetaerolite formation made impossible the

calculation of the solid solution composition from the cell content and the coulombs delivered.

Table (4.2) shows that no significant change of the electrolyte composition occurred during the second horizontal plateau.

The overall cell reaction was

$$2MnO_2 + Zn \longrightarrow Mn_2O_3.ZnO \qquad (4.5)$$

where MnO_2 is a component of the solid solution.

At the end of this plateau, the progressively more negative zinc electrode potential resulted from the increase of the NH_4Cl concentration. The overall reaction was

$$2MnOOH + Zn(NH_3)_2Cl_2 \longrightarrow Mn_2O_3.ZnO + 2NH_4Cl \qquad (4.6)$$

where MnOOH is also a component of the solid solution.

The net result of equation (4.6) was an increase of the positive electrode potential due to an increase of the oxidation degree of the solid solution and a decrease of the zinc electrode potential due to the increase of the NH_4Cl concentration caused by the dissolution of the $Zn(NH_3)_2Cl_2$ precipitate. Reaction (4.6) did not occur as a reaction between two solids but was the result of

$$2MnOOH + Zn^{2+} \longrightarrow Mn_2O_3.ZnO + 2H^+ \qquad (4.4)$$

followed by

$$Zn(NH_3)_2Cl_2 + 2H^+ \longrightarrow Zn^{2+} + 2NH_4^+ + 2Cl^- \qquad (4.7)$$

The electrolyte was squeezed out of the cell number 8 during a period of fast hetaerolite formation, i.e. when equation (4.4) was consuming Zn^{2+} and producing H^+ at a relatively high rate. The low pH and the low $ZnCl_2$ concentration for this cell show that the rate of equation (4.7) was insufficient to absorb the protons formed by equation (4.4) and to regenerate the Zn^{2+} consumed by the hetaerolite formation. The lowering of the pH increased the rate of the reaction

$$2MnOOH + 2H^+ \longrightarrow MnO_2 + Mn^{2+} + 2H_2O \qquad (4.8)$$

and therefore the Mn^{2+} concentration increased in the electrolyte. The NH_4Cl concentration remained unaffected because it was controlled by the fast NH_4Cl dissolution-precipitation equilibrium.

The Mn^{2+} concentration remained very low throughout the discharge (except for the cell number 8 discussed above). This was probably due to the fact that the hetaerolite formation kept the true oxidation degree of the solid solution at a high value where it was in equilibrium with very low Mn^{2+} concentration (equilibrium 1.27). The low Mn^{2+} concentration was probably also due to the reaction

$$MnO_2 + Mn^{2+} + Zn^{2+} + 2H_2O \longrightarrow Mn_2O_3.ZnO + 4H^+ \qquad (1.29)$$

as proposed by McMurdie *et al.* [50]. This interpretation is supported by the very low Mn^{2+} concentration found in the electrolyte of cells number 6 and 7 analyzed in a period of high hetaerolite formation rate, at a stage in the discharge when $Zn(NH_3)_2Cl_2$ was still abundant and therefore could easily buffer the electrolyte (this was not the case for cell number 8 analyzed after hetaerolite formation had dissolved a large amount of $Zn(NH_3)_2Cl_2$, as revealed by the high NH_4Cl concentration).

The length of the first stage of discharge and the results of the analysis of the electrolyte squeezed out of the undischarged cell (see calculations in appendix 2), reveal that Faradiser M adsorbed more zinc and less NH_4^+ than EMD. These results are in agreement with the known [89] higher ion-exchange capacity of Faradiser M and suggest that the ZnO content of the cells should be increased.

4.2.3 The open circuit voltage

Figure (4.7) shows the open circuit voltage after recovery of the cell discharged at the 15 minutes per day rate. The open circuit voltage of the cell shows the characteristics of the positive electrode potential, i.e. a very steep decrease at the beginning of the discharge and the large recovery of the OCV due to hetaerolite

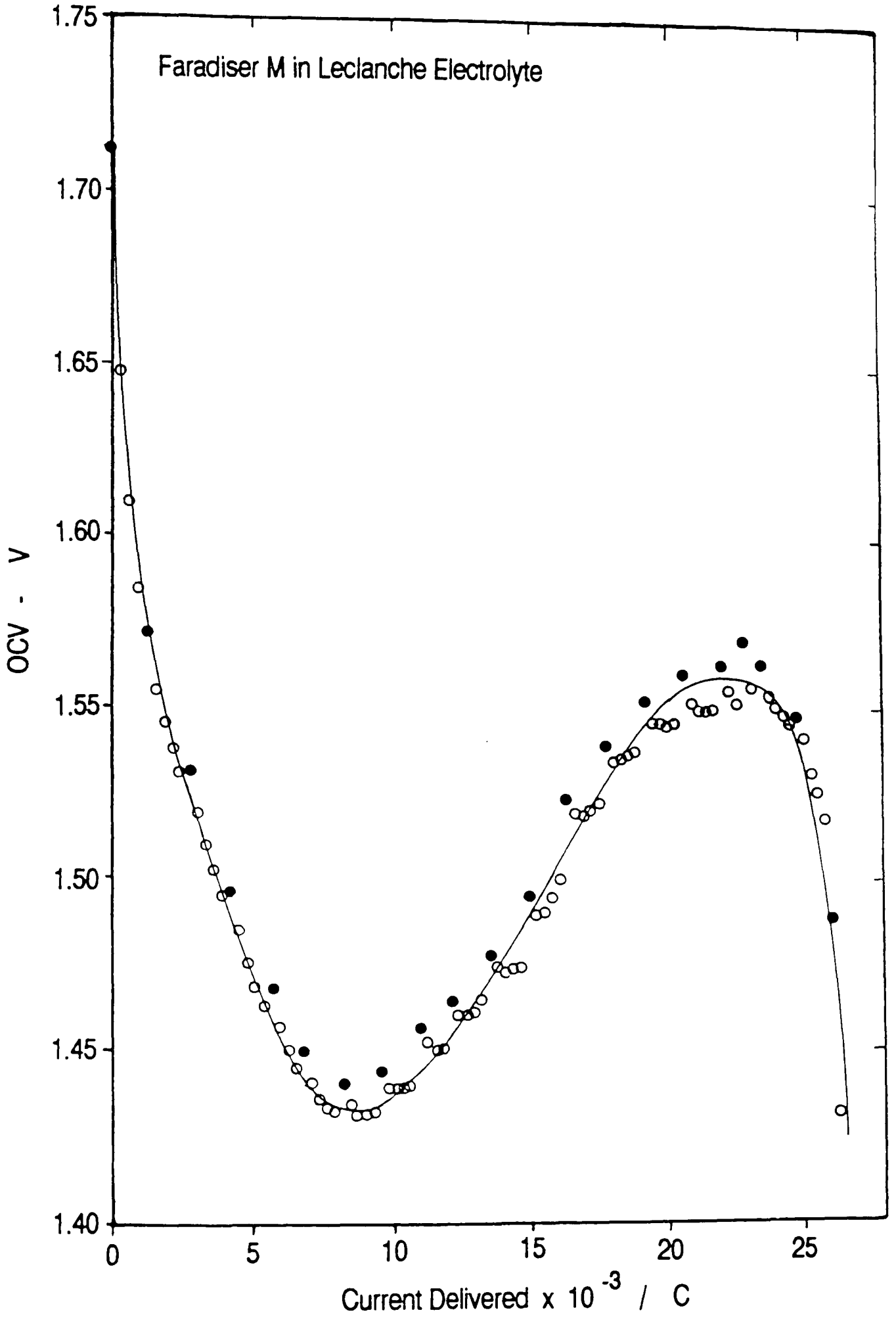

Figure 4.7 : Open circuit voltage of Faradiser M in Leclanché electrolyte discharged though 4 Ω for 15 min d^{-1}. o 23.75 hour recovery, ● 71.75 hour recovery

formation causing a substantial increase of the oxidation state of the solid solution. The OCV curve exhibits no clear influence of the zinc electrode potential because of the very limited variations in its value.

4.3 Intermittent discharge in pure zinc chloride electrolyte

Three cells containing EMD, Faradiser M and Faradiser WSZ were discharged through 4 ohms for 30 minutes a day down to a 0.9 V closed circuit potential.

4.3.1 Zinc electrode potential

The potential curves are shown in figure (4.8) as a function of the current delivered in faraday per mole of MnO_2 ($r-r_0$ where r_0 is the oxidation degree of the starting material) and in figure (4.9) as a function of the current delivered by the cells. The r_0 values were 0.082 for EMD and 0.104 for both CMDs. The zinc electrode potential curves show the change towards more negative values corresponding to the third stage of the discharge in mixed NH_4Cl-$ZnCl_2$ electrolyte. The small increase at the beginning of the discharge suggests that the electrolytes of the starting cells were not fully buffered. The three curves are very similar up to a discharge of about 0.3 faraday per mole (about 7,000 coulombs per cell) and then the slope of the curve for the cell containing Faradiser M decreased. This may be understood by considering that some hetaerolite was formed by Faradiser M from that point. The hetaerolite formation is supported by the zinc electrode potential significantly higher than the smoothed curve after a week-end long rest period.

4.3.2 The manganese dioxide electrode potential

The manganese dioxide electrode potential curves show the continuous decrease with reduction typical of the homogeneous reduction. The steep decay of the curves at the beginning of the discharge may also be explained by the increase of the electrolyte pH that occurred in the early stage of the discharge until the electrolytes became fully buffered. The curve for EMD is very similar to its

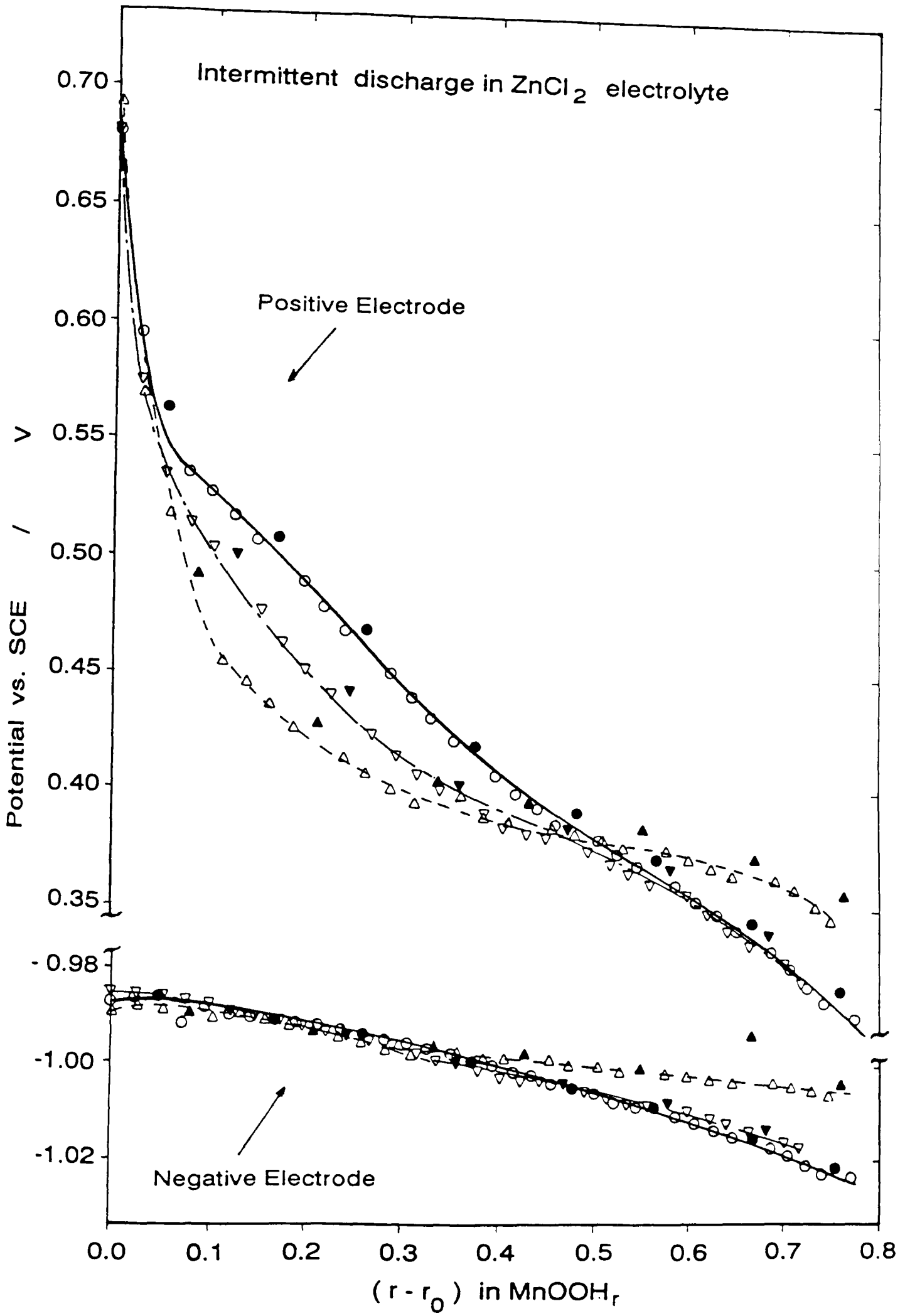

Figure 4.8 : Discharge through 4 Ω for 30 min d^{-1}; ○● EMD, ▵▲ Far M, ▽▼ Far WSZ, filled symbols: 71.5 hour recovery ; r_0 is the oxidation stage of the starting material

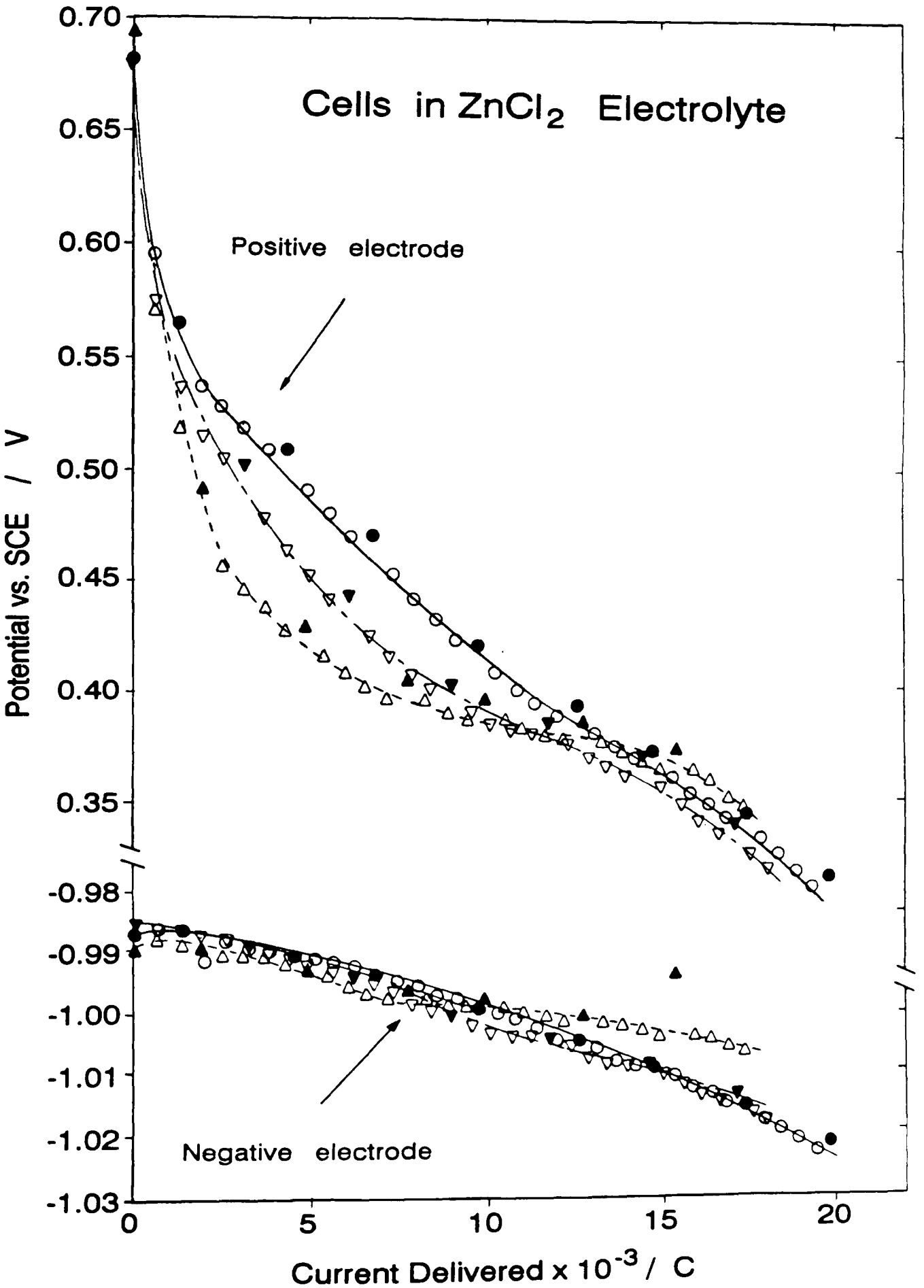

Figure 4.9 : Intermittent discharge through 4 Ω for 30 min d^{-1}; ○● EMD, △▲ Far M, ▽▼ Far WSZ; filled symbols after 71.5 hour recovery

equivalent in the mixed electrolyte; the electrode potential of the CMDs decreased faster than for the EMD, but did not exhibit the increase observed in the mixed electrolyte. The only sign of hetaerolite formation is the flattening of the curve for Faradiser M, especially apparent in figure (4.8).

Table (4.3), in section (4.3.4), gives the pH of the electrolyte at the end of the test. Table (6.8), in chapter 6, shows the pH of the electrolyte after a discharge of about 10,000 coulombs. Intermediate values were calculated by linear interpolation between these two values, assuming a linear increase of the pH with the current delivered by the cell. Although this relationship provides only a first approximation, the error could not be large due to the small variation of the pH (about 0.4 pH units) between these two points. The error made by using this assumption was certainly larger for the very beginning of the discharges due to the necessity to buffer the electrolyte during this stage.

The estimated pH values were used to calculate the potential of the manganese dioxide electrode at pH 0 (0.059 V pH^{-1} [13]); for the undischarged cells, the measured pH value was used. The results are shown in figures (4.10) to (4.12). The calculated potentials have also been compared to the potential - composition equations (see chapter 7)

$$E = E_0 + \frac{RT}{F}\ln\frac{(0.5-r')\ (1-r')}{4r'^2} \tag{4.1}$$

$$E = E_0 + 2\frac{RT}{F}\ln\frac{1-r'}{r'} \tag{4.2}$$

and

$$E = E_0 + \frac{RT}{F}\ln\frac{1-r'}{r'} \tag{4.9}$$

with

$$r' = \frac{r - y}{1 - y} \tag{4.3}$$

where the E_0s and y are considered as fitting parameters.

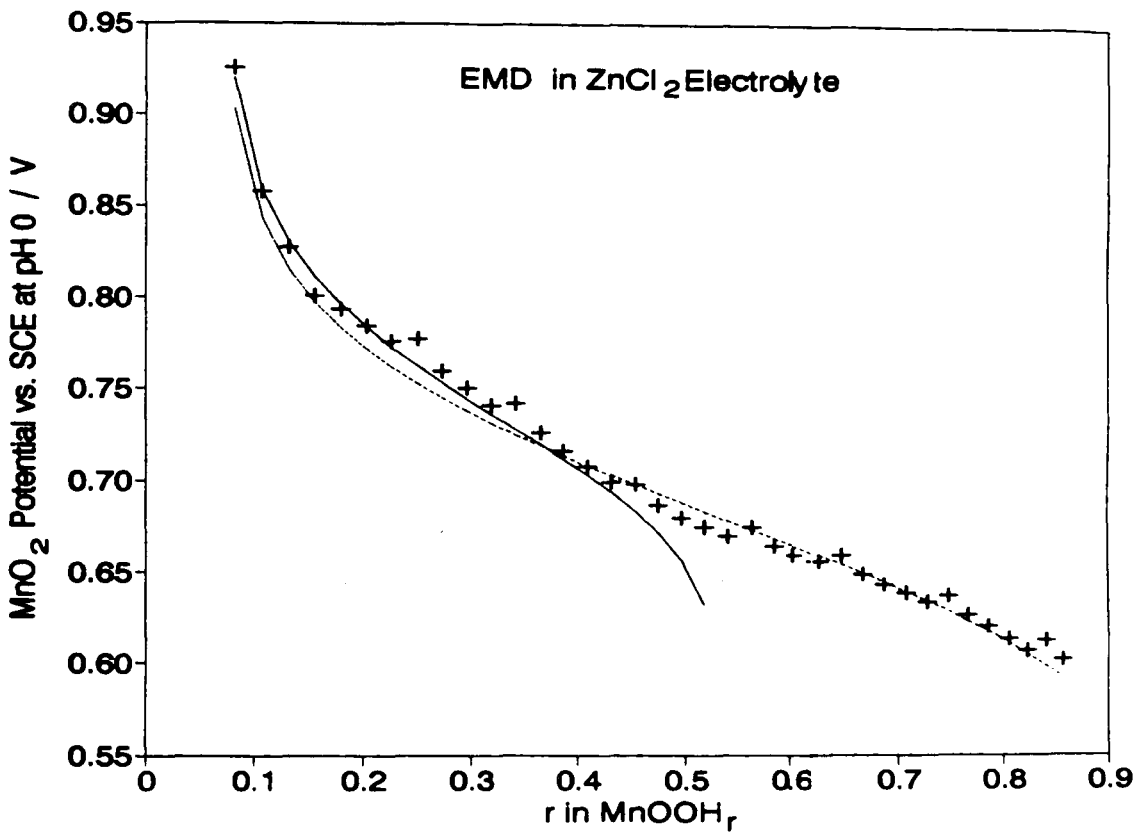

Figure 4.10 : + MnO_2 electrode potential at pH 0 compared to equations 4.1 (——) and 4.2 (- - -) with E_0 = 0.75 and 0.68 V, respectively and y = 0.07

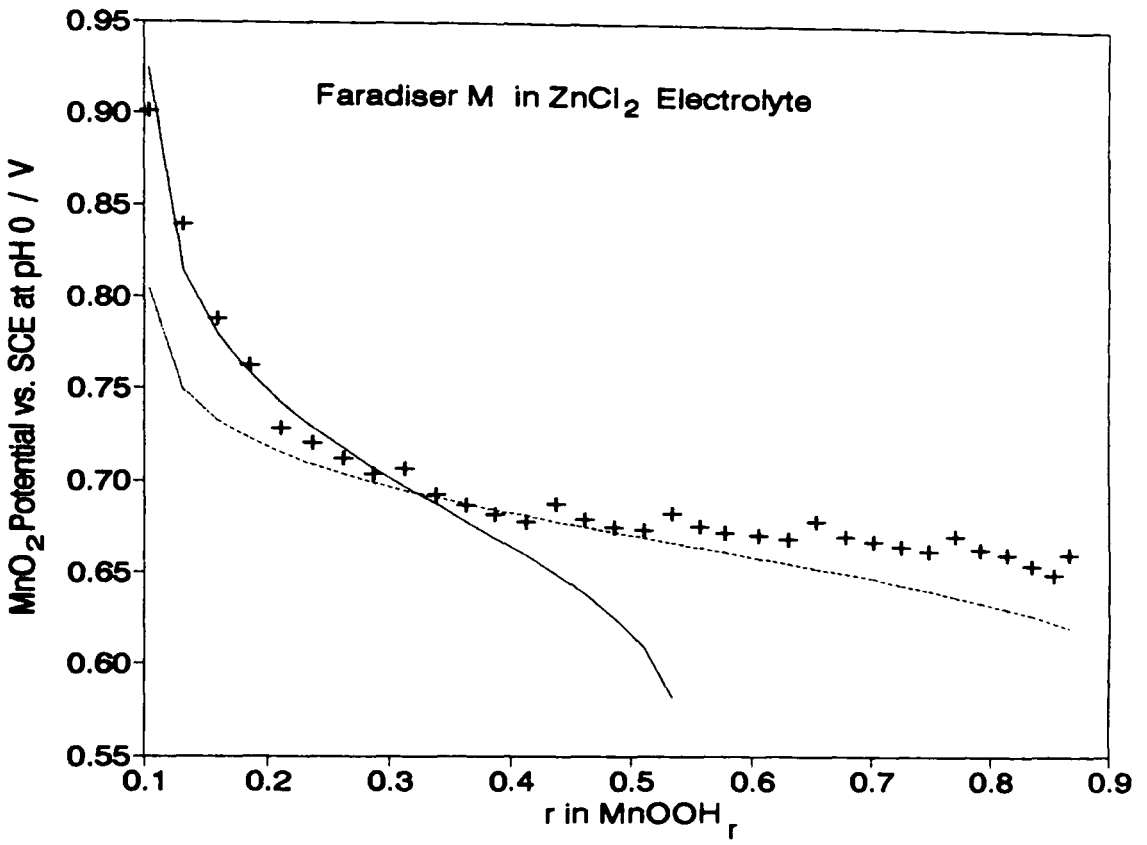

Figure 4.11 : + MnO_2 electrode potential at pH 0 compared to equations 4.1 (——) and 4.9 (- - -) with E_0=0.70 and 0.665 V, respectively and y=0.100

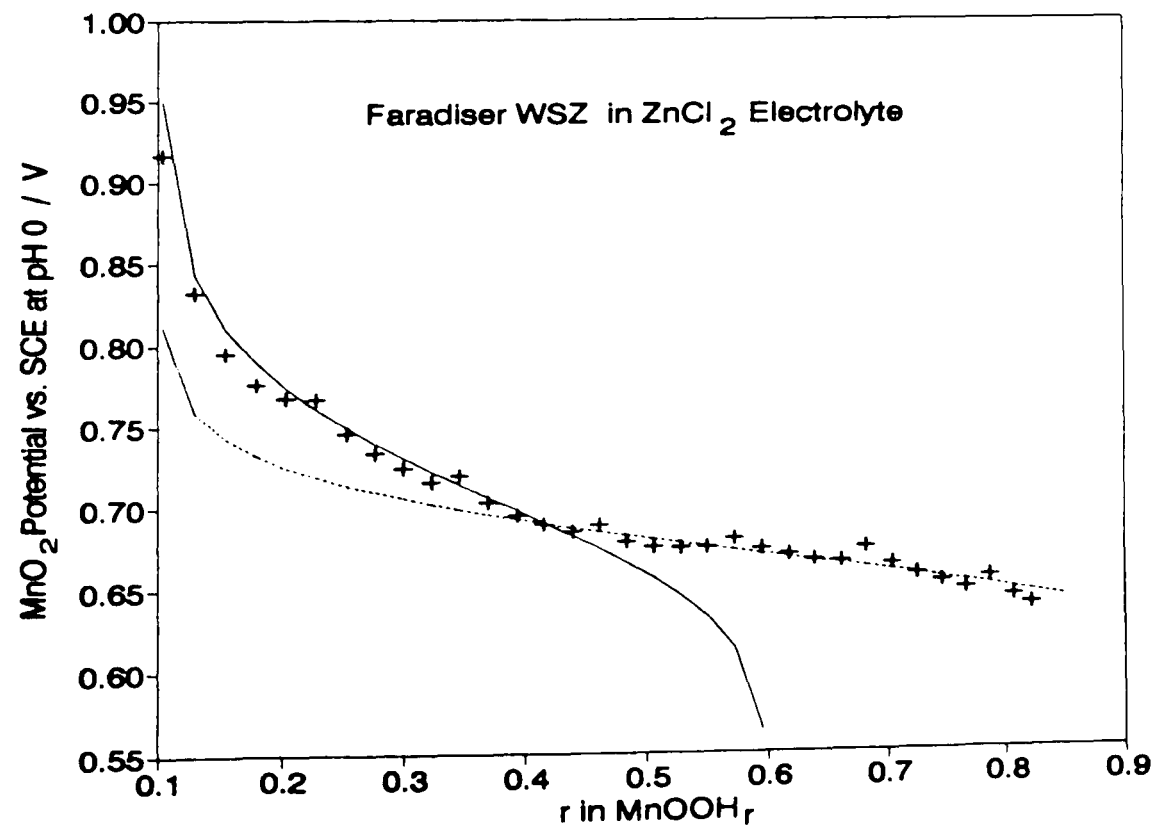

Figure 4.12 : + MnO_2 electrode potential at pH 0 compared to equations 4.1 (——) and 4.9 (- - -) with E_0=0.72 and 0.67 V, respectively and y=0.100

For EMD and Faradiser WSZ, the break at about mid-reduction ($0.4 < r < 0.5$) appears clearly and the agreement between the electrode potentials and the curves is very good, except for the points measured after a long recovery which are systematically above the curves. For Faradiser M, the break occurred earlier in the discharge (at about $MnOOH_{0.3}$) but also, all the potentials measured after $r = 0.6$ were above the curve. Although the difference was never very large, it suggests that some hetaerolite was formed during the second half of the discharge.

The use of a different equation for the CMDs than for the EMD is discussed in chapter 7.

4.3.3 The open circuit voltage

The curves are given in figure (4.13) as a function of the current delivered in faraday per mole and in figure (4.14) as a function of the current delivered by the cells. These curves are very similar to the positive electrode potential curves because of the small differences (about 35 mV) between the initial and the final zinc electrode potentials. The modest favourable effect of the hetaerolite formation on the Faradiser M positive electrode (compared to the EMD curve) was counteracted by the effect of this formation on the zinc electrode potential.

Comparison of figures (4.13) and (4.14) shows that although cells delivered significantly different quantities of coulombs, the rates of use were very similar for all the materials (about 0.7 to 0.8 faraday per mole)

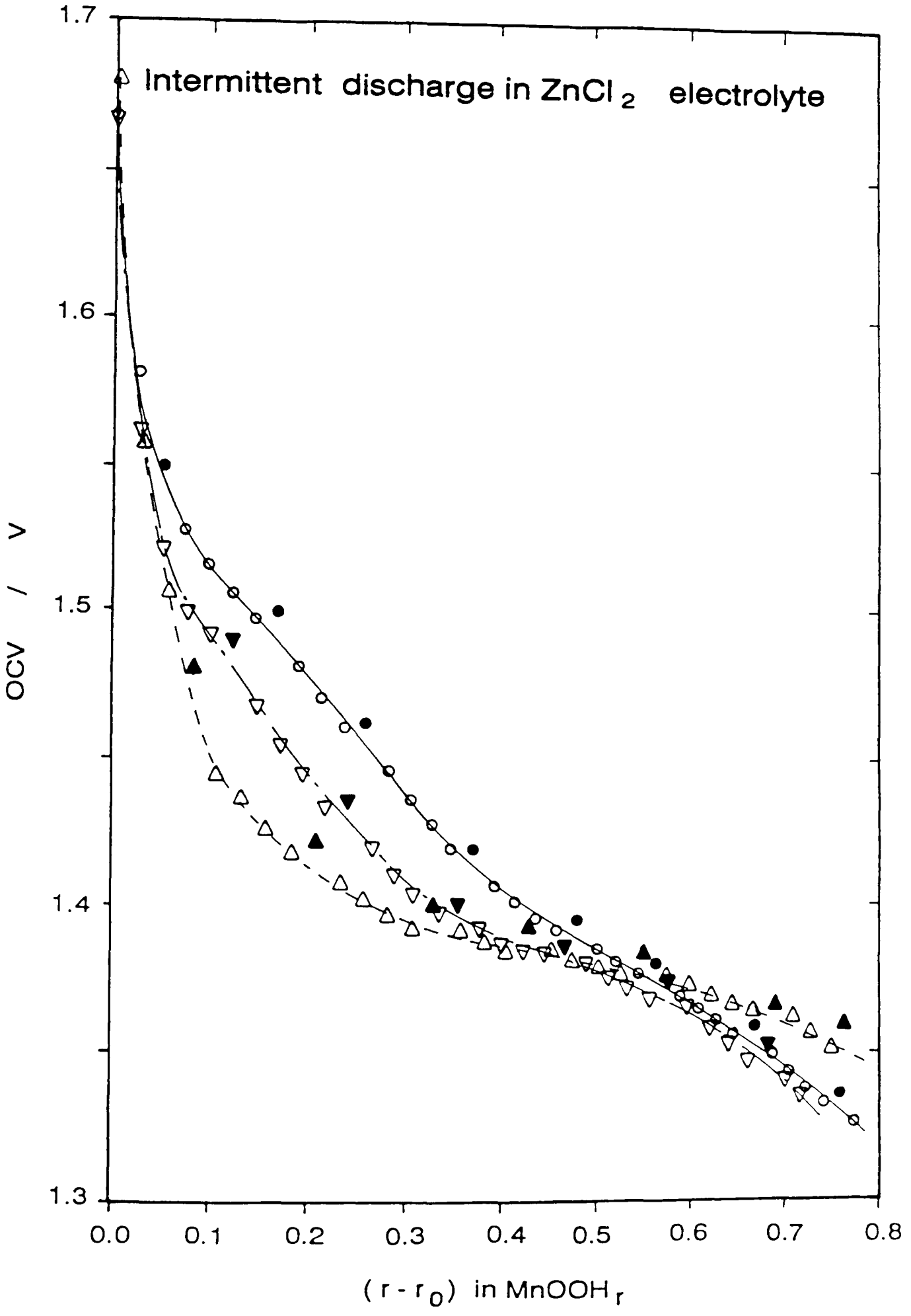

Figure 4.13 : OCV vs. current delivered (F mol^{-1}); ○● EMD, △▲ Far M, ▽▼ Far WSZ; r_0 is the oxidation degree of the starting material; 30 min. d^{-1} through 4 Ω; filled symbols after 71.5 hour recovery

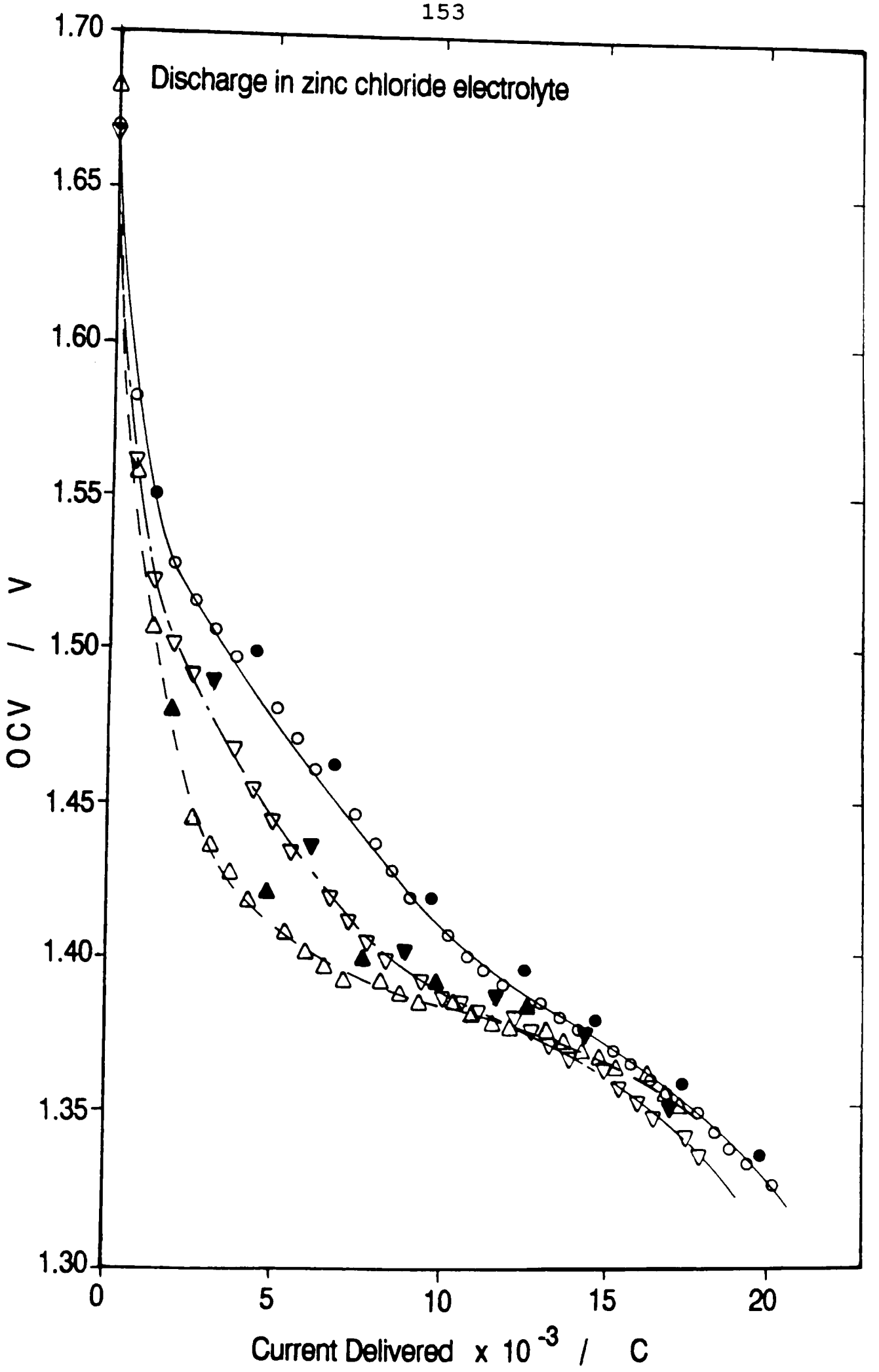

Figure 4.14 : OCV vs. current delivered (coulombs); ○● EMD, △▲ Far M, ▽▼ Far WSZ; 30 min. d^{-1} through 4 Ω; filled symbols after 71.5 hour recovery

4.3.4 Chemical analyses of the electrolyte

The results are given in table (4.3) for the undischarged and the discharged cells.

Table 4.3 : Chemical analyses of $ZnCl_2$ electrolyte

Cell	pH	$ZnCl_2$ w/w %	Mn^{2+} ppm
EMD			
undischarged	4.10	27.0	40
20,137 coulombs	5.45	8.5	22100
Faradiser M			
undischarged	3.53	26.5	70
17,551 coulombs	5.15	16.7	14600
Faradiser WSZ			
undischarged	3.95	26.4	160
17,841 coulombs	5.39	11.7	15800

These results confirm the conclusion of the previous section, namely that the electrolyte of the undischarged cells was far from fully buffered, especially for Faradiser M.

It has not been possible to calculate the zinc chloride concentration in the undischarged cells on the basis of the cell formulations (see section A2.2 in appendix 2), the calculated $ZnCl_2$ concentrations were 28.9, 28.6 and 28.8 w/w % for EMD, Faradiser M and Faradiser WSZ, respectively, higher than the measured values because of the ion-exchange phenomenon. From the electrolyte composition and the cell formulations it has been calculated (section A2.2) that the precipitate was $2ZnCl_2.5Zn(OH)_2.H_2O$ rather than $ZnCl_2.4Zn(OH)_2.H_2O$. The overall cell reaction was thus

$$5Zn + 2Zn^{2+} + 4Cl^- + 10MnO_2 + 11H_2O \longrightarrow 2ZnCl_2.5Zn(OH)_2.H_2O + 10MnOOH \quad (4.10)$$

The concentrations at the end of the discharge, calculated on the basis of equation (4.10) are 8.2, 13.0 and 11.4 w/w % $ZnCl_2$ for EMD, Far M and Far WSZ, respectively. These results fairly agree with the measured concentrations for

EMD and Far WSZ but not for Faradiser M. For the latter MnO_2, the measured zinc chloride concentration corresponds to a 0.151 faraday discharge following equation (4.10). The discharge actually produced 0.182 faraday of current, the difference showing that about 17 % of the current corresponded to the overall reaction

$$Zn + 2\ MnO_2 \longrightarrow Mn_2O_3.ZnO \qquad (4.5)$$

which did not affect the electrolyte composition.

The formation of Mn^{2+} was much larger in pure zinc chloride electrolyte than in the mixed Leclanché electrolyte for an electrolyte pH only 0.1 to 0.2 unit lower in the $ZnCl_2$ electrolyte. The greater Mn^{2+} concentration in the case of EMD was probably caused by a deeper discharge than for CMDs and the lowest manganous ion concentration in the case of Faradiser M is compatible with its role in hetaerolite formation.

4.4 Conclusions

The performances of the different cells in mixed Leclanché and in pure $ZnCl_2$ electrolytes are summarized in table (4.4).

Table 4.4 : performances on intermittent discharge

Discharge type	Current delivered by the cell / C	Faraday mole $^{-1}$
Leclanché		
EMD 30 and 15 min day^{-1}	24,400	0.647
Far M 15 min day^{-1}	26,434	0.808
Far M 60 min day^{-1}	24,875	0.760
Zinc chloride		
EMD 30 min day^{-1}	20,137	0.775
Far M 30 min day^{-1}	17,551	0.763
Far WSZ 30 min day^{-1}	17,841	0.718

The performances of the cells in both electrolytes were in agreement with the reports of Ohta *et al.* [186] and Uetani *et al.* [187,188], both in mixed Leclanché and in pure zinc chloride electrolytes. In the mixed electrolyte, because of hetaerolite formation, Faradiser M was much better than EMD either in absolute (coulombs per cell) or in specific performance (faraday per mole of MnO_2), even though the discharge regime was more severe for Faradiser M (60 min day^{-1}) than for the electrodeposited material (when the CCV had reached 0.9 V on the 30 minutes a day regime, the discharge was continued for 15 min day^{-1}).

The performances of the cells were worse in pure zinc chloride electrolyte than in the mixed Leclanché electrolyte. This is partly due to the lower quantity of manganese dioxide contained by the cells using the $ZnCl_2$ electrolyte than for those using a mixed electrolyte formulation. The performance based upon one mole of manganese dioxide supports this conclusion. The specific capacity of EMD and Faradiser M were very similar and higher by about 6 % than the capacity of Faradiser WSZ. Among the chemically prepared materials, the better specific capacity of Faradiser M resulted from the formation of some hetaerolite, although in lower quantity than in the mixed Leclanché electrolyte.

The cells produced more Mn^{2+} in pure zinc chloride than in the Leclanché electrolyte. The reason for this is not well understood as it is difficult to believe that it was the result of the pure zinc chloride electrolyte being more acidic (by about 0.1 - 0.2 pH unit) than the mixed electrolyte. In both electrolytes, lower manganous ion concentrations were found in the cells containing the hetaerolite-former Faradiser M than in the other cells. This supports the suggestion of McMurdie *et al.* [50] concerning the involvement of Mn^{2+} in the formation of hetaerolite. Although the amount of Mn^{2+} formed during the discharge seems to have increased with the discharge depth, at least in zinc chloride electrolyte (see table 6.8 for the results at about r=0.54), its concentration remained much lower than the concentrations measured by Shaw [118,13]. The reason for this is not known.

In the Leclanché electrolyte, the discharge of a cell containing electrodeposited manganese dioxide can be divided into the three stages predicted by Tye [13,18]. The duration of the first stage can be calculated on the basis of the cell formulation and the overall discharge reaction only if the removal, by ion-exchange on the manganese dioxide, of some NH_4Cl from the electrolyte is taken into consideration. The duration of the second discharge stage can also be predicted from the cell formulation, the overall discharge equations and the knowledge of the electrolyte composition which corresponds to the end of the $Zn(NH_3)_2Cl_2$ formation as the only reaction product (reported in chapter 3).

The change of the manganese dioxide electrode potential on discharge (corrected for the variations of the electrolyte pH) agreed with the solid solution reduction model and with the equations proposed by Tye [141].

During the third stage of the discharge, the slow recovery of the zinc electrode recovery changed the electrode potential towards more negative values. This slowness suggests that the discharge caused the precipitation of $Zn(NH_3)_2Cl_2$ which subsequently re-dissolved to form $ZnCl_2.4Zn(OH)_2.H_2O$, as was observed on ZnO addition (see section 3.2).

In cells containing Faradiser M, the duration of the first stage of the discharge shows that the CMD adsorbed more zinc and less ammonium than EMD. The amount of ZnO incorporated into the electrode mix was insufficient to neutralize the protons released by the important ion exchange and therefore the electrolyte of the undischarged cells was not fully buffered. The increase of the electrolyte pH that occurred in the early stage of the discharge, and which does not occur in fully buffered electrolyte, added about 50 mV to the potential loss caused by the reduction of the manganese dioxide on discharge.

Hetaerolite started to form very early in the discharge ($r = 0.32$ in $MnOOH_r$). After about 9,000 coulombs, hetaerolite formation became faster than the overall discharge rate and the positive electrode potential increased due to enhancement of the oxidation state of the solid solution. The cell open circuit voltage also increased. Hetaerolite formation caused the dissolution of the $Zn(NH_3)_2Cl_2$ formed in the earlier stage of the discharge causing the electrolyte to become saturated in NH_4Cl again. This drove the zinc electrode potential towards more

negative values and thus participated a little to the increase of the open circuit voltage of the cell. Although this NH_4Cl regeneration was mentioned by Divers [111], no experimental report of this phenomenon has been found in the literature. The dissolution of the precipitate due to hetaerolite formation must also have improved the behaviour of the cell during subsequent discharge by improving the mass transport through the electrolyte. Even when hetaerolite was formed, the current producing reaction was the solid solution reduction (equation 1.25), hetaerolite being formed as a purely chemical subsequent step.

Faradiser M did not form as much hetaerolite in pure zinc chloride as in the Leclanché electrolyte, although its effect on both negative and positive electrode potentials was apparent. Hetaerolite formation was probably the cause of the good specific (faraday $mole^{-1}$) performance of Faradiser M. In zinc chloride cells, hetaerolite formation is not beneficial to the zinc electrode potential as it makes it less negative.

The manganese dioxide electrode potential (calculated at pH 0) showed the continuous decrease on discharge typical of solid solution reduction. For EMD, the potential - composition relationship has been fitted to the equations proposed by Tye [143], using, for the EMD, almost the same parameters for the E_0s and y (the inactive MnIII) in both electrolytes. By contrast, the potential - composition relationships for the CMDs were the same as for the EMD only in the first part of the reduction. In the second part of the discharge, they could be fitted to an equation proposed by Tye [215] for the early stage of the reduction of a form of manganese dioxide normally inactive in batteries (β-MnO_2). More details about this phenomenon are given in chapter 7. This difference between EMD and CMDs is a new finding.

The chemical analyses of the electrolyte squeezed out of discharged cells have revealed that the precipitate formed on discharge in pure zinc chloride cells was not $ZnCl_2.4Zn(OH)_2.H_2O$ but was very close to the formula $2ZnCl_2.5Zn(OH)_2.H_2O$. This contrasts with Leclanché cells for which the electrolyte composition at the end of stage three is compatible with the formation of the former precipitate and not with the latter. This difference between Leclanché and zinc chloride cells has not been reported before.

Chapter 5. Development of the probe system

This chapter reports the development of the technique used in the investigation of the cell behaviour during continuous discharge tests. In this section, the expression "usual reference electrode" refers to the reference electrode connected to the electrolyte of the negative compartment by a Luggin capillary inserted into the cell through the zinc electrode. This arrangement is described in section (2.4.3).

5.1. Zinc probes in the negative electrode compartment

Zinc probes were positioned adjacent to the negative electrode surface (see section 2.5.1). They were expected to take a potential identical to the zinc electrode open circuit potential at the time of the measurement and thus permit the monitoring of the negative electrode concentration overpotential.

5.1.1 Discharge curves

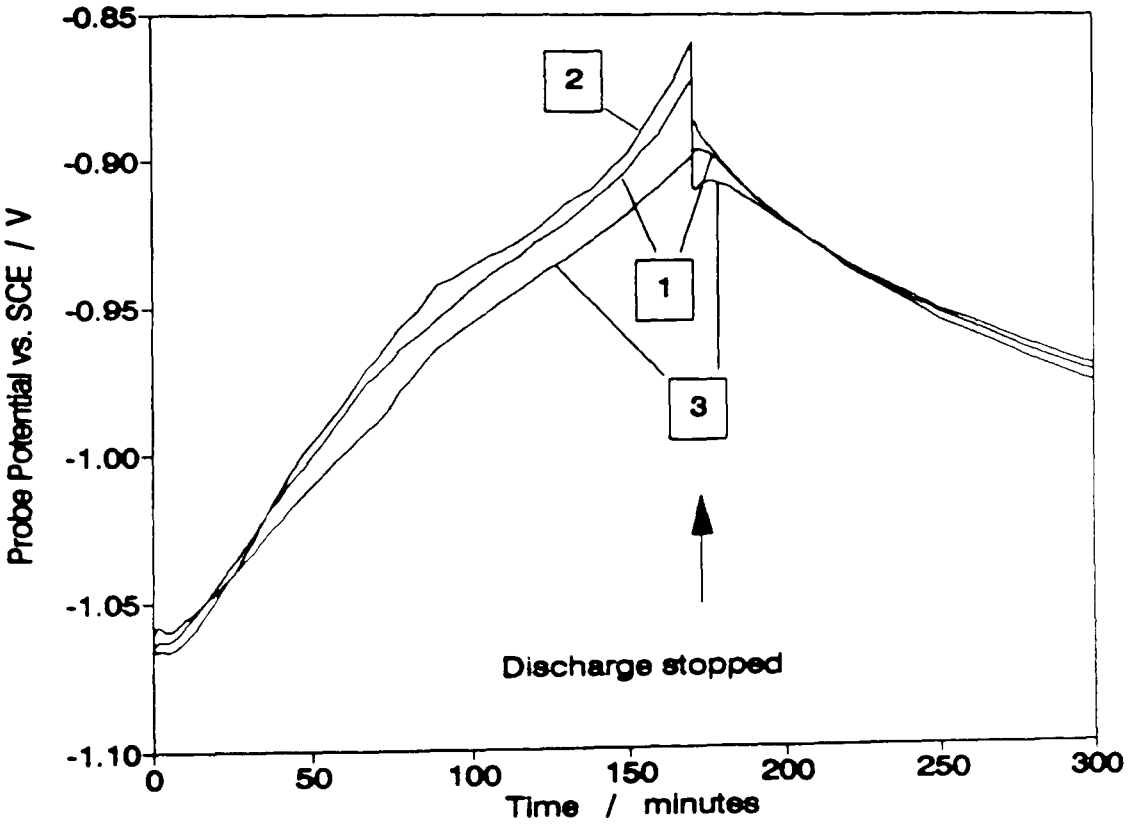

Figure 5.1 : Probes inserted at different depths into the cell; (1), 0.3 mm; (2), 0.35 mm; (3), 0.4 mm. Holes drilled *after* cell manufacture; commercial Leclanché cell; 4 Ω discharge

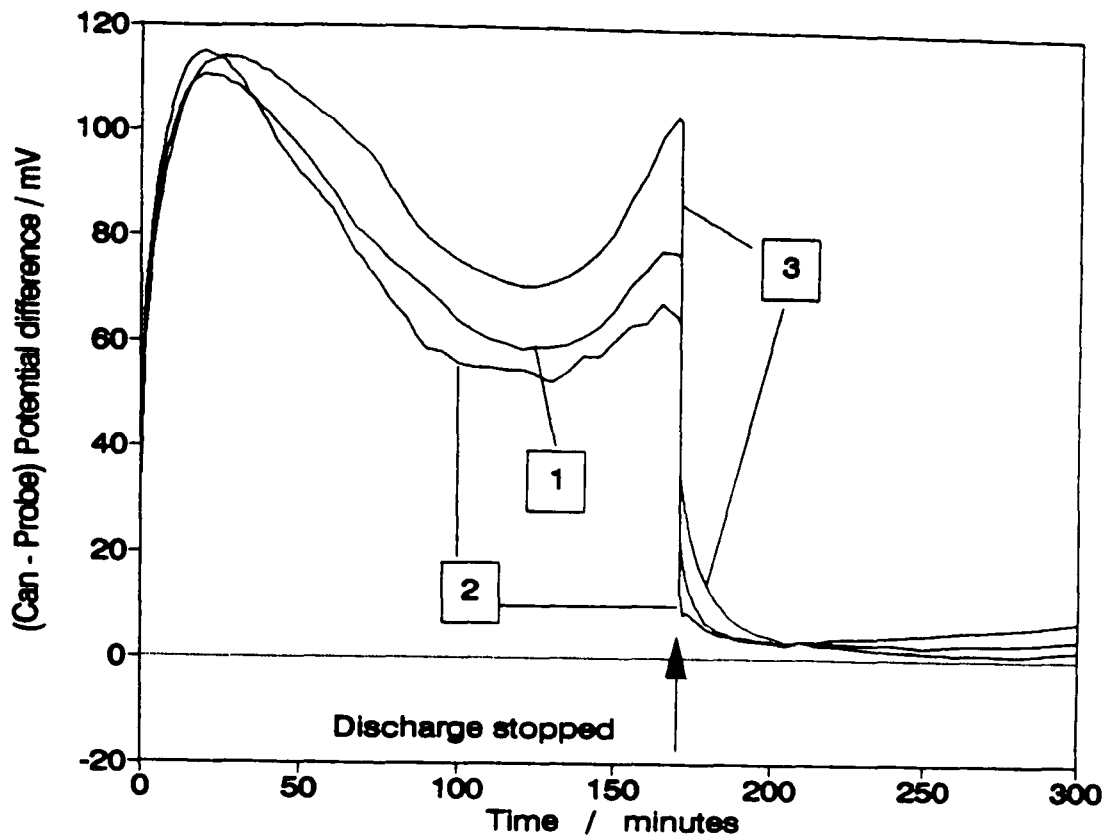

Figure 5.2 : Potential difference between the probes and the zinc electrode, hole drilled *after* cell manufacture; commercial Leclanché cell; 4 Ω discharge; same probes as in fig. (5.1)

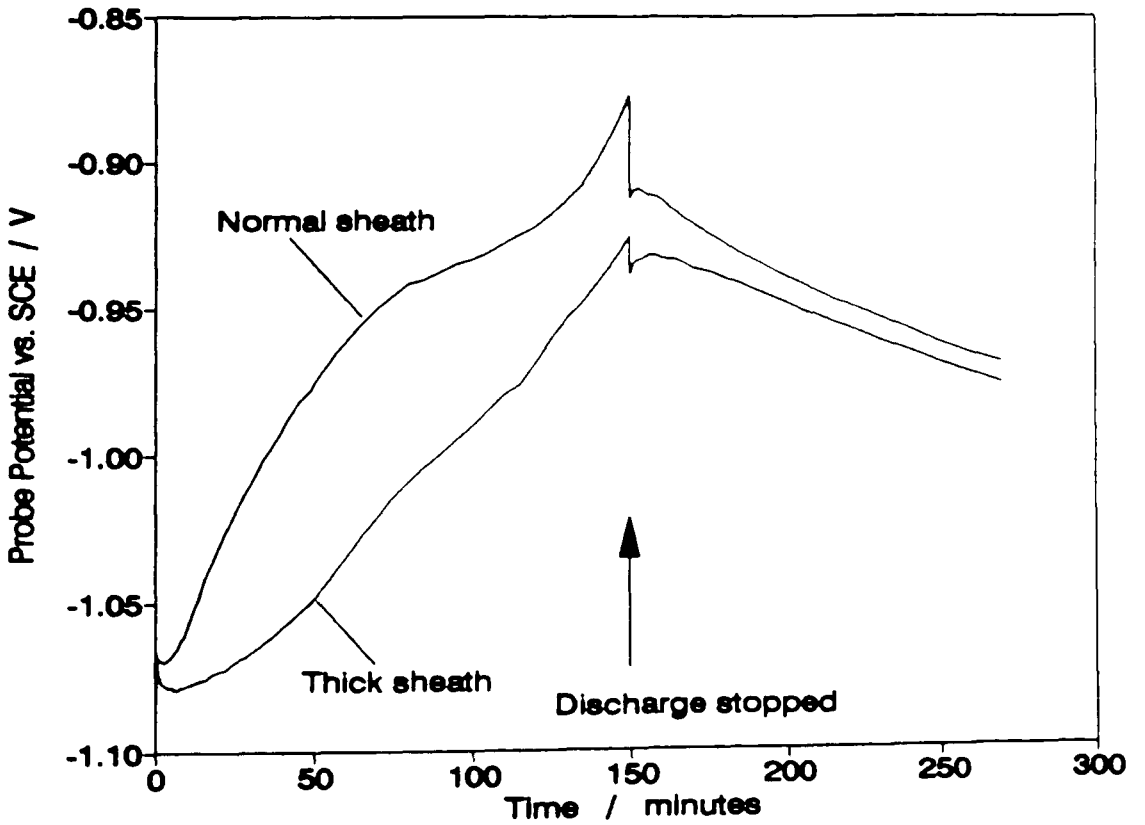

Figure 5.3 : Influence of the sheath thickness on the probe potential vs SCE curve, holes drilled *after* cell manufacture; commercial Leclanché cell; 4 Ω discharge

Figure (5.1) shows the potentials versus the usual reference electrode of three probes inserted into the same commercial cell with the tips of the probes located at different distances from the outside surface of the can and thus at different distances from the electrode active surface (this distance is called "wall thickness" in figure 2.7), 0.3, 0.35 and 0.4 mm for the probes 1, 2 and 3, respectively. The potential of the 3 probes remained stable for about 5 minutes at the beginning of the discharge, they all decreased by 10 to 30 mV when the discharge was stopped and then increased again, from about 1 mV over the first minute of recovery for probe 2 to about 3 mV over the first 7 minutes of recovery for probe 3. During the recovery, the probe potentials did not take the value of the negative electrode potential as soon as the discharge was stopped; as shown in figure (5.2), it took around 30 minutes for the difference to decrease to about 5 mV. Figure (5.3) shows the curves measured using two probes with different sheath thickness (0.4 mm for the normal sheath and 1.2 mm for the thicker sheath) during the discharge of the same type of commercial cell. The increase of the sheath thickness dramatically increased the discharge time before the probe potential started to become less negative. Figure (5.4) shows that a thicker probe sheath also increased significantly the time after the discharge was stopped during which the probe potential continued to increase, and the time necessary for the probe potential to come close to the zinc electrode potential. The change of the probe sheath thickness did not increase the jump in the probe potential when the discharge was stopped.

Three probes were inserted into a cell through holes drilled into the can before the cell assembly. The potentials they gave are compared in figure (5.5) to the negative electrode open circuit potential determined using the interruption technique (see section 5.2), all potentials being measured against the usual reference electrode. The spread of the probe potentials at a given moment of the discharge was quite large (about 40 mV by the end of the discharge). There was also a short delay between the end of the discharge and the beginning of the smooth continuous decrease of the potential occurring during the recovery.

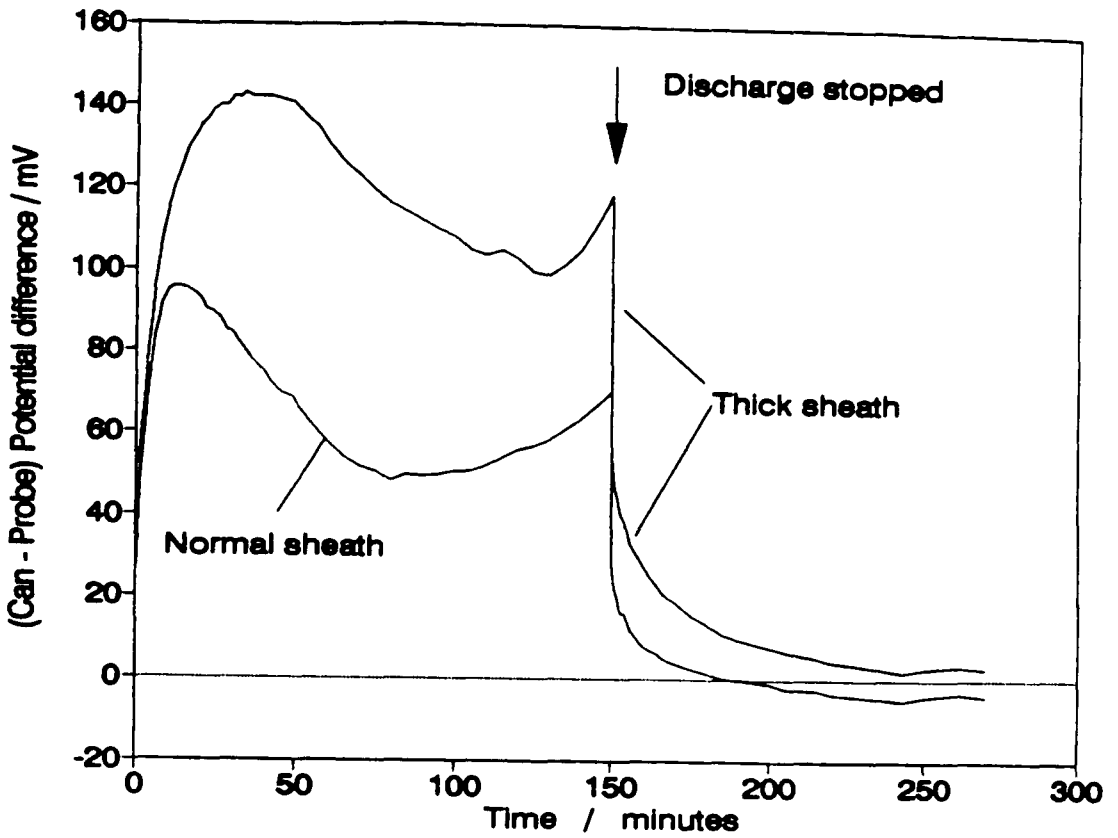

Figure 5.4 : Influence of the sheath thickness on the potential difference between the probe and the zinc electrode; holes drilled *after* cell manufacture; commercial Leclanché cell; 4 Ω discharge

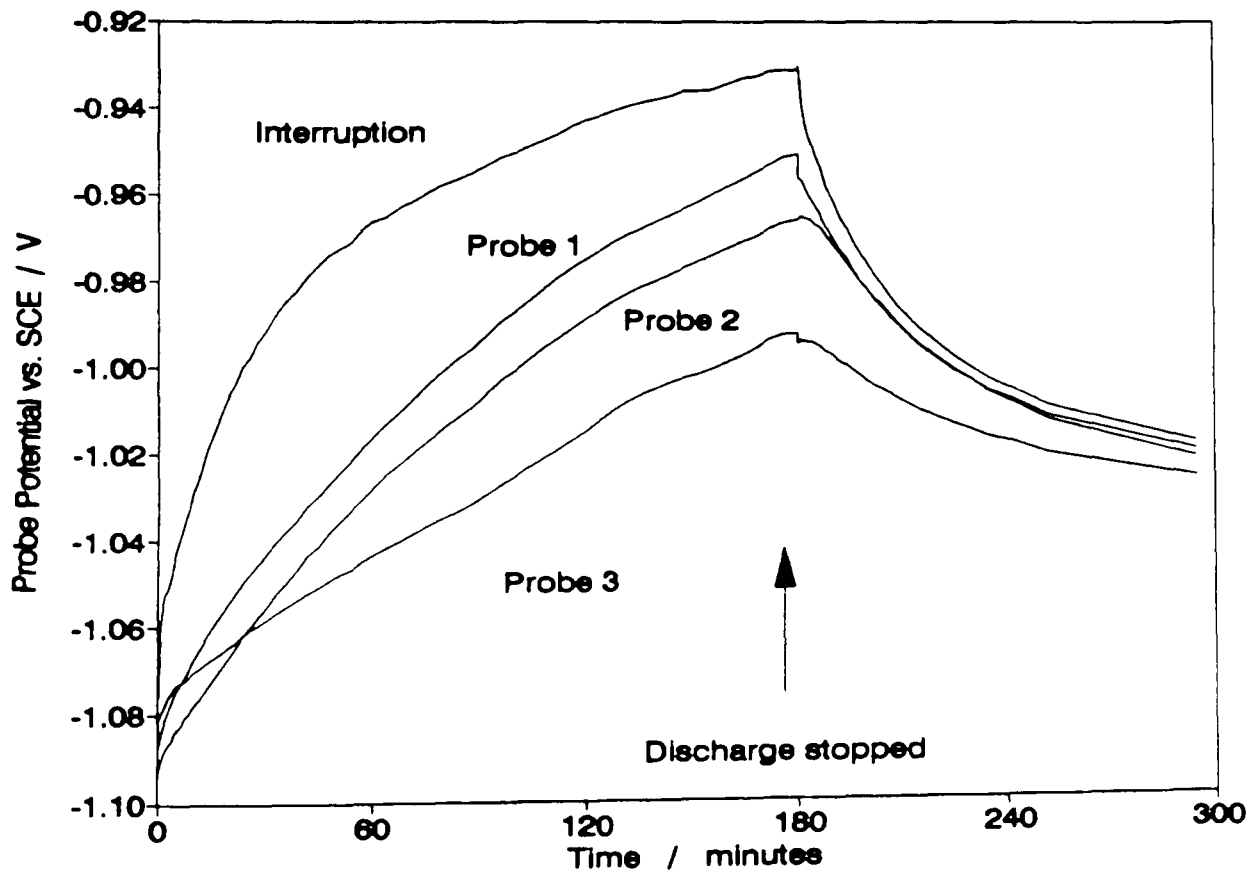

Figure 5.5 : Probe potentials and zinc open circuit potential (vs. SCE) measured by the interruption method; holes drilled *before* cell manufacture; Faradiser M in Leclanché electrolyte; 4 Ω discharge

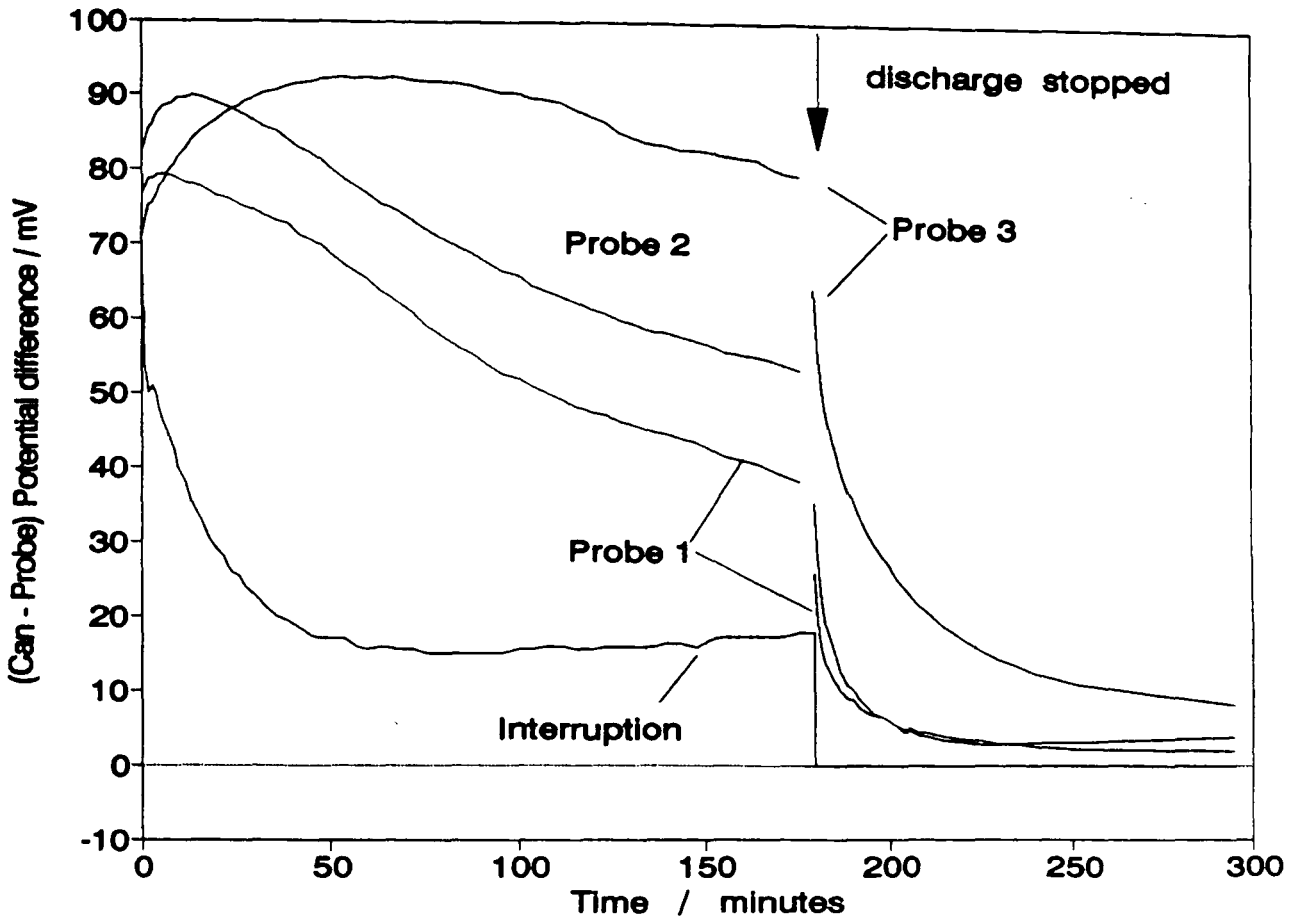

Figure 5.6 : Probes - zinc electrode potential differences and (ohmic + activation) overpotential measured by the interruption technique; Faradiser M in Leclanché electrolyte; 4 Ω discharge

The very fast potential jumps when the discharge was stopped were small (less than 6 mV) and occurred either towards more positive or more negative values. The curve measured using the interruption technique was very smooth, both during the discharge and during the recovery. Figure (5.6) shows that the probe potentials approached the negative electrode potential (within 5 mV) only about half an hour after the discharge was stopped and even longer for the probe number 3. The (ohmic + activation) overpotential, measured by the difference between the probe potential and the zinc electrode potential or by the change of the zinc electrode potential on discharge interruption, were very different (figure 5.6) when measured by the probe technique or by the interruption method. The interruption method gave a total transient overpotential (ohmic + charge transfer overpotential) decreasing rapidly during the first hour of the discharge and then remaining almost unchanged until the discharge was stopped. By contrast, the curves measured with the probes showed an increase of the ohmic + activation

overpotential during a period depending on which probe was used for the measurement.

When the discharge was stopped, the potential difference between the probes and the zinc electrode, as well as the zinc electrode potential, showed a similar potential jump of about 15 mV.

5.1.2 Discussion of the results

The response time of the zinc probes increased with increasing sheath thickness or in other words with increasing distance between the dissolving zinc electrode surface and the tip of the probe. The effects of this response time were apparent when the discharges were started and also when they were stopped. In the absence of convection as in Leclanché type cells and of electrical migration due to the absence of current between the negative electrode and the probe, transport to or from the probe tip occurred exclusively by diffusion, i.e. when a concentration difference existed. Outside equilibrium conditions, it was therefore impossible to have the same electrolyte composition at the probe tip and at the zinc electrode surface. At the start of discharge, the zinc activity increased faster at the electrode surface than at the probe extremity; thus the potential difference between the probe and the negative electrode increased with discharge time. This phenomenon became more apparent with the increase of the diffusion path length (thicker sheath or deeper probe). The potential difference between the probes and the zinc electrode started to decrease as the rate of increase of the zinc activity at the electrode surface began to lessen, but it remained larger than the electrode activation overpotential. When the discharges were stopped, diffusion continued to increase the zinc activity, and therefore the probe potentials, at the probe surfaces, for a time dependent on the magnitude of the difference between the concentrations at the can and probe surfaces and thus for a time which increased with increasing diffusion path length. During the recovery, the probe potentials came closer to the zinc electrode potential as diffusion reduced the concentration differences.

The probe potential jumps when the discharges were stopped were due to the ohmic potential difference existing within the electrolyte between the locations of the salt bridge tip and the zinc probe extremities. When both salt bridge and probes were correctly positioned, these potential jumps were small and occurred in a direction which depended on the respective positions of the Luggin capillary and the zinc probe as illustrated in figure (5.5).

The decrease of the probe potentials at the beginning of the discharge is not well understood. It was not observed for the probes inserted through holes drilled into the can before cell assembly (compare figures 5.1 and 5.5) and might therefore have been due to the deformation of the zinc can caused by the drilling of the holes into the zinc electrode of already assembled cells.

During a discharge in NH_4Cl - $ZnCl_2$ electrolyte, the ammonium chloride concentration decreases at the zinc electrode surface [34,80] and eventually vanishes [80]. The zinc charge transfer overpotential is much higher in the mixed electrolyte than in pure zinc chloride solutions [61] and therefore the decrease of the total transient overpotential (ohmic + activation overpotential) measured with the interruption method which occurred during the first hour of the discharge showed the effect of decreasing NH_4Cl concentration at the electrode interface on the anodic dissolution activation overpotential.

Figures (5.5) and (5.6) show that the difference between the probe potentials and the zinc electrode open circuit potential was maximum after about 1 hour of discharge when it amounted to about 70 mV and then slowly decreased with time down to about 30 - 50 mV when the discharge was stopped. This represented a significant part of the total concentration overpotential, which was about 130 mV towards the end of this discharge (three hours through 4 Ω in Leclanché electrolyte), making very inaccurate the use of zinc probes to monitor the negative electrode concentration overpotential.

5.2. Potential transients

In this section the interpretation of the potential transients which occurred during the first milliseconds following the start or the interruption of a discharge is reported. The time at which the interruption of the discharge happened, was revealed by the step change of the electrode potential (ohmic overpotential).

5.2.1 The zinc electrode potential transients

A typical zinc electrode potential transient recorded during the discharge of a Leclanché cell is shown in figure (5.7). On the oscilloscope screen, the ohmic overpotential appeared as a discontinuity in the trace (the change being too fast for a measurement) and therefore was easily measured.

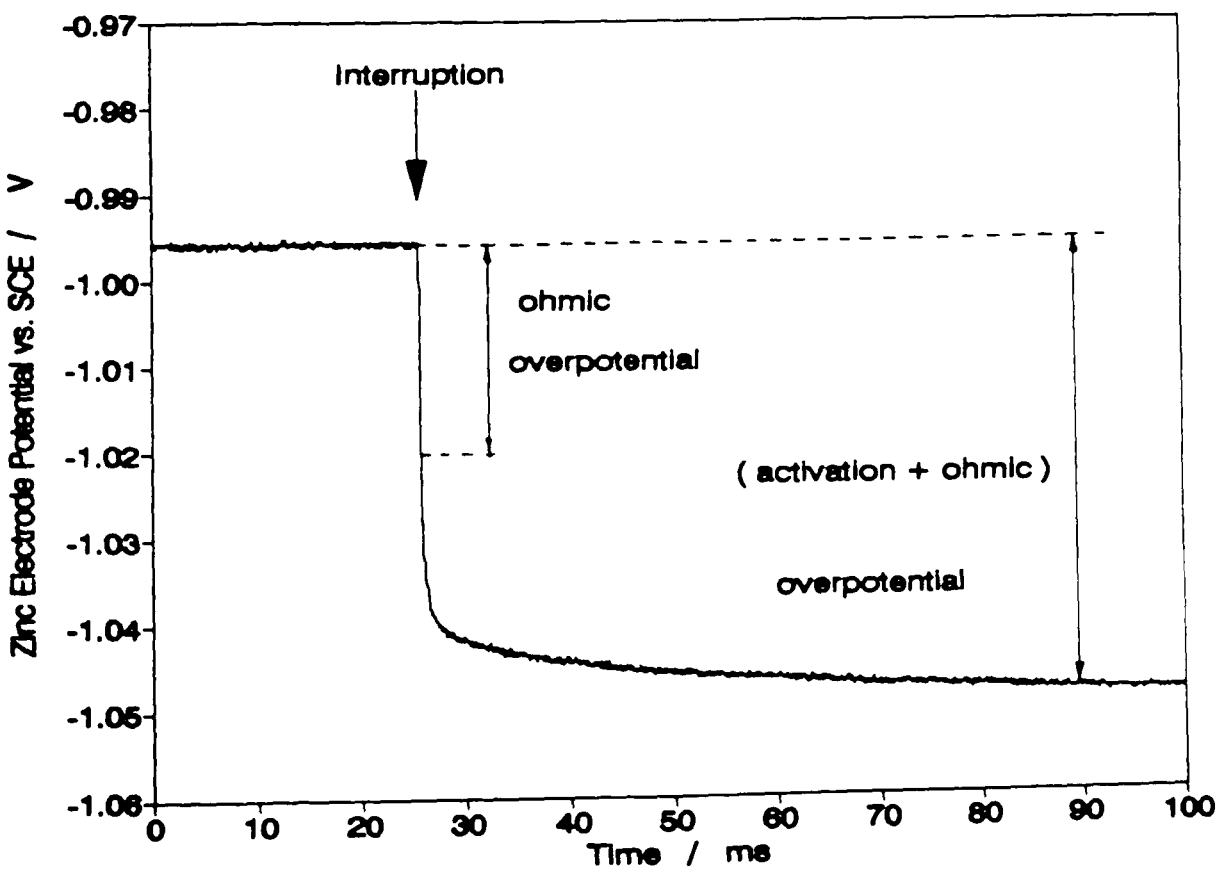

Figure 5.7 : A typical zinc electrode potential vs. SCE transient on discharge interruption; Faradiser M in Leclanché electrolyte, discharge through 4 Ω

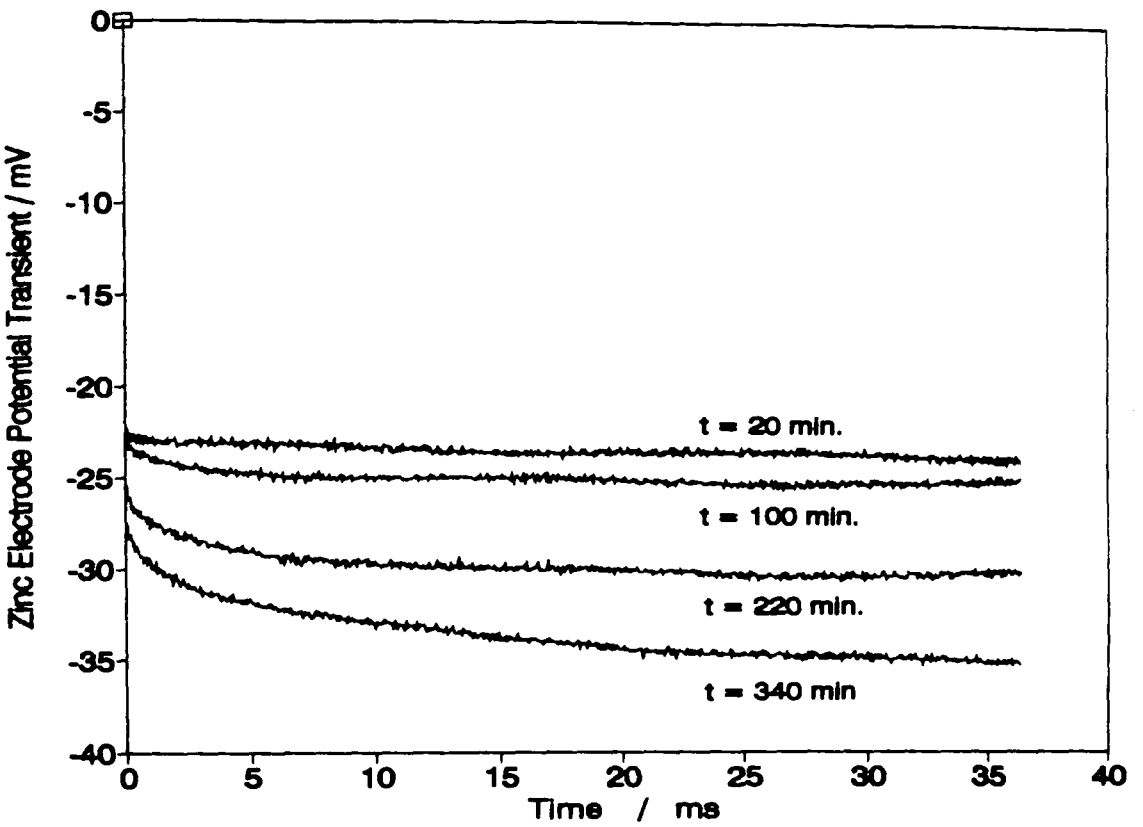

Figure 5.8 : Zinc electrode potential transients vs. SCE at different discharge depths, EMD in $ZnCl_2$ electrolyte through 2.2 Ω.

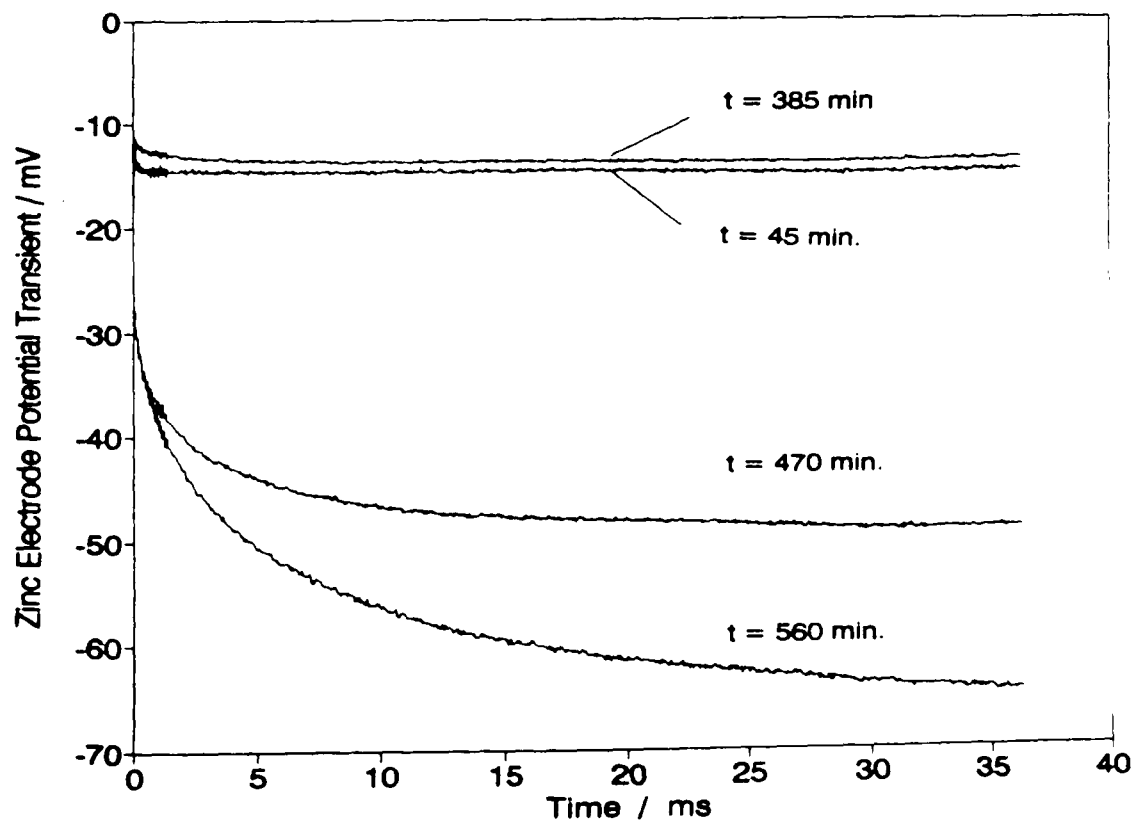

Figure 5.9 : Zinc electrode potential transients vs. SCE, at different discharge depths; EMD in Leclanché electrolyte through 4 Ω

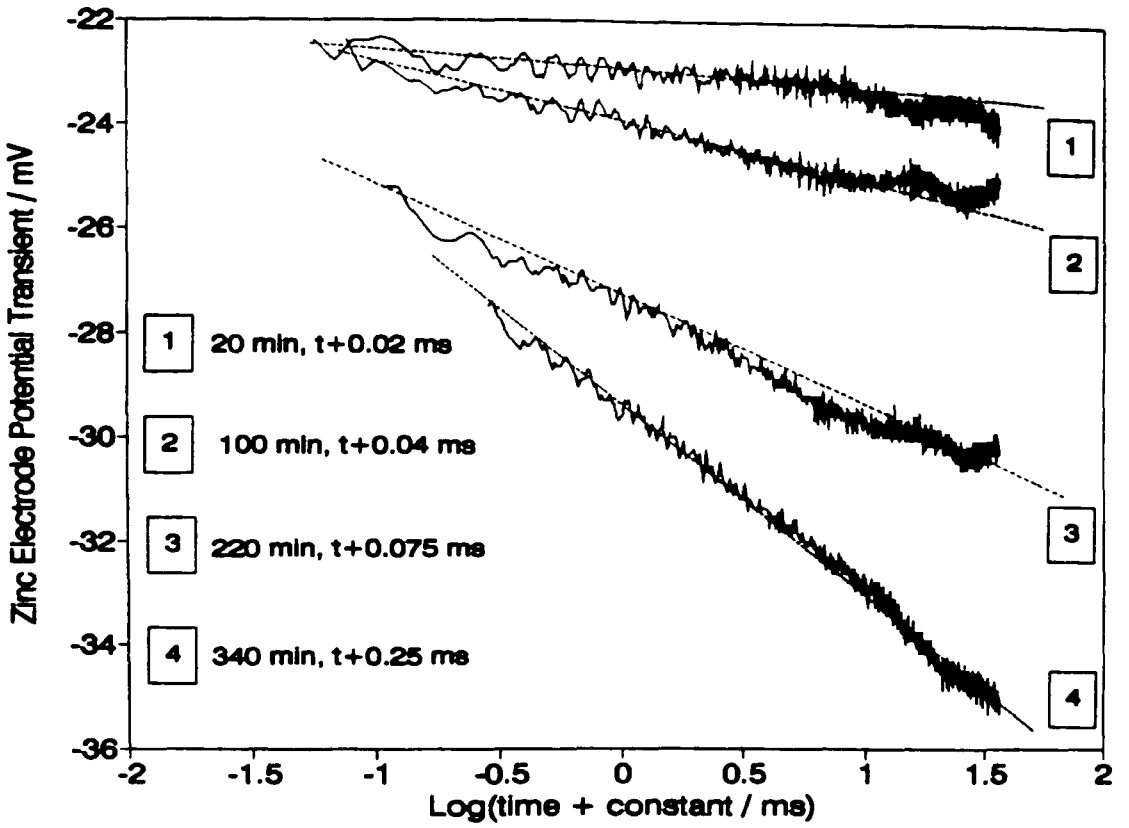

Figure 5.10 : Zinc electrode potential transient vs. SCE, on a logarithmic time scale; EMD in $ZnCl_2$ electrolyte through 2.2 Ω

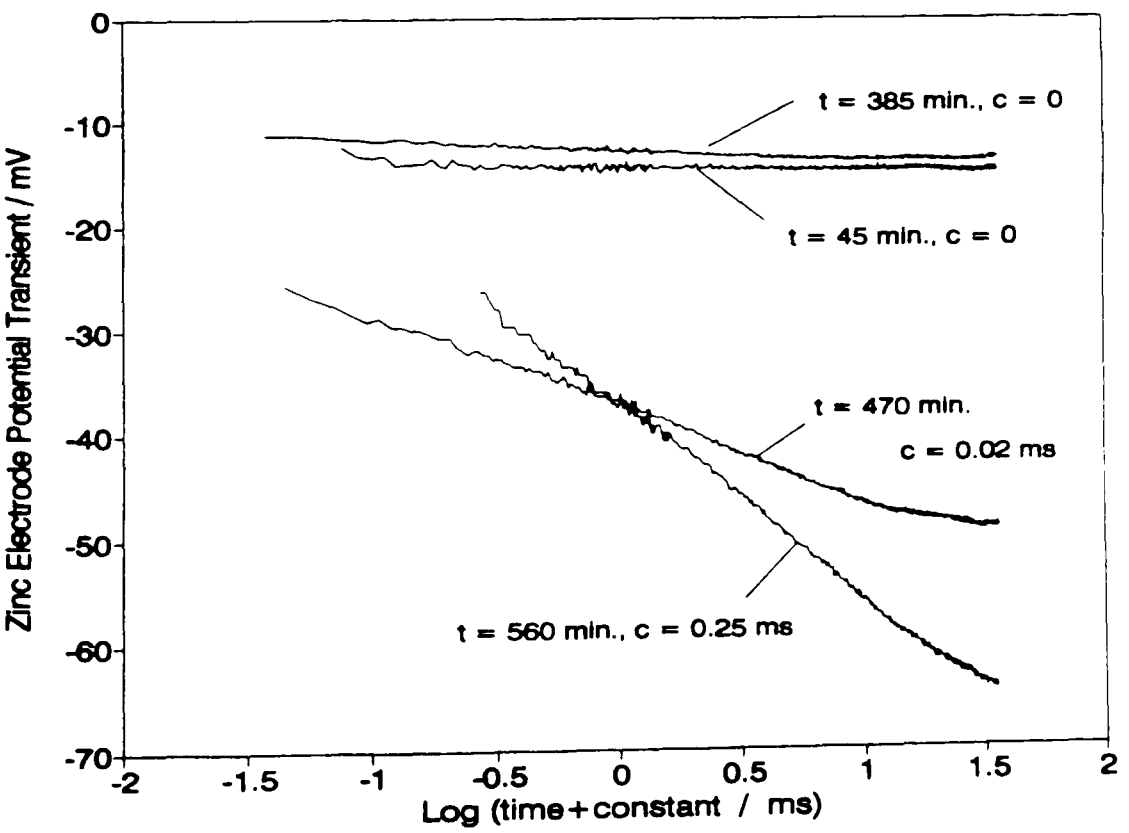

Figure 5.11 : Zinc electrode potential vs. SCE transients on logarithmic time scale; Faradiser M in Leclanché electrolyte through 4 Ω.

The shape of the transient potential curve changed during the discharge. Figure (5.8) shows a set of curves recorded after the interruption at different stages of the discharge of a zinc chloride cell and figure (5.9) the similar curves recorded in Leclanché electrolyte. The value of the potential step which occurred on interruption of the current only slightly increased with increasing discharge depth but during the 35 ms following the interruption, the potential changed from about 2 mV (after 20 minutes of discharge) to more than 10 mV in zinc chloride and more than 30 mV in Leclanché electrolyte towards the end of the test. The curvature of the plot also increased with discharge time.

Figure (5.10) shows the same potential transients as in figure (5.8) using a logarithmic scale of the time modified by addition of a constant adjustable value (figure 5.11 shows the graphs corresponding to figure (5.9), in the Leclanché electrolyte). The same type of semi-logarithmic relationship has already been reported [182,183,216-218] and explained on the basis of discharge of the electrode double layer by a current proportional to the exponential of the electrode overpotential [216,218]. Grahame [218] showed that if the electrode double layer capacitance (C) was independent of the electrode potential (E) and that if for example during an anodic reaction the cathodic process could be neglected, the relation was

$$E = E_0 - \frac{RT}{(1-\alpha)nF} \ln\left[1 + \frac{(1-\alpha)nF\ i_0\ t}{RT\ C}\right] \qquad (5.1)$$

where E_0 is the electrode potential after the ohmic potential step, α is the transfer coefficient, n the number of electrons involved in the reaction, i_0 is the exchange current density and R, T and F the gas constant, the absolute temperature and the faraday, respectively.

The linear relationships shown in figures (5.10) and (5.11) therefore indicate that during the anodic dissolution of zinc, during the heavy drain discharge tests, the reverse reaction occurred at a rate negligible compared to the dissolution rate, in agreement with the finding of Brouillet and Jolas [64]. The increase of the time shift used in the equation with increasing discharge depth suggests that the double

layer capacitance increased during the test, probably due to an increase in electrode roughness.

Despite careful shielding of all the leads used in the set-up, the measurements of the potential transients were affected by two types of noise as is evident for example in figure (5.10). The high frequency noise was virtually constant throughout all of this work (about 0.2 mV peak to peak) while the level of the low frequency (50 Hz) noise was very variable and could change very rapidly from less than 0.5 mV (peak to peak) to more than 5 mV or, as rapidly, from a high to a low value. To minimise the effect of these noises on the measured overpotentials, the readings were taken between the apparent average value of the signal before interruption and the first value after the interruption (ohmic overpotential) or the apparent average value after about 35 ms (ohmic + activation overpotential).

5.2.2 Manganese dioxide electrode potential transients

The positive electrode potential, between the carbon rod and the usual reference electrode, transients recorded at different moments of a discharge are shown in figure (5.12). This figure presents the transients measured in a cell containing the mixed Leclanché electrolyte discharged on 4 ohms, but similar results were found in pure $ZnCl_2$ electrolyte during 2.2 ohm continuous discharge tests.

The ohmic overpotential remained practically unchanged throughout the discharge but, as for the zinc electrode potential transients in figures (5.8) and (5.10), the shape of the curve changed from a step-like transient at the beginning of the test to a more curved profile with increasing discharge depth. Figure (5.13) shows that for times longer than about 1 ms, the curves could be approximated by straight lines in a potential versus $\sqrt{t}$ graph.

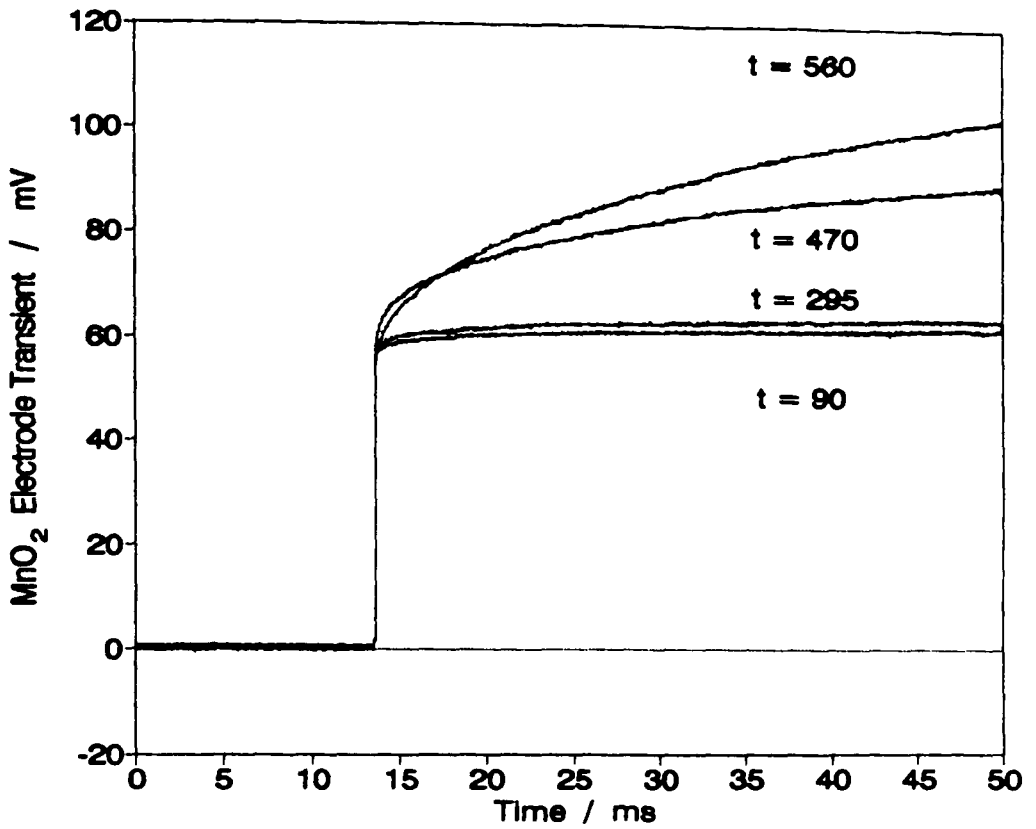

Figure 5.12 : Manganese dioxide electrode vs. SCE transients; Faradiser M in Leclanché electrolyte discharged continuously through 4 Ω.

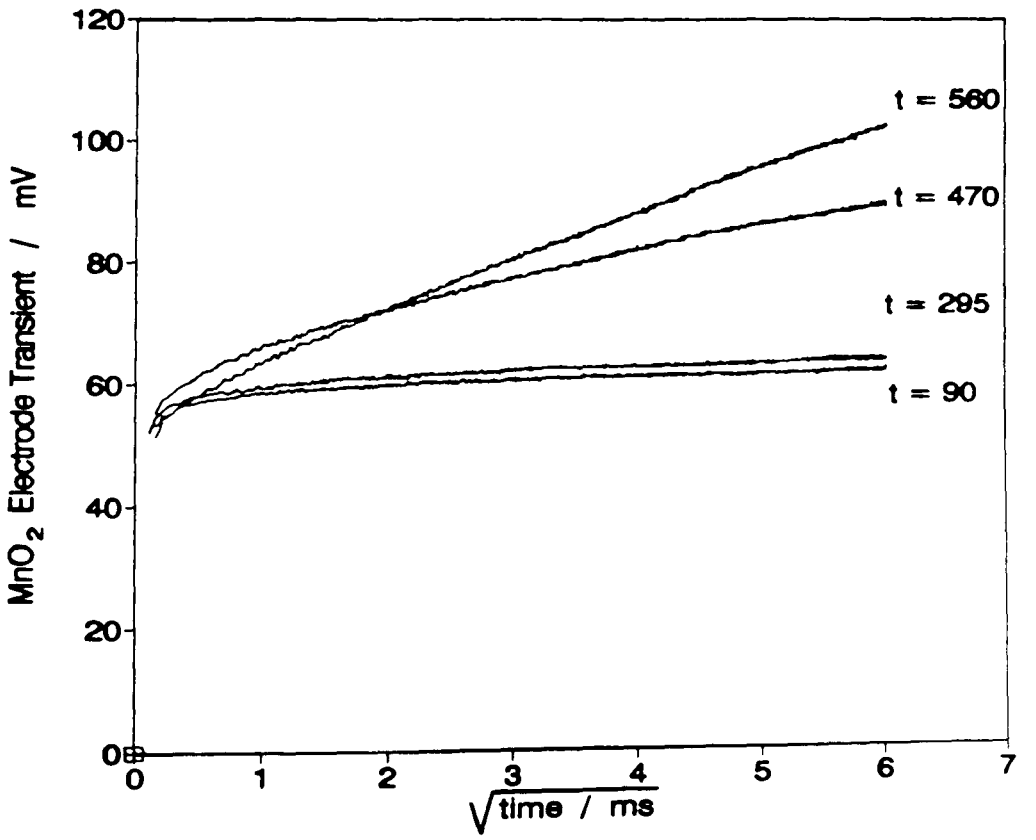

Figure 5.13 : Positive electrode (vs. usual reference electrode) transients on a $\sqrt{t}$ scale; Faradiser M in Leclanché electrolyte discharged continuously through 4 Ω

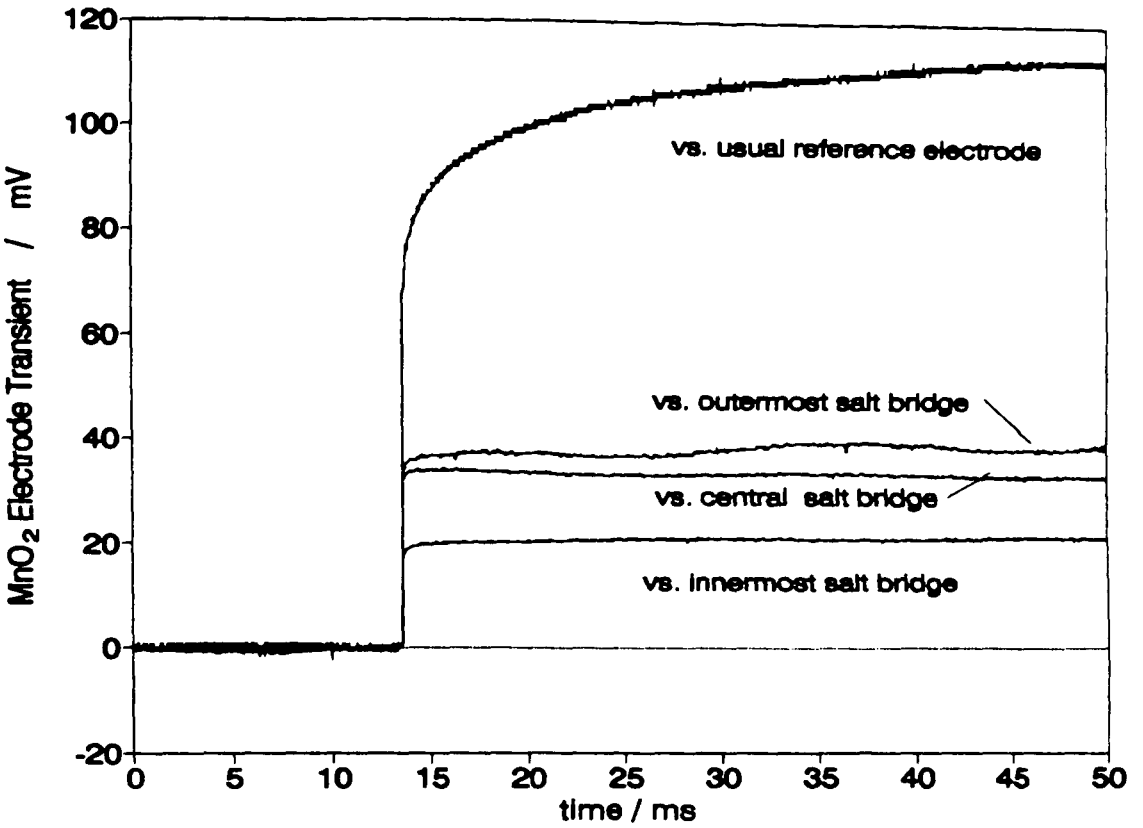

Figure 5.14 : Transients of the MnO_2 electrode potential versus reference electrodes at different positions into the electrode (salt bridges); Faradiser M in Leclanché electrolyte through 4 Ω after about 500 min. on load

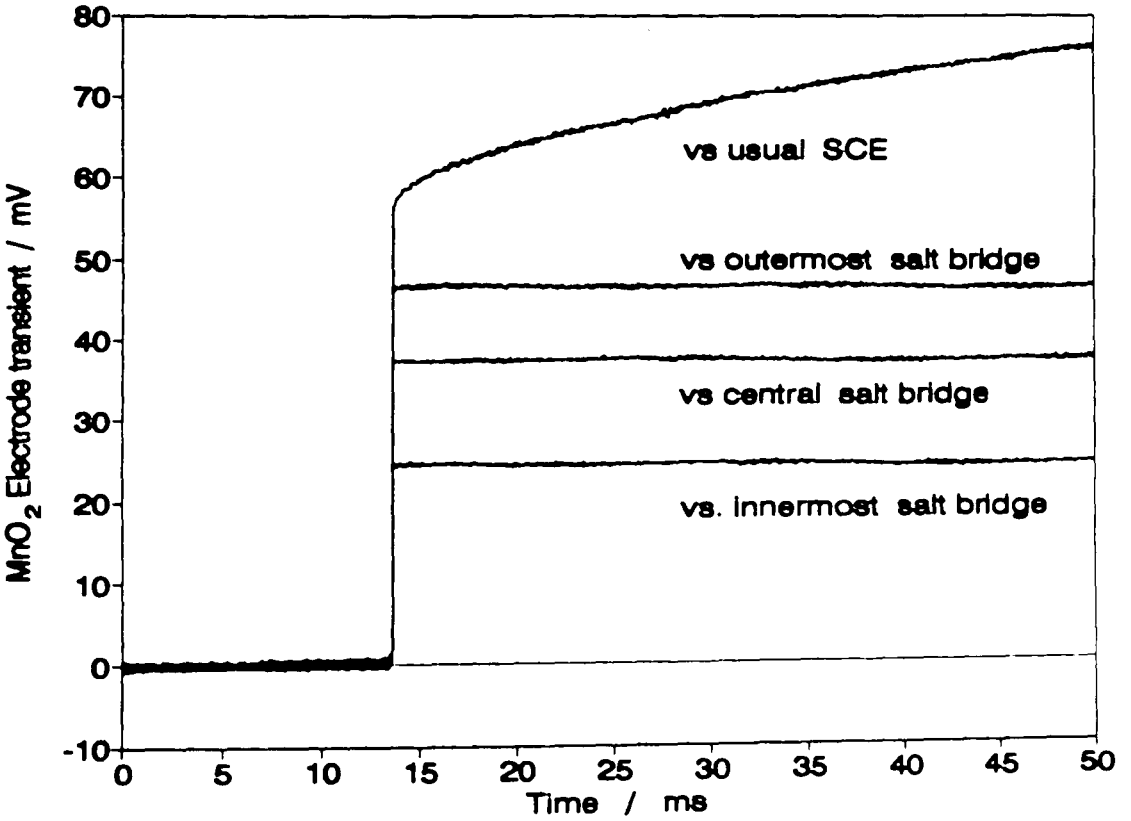

Figure 5.15 : Transients of the MnO_2 electrode potential versus reference electrodes at different positions into the electrode (salt bridges); EMD in $ZnCl_2$ electrolyte through 2.2 Ω after about 300 min.

A $\sqrt{t}$ dependence was predicted by Brouillet *et al.* (equation 1.33) [147] and by Era *et al.* (equation 1.34) [150] for the electrode recovery after discharge interruption and therefore figure (5.13) suggests that the electrode started to recuperate during the suspension of the discharge. The possibility of the electrode recovery during the interruption is supported by the finding of Garche *et al.* [219] who reported a recuperation of the PbO_2 electrode during the pause of the discharge.

Salt bridges were inserted at different locations into the positive electrode mass and connected to reference electrodes. The electrode potential transients were occasionally measured with respect to these electrodes. Figures (5.14) and (5.15) show such transients after about 500 minutes of discharge in Leclanché cell (figure 5.14) and after about 300 minutes of discharge in pure $ZnCl_2$ electrolyte cell (figure 5.15), i.e. towards the end of the test for both cells. They also compare these transients to the curve recorded using the SCE inserted through the zinc electrode. The transients measured with respect to a reference electrode connected inside the manganese dioxide mix displayed very little curvature, especially in the pure $ZnCl_2$ electrolyte cell where the transients were practically step potential changes. This clearly rules out the possibility of a significant electrode recovery during the short time of the measurement and directs attention to the space between the outermost salt bridge and the zinc electrode compartment, i.e. to the separator region as the cause of the curvature in the manganese dioxide transients.

5.2.3 Transients measured with salt bridges

In the following, the expression "salt bridge potential" refers to the potential taken by a reference electrode connected to the positive electrode mass by a salt bridge inserted into this mass, with respect to the usual reference electrode inserted through the zinc can. By analogy with the previous sections, the change of this potential on current interruption is called "salt bridge transient".

Figure (5.16) shows some of the outermost salt bridge transients recorded at different moments of the discharge of a $ZnCl_2$ cell. There is a great similarity with the positive electrode transients shown in figure (5.12).

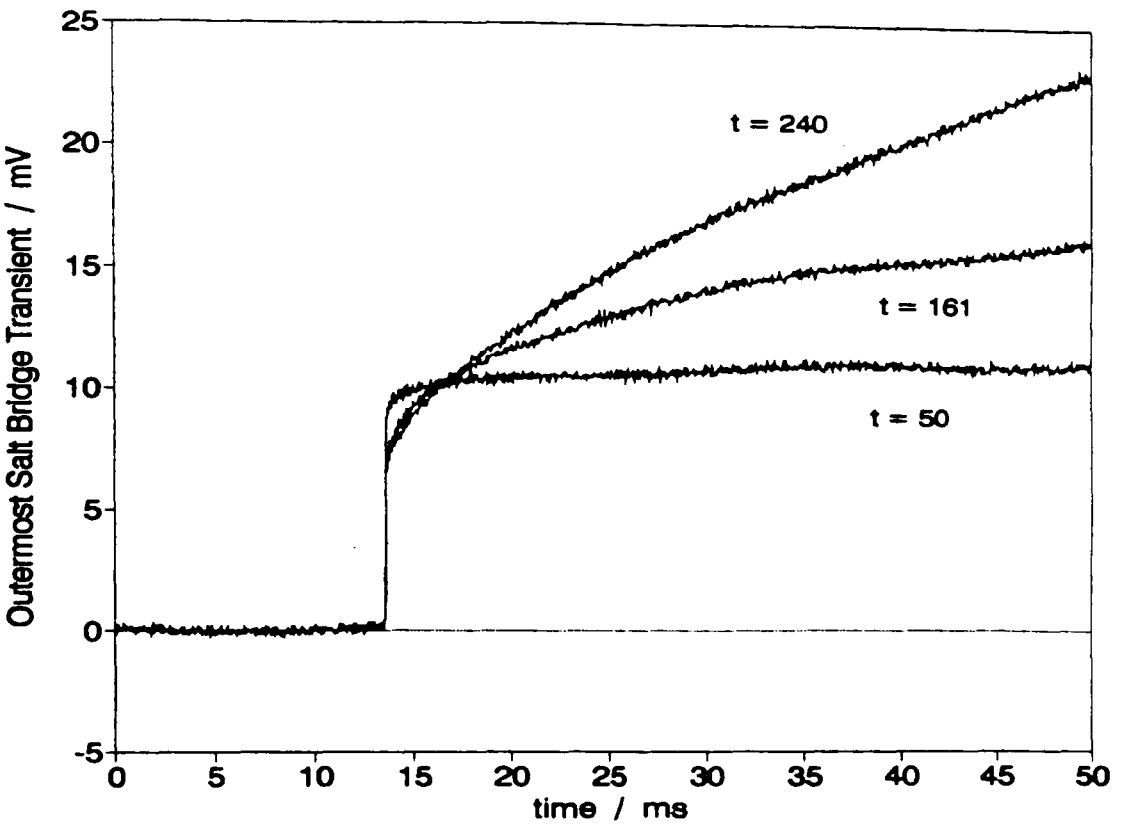

Figure 5.16 : Outermost salt bridge transients at different depths of discharge; Faradiser WSZ in $ZnCl_2$ electrolyte on continuous discharge through 2.2 Ω

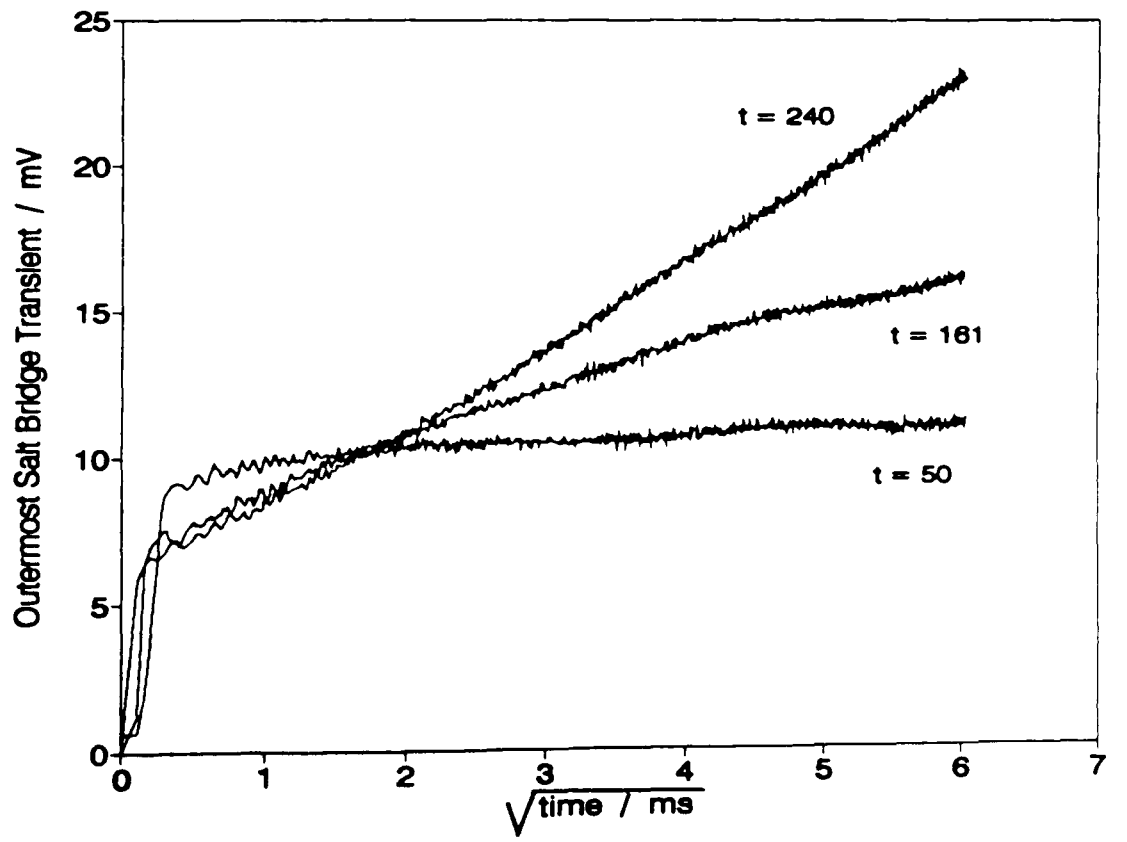

Figure 5.17 : Outermost salt bridge transients (as in figure 5.16), as a function of √t; Faradiser WSZ in $ZnCl_2$ electrolyte on continuous discharge though 2.2 Ω.

There is also a great similarity in the shape of the curves between figure (5.17) which shows the same transients as in figure (5.16) drawn as a function of $\sqrt{t}$ and the equivalent plots in figure (5.13). Figure (5.18), recorded when the discharge was stopped, shows that the linearity of the plot lasted about 500 ms and that the complete decay of the salt bridge potential occurred in about 1 second.

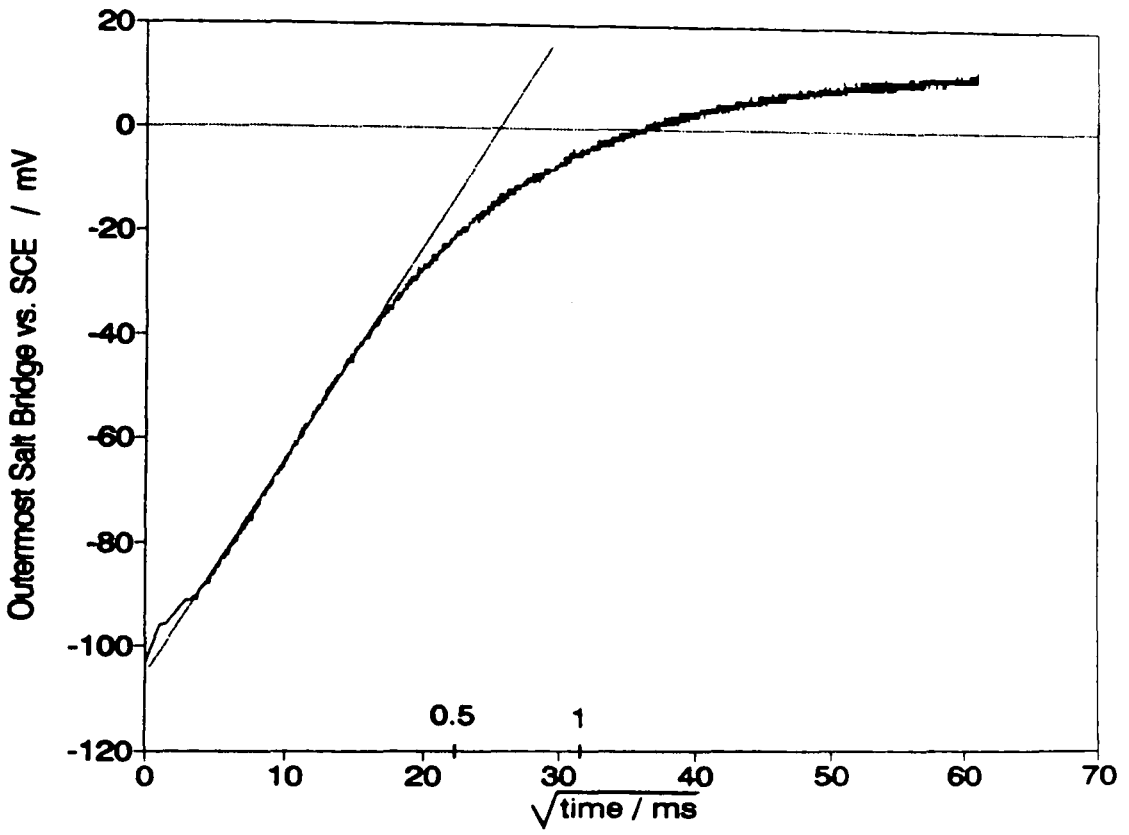

Figure 5.18 : Outermost salt bridge transient (against the usual reference electrode) at the end of the discharge; Faradiser WSZ in $ZnCl_2$ electrolyte on continuous discharge through 2.2 Ω; end of the discharge

Figures (5.19) and (5.20) show the salt bridges transients recorded during the seventh hour of the discharge of a zinc chloride cell, as a function of time and as a function of $\sqrt{t}$, respectively. The three curves are practically parallel in both plots suggesting that they were caused by the same phenomenon, occurring between the outermost salt bridge and the negative electrode compartment, modified by a constant potential difference depending on the location of the salt bridge.

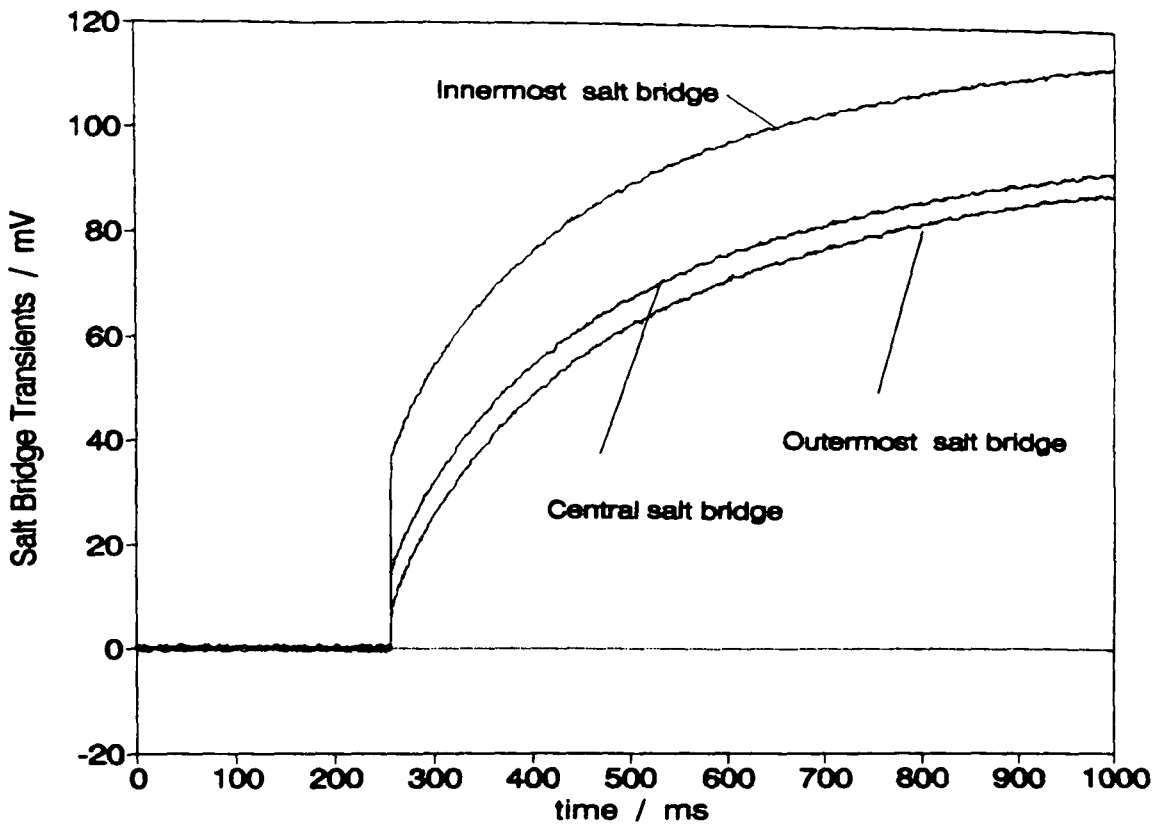

Figure 5.19 : Salt bridge transients; Faradiser WSZ in $ZnCl_2$ electrolyte, sixth hour of a continuous discharge through 2.2 Ω

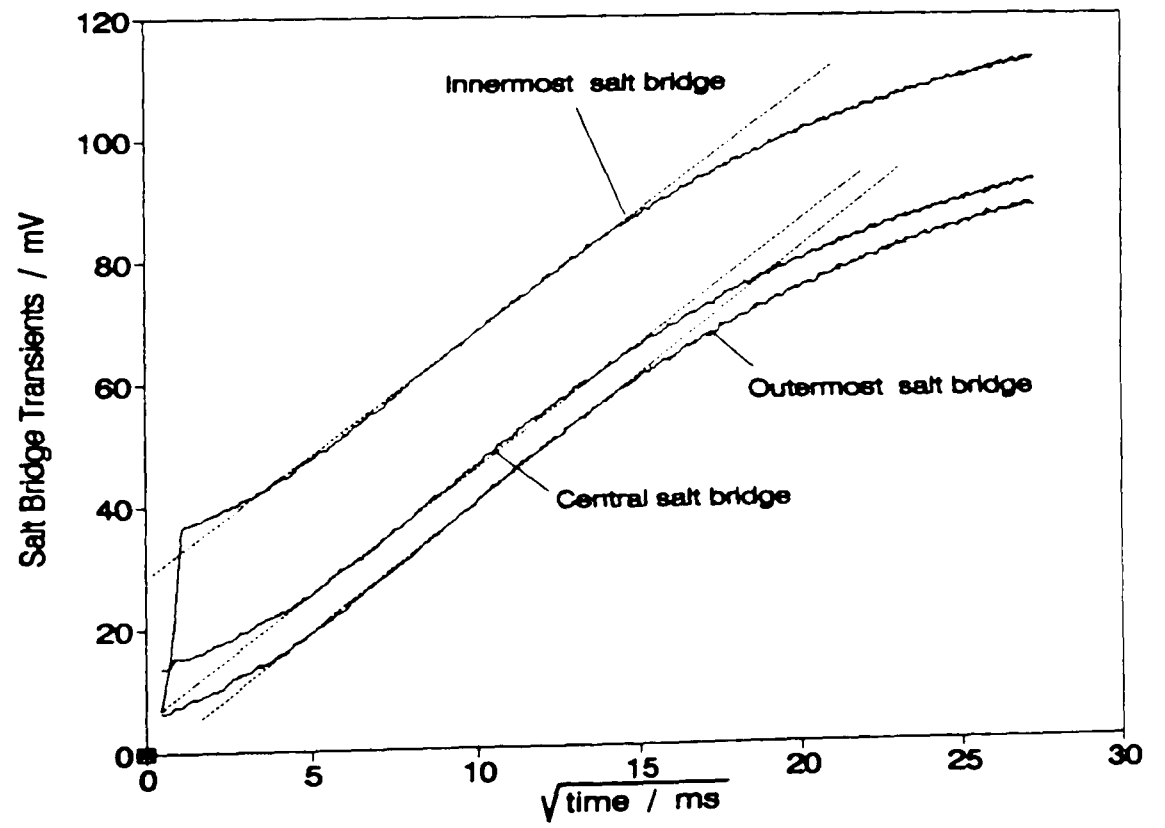

Figure 5.20 : Salt bridge transients as in figure (5.19) on a √t scale; Faradiser WSZ in $ZnCl_2$ electrolyte, sixth hour of a continuous discharge through 2.2 Ω

The common origin of the potential difference is confirmed by the fact that the linear range (in figure 5.20) was the same for the three curves, namely between 2 and about 400 ms after the interruption of the discharge.

When used in a medium having both electronic and ionic conductivity as is the case for the positive electrode mass of a Leclanché cell, ionic probes (salt bridges) can only detect potential differences across the ionic conductor phase [220,221] and therefore the origin of the potential difference between the reference electrodes connected to the electrolyte phase on each side of the separator has to be found within this electrolyte phase in the separator region. A blockage of the separator pores would increase the length and the tortuosity of the path of ionic transport and increase the electrolyte resistance [73] across the separator. This would appear in the transient just as a potential step on current interruption, which was not the case. Another possible explanation is the formation of a diffusion potential across the separator due to the build up of concentration gradients during the discharge. On interruption of the current, the external electric field existing between the electrodes is cut off and diffusion reduces the concentration gradients and the associated diffusion potential. A diffusion-controlled process is very likely to exhibit a $\sqrt{t}$ dependence and is therefore compatible with the experimental observations.

5.2.4 Carbon probe potential transients

Figures (5.21) and (5.22) show the outermost probe potential transients as a function of time and $\sqrt{t}$ respectively, as they were recorded at different moments of a Leclanché cell discharge. The similarity of these curves with the manganese dioxide electrode potential transients (figures 5.12 and 5.13) is obvious and confirms the existence of a process controlling the shape of all the potential transients measured into the positive electrode compartment.

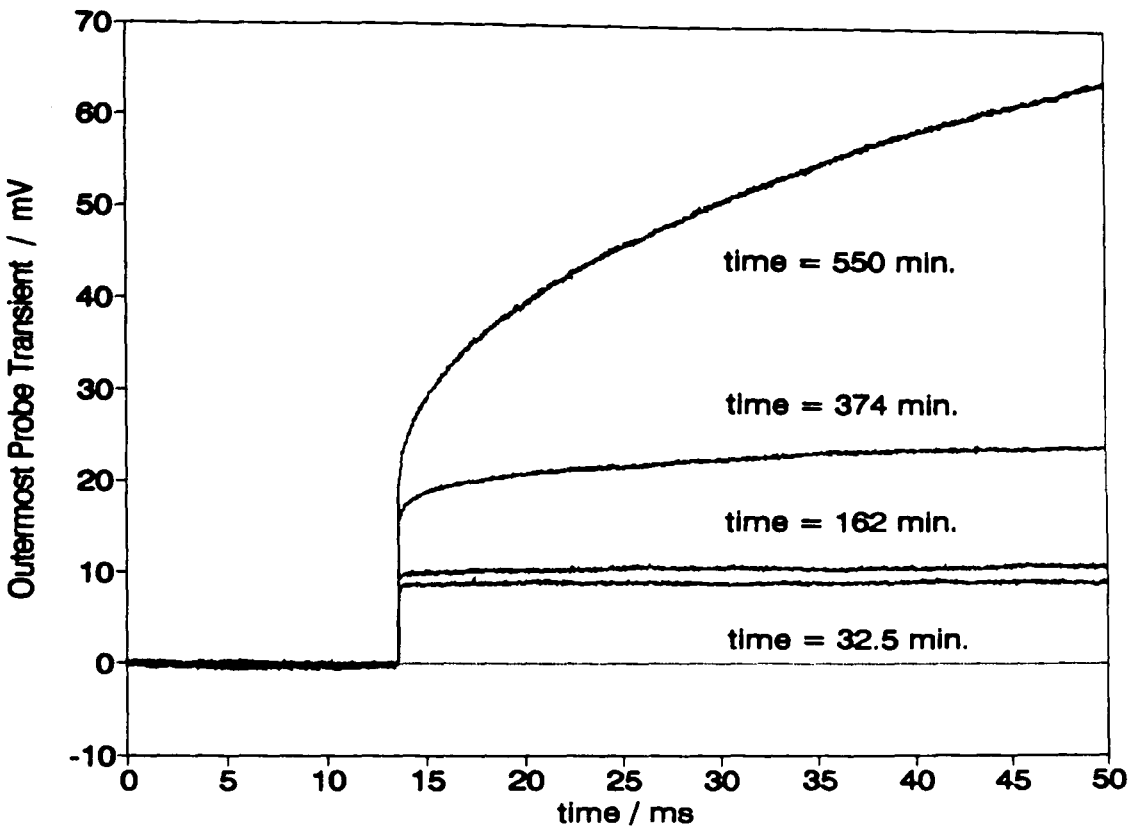

Figure 5.21 : Outermost carbon probe potential (vs. usual SCE) transient at different discharge depths; EMD in Leclanché electrolyte discharged continuously through 4 Ω

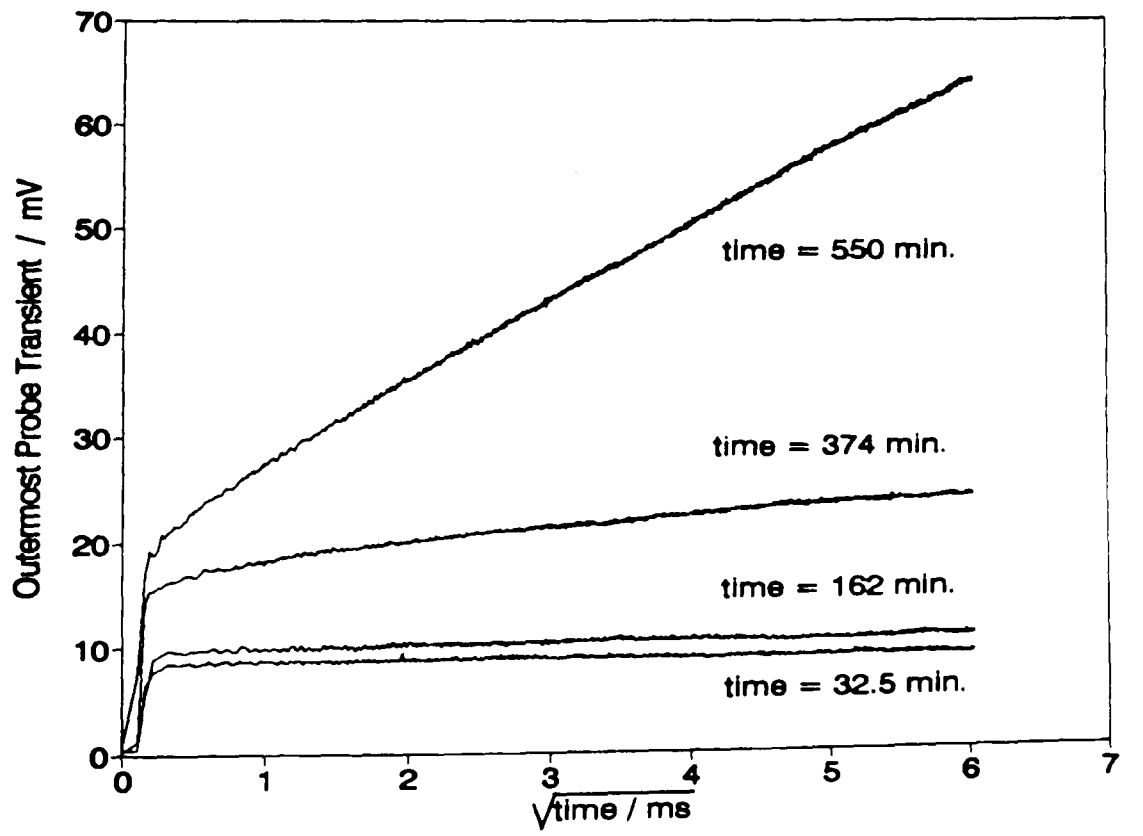

Figure 5.22 : Outermost carbon probe potential as in figure (5.21) as a function of $\sqrt{t}$; EMD in Leclanché electrolyte discharged continuously through 4 Ω.

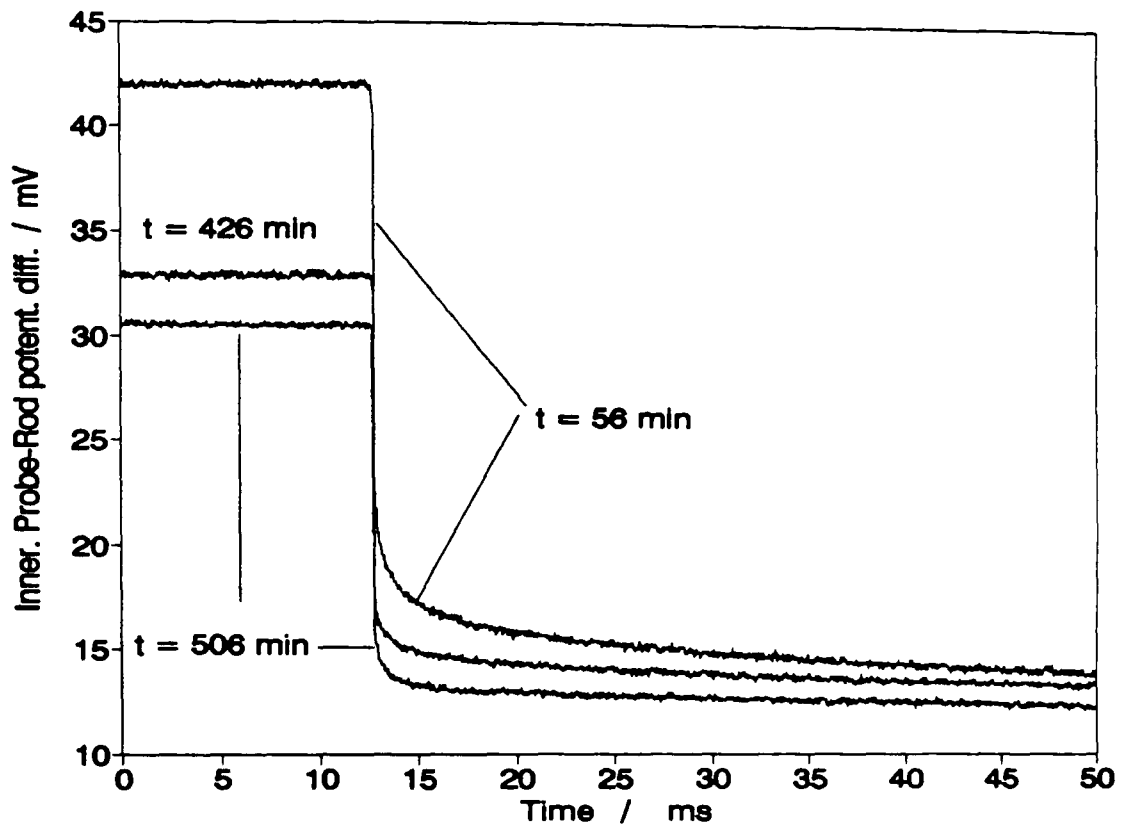

Figure 5.23 : Innermost carbon probe versus positive terminal; Faradiser M in Leclanché electrolyte discharged continuously through 4 Ω

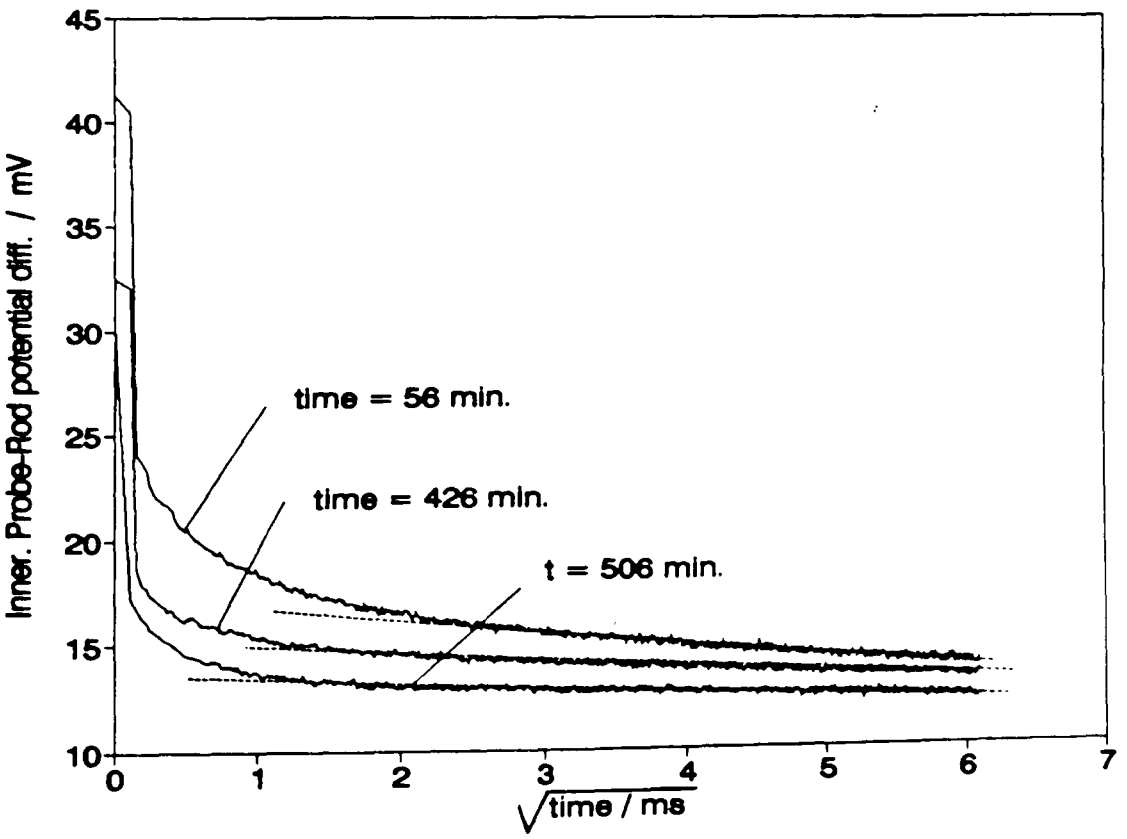

Figure 5.24 : Innermost carbon probe versus positive terminal versus √t; Faradiser M in Leclanché electrolyte discharged continuously through 4 Ω

During the discharge, a potential difference appeared between the carbon probes and the cell positive terminal. Figures (5.23) and (5.24) show how this potential difference changed on discharge interruption, on a linear time scale (fig. 5.23) or on a $\sqrt{t}$ scale (fig. 5.24). The potential difference between the carbon probe (the innermost probe in this case but the other probes exhibited similar behaviour) and the cell positive terminal (carbon rod) did not vanish on discharge interruption but just decreased down to about 10 - 20 mV and then the decay showed a $\sqrt{t}$ dependence. No reference electrode was used in these measurements and therefore the $\sqrt{t}$ dependence could not be due to the same effect which affected the potentials measured with respect to the usual SCE. In this case, the decay of the potential difference was due to a levelling of the non-uniformity of the manganese dioxide potential within the electrode, the potential of each part changing according to equation (1.33) or (1.34) with the resulting effect shown in figure (5.24). In this case, both the carbon rod and the probe were electronic conductors and therefore only sensitive to electronic conductivity [220,221]. All the electronic conductors inserted into the positive electrode mix (current collector and carbon probes) were connected to each other through the conductive electrode matrix (the acetylene black) and therefore any potential difference between two of them reflected the ohmic loss due to the passage of the current through the electronic conductive phase of the electrode between the points under consideration. On this basis, the potential difference existing on open circuit between the positive terminal and a carbon probe, with the probe positive with respect to the rod, means that electrons were flowing from the region surrounding the rod to the outer parts of the electrode, in other words during the interruption, the outer part of the electrode was recharging the inner part. The higher open circuit potential at the periphery of the electrode compared to its centre may have been the result of a greater reduction rate deep inside the electrode compared with the external layer or to the electrolyte pH being more acidic in the external layer than close to the current collector [78].

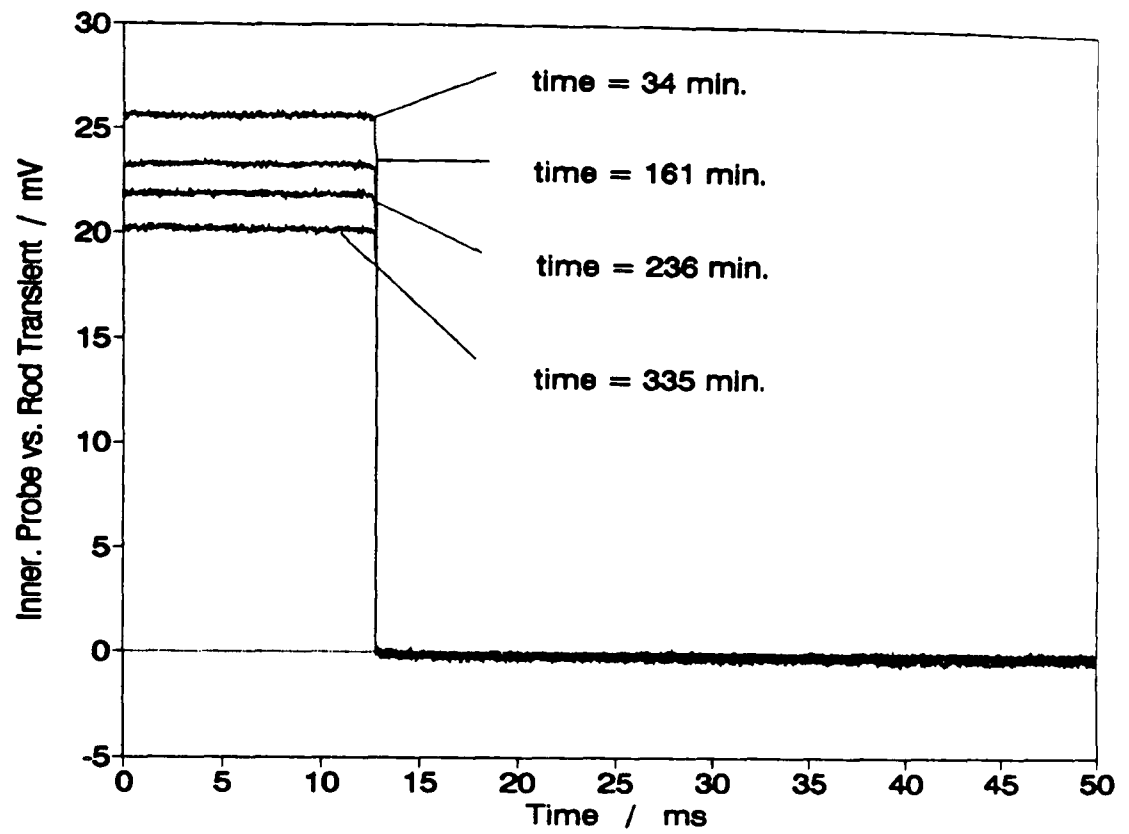

Figure 5.25 : Innermost carbon probe potential with respect to the carbon rod; EMD in $ZnCl_2$ electrolyte discharged continuously through 2.2 Ω

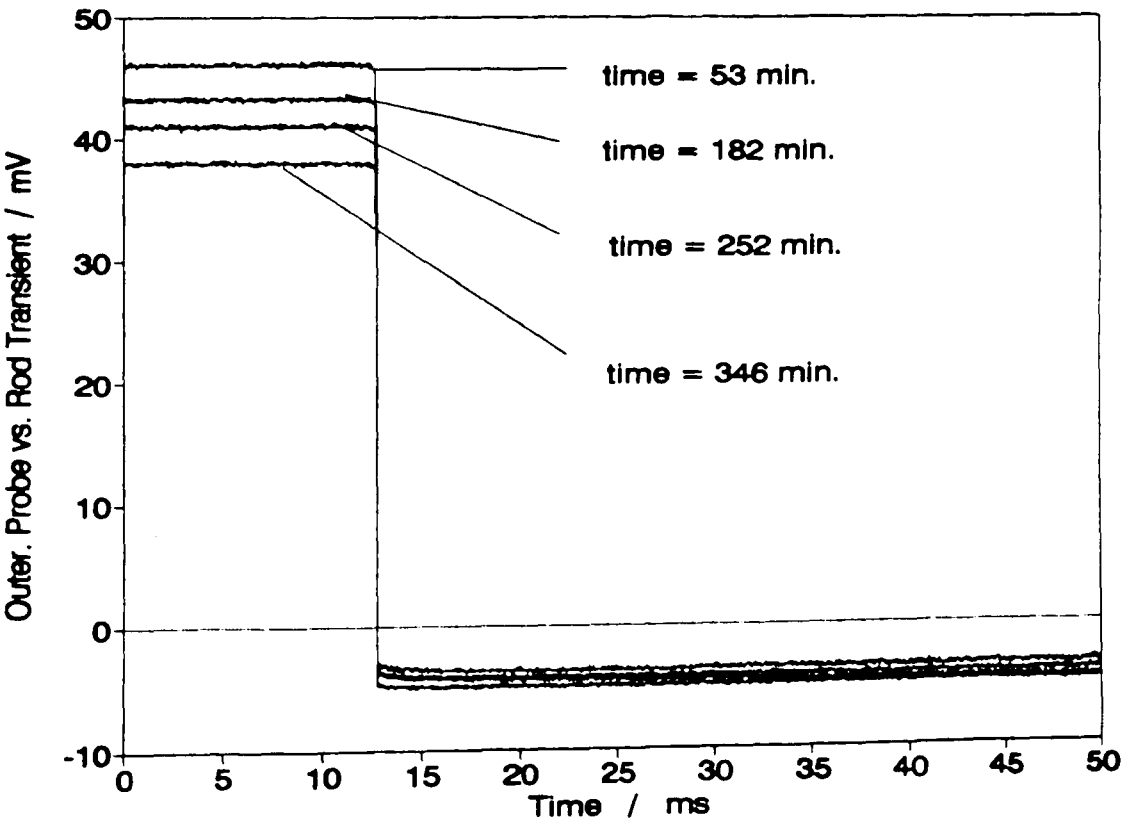

Figure 5.26 : Outermost carbon probe potential with respect to the carbon rod; EMD in $ZnCl_2$ electrolyte discharged continuously through 2.2 Ω

Figures (5.25) and (5.26) show how the potential difference between the innermost probe and the rod (figure 5.25) and between the outermost probe and the rod (figure 5.26) changed on interruption of the discharge in $ZnCl_2$ electrolyte. The innermost potential fell to the same potential as the current collector without any measurable delay indicating the same reduction degree around the rod as around the innermost probe. By contrast, the outermost probe potential also fell very rapidly but to a potential lower than the rod potential. The central probe (not shown) exhibited a behaviour intermediate between the other two probes with an open circuit potential slightly negative with respect to the rod). This suggests a higher reduction level at the periphery than in the interior of the electrode.

Figures (5.14) and (5.15) show that in both Leclanché and $ZnCl_2$ electrolytes, the response of the manganese dioxide electrode to a step change of the current may be considered to be a step change of the electrode potential. No capacitive effect can be seen in the transients of figure (5.25) and (5.26). This means that the time constant of the manganese dioxide electrode equivalent circuit [153,179] was very small. The double layer capacitance of porous electrode is very large and therefore the small time constant of the equivalent circuit was due to a very small value of the charge transfer resistance. The combination of a small charge transfer resistance with the low effective current density typical of a porous electrode, gave the positive electrode a very small activation overpotential.

5.2.5 Transients at the starting of the discharge

Figure (5.27) shows the cell's electrode transients when the discharge was started. Both electrode overpotentials passed through a maximum and then decreased (they increased again later when the concentration overpotentials became significant). This behaviour was common to Leclanché and $ZnCl_2$ cells. Figure (5.28) shows that the positive electrode overpotential also exhibited this

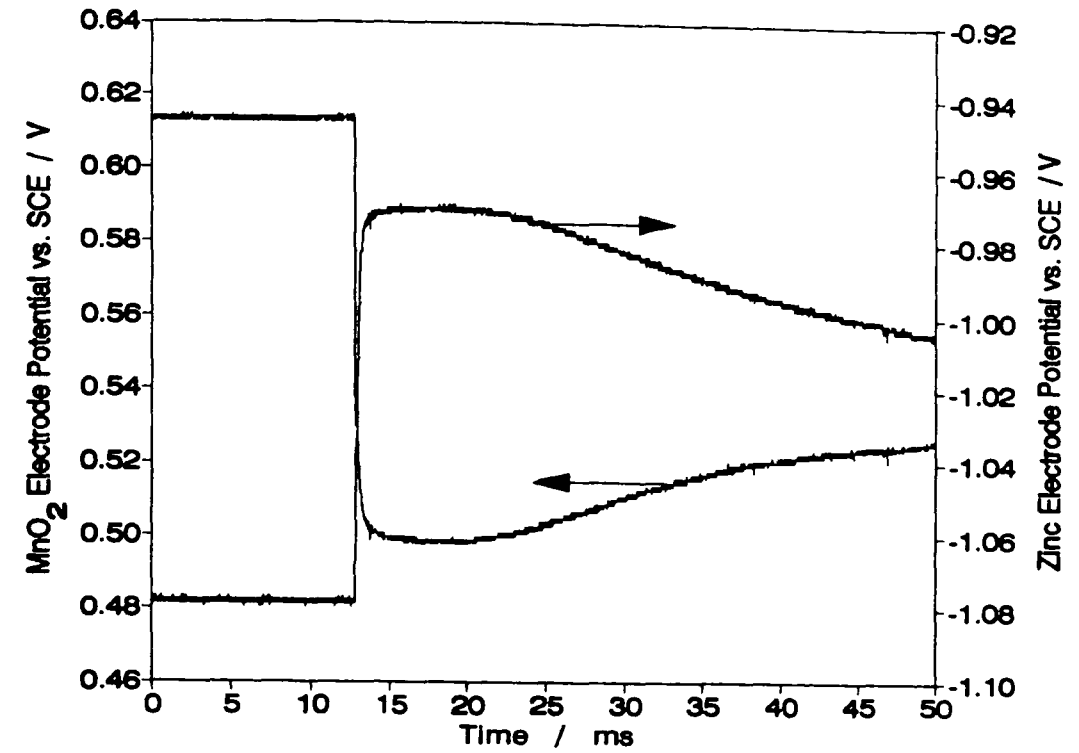

Figure 5.27 : Electrodes (vs. the usual SCE) transients at the beginning of the discharge through 4 Ω; Faradiser M in Leclanché electrolyte

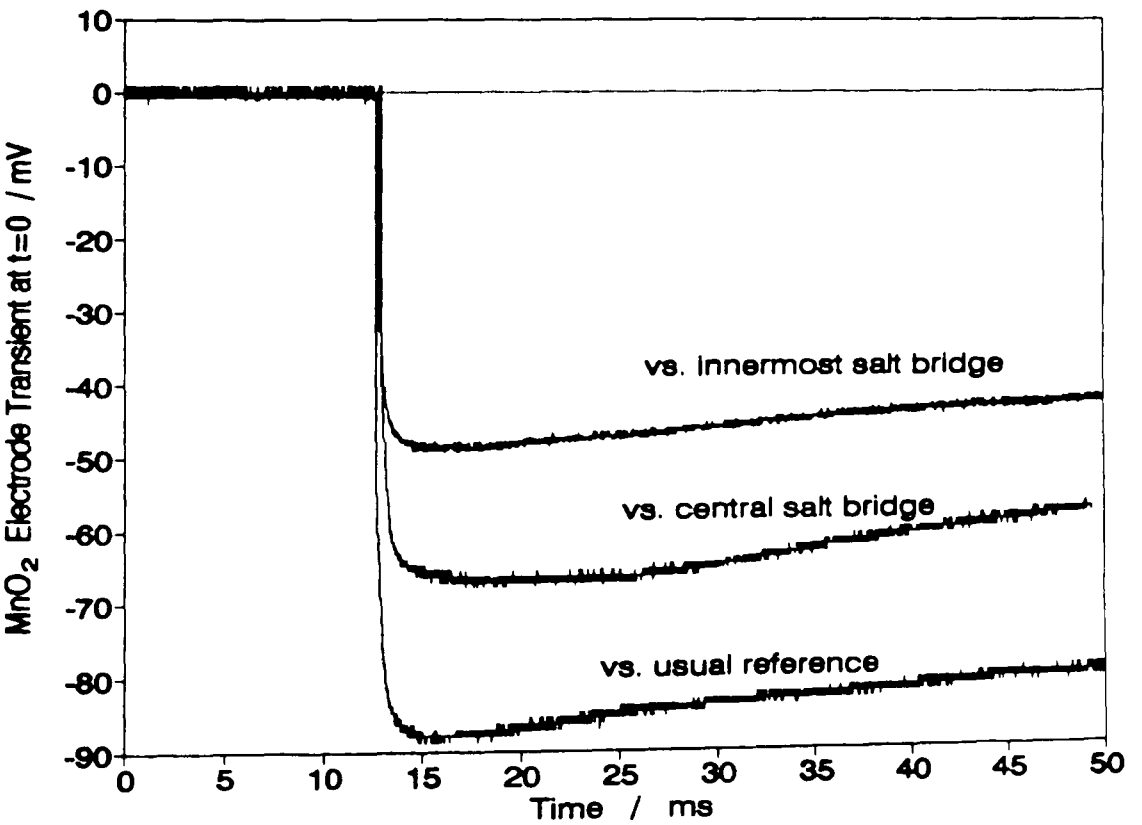

Figure 5.28 : Transients of the MnO_2 electrode potential versus salt bridges at the beginning of the discharge through 4 Ω; Faradiser M in Leclanché electrolyte

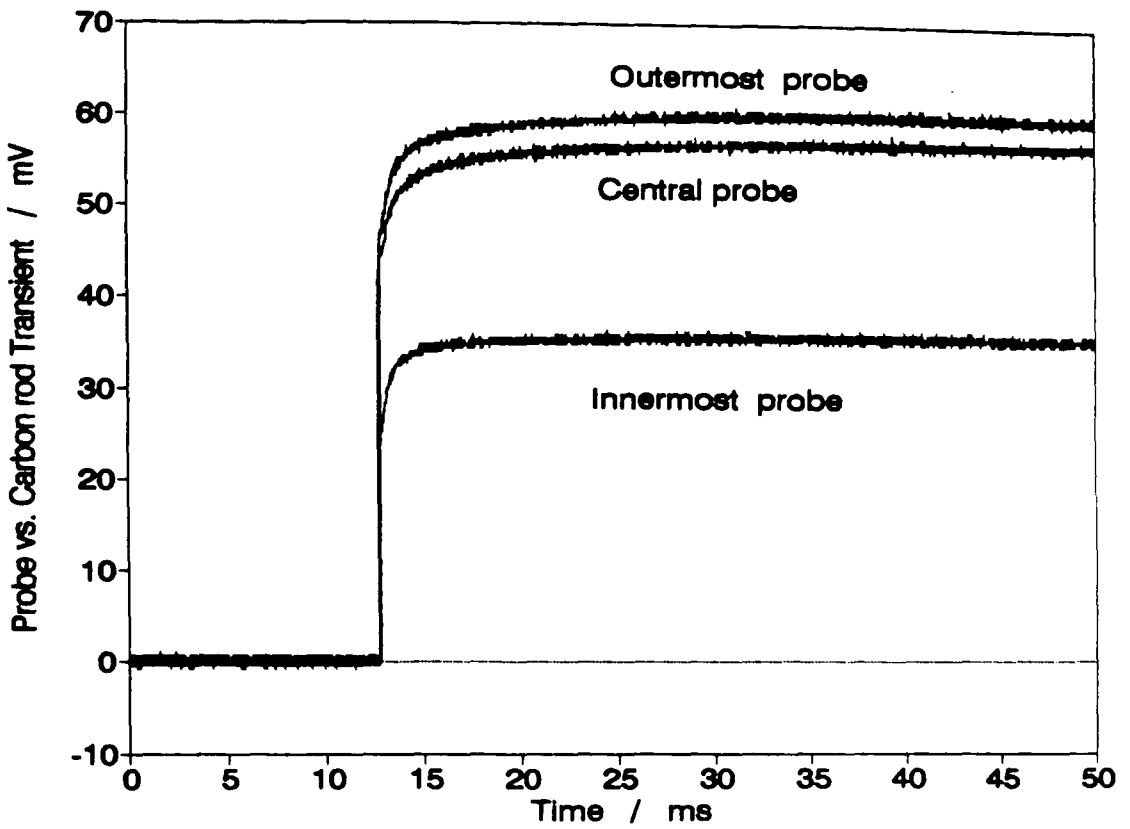

Figure 5.29 : Transients of the probe potentials with respect to the carbon rod; measured at the beginning of discharge through 4 Ω; Faradiser M in Leclanché electrolyte

local maximum when expressed with respect to reference electrodes connected to the electrolyte inside the cathode mass (salt bridges). The transients in figure (5.28) were recorded during short (about 0.2-0.3 s) discharge pulses separated by about 10 minute recovery periods. This accounts for the slightly dissimilar shape of the central salt bridge transient curve. The behaviour of the zinc electrode on starting of the discharge was similar to the behaviour of the magnesium electrode reported by Narayanan and Sathyanarayama [222] who explained the overshoot by the dissolution at the beginning of the discharge of a passivation layer formed on the electrode surface. The similarity of the transients suggests that the dissolution of a surface film on the zinc electrode was also the cause of the observed maximum of the electrode overpotential. The reason for the manganese dioxide electrode behaviour is not well understood. The transients between the carbon probes and the current collector shown in figure (5.29) do not exhibit any sign of a maximum after a few milliseconds of discharge. This suggest that the

cause of the maximum in the electrode overpotential is to be found in the electrolyte, possibly in a change of the ohmic loss induced by the change of the discharge current.

5.3. Conclusions

The potential of a zinc probe inserted into a cell through a hole drilled into the zinc electrode will be different from the open circuit potential of the zinc electrode itself whenever the concentrations in the cell are not uniform, e.g. during a discharge or the recovery after discharge of the cell. This makes it impossible the use a zinc probe to monitor the zinc electrode concentration overpotential during a discharge.

The change of the zinc electrode potential on interruption of the discharge is the sum of the electrode activation overpotential and the ohmic overpotential existing between the electrode and the extremity of the Luggin capillary used as connection to the reference electrode. The electrode closed circuit potential corrected for this overvoltage provided a much better measure of the electrode open circuit potential than the potential measured using a zinc probe. The changes of the zinc electrode activation overpotential may be understood qualitatively by considering the variation of the NH_4Cl concentration at the electrode with discharge time and the influence of this concentration on the charge transfer overpotential. Zinc probes might however be very useful to monitor the change on discharge of the zinc activity into the positive electrode where concentration gradients are unlikely to be as important as at the zinc electrode.

The zinc electrode transients on interruption revealed a charge transfer overpotential corresponding to the discharge of the electrical double layer by the zinc dissolution reaction, without any significant influence of the reverse reaction. The plot of the overpotential decay on a logarithmic scale of time after interruption suggested that the electrode double layer capacity increased with

increasing discharge depth, probably due to an increase of the electrode roughness. The open circuit potential may be calculated by adding the ohmic and the charge transfer overpotentials (measured after about 35 ms) to the closed circuit electrode potential. The validity of this procedure is supported by the absence of significant discontinuity in the zinc electrode open circuit potential curve shown in figure (5.5). The interruption method is a very useful technique for estimating the zinc electrode concentration overpotential.

The manganese dioxide electrode exhibited negligible charge transfer overpotential. This was apparent on the plot of the electrode potential transients using a square root of time scale which showed little deviation from linearity during the beginning of the interruption periods. The very low activation overpotential of the manganese dioxide electrode was confirmed by the step-like transients measured between the current collector and carbon probes inserted into the electrode mix. As a consequence, the open circuit potential of the electrode may be calculated by correction of the closed circuit potential for the ohmic overpotential only. No significant recovery of the positive electrode was observed during the discharge interruptions.

All the potentials within the positive electrode mass which were measured with respect to the reference electrode inserted into the negative electrode compartment were affected by a diffusion potential which decayed with a $\sqrt{t}$ dependence as soon as the discharge was interrupted. This diffusion potential vanished in about one second at the end of the discharge suggesting a very short diffusion path [223], possibly the separator thickness or the thickness of a precipitate layer on its surface. Salt bridges inserted at different locations in the cell permitted the measurement of the potential differences existing between different points of the electrolyte phase.

The potential difference existing between the current collector and the carbon probes on open circuit has been interpreted as an ohmic potential difference across

the electronic conductor in the electrode mass. It shows that the positive electrode reduction was not uniform and that the electrochemical current distribution was probably different in Leclanché electrolyte through 4 ohm discharge and in $ZnCl_2$ electrolyte on 2.2 ohm discharge. Carbon probes are very useful to study the electronic current distribution within the positive electrode mass and permit the calculation of the electrochemical reaction rate distribution within the volume of the electrode (rate of discharge of the manganese dioxide, e.g. in A cm^{-3}, see section 6.3).

Chapter 6. Continuous discharges

The results of the continuous discharge tests through a 4 ohm load in the Leclanché electrolyte and through a 2.2 ohm load in $ZnCl_2$ electrolyte are reported in this chapter. The discharge tests were stopped when the cell voltage reached 0.9 V. In Leclanché electrolyte, the cells contained either EMD or Faradiser M; in $ZnCl_2$ electrolyte, they contained either EMD, Faradiser M or Faradiser WSZ. Two different formulations were used for zinc chloride cells containing Faradiser WSZ to study the influence of the electrolyte content on the cell performance.

6.1. The cell voltages and the electrolyte analyses

These voltages were calculated as the difference between the manganese dioxide electrode and the zinc electrode potentials, both potentials measured with respect to the usual reference electrode, i.e. the saturated calomel electrode inserted through the zinc electrode.

6.1.1 Cell voltage in Leclanché electrolyte, 4 Ω discharges

Figures (6.1) and (6.2) show the cell voltages for a battery containing electrodeposited manganese dioxide (EMD) and Faradiser M (Far M) for a discharge of a cell with salt bridges and carbon probes, respectively. The cells containing EMD performed better than those containing the CMD, as previously reported by Ohta *et al.* [186]. The similarity of the respective curves in these figures shows that the insertion of salt bridges or carbon probes into the positive electrode mass did not change the battery behaviour to any significant extent. Both figures show the double-inflection curve characteristic of discharges with Faradiser M. This characteristic is also visible in reports by other workers [186].

Figures (6.1) and (6.2) show that throughout the whole discharge, the voltage, and therefore the current, was lower for the cell containing the CMD than for the cell containing the electrodeposited material. Tables (6.1) and (6.2) summarise the discharge performances of cells made with the EMD and with the CMD, respectively.

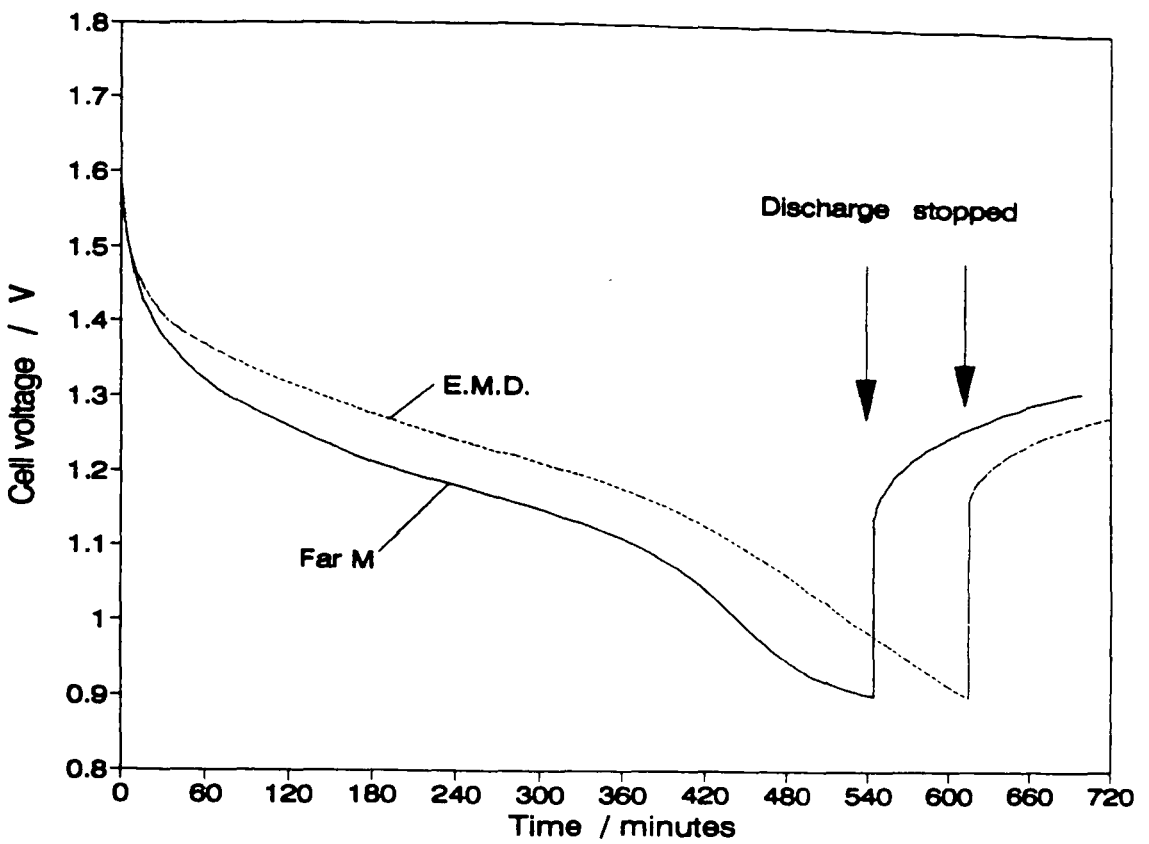

Figure 6.1 : Cell voltage in Leclanché electrolyte with salt bridges inserted into the MnO_2 electrode; continuous discharge through 4 Ω

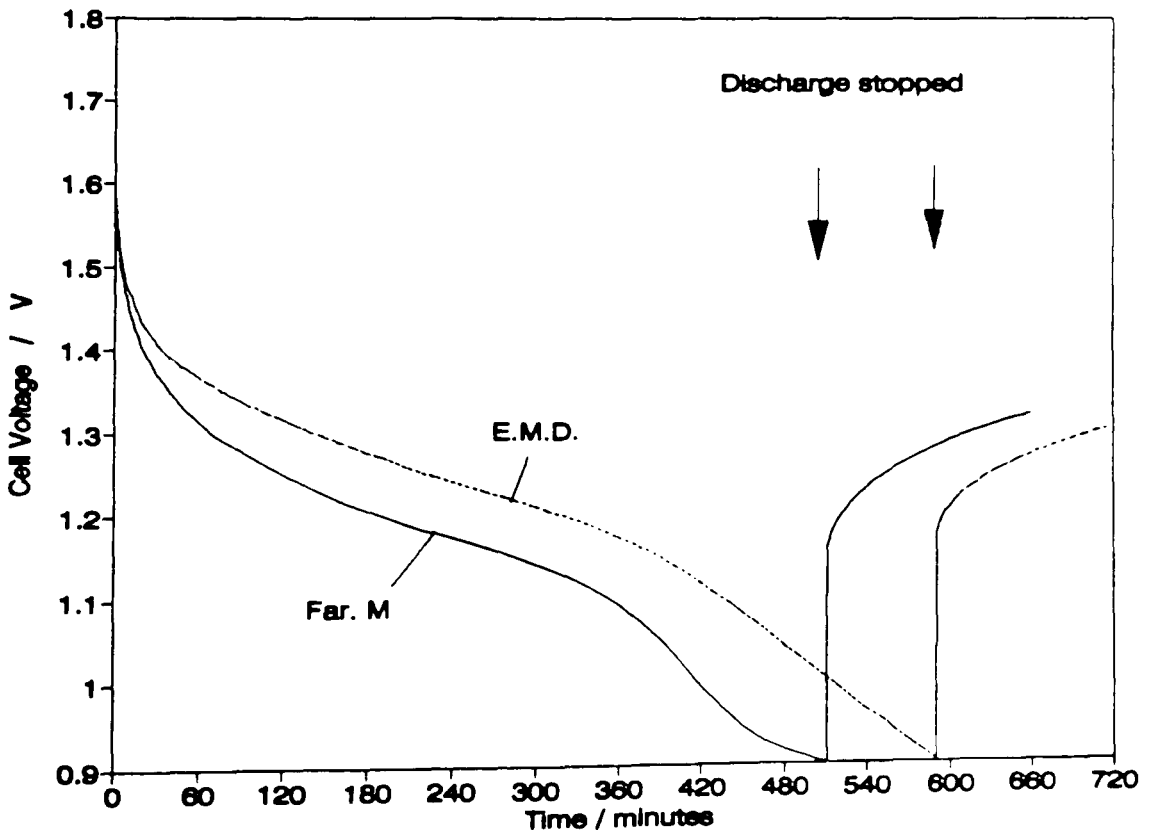

Figure 6.2 : Cell voltage in Leclanché electrolyte with carbon probes inserted into the MnO_2 electrode; continuous discharge through 4 Ω

Table 6.1 : Performance of cells containing EMD on 4 Ω down to 0.9 V CCV.

Cell	Duration / min.	Coulombs delivered
2	580	10352
5	540	9886
7	584	10478
12	590	10567
13 *	615	10989
15 *	620	11102
average	588	10562

* cell discharged with salt bridges

Table 6.2 : Performance of cells containing Faradiser M on 4 Ω down to 0.9 V CCV.

Cell	Duration / min.	Coulombs delivered
4	535	9152
6 *	565	9743
8	525	9069
12 *	595	10215
13	525	9089
15 *	545	9444
average	548	9452

* cells discharged with salt bridges

The average performance of cells containing EMD was about 7 % longer than for those with CMD, but due to the higher closed circuit voltage, the former delivered about 12 % more coulombs than the latter. Cells made with EMD contained more MnO_2 (36.04 g or 0.391 mol) than the cells made with Faradiser M (31.0 g or 0.339 mol), see tables (2.1) and (2.4). When the average performance is expressed in terms of specific performance, the figures are 0.280 and 0.288 faraday per mole (or 293 and 304 coulombs per gram) for EMD and CMD, respectively. Thus the apparent inferiority of the CMD relates only to the smaller amount that is packed into a cell, although the on-load voltage is lower.

6.1.2 Electrolyte analyses, discharge of Leclanché cells

The composition of the electrolyte squeezed out of the manganese dioxide electrode mass after discharge and one week of recovery are given in tables (6.3) and (6.4) for cells containing EMD and CMD, respectively. No analyses were performed on cells number 2, 5 and 7 containing EMD.

The cells used for the continuous discharge tests were of a different batch than those used for the intermittent discharge experiments and thus the slightly different results for the electrolyte analyses (see tables 4.1 and 4.2).

Table 6.3 : Electrolyte composition after one week of recovery, EMD in Leclanché electrolyte

Cell	pH	NH_4Cl w/w %	$ZnCl_2$ w/w %	Mn^{2+} / ppm
4 *	5.55	29.3	16.9	20
12	5.70	19.3	18.2	120
13	5.80	16.9	17.0	30
15	5.89	16.1	16.4	30

* undischarged cell

Table 6.4 : Electrolyte composition after one week of recovery, Faradiser M in Leclanché electrolyte

Cell	pH	NH_4Cl w/w %	$ZnCl_2$ w/w %	Mn^{2+} / ppm
2 *	5.07	29.0	14.5	40
4	5.68	21.5	16.0	550
6	5.90	18.1	14.1	1060
8	5.81	21.7	15.5	610
12	5.88	18.5	13.6	600
13	5.72	21.1	15.6	800
15	5.80	20.1	14.5	520

* undischarged cell

The electrolyte of undischarged cells containing Faradiser M was more acidic and its $ZnCl_2$ concentration was lower than for the cells containing EMD. This is consistent with the higher ion-exchange capacity of Faradiser M already mentioned in section (4.2) and the incomplete buffering of the electrolyte by the ZnO incorporated in the positive electrode mass. The lower $ZnCl_2$ concentration

in cells containing Faradiser M was also observed after the discharge, suggesting that the partially reduced CMD retained a higher ion-exchange capacity than the partially reduced EMD. The lower zinc chloride concentration in cells made with CMD increased the pH at which the electrolyte was buffered [76,78,224]. During the continuous discharge, i.e. far from the equilibrium conditions that were approached more closely on the intermittent discharges, the pH in the positive electrode increased probably to higher values in the cells with CMD than in those with EMD thus decreasing more the manganese dioxide potential and the cell voltage for the former material than for the latter.

Comparison of tables (6.3) and (6.4) with tables (6.1) and (6.2) shows that the NH_4Cl concentration after recovery was related to the discharge duration, the longer the discharge, the lower the NH_4Cl. However, for a similar discharge performance (e.g. cell 12 in table 6.1 and 6.2) and a lower NH_4Cl and higher water content of the cell with CMD than with EMD (see table 2.1), the NH_4Cl concentration after one week of recovery was practically the same in the cell with Faradiser as in the cell with EMD showing that some hetaerolite was formed during the recovery period (see section 4.2). Hetaerolite formation is a slow process (section 4.2) and therefore it did not affect the manganese dioxide behaviour during the discharge.

Cells with CMD produced more manganous ions than those with EMD, possibly because of the slightly higher reduction degree of the manganese dioxide in the former cells (see tables 6.5 and 6.6) or due to a lower oxidation stage of the surface of CMD (caused by a lower proton/electron diffusion coefficient) during the discharge than of the surface of EMD.

Tables (6.5) and (6.6) show the electrode potentials before discharge and for the discharged cells, after one week of recovery. They also show the average oxidation degree of the manganese dioxide after discharge, calculated from the data in tables (2.1), (2.4), (6.1) and (6.2). The potentials at pH 0 were calculated assuming a slope of 0.0592 V pH^{-1} [13].

Table 6.5 : Electrode potentials versus SCE in Leclanché cells with EMD, initially and after discharge and one week of recovery.

	undischarged		discharged and 1 week of recovery	
Cell	E_{Zn} / V	E_{Mn} / V	E_{Zn} / V	E_{Mn} / V
5	-1.082	0.589	-	-
7	-1.078	0.614	-1.031	0.424
12	-1.076	0.590	-1.045	0.438
13	-1.079	0.610	-1.046	0.429
15	-1.079	0.603	-1.048	0.427
average	-1.079	0.603	-1.043	0.430
at pH 0		0.932		0.773

average r in $MnOOH_r$: 0.362

Table 6.6 : Electrode potentials versus SCE in Leclanché cells with Faradiser M, initially and after discharge and one week of recovery.

	undischarged		discharged and 1 week of recovery	
Cell	E_{Zn} / V	E_{Mn} / V	E_{Zn} / V	E_{Mn} / V
4	-1.076	0.628	-1.051	0.364
6	-1.079	0.602	-1.059	0.350
8	-1.076	0.630	-1.054	0.371
12	-1.073	0.622	-	-
13	-1.079	0.609	-1.050	0.356
15	-1.077	0.628	-1.058	0.362
average	-1.077	0.620	-1.054	0.361
at pH 0		0.919		0.704

average r in $MnOOH_r$: 0.393

The higher initial MnO_2 potential of Faradiser M was due to a difference in the electrolyte pH as revealed by the potential calculated at pH 0. In spite of similar reduction degree and the increase of the potential caused by hetaerolite formation, Faradiser M had a significantly lower electrode potential after discharge and recovery than EMD.

6.1.3 Cell voltage in $ZnCl_2$ electrolyte, 2.2 Ω discharges

Figure (6.3) shows the cell voltage during the discharge and the first hours of recovery for the normal formulations with EMD, Faradiser M and Faradiser WSZ. As in the Leclanché electrolyte, the voltages of cells with CMD were lower than those with EMD throughout the discharge.

Figure (6.4) shows that the addition of one ml of electrolyte in excess of the normal moisture content of the cell, increased the cell voltage by about 20 mV for most of the discharge duration.

The discharge performances summarised in table (6.7) are given as the time necessary to reach a closed circuit voltage of 0.9 V.

Although there were some variations within a given formulation, the performance increased in the order

Far M << Far WSZ < EMD < Far WSZ + extra electrolyte

when expressed in terms of discharge duration or coulombs delivered by the cell, and in the order

Far M < Far WSZ, EMD, << Far WSZ + extra electrolyte,

when expressed in terms of specific capacity (F mol^{-1} or C g^{-1}).

For normal formulations (identical apparent wetness of the manganese dioxide electrode mix), EMD was therefore superior to CMDs, especially to Faradiser M (about 17 % in terms of duration or coulombs delivered), on heavy continuous drain. When the performances were reported per unit mass of MnO_2 (faraday per mole or coulombs per gram), they came closer to each other, Faradiser WSZ was equivalent to EMD and Faradiser M delivered only about 3 % less coulombs than EMD. These conclusions are in agreement with the reports by Ohta *et al.* [186] and Uetani *et al.* [106,187,188]. The latter also reported the improved performance of cells containing more electrolyte [106,187,188]. Faradiser WSZ was not studied by these workers.

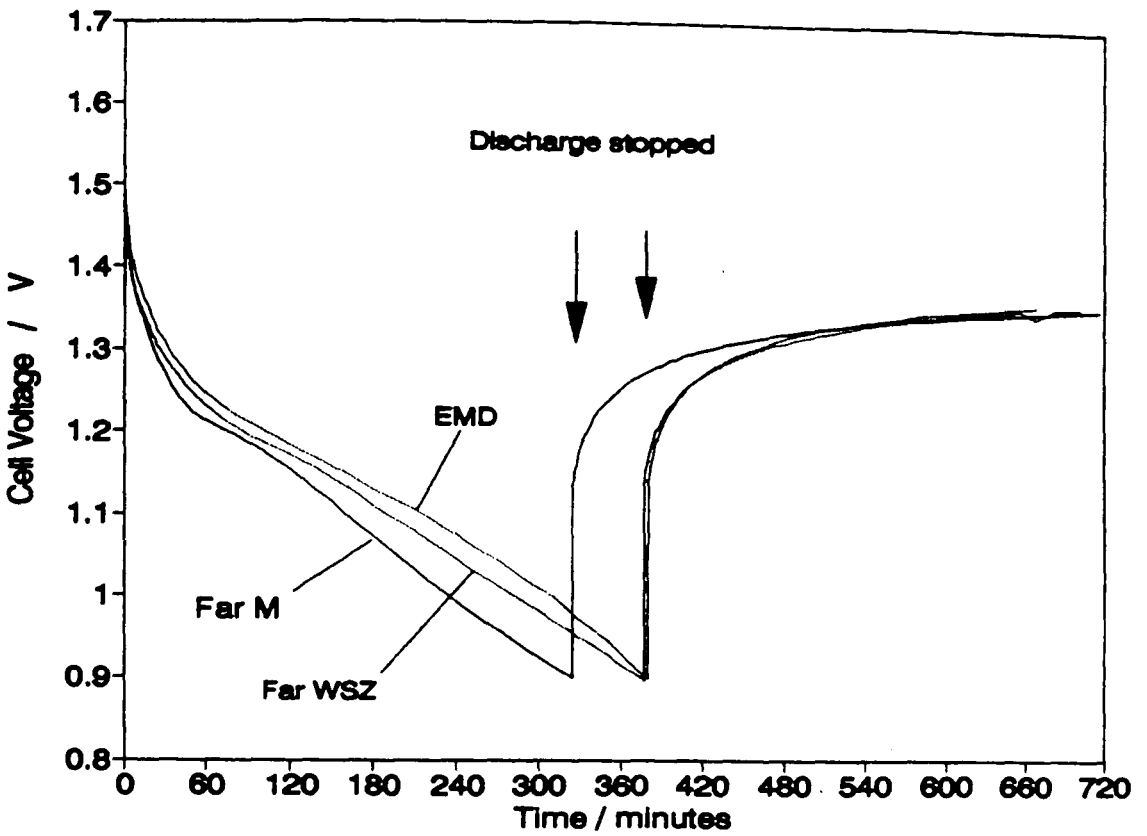

Figure 6.3 : Cell voltage in $ZnCl_2$ electrolyte, with salt bridges inserted into the MnO_2 electrode; continuous discharge through 2.2 Ω

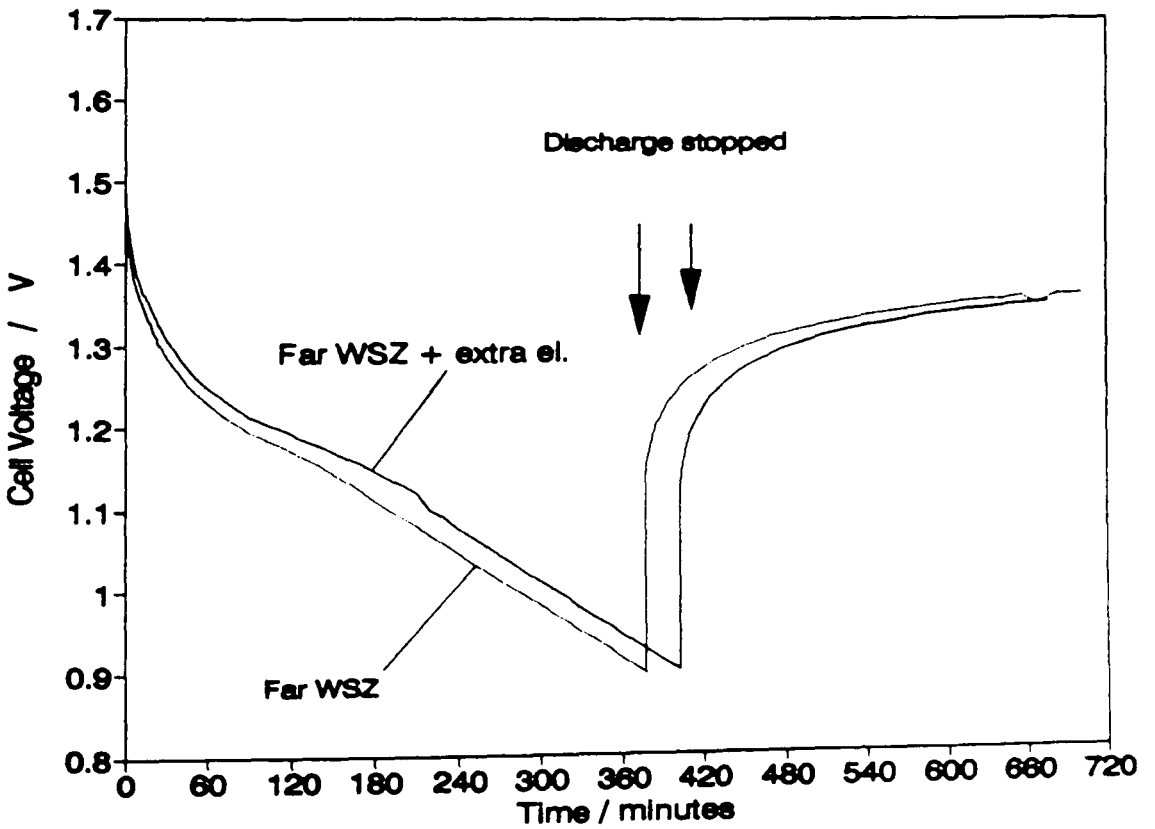

Figure 6.4 : Effect of added electrolyte on the cell voltage in $ZnCl_2$ electrolyte, with salt bridges inserted into the MnO_2 electrode; continuous discharge through 2.2 Ω

Table 6.7 : Performances in $ZnCl_2$ electrolyte on continuous discharge through 2.2 Ω

Cell	Duration / min.	Coulombs delivered
EMD		
4	397	12112
6	360	10998
11 *	380	11643
14	390	11876
17 *	378	11480
average	381	11622 (0.446 F mol^{-1} or 467 C g^{-1})
Far M		
5	327	9789
7	355	10783
11 *	312	9391
12	309	9291
13 *	335	10058
16 *	325	9572
average	327	9845 (0.426 F mol^{-1} or 453 C g^{-1})
Far WSZ		
8	348	10478
9 *	377	11358
10	345	10340
17 *	379	11369
18	367	10947
average	363	10898 (0.437 F mol^{-1} or 465 C g^{-1})
Far WSZ + extra electrolyte		
6 *	403	12287
8	407	12344
12 *	416	12609
13	399	12036
14	397	12020
average	404	12260 (0.491 F mol^{-1} or 524 C g^{-1})

* cells discharged with salt bridges.

6.1.4 Electrolyte analyses, discharge of zinc chloride cells

The electrolyte was squeezed out of the positive electrode mass after one week of recovery. The results of the chemical analyses are given in table (6.8). The zinc and the MnO_2 electrode potentials against SCE, after discharge and recovery are also given.

Table 6.8 : Electrolyte analyses after one week of recovery. The potentials are against SCE.

Cell	pH	$ZnCl_2$ w/w %	Mn^{2+} / ppm	E_{Zn} / V	E_{Mn} / V
EMD					
7 *	4.10	27.0	40	-0.985	0.676
4	4.91	21.8	4770	-0.990	0.427
6	4.93	21.1	4150	-0.992	0.425
11	5.13	18.9	6720	-1.008	0.407
14	5.11	19.7	6970	-1.000	0.410
17	4.96	19.1	7090	-1.003	0.406
Far M					
4 *	3.53	26.5	70	-0.988	0.679
5	4.83	21.2	6580	-0.995	0.426
7	4.93	20.4	6140	-0.997	0.421
11	4.78	21.1	6240	-0.994	0.430
12	4.80	21.8	7210	-0.994	0.427
13	5.04	19.0	9190	-1.001	0.403
16	4.92	20.3	7130	-0.997	0.420
Far WSZ					
3 *	3.95	26.4	160	-0.986	0.673
8	5.04	20.8	2650	-0.998	0.423
9	4.93	19.2	4690	-1.001	0.409
10	4.77	20.8	3970	-0.998	0.419
17	5.13	19.0	5760	-0.981	0.396
18	5.00	20.2	5590	-1.000	0.409
Far WSZ + extra electrolyte					
18 *	3.94	16.2	90	-0.986	0.675
6	4.90	19.7	7360	-0.997	0.404
8	4.77	19.6	6930	-0.999	0.403
12	4.97	19.2	5970	-1.001	0.403
13	4.86	20.6	4300	-0.997	0.413
14	5.10	20.1	2860	-1.000	0.418

* undischarged cells

The electrode potentials given in table (6.8) for the undischarged cells are the average of the potentials measured, before discharge, on the other cells of the same formulation. Results from table (6.8) have been combined with data from tables (6.7) and (2.2) to calculate the oxidation degree of the manganese dioxide corrected for the Mn^{2+} by equation (2.18), for each discharged cell. The average for each formulations are shown in table (6.9). The manganese dioxide potential was calculated at pH 0 assuming a slope of 0.0592 V pH^{-1} [13].

Table 6.9 : Oxidation degree after discharge in $ZnCl_2$ electrolyte and potential vs. SCE after one week of recovery. The values for the discharged cells are average results.

Cell	r in $MnOOH_r$	E_{Mn} vs. SCE at pH 0 / V
EMD		
undischarged	0.082	0.918
discharged	0.528	0.711
Faradiser M		
undischarged	0.104	0.888
discharged	0.530	0.710
Faradiser WSZ		
undischarged	0.104	0.907
discharged		
normal formulation	0.541	0.707
+ extra electrolyte	0.595	0.699

The reason for the difference in the pH of the electrolyte of fresh cells, namely the different levels of buffering, has already been discussed in section (4.3.3). There were no other significant differences in electrolyte composition or manganese dioxide electrode potential between the different formulations, except the potential of the undischarged Faradiser M being lower than the potential of the other undischarged materials. As previously observed for intermittent discharge tests (chapter 4), much more manganous ions were formed in the zinc chloride than in Leclanché electrolyte. The pH difference between the Leclanché and the zinc chloride electrolyte after continuous discharge and one week recovery

(about 0.8 pH unit) was probably too small to explain a tenfold (for CMD) or sixtyfold (for EMD) increase of the Mn^{2+} concentration and was not applicable to intermittent discharge results where the pH were very similar in both electrolytes. The reason for this difference is not known.

6.2. The zinc electrode potential

The potentials reported in this section were measured against the "usual reference electrode", i.e. the SCE connected to the electrolyte through the zinc electrode.

The expression "temporary equilibrium potential" refers to potential the electrode would take, against the specified reference electrode, if it were in equilibrium with the adjacent solution. The difference between this "temporary equilibrium potential" and the potential of the electrode after full recovery of the cell was the concentration overpotential.

6.2.1 Zinc potential in Leclanché electrolyte, 4 Ω discharges

The negative electrode potential with respect to the usual reference electrode is shown in figure (6.5) on closed circuit for the duration of the discharge and on open circuit after the cessation of discharge. Figure (6.6) shows the temporary zinc equilibrium potential calculated by subtracting the total transient (ohmic + activation) overpotential from the closed circuit potential of figure (6.5).

The curves are very similar for EMD and CMD. The beginning of the discharge was characterised by a very steep increase of the negative electrode potential, both on closed and on open circuit.

Figure (6.7) shows the variation of the temporary zinc electrode equilibrium potential as a function of $\sqrt{t}$ for a cell with EMD and with Faradiser M; a change of the slope after about 35 minutes on load is clearly visible. The zinc electrode potential for a given $ZnCl_2$ concentration changes almost linearly with NH_4Cl concentration (section 3.3) and for a given NH_4Cl with $ZnCl_2$ concentration (see figure 1.1). On the basis of the treatment of electrode concentration polarisation, e.g. the equations (1.19) and (1.20), given by Dewhurst [65] and of the

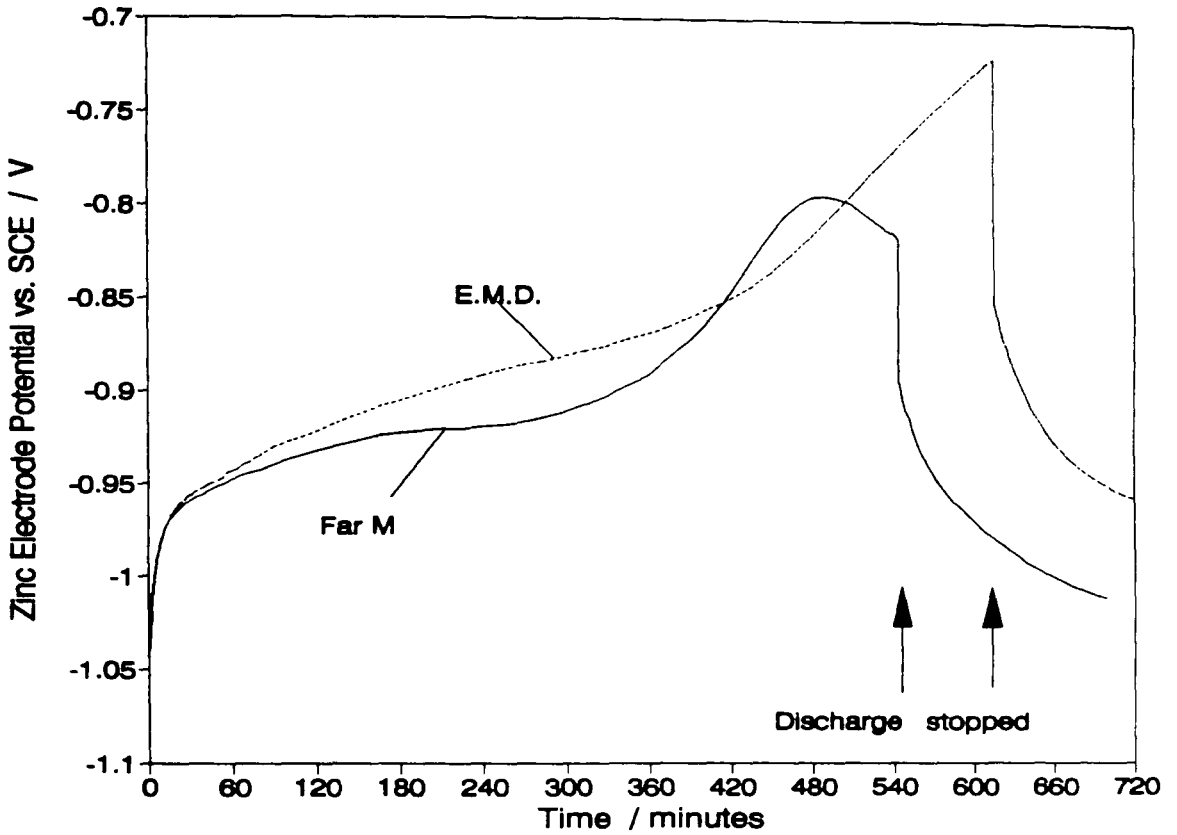

Figure 6.5 : Closed-circuit zinc electrode potential (vs. SCE) in Leclanché electrolyte; continuous discharge through 4 Ω

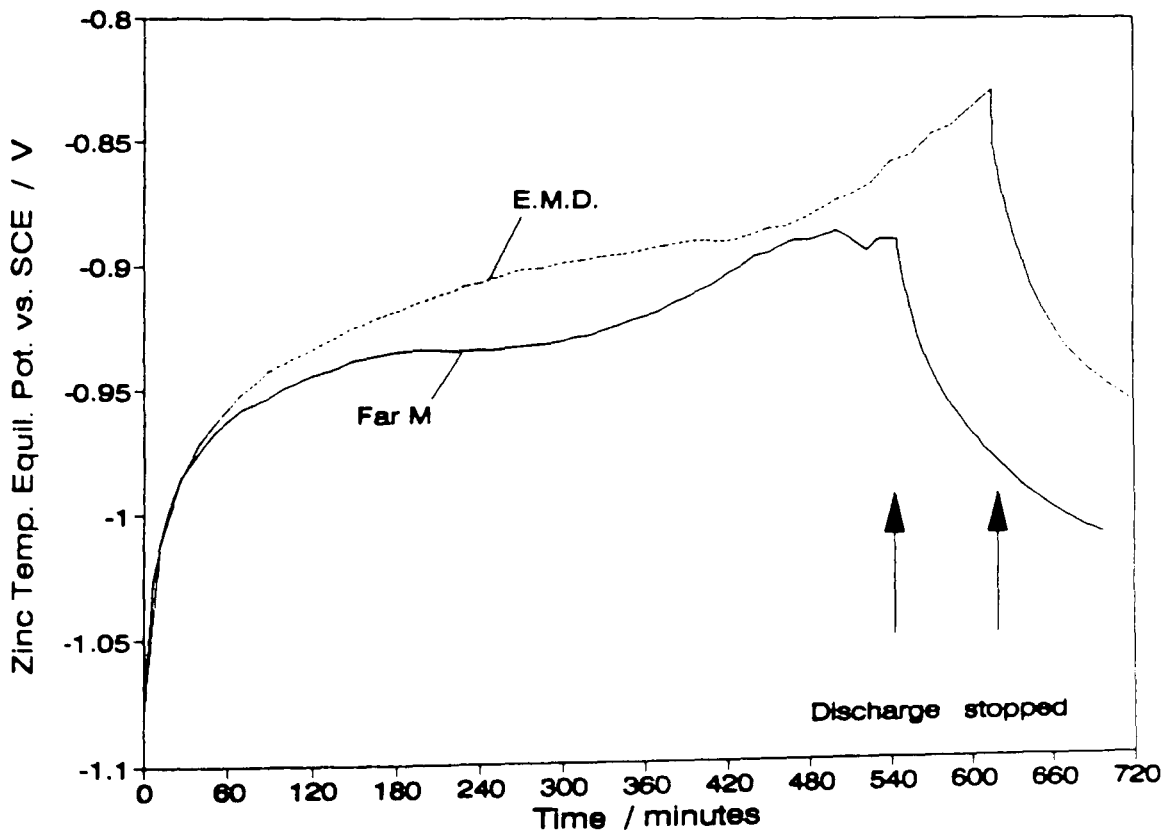

Figure 6.6 : Zinc electrode temporary equilibrium potential (vs. SCE) in Leclanché electrolyte; continuous discharge through 4 Ω

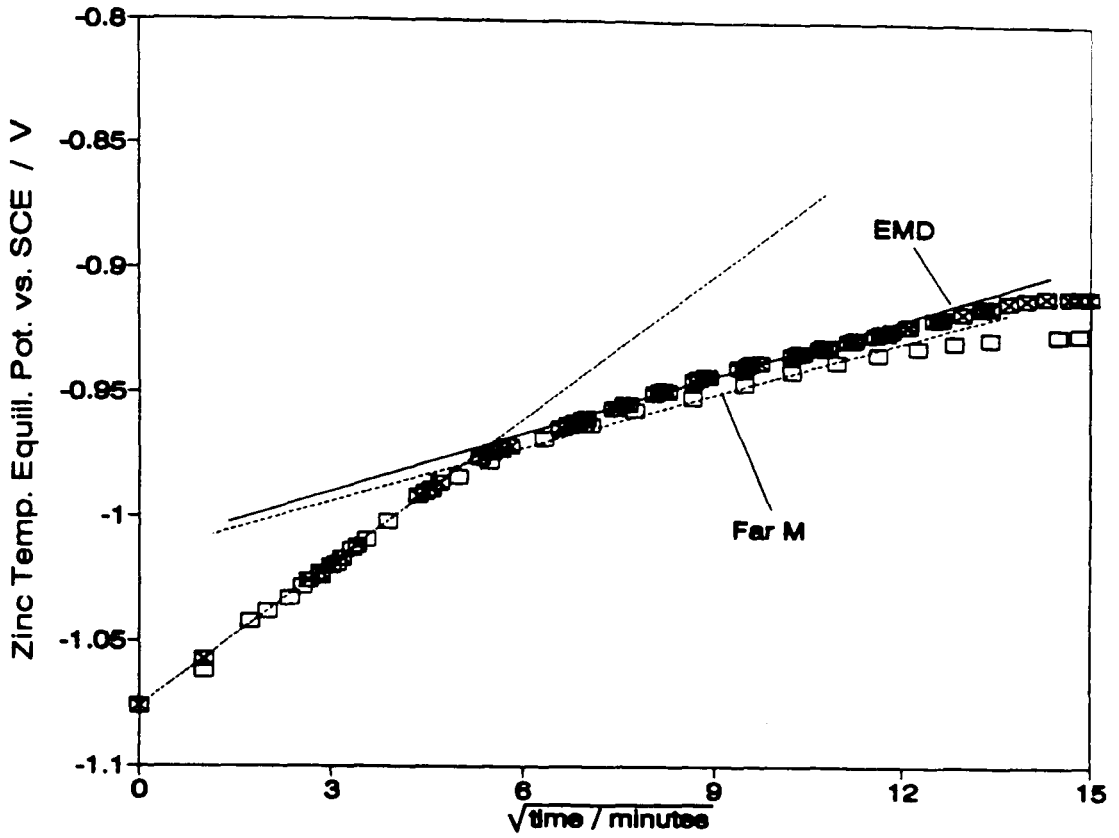

Figure 6.7 : Zinc electrode temporary equilibrium potential (vs. SCE) vs. $\sqrt{t}$ in Leclanché electrolyte; continuous discharge through 4 Ω

approximate potential-concentration relationship, the change of the slope in figure (6.7) suggests a change in the transference number of some of the electrolyte species. This change corresponded to the elbow of the curves in figure (6.5). This may be interpreted on the basis of the findings of Agopsowicz *et al.* [80] and Atlung *et al.* [34]. The first part of the curves show the accumulation of zinc species at the electrode interface (due to the negative zinc transference number in the Leclanché electrolyte [80]) combined with the effect on the electrode potential of the decreasing NH_4Cl concentration [80,34]. When the NH_4Cl concentration at the electrode reached zero, after about 30 - 40 minutes on the 4 Ω load, the zinc transference number changed to a positive value [80], more zinc was carried away by migration and the rate of potential increase diminished. After about two hours, the assumption of semi-infinite diffusion used in the derivation of Dewhurst's equation [65] ceased to be valid and the potential increase became lower than predicted by the equation.

The zinc electrode potential was more negative for the CMD than for the EMD during the first seven hours of the discharge, due to lower current in the former cells. For Faradiser M, the steep increase of the closed circuit potential, followed by an unexpected decrease seems to correspond to the second inflection of the cell voltage curve in figures (6.1) and (6.2). For both materials, the steeper increase of the concentration overpotential towards the end of the discharge, i.e. at a period of decreasing current, is not well understood. It was possibly caused by an obstruction of the diffusion path of the zinc ions resulting from the formation of a precipitate layer on the separator surface.

Figure (6.8) shows the zinc electrode activation overpotential, taken as the difference between the total transient overpotential (measured about 35 ms after the current interruption) and the ohmic potential step. The two curves are virtually identical for the first eight hours of discharge. The very steep increase of the activation overpotential towards the end of the discharge is not understood. The reason for the final decrease of the activation overpotential observed at the end of the discharge with Faradiser M and which corresponded to the maximum in the closed circuit potential curve (figure 6.5) remains unclear.

Figures (6.9) and (6.10) show the change of the charge transfer overpotential during the first hours of the discharge of a cell with EMD and with Faradiser M, respectively on a $\sqrt{t}$ scale. A linear relationship seems to exist between the activation overpotential and the square root of the time on load, for both cells, between about 5 and 35-40 minutes. The end of the linear decrease corresponded closely to the change of slope in figure (6.7). The same relationship was also observed on a 2.2 Ω discharge of a cell containing Faradiser M in Leclanché electrolyte (figure 6.11).

Baugh and White [61] found that the charge transfer overpotential of a zinc electrode was much larger in NH_4Cl-$ZnCl_2$ solutions than in pure $ZnCl_2$ solutions; Agopsowicz *et al.* [80] reported the decrease of the ammonium chloride concentration at the zinc electrode surface during anodic dissolution, and the linearity of the $\sqrt{t}$ plots of the charge transfer overpotential curves suggests that it was related to a migration-diffusion phenomenon which obeyed Dewhurst's

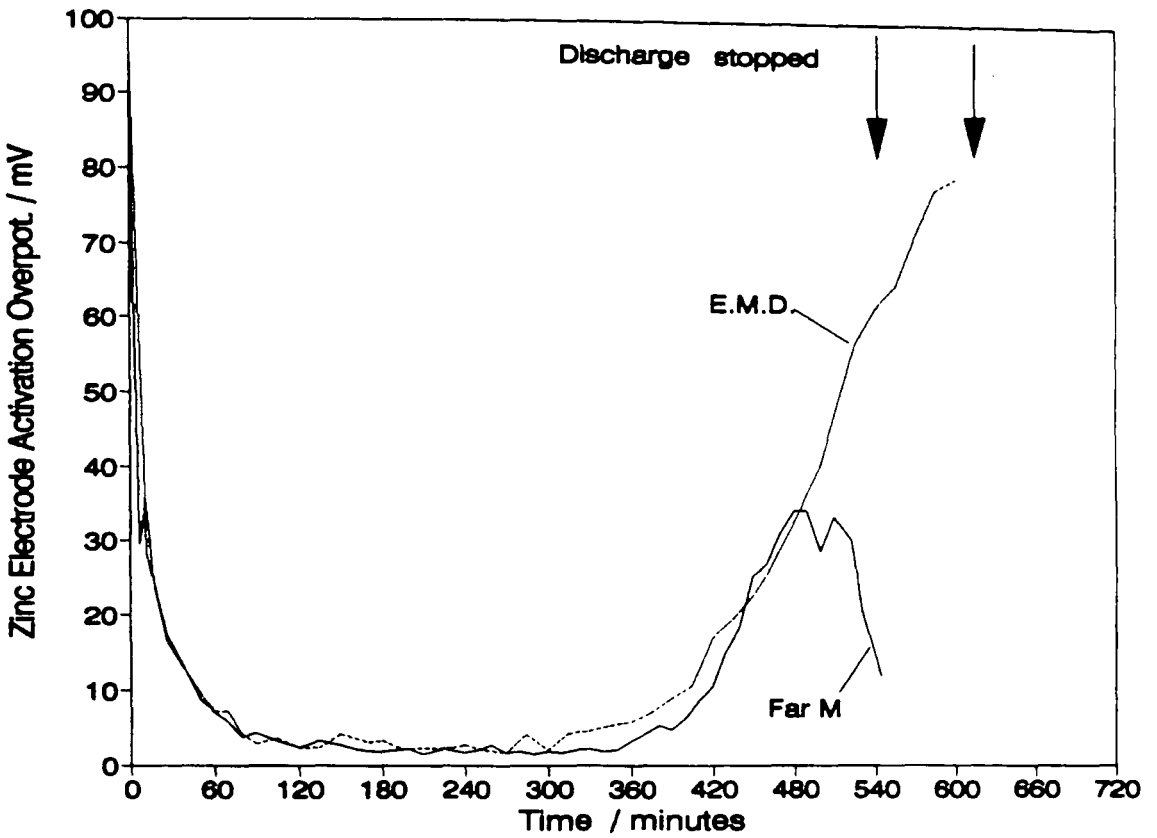

Figure 6.8 : Charge transfer overpotential in Leclanché electrolyte; continuous discharge through 4 Ω

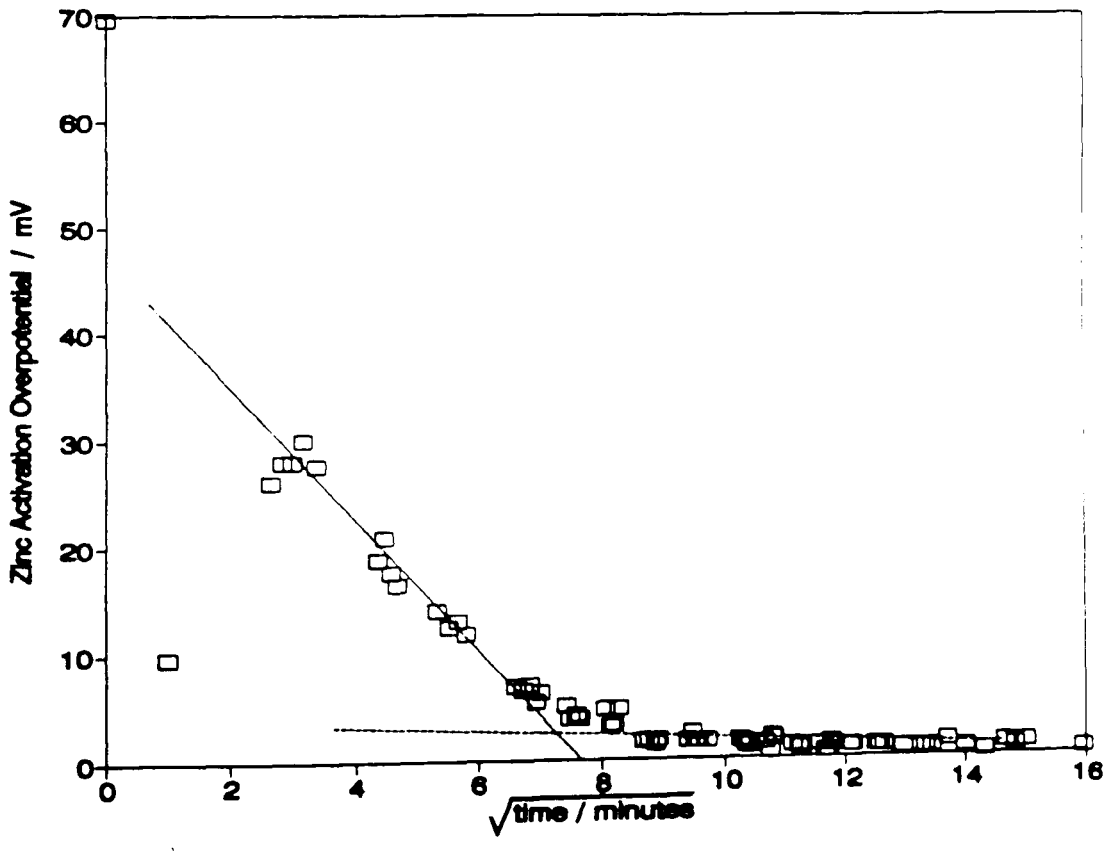

Figure 6.9 : Charge transfer overpotential vs. √t; EMD in Leclanché electrolyte; continuous discharge through 4 Ω

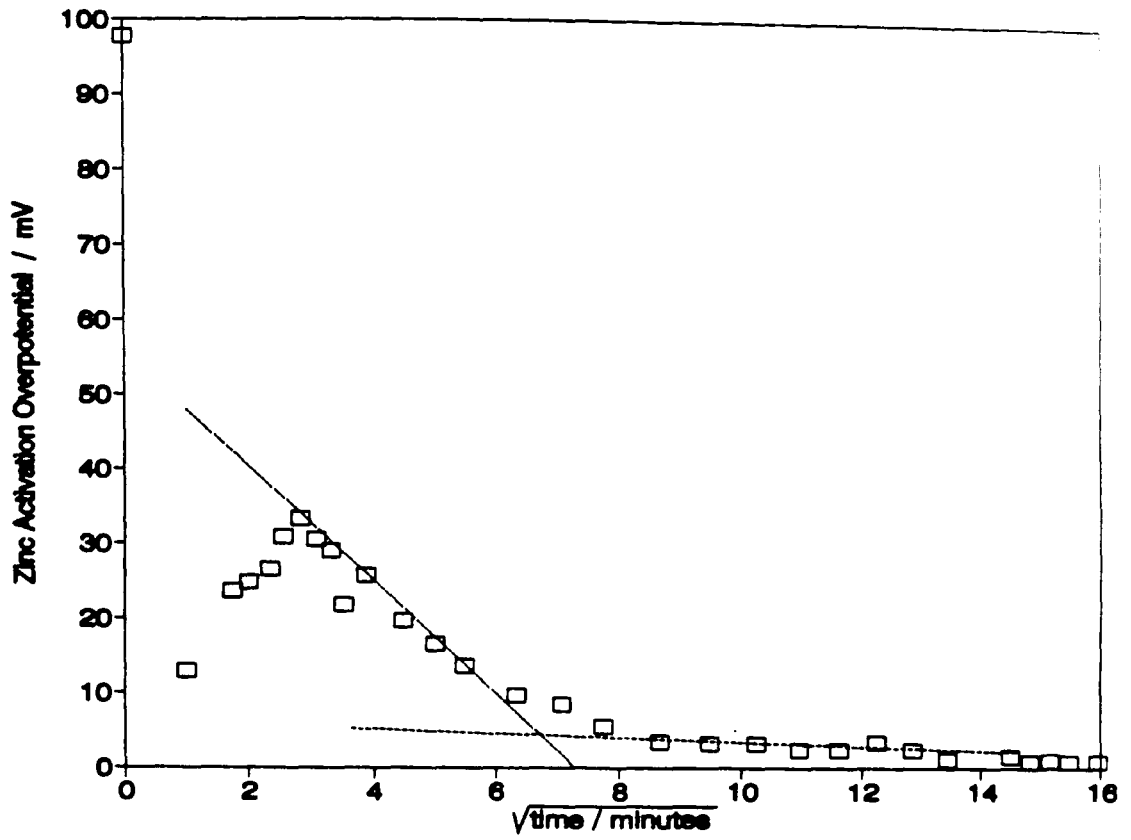

Figure 6.10 : Charge transfer overpotential vs $\sqrt{t}$; Faradiser M in Leclanché electrolyte; continuous discharge through 4 Ω

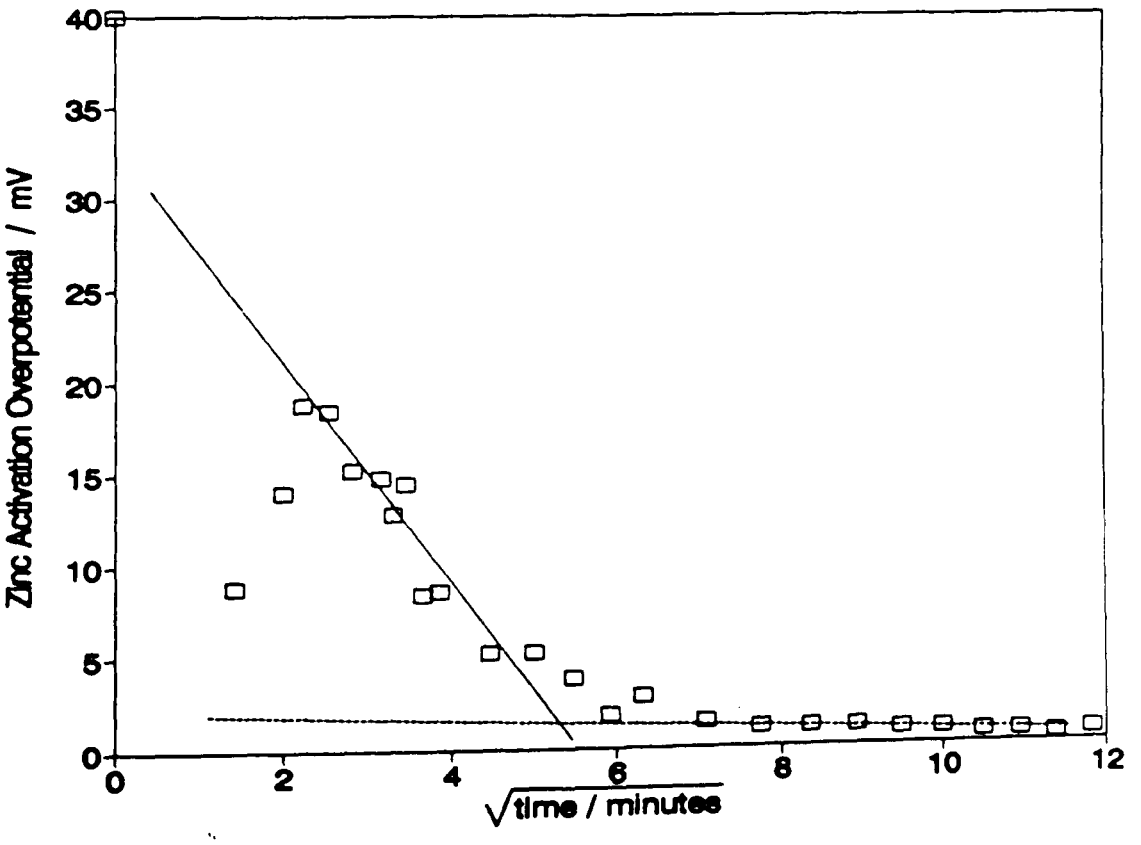

Figure 6.11 : Charge transfer overpotential vs $\sqrt{t}$; Faradiser M in Leclanché electrolyte; continuous discharge through 2.2 Ω

equation [65]. At higher current density (on 2.2 Ω), the NH_4Cl concentration at the electrode surface fell to zero in a shorter time than at lower current density (on 4 Ω) and therefore the activation overpotential reached a practically constant low value earlier in discharge at the higher current density, as was observed during the 2.2 Ω discharge in figure (6.11). These results therefore support the explanation of the zinc electrode potential curve given earlier in this section and are an experimental evidence, in an actual cells, of the moving boundary phenomenon reported by Agopsowicz *et al.* [80] in an experiment simulating the separator region of a Leclanché cell. The data also suggest a practically linear relationship between the zinc electrode activation overpotential and the NH_4Cl concentration.

The shape of the activation overpotential curves on a $\sqrt{t}$ scale during the first 4-5 minutes of the discharges are not clearly understood. It is probably related to a change of the zinc electrode surface due to dissolution by the discharge of the passivation film as reported in chapter 5.

6.2.2 Zinc potential in $ZnCl_2$ electrolyte, 2.2 Ω discharges

Figures (6.12) and (6.13) show the closed circuit and the temporary equilibrium electrode potentials, respectively, in the zinc chloride cells with normal formulations. The on-load potential curves were very similar for the three cells and the difference between EMD and either Faradiser M or Faradiser WSZ was always small (less than 20 mV). The more negative electrode potential for Faradiser M was due to the lower closed circuit voltage and thus the lower discharge current for this cell.

The curves of the temporary equilibrium zinc electrode potential are even closer to each other than the closed circuit potential curves, with a maximum potential difference of about 10 mV. The steep increase of the concentration overvoltage during the first two hours of the discharge shows the build-up of the zinc chloride concentration at the electrode. The influence of diffusion on the concentration at the zinc electrode surface increased with time and a steady-state situation was nearly reached after about three hours.

The concentration increase became slightly steeper again towards the end of the discharge, probably due to partial blockage of the separator porosity. The

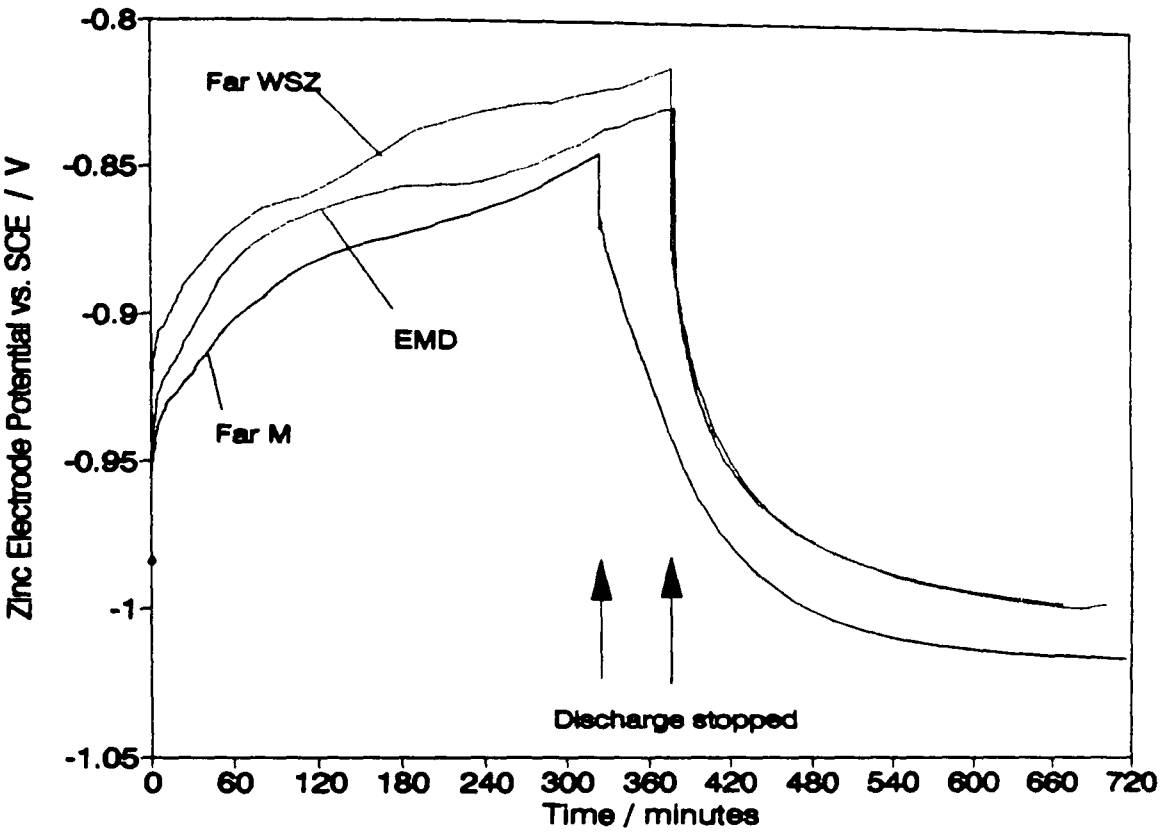

Figure 6.12 : Zinc electrode potential (vs. SCE) in $ZnCl_2$ electrolyte; continuous discharge through 2.2 Ω

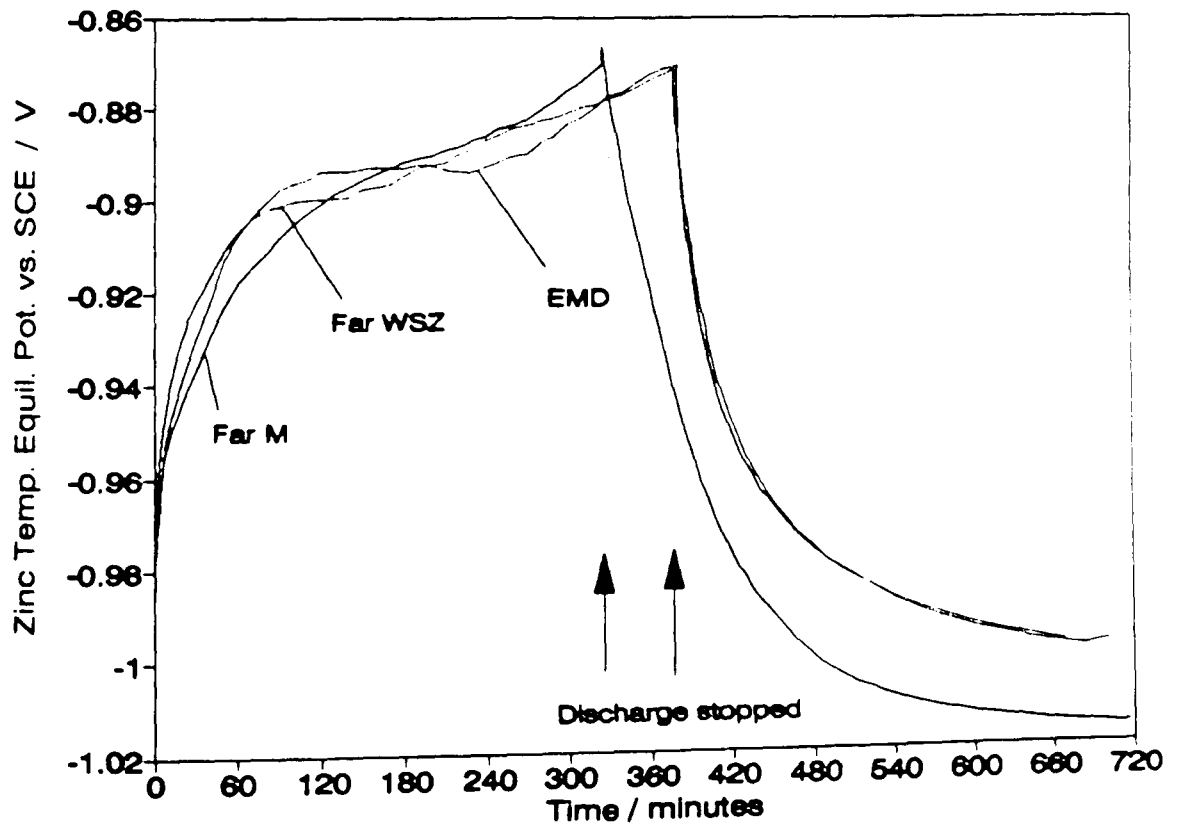

Figure 6.13 : Zinc electrode temporary equilibrium potential (vs. SCE) in $ZnCl_2$ electrolyte, continuous discharge through 2.2 Ω

faster increase of the concentration overpotential for Faradiser M towards the end of the discharge, even though the discharge current was lower for this cell than for the others suggests that the diffusion of the zinc ions in this cell became more hindered than in the other two.

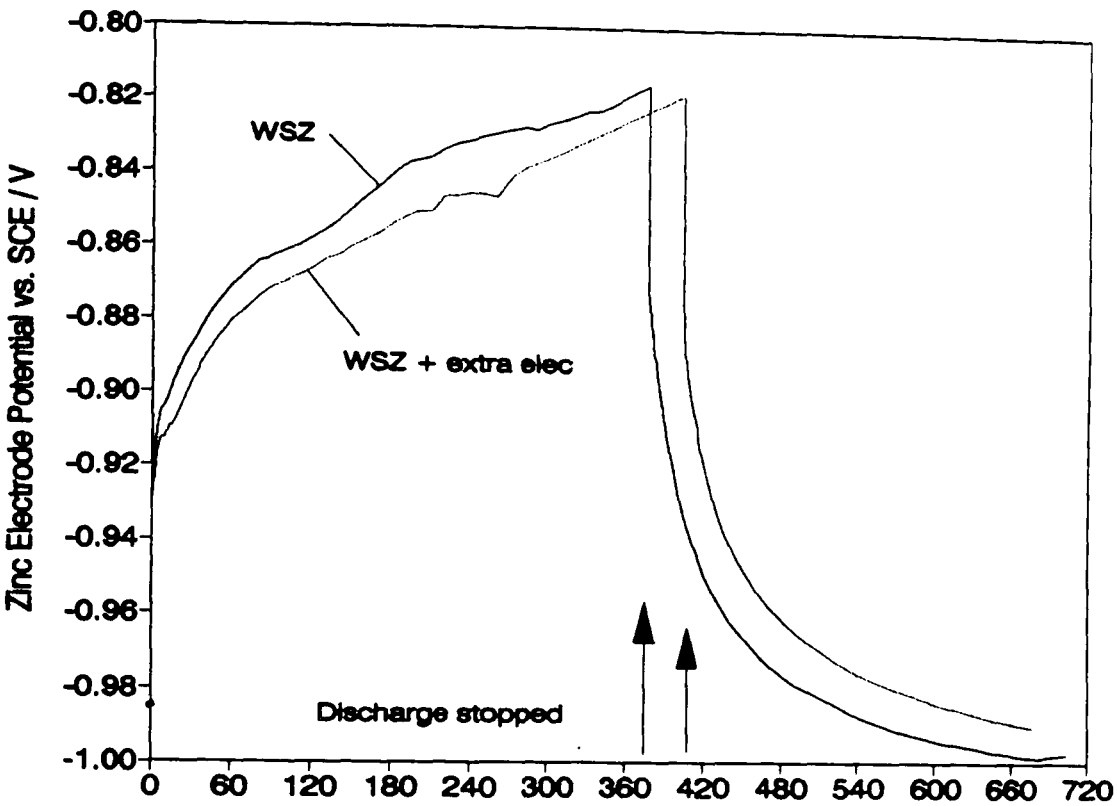

Figure 6.14 : Effect of added electrolyte on the zinc electrode on-load potential (vs. SCE); Faradiser WSZ in $ZnCl_2$ electrolyte; continuous discharge through 2.2 Ω

The extra electrolyte had little effect on the zinc electrode potentials both on-load (figure 6.14) and on open circuit (temporary equilibrium potential, not shown), with a difference of less than 10 mV during most of the discharge.

Figure (6.15) shows the zinc electrode activation overpotential for the cells with normal formulations. The charge transfer overpotential was much lower in zinc chloride than in Leclanché electrolyte, especially at the beginning of the discharge, due to the absence of NH_4Cl, in agreement with the findings of Baugh and White [61]. The increase after one to two hours on load is not explained, it seems to correspond to the equivalent increase observed in the Leclanché electrolyte towards the end of the discharge. In both electrolytes, the increase of the charge transfer overpotential occurred when the temporary equilibrium

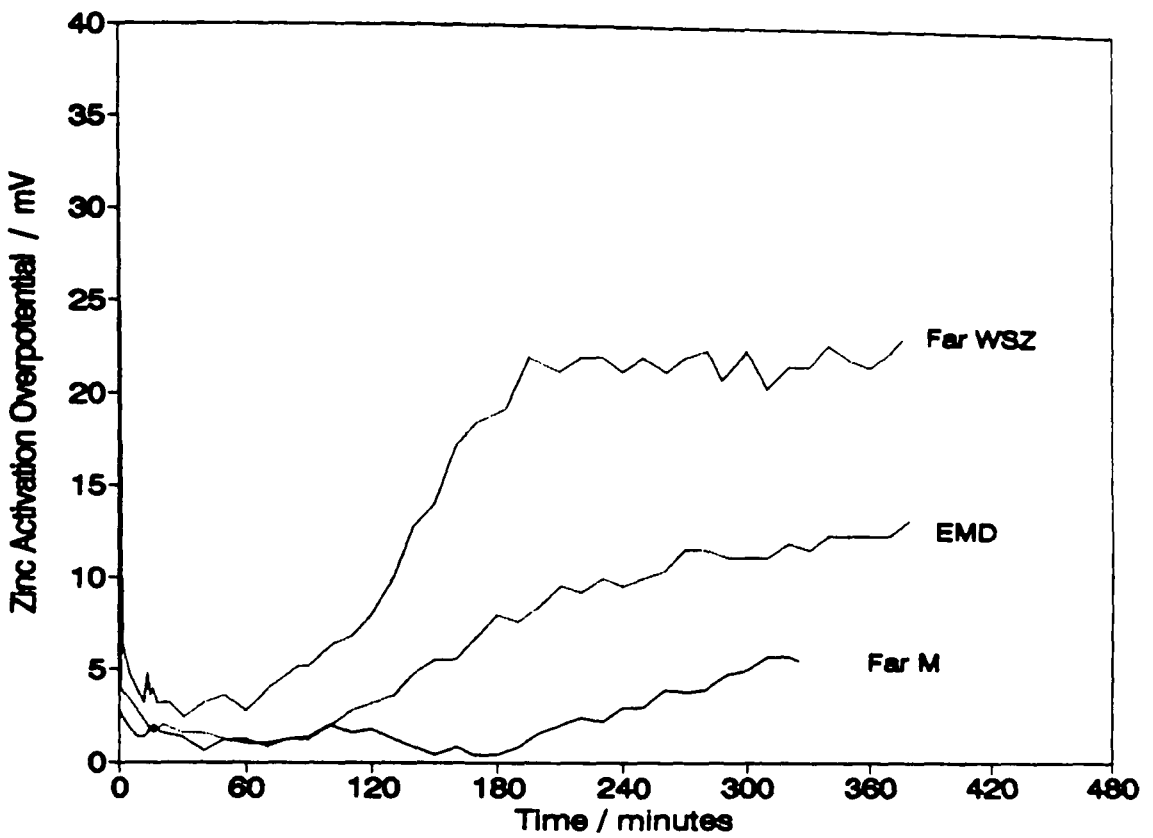

Figure 6.15 : Zinc electrode charge transfer overpotential in $ZnCl_2$ electrolyte; continuous discharge through 2.2 Ω

potential reached about -0.9 V vs. SCE (corresponding to about 5 molar or about 7 molal $ZnCl_2$, see section 3.3), suggesting a dependence of the charge transfer overpotential on the zinc chloride concentration.

The addition of one milli-litre of extra electrolyte in the Faradiser WSZ cell had very little effect (the largest difference being about 5 mV, lower for the cell with extra electrolyte) on the activation overpotential.

The densities measured in section (3.1) have been used to convert the zinc electrode potentials (versus SCE) measured in section (3.3) from the molal to the molar scale. The concentration C, in mol l^{-1}, of the solution was then determined by the empirical relation

$$C = -8.327 + 32.902\sqrt{E + 1.1} - 5.762(E + 1.1) - 3.2678(E + 1.1)^2 \qquad (6.1)$$

where E is the electrode temporary equilibrium potential versus SCE (V). Equation (6.1) gives an average difference of about 0.04 mol l^{-1} between the

experimental and the calculated molarities in the range $0.8 \leq C \leq 7.4$ molar $ZnCl_2$. The results of this curve fitting are shown in figure (6.16).

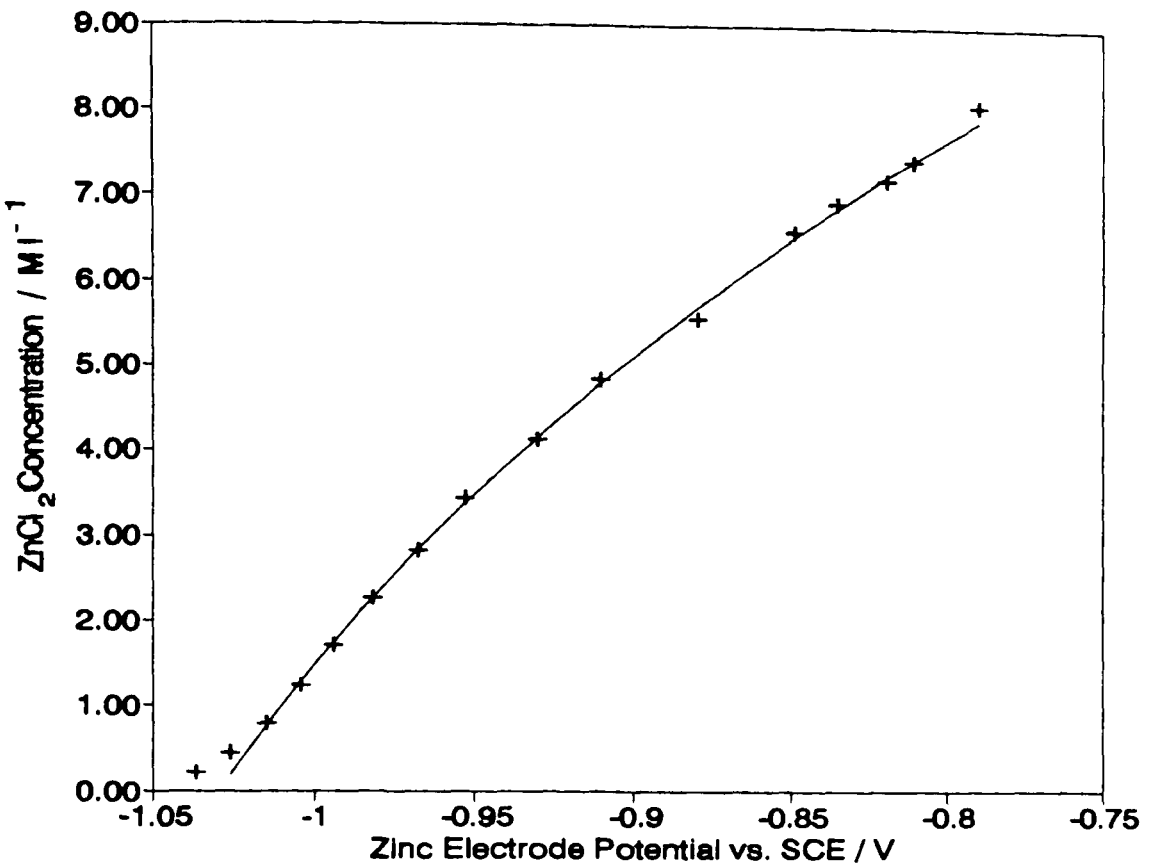

Figure 6.16 : Zinc chloride molarity vs. zinc electrode potential; + results from section 3.3, —— equation (6.1)

Equation (6.1) has been applied to the temporary equilibrium zinc electrode potentials (from figure 6.13) and plotted as a function of the square root of the time counted from the discharge start as suggested by equation (1.19). The results of these calculations are shown in figure (6.17). The linearity of the plots between about 5 and more than 60 minutes on load is very good and confirms, in actual cells, the results of Agopsowicz *et al.* [80] in a simulated separator region. The steeper slope of the curve observed at the beginning of the discharges was due to the higher discharge current at that moment, and the breakdown of the linearity after more than one hour on test was due to the end of the applicability of the semi-infinite diffusion model (when the concentration change reached the positive electrode mass).

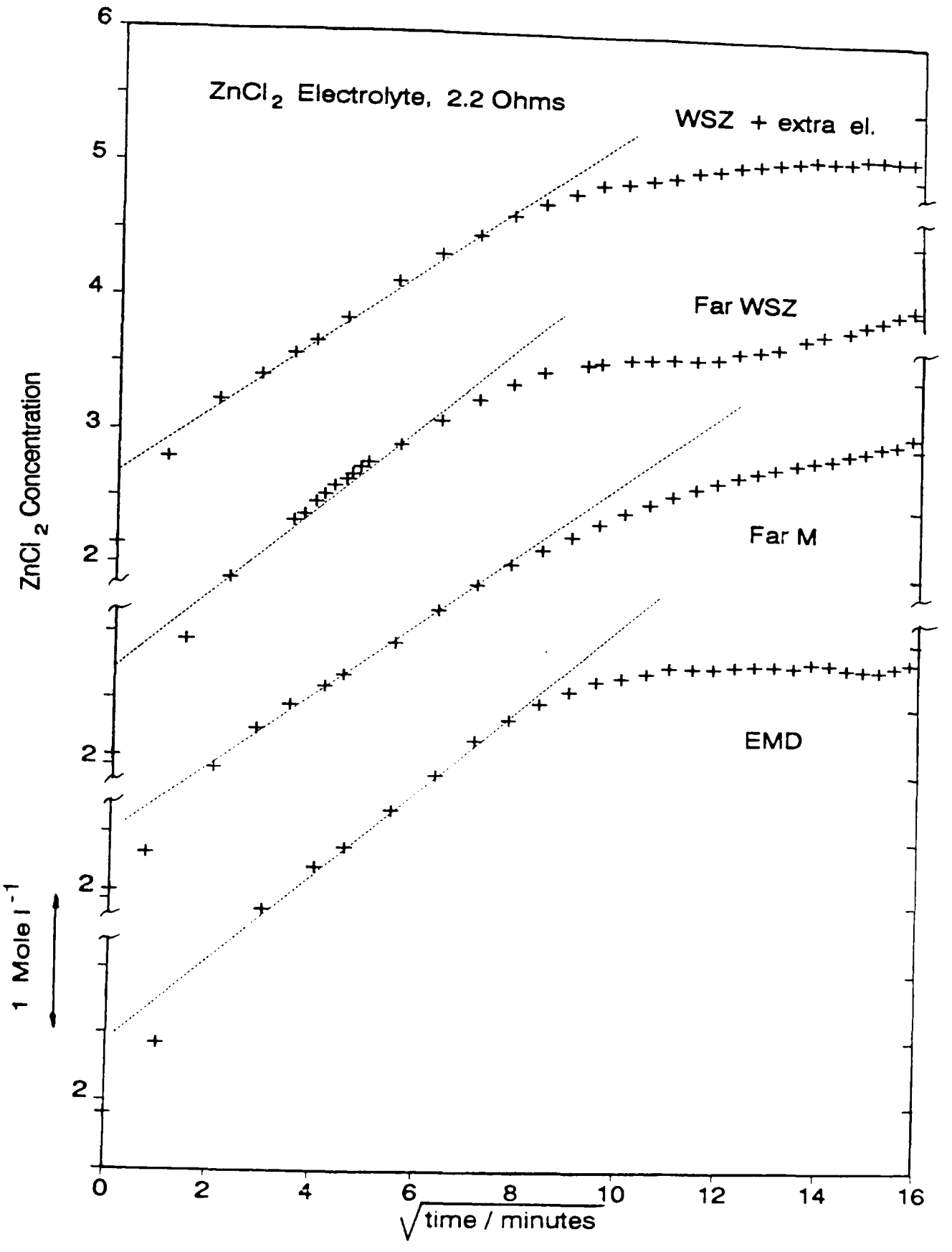

Figure 6.17 : Zinc chloride concentration at the electrode interface as a function of $\sqrt{t}$ in $ZnCl_2$ electrolyte; continuous discharge through 2.2 Ω.

6.3. The voltage loss in the separator region

The loss of voltage in the separator region has been measured between two saturated calomel electrodes connected to the electrolyte in the zinc electrode compartment (the usual reference electrode) and in the outer part of the positive electrode (the outermost salt bridge), respectively.

6.3.1 Voltage loss in the separator region, Leclanché electrolyte, 4 Ω discharges

Figure (6.18) shows the potential of the three salt bridges inserted at three different locations (see section 2.5.3) in the positive electrode mass. The three curves are parallel, suggesting they were the result of the shift by a constant value, depending on the probe location, of the same potential difference which varied with the discharge stage. A similar comment has already been made in section (5.2.3) about the transients recorded on interruption of the discharge.

Figures (6.19) and (6.20) show the potential differences measured between the usual reference electrode and the outermost salt bridge on load and when corrected for the ohmic loss. The curves, both on-load and corrected for the ohmic loss, were similar for EMD and CMD for about 8 hours, after which the potential difference became more important for Faradiser M than for EMD (about 40 mV difference by the end of the discharge). Figure (6.20) shows clearly that this potential difference was not ohmic, as it did not vanish on current interruption. The only other possible voltage loss across the electrolyte is a diffusion potential, therefore figure (6.20) indicates that a diffusion potential was responsible for a significant part (about 100 mV out of a total of about 800 mV) of the voltage decay of the cell during the test. No report of this phenomenon has been found in the literature.

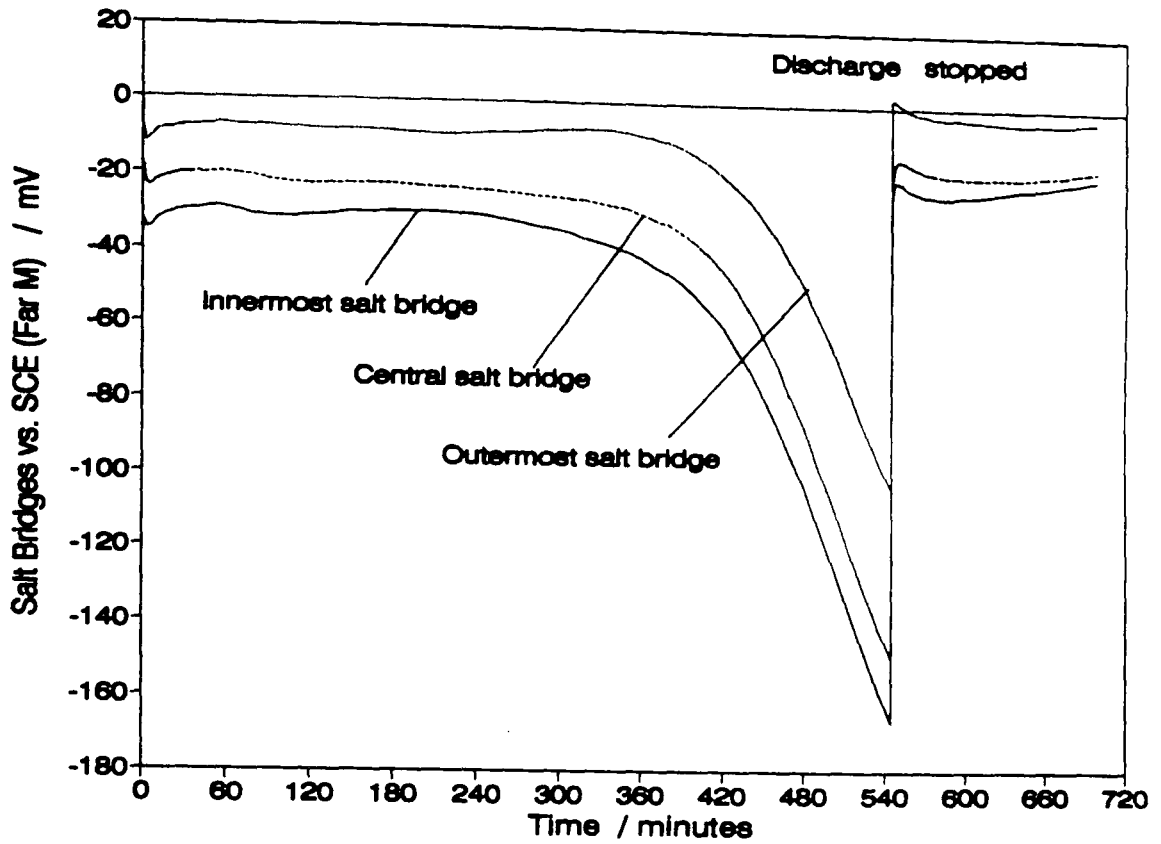

Figure 6.18 : Salt bridge potentials (vs. usual SCE); Faradiser M in Leclanché electrolyte; continuous discharge through 4 Ω

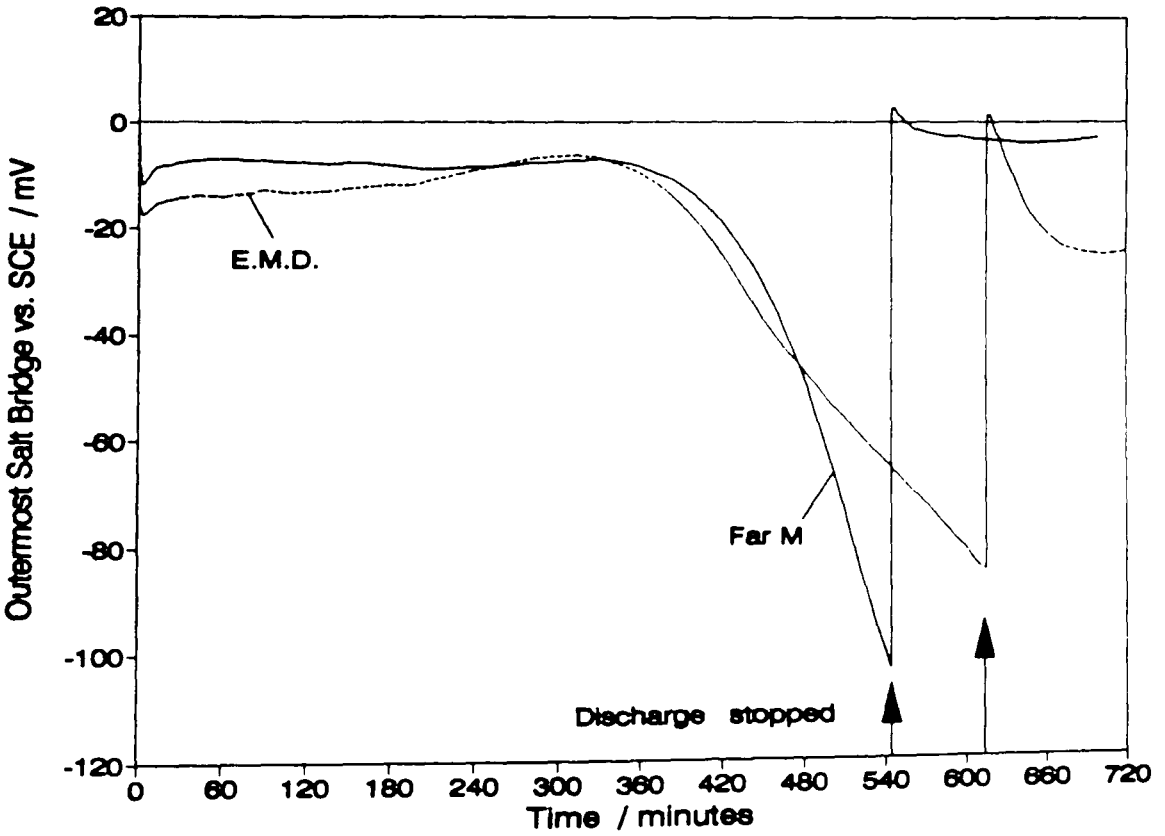

Figure 6.19 : Outermost salt bridge on-load potential (vs. SCE) in Leclanché electrolyte; continuous discharge through 4 Ω

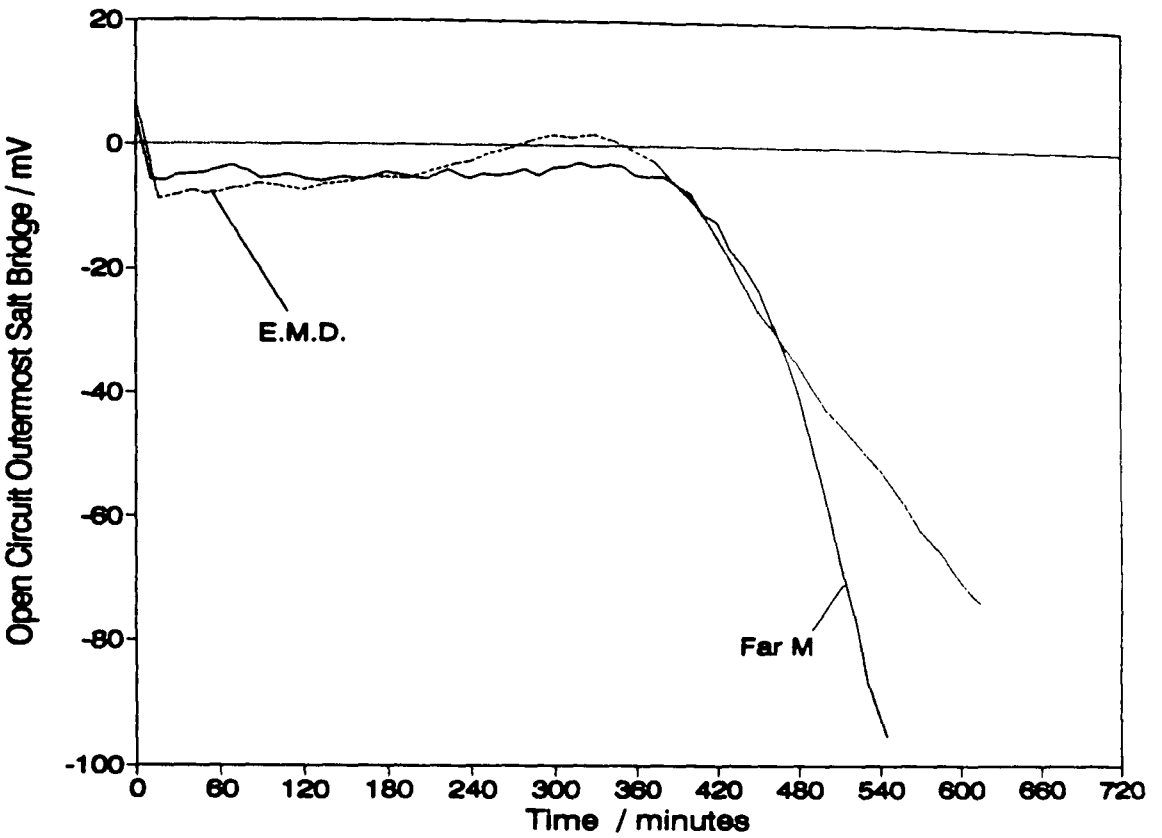

Figure 6.20 : Outermost salt bridge potential (vs. SCE) corrected for ohmic loss in Leclanché electrolyte; continuous discharge through 4 Ω

6.3.2 Voltage loss in the separator region, zinc chloride electrolyte, 2.2 Ω discharge

The outermost salt bridge potentials on-load and corrected for the ohmic loss are shown in figures (6.21) and (6.22), respectively. There was very little difference between the on-load and the open circuit outermost salt bridge potential, confirming the essentially non-ohmic nature of the potential difference across the separator region. Both curves exhibited a minimum (in absolute value) after about two to three hours of discharge, followed by an increase with a steepness following the order EMD < Far WSZ < Far M. By the end of the discharge, the voltage loss reached about one fifth of the total polarisation of the cell containing Faradiser M.

Figure (6.23) shows that the addition of one milli-litre of electrolyte to the cell with Faradiser WSZ reduced the voltage loss in the separator region from more than 100 mV to about 60 mV. This was the most significant difference caused by the change in the moisture content of the cell.

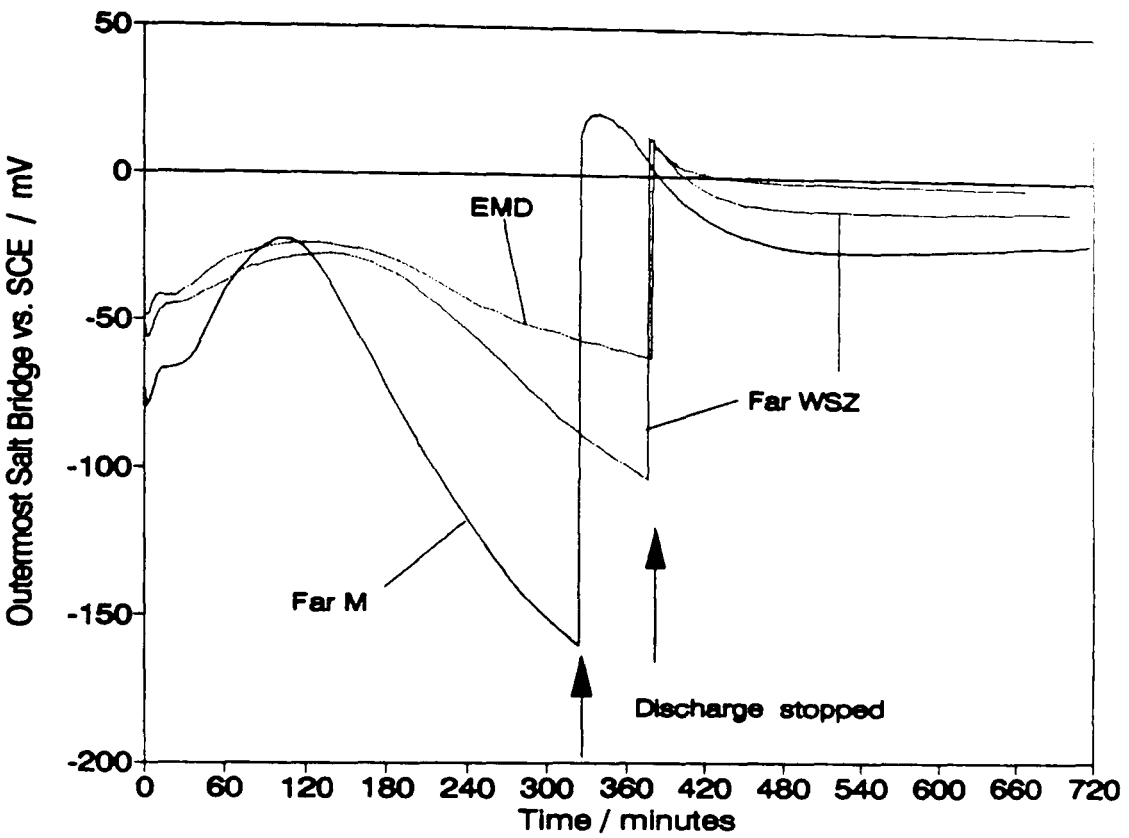

Figure 6.21 : Outermost salt bridge potential (vs. usual SCE) in $ZnCl_2$ electrolyte; continuous discharge through 2.2 Ω

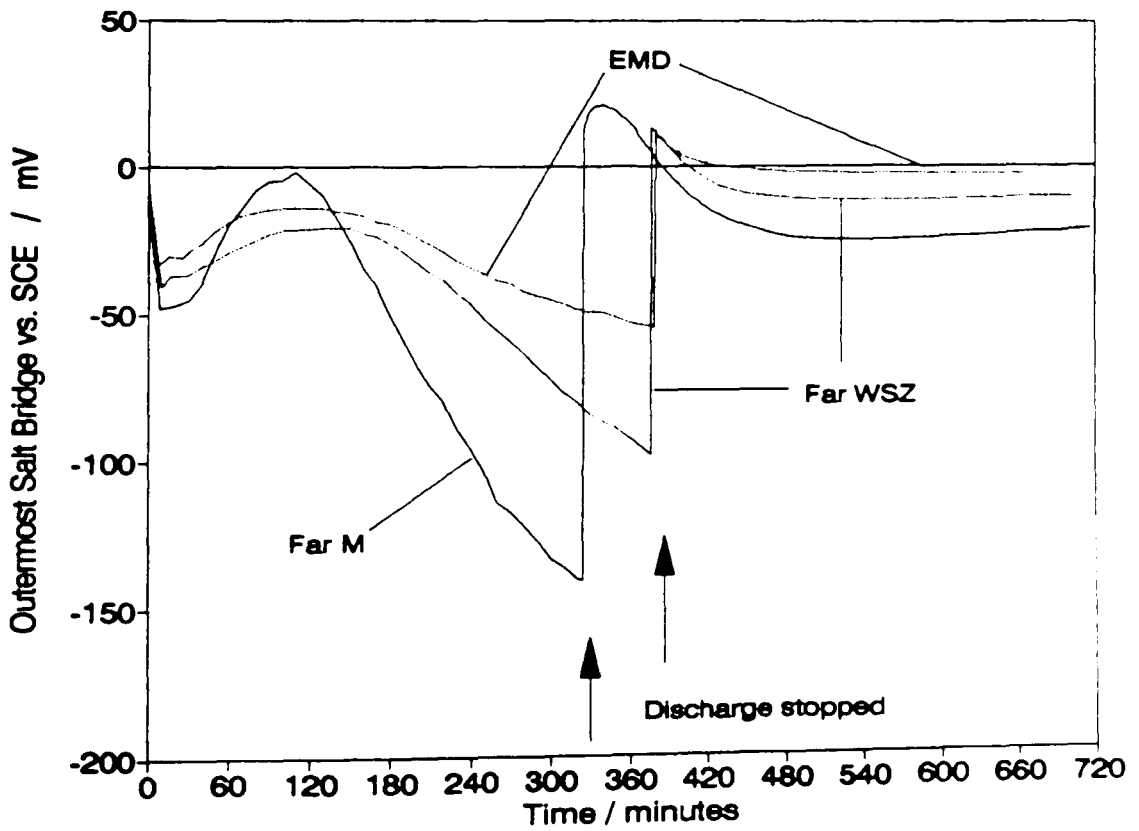

Figure 6.22 : Outermost salt bridge potential (vs. SCE) corrected for the ohmic loss in $ZnCl_2$ electrolyte; continuous discharge through 2.2 Ω

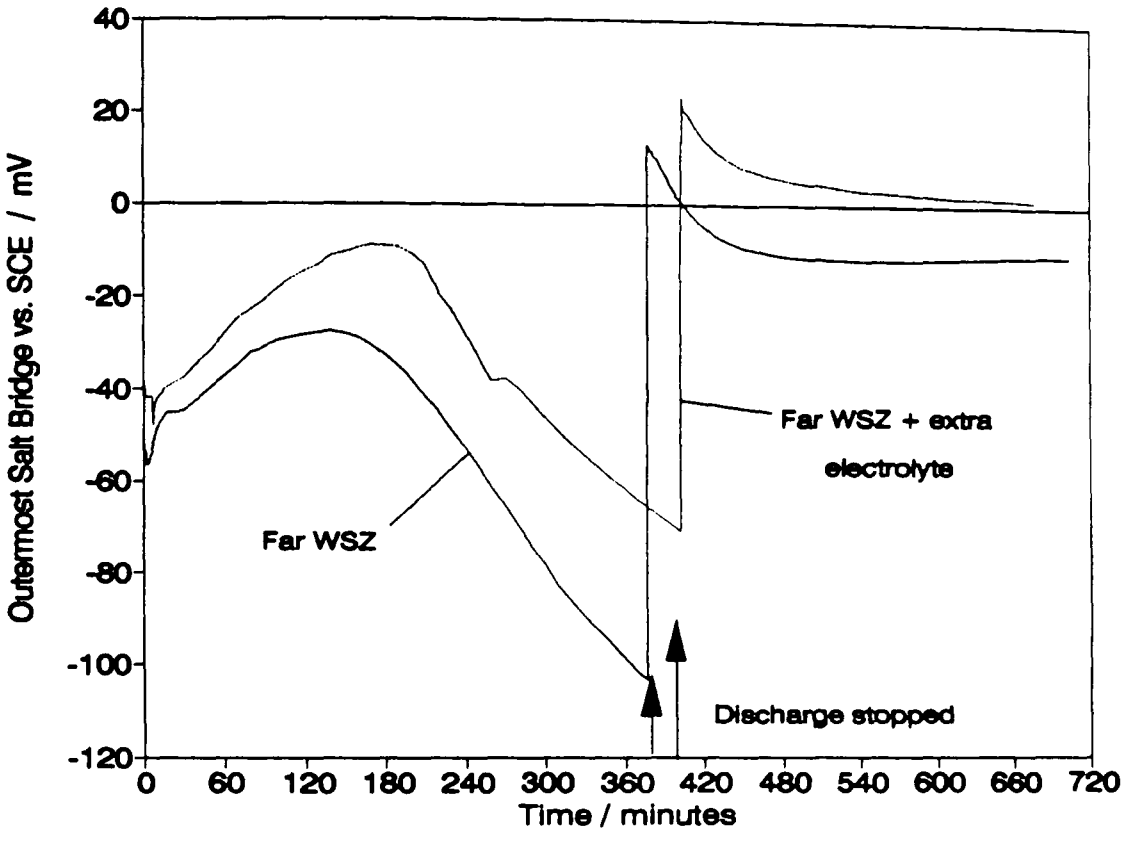

Figure 6.23 : Effect of added electrolyte on the on-load outermost salt bridge potential (vs. usual SCE) in $ZnCl_2$ electrolyte; continuous discharge through 2.2 Ω

The minimum of the voltage loss curve was observed about one hour later in the cell containing extra electrolyte than in the cell with normal formulation. Both effects, namely the lower voltage loss across the separator region and its delayed build up in the final part of the discharge, were probably caused by the larger electrolyte volume available to accommodate the zinc ions produced by the anodic reaction. This lowered the zinc concentration and thus delayed the conditions favourable to the build-up of the large concentration differences necessary to the formation of significant diffusion potentials. Diffusion potentials are usually small [60], but the very large dependence of zinc activity on electrolyte composition (see section 3.3) can explain the magnitude of the observed diffusion potential, for example, a zinc electrode potential difference of more than 100 mV exists for a less than fivefold change of the $ZnCl_2$ concentration between about 1.5 and 7 molal (1.4 and 5.5 molar, see section 3.3).

6.4. The manganese dioxide electrode potential

The manganese dioxide electrode potential with respect to the usual reference electrode (connected to the electrolyte within the negative electrode compartment) included the potential difference which existed in the separator region throughout the discharge. The positive electrode potential versus the outermost salt bridge did not contain the effect of the separator region and was therefore more suitable to monitor the potential loss of the positive electrode (ideally, the tip of the Luggin capillary should be adjacent to the outside electrode surface [153], but the difference is thought to be small).

6.4.1 MnO_2 electrode potential in Leclanché electrolyte, 4 Ω discharge

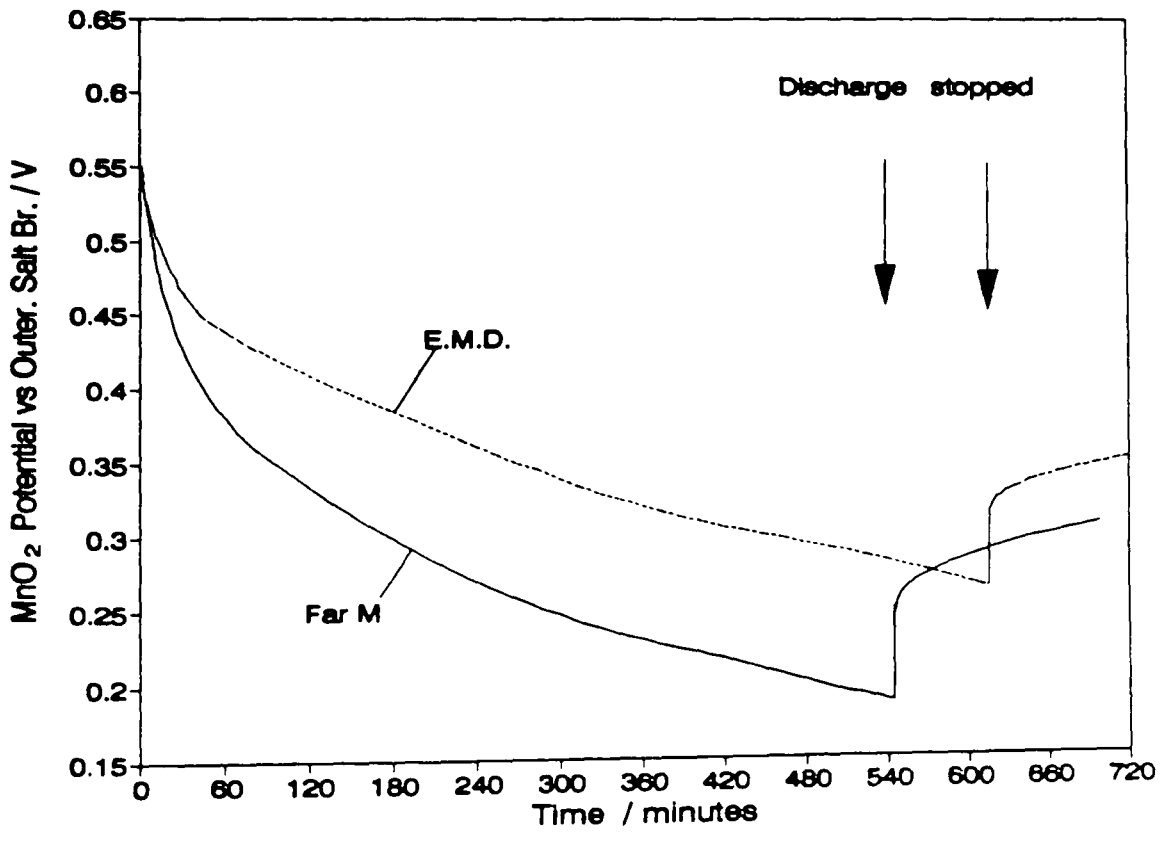

Figure 6.24 : Closed circuit positive electrode potential versus outermost salt bridge in Leclanché electrolyte; continuous discharge through 4 Ω

Figure (6.24) shows the closed circuit positive electrode potential with respect to the outermost salt bridge during the discharge through 4 Ω in Leclanché electrolyte. The potential of the positive electrode with Faradiser M was lower

than with EMD throughout the discharge, with a difference amounting to about 90 mV towards the end of the test. The addition of a higher voltage loss in the separator region for CMD than for EMD (see figure 6.19) and a lower positive electrode potential for the former material than for the latter on the 4 Ω continuous discharge test, caused the lower performance of CMD compared to EMD.

6.4.2 MnO_2 electrode potential in zinc chloride electrolyte, 2.2 Ω discharge

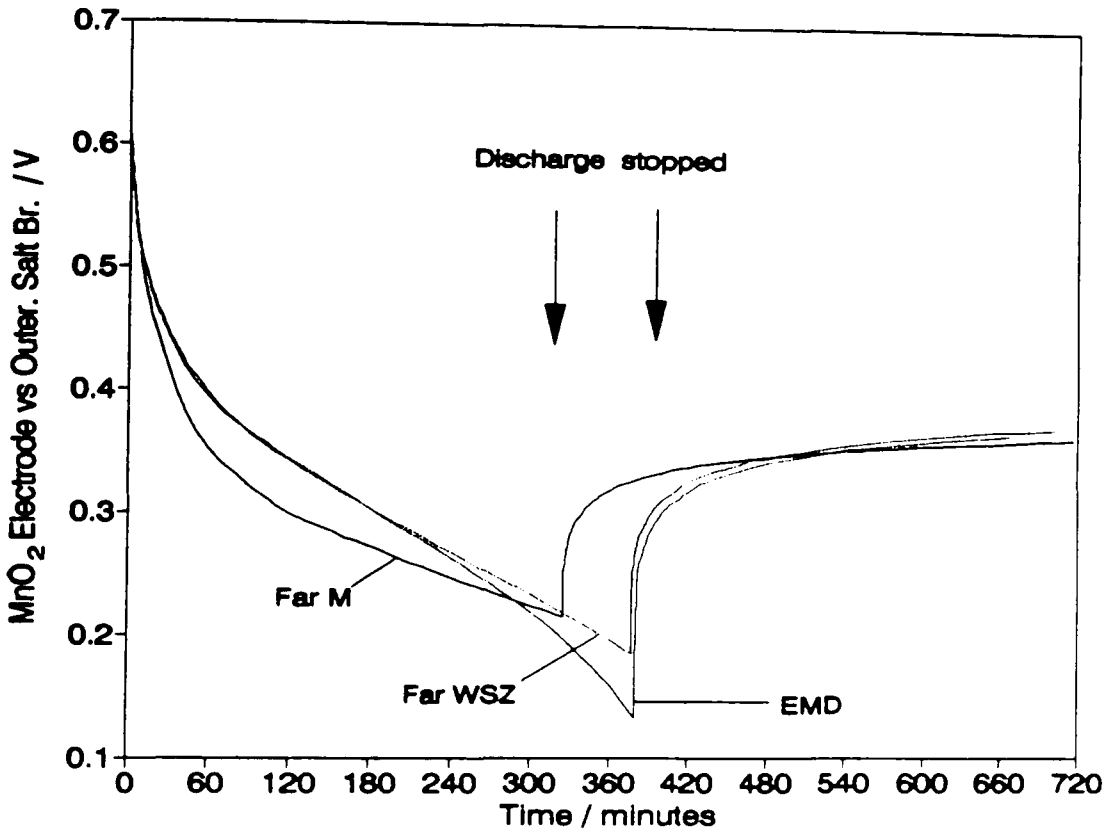

Figure 6.25 : Closed circuit positive electrode potential versus outermost salt bridge in $ZnCl_2$ electrolyte; continuous discharge through 2.2 Ω

Figure (6.25) shows the on-load MnO_2 electrode potential with respect to the outermost salt bridge during a discharge through 2.2 Ω in zinc chloride electrolyte. The curves were much closer to each other than in the Leclanché electrolyte (figure 6.24), but Faradiser M had, again, a lower electrode potential than the other materials throughout most of the discharge. The positive electrode potential of Faradiser WSZ was very similar to the potential of EMD and even higher at

the end of the test; the MnO_2 electrode potential was therefore not the reason for the lower performance of Faradiser WSZ compared to EMD.

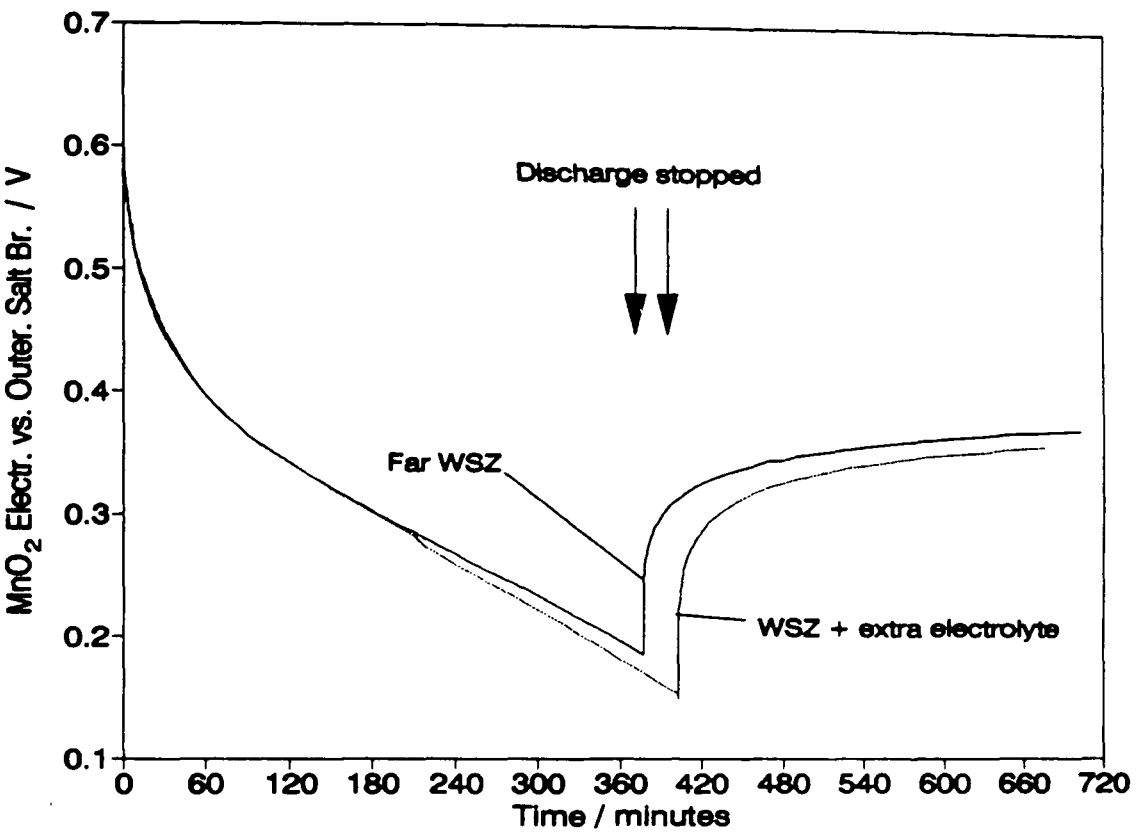

Figure 6.26 : Effect of extra electrolyte on the MnO_2 electrode potential vs. outermost salt bridge in $ZnCl_2$ electrolyte; continuous discharge through 2.2 Ω

Figure (6.26) shows that the addition of extra electrolyte to Faradiser WSZ had a very limited influence on its positive electrode potential (with respect to the outermost salt bridge).

6.4.3 Manganese dioxide electrode concentration overpotential

The manganese dioxide equilibrium potential including the effect of the reduction of the material and of the change of the pH of the electrolyte was calculated as in section 4.3.2. The MnO_2 electrode temporary equilibrium potential (versus the outermost salt bridge) was calculated from the closed circuit potential (with respect to the usual reference electrode) corrected for the ohmic overpotential, taken as the difference between the MnO_2 electrode and the outermost salt bridge ohmic overpotentials, and the voltage loss in the separator region, taken as the outermost salt bridge potential (versus the usual SCE)

corrected for the ohmic loss, see section 6.3. The manganese dioxide electrode concentration overpotential was the difference between these two potentials.

The results in Leclanché electrolyte are shown in figure (6.27). The slightly lower overpotential of Faradiser M compared with EMD was probably due to the lower discharge current of the cell containing the CMD, suggesting that the product $A\ D$ (see equation 1.33) of the electrochemically active surface area (A) by the H^+/e diffusion coefficient (D) was very similar for the two materials.

Figure (6.28) shows the results in $ZnCl_2$ electrolyte. The concentration overpotentials were very similar for Faradiser M and Faradiser WSZ, both being much lower than for EMD. The lower concentration overvoltage of Faradiser M compared to Faradiser WSZ was probably due to the lower discharge current (see figure 6.3), but this factor does not explain the difference between EMD and Faradiser WSZ as the closed circuit voltages and therefore the discharge currents were very similar for these cells (see figure 6.3). The cells contained about the same quantities of EMD and of Faradiser WSZ and almost the same amount of electrolyte (see table 2.2), suggesting that the difference was due to the materials, possibly the difference between their surface areas (see table 2.4). The addition of some extra electrolyte to the cell had little influence on the concentration overvoltage as revealed by the similarity of the curves for both formulations with Faradiser WSZ.

6.5. Internal resistance of the cell

The total ohmic loss in the cell was calculated by addition of the ohmic overpotential of the zinc and the MnO_2 electrodes, both measured against the usual reference electrode (inserted through the zinc can). This total ohmic loss has been divided by the discharge current (CCV divided by the load) to give the cell internal resistance. The calculated internal resistances are shown in figures (6.29) and (6.30) for the Leclanché and the $ZnCl_2$ electrolyte, respectively. All the curves, except for Faradiser M in Leclanché electrolyte, show a progressive increase of the internal resistance, with no indication of a steeper increase at any stage of the discharge. In zinc chloride electrolyte, the progressive build-up of

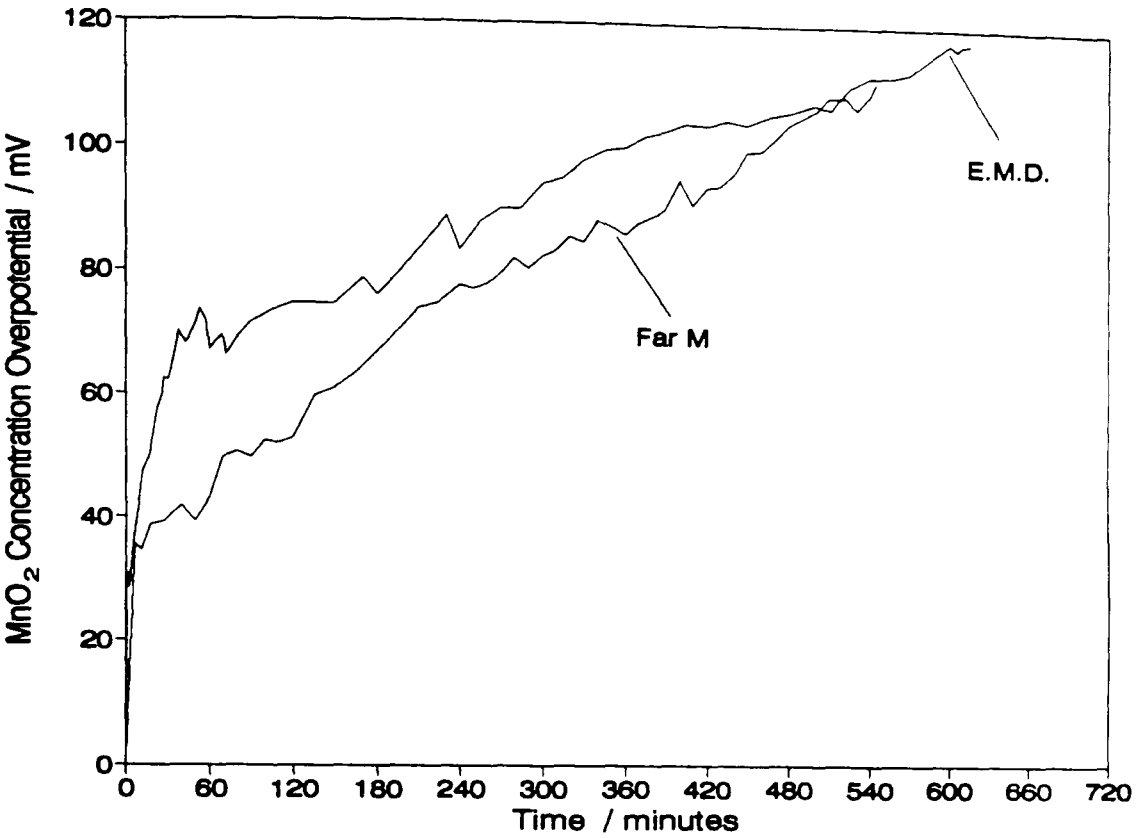

Figure 6.27 : Manganese dioxide concentration overpotential in Leclanché electrolyte; continuous discharge through 4 Ω

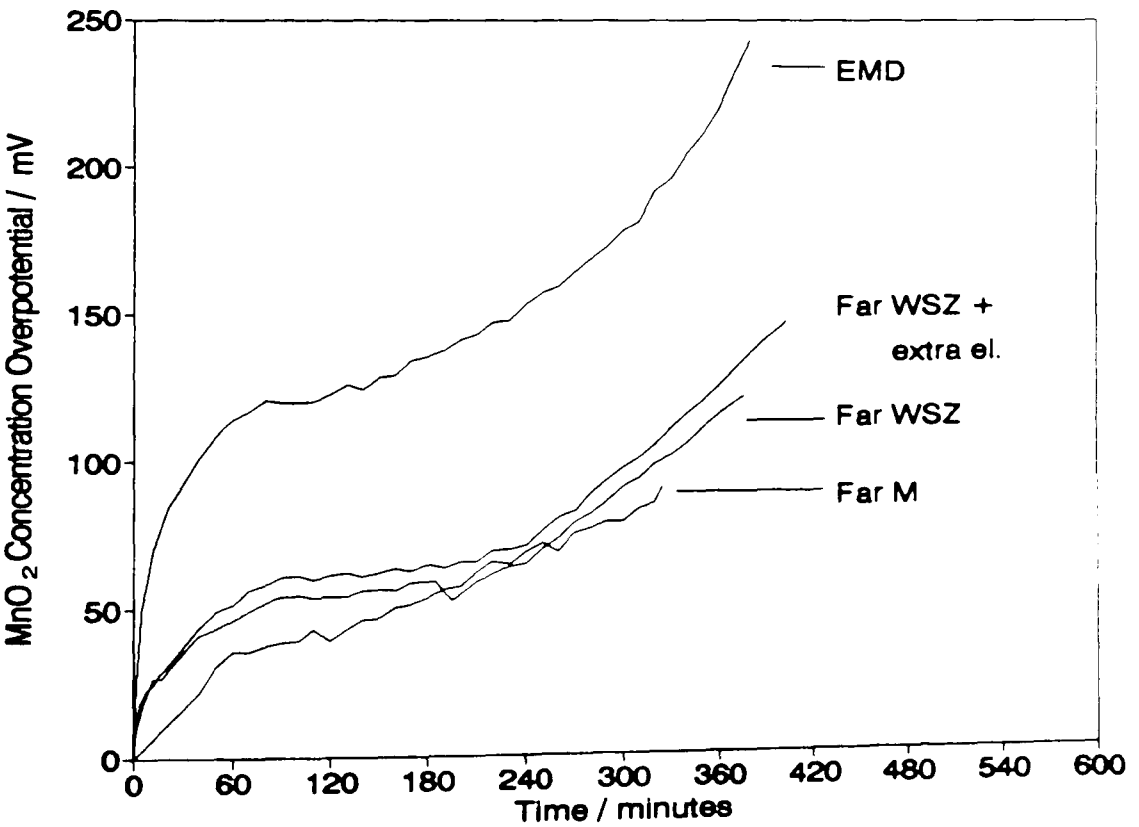

Figure 6.28 : Manganese dioxide electrode concentration overpotential in $ZnCl_2$ electrolyte; continuous discharge through 2.2 Ω

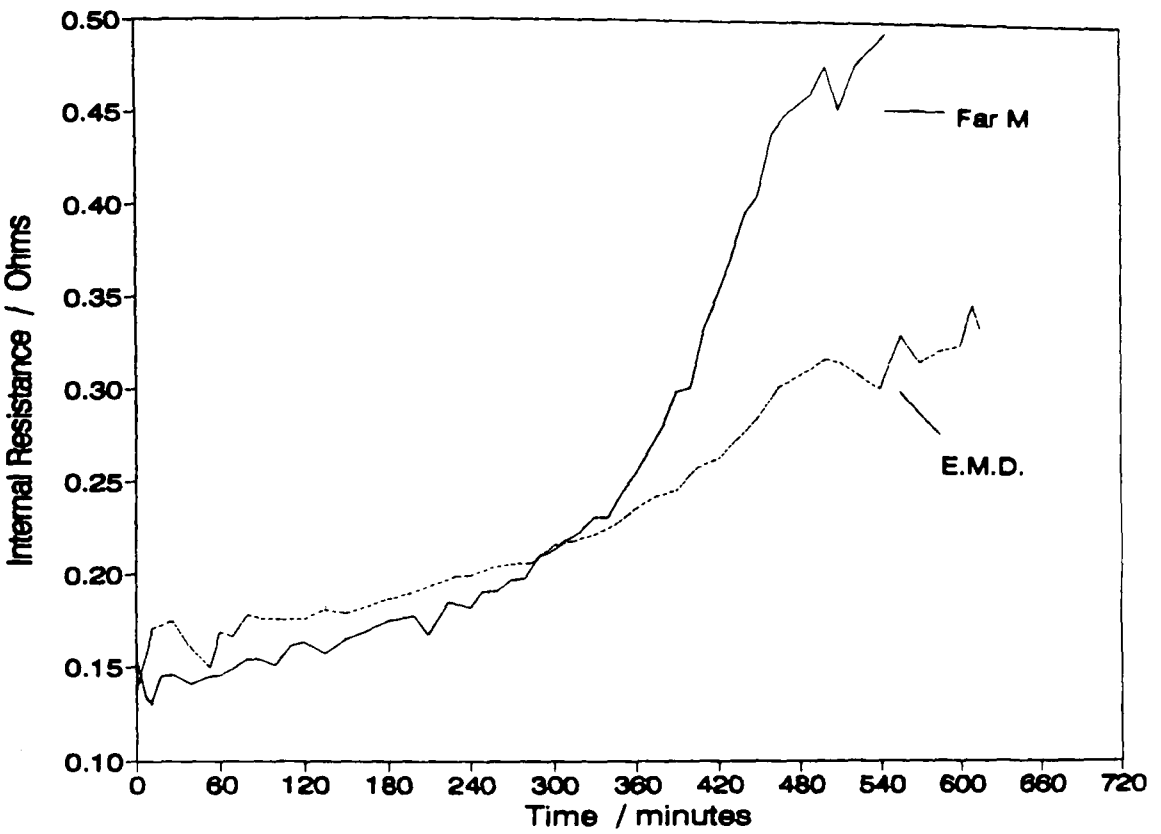

Figure 6.29 : Internal resistance in Leclanché electrolyte; continuous discharge through 4 Ω

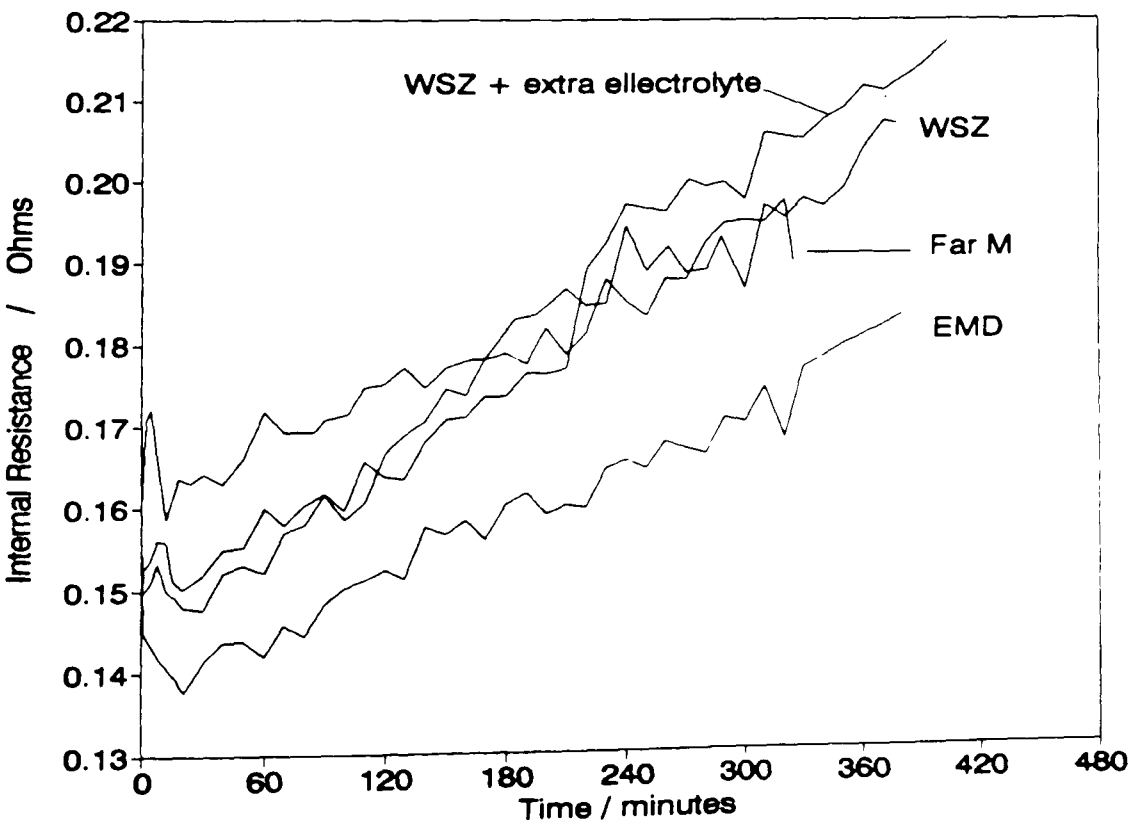

Figure 6.30 : Internal resistance in zinc chloride electrolyte; continuous discharge through 2.2 Ω

the internal resistance was probably due to the decrease of the electrolyte conductivity with increasing $ZnCl_2$ concentration [225]. In the Leclanché cells, the electrolyte conductivity also decreased [19] due to the decrease of the NH_4Cl concentration during the discharge and this may explain the curve observed for the EMD. Figure (6.26) shows that for Faradiser M the increase of the internal resistance with discharge time became steeper after about five hours on load. This suggests that from that moment, the separator porosity became partially clogged by a layer of precipitate. This clogging hindered the diffusion of the zinc species, increased the anodic concentration overpotential (observed at that moment, see figure 6.6) and favoured the formation of the high concentration difference across the separator region necessary to the formation of high diffusion potential (see figure 6.19).

6.6. Voltage loss distribution

The discharge of a cell causes permanent changes to its components, precipitation of some of the electrolyte salts and reduction of the manganese dioxide, and thus modifies the potential on both zinc and manganese dioxide electrodes. For EMD and Faradiser WSZ which did not form hetaerolite, the intermittent discharge curves (see chapter 4) give a very good approximation of the effect of the chemical changes on the electrodes potential. For Faradiser M, which formed hetaerolite during the intermittent discharge tests, the initial parts of the zinc electrode potential curves (in Leclanché and in zinc chloride electrolytes) can be extrapolated to give the estimated negative electrode potential that would apply if hetaerolite had not been formed. The manganese dioxide electrode potential after full recovery, can be calculated from the potential-composition equations and the estimated electrolyte pH (see section 6.4.3).

During a continuous discharge test, the voltage loss of the cell may be divided into permanent changes due to the chemical modifications of the cell, and overpotential, which is the difference between the cell closed circuit voltage and the voltage after full recovery of an identical cell discharged to the same extent. The total overvoltage is the sum of the ohmic loss (due to the internal resistance

of the cell), the electrode charge transfer overpotential (limited to the zinc electrode activation overpotential as the MnO_2 electrode activation overpotential was negligible, see chapter 5), the zinc and manganese electrode concentration overpotentials (difference between the temporary equilibrium electrode potential and the electrode potential after full recovery of an identical cell discharged to the same extent) and finally the voltage loss resulting from a diffusion potential in the separator region.

The ohmic loss has been determined as in section (6.5) by addition of the zinc and manganese dioxide electrode ohmic overpotentials measured on discharge interruption.

The zinc electrode activation overpotentials were directly measured (see figures 6.8 and 6.15).

The zinc concentration overpotential was taken as the difference between the temporary equilibrium electrode potential (closed circuit potential – (ohmic + activation) overpotential) and the electrode potential, at the same stage (coulombs delivered) of the intermittent discharge of the cell with the same formulation.

The voltage loss in the separator region was taken as the potential difference, corrected for the ohmic drop, between the usual reference electrode (connected to the negative electrode compartment) and the outermost salt bridge.

The oxidation degree of the manganese dioxide has been calculated from the coulombs delivered and the amount of MnO_2 contained in the cell. No correction has been applied for the Mn^{2+} formed due to the negligible effect it had on the average oxidation stage. The manganese dioxide electrode potential after full recovery has been calculated from the calculated oxidation stage and using the same equations and pH evaluations as in chapter 4.

The open circuit of the cell after full recovery has been calculated from the manganese electrode potential calculated as in the previous paragraph, and the interpolated (extrapolated from the 30 minute a day discharge curves in the case of Faradiser M due to hetaerolite formation) zinc electrode potential. The difference between the open circuit after full recovery and the closed circuit is the

total overpotential. The temporary equilibrium manganese dioxide electrode potential was calculated as in section 6.4.3.

The permanent change of the zinc electrode potential was the difference between the initial open circuit zinc electrode potential and its value after full recovery.

The total voltage loss was the difference between the closed circuit voltage and the initial cell open circuit voltage.

The results of these calculations are presented in figures (6.31) to (6.36).

Figures (6.31) and (6.32) summarise the main differences on discharge through four ohms in Leclanché electrolyte between EMD and Faradiser M, namely the larger permanent (chemical) change and the larger voltage loss in the separator region (especially towards the end of the discharge) for the CMD than for the EMD. The larger zinc electrode concentration overpotential and permanent potential change for the cell containing EMD was due to the higher discharge current and greater amount of charge delivered for that cell than for the cell with CMD. The manganese dioxide concentration overpotential was very similar for Faradiser and EMD (see section 6.4.3).

In zinc chloride electrolyte (figures 6.33 to 6.36) the permanent change of the zinc electrode potential was small and negative (i.e. increasing the cell voltage). The main difference between EMD and the CMDs was observed in the permanent decrease of the manganese dioxide electrode potential and in the voltage loss in the separator region.

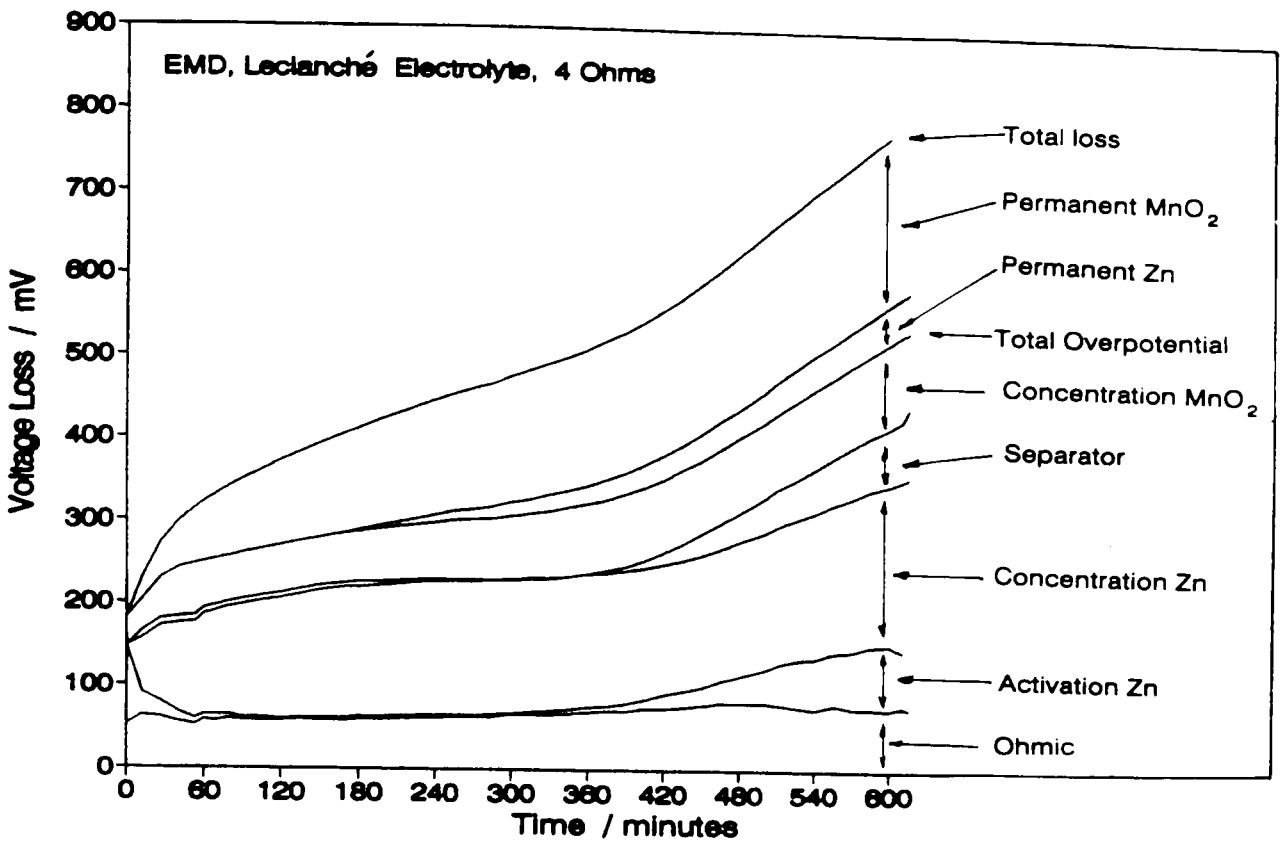

Figure 6.31 : Voltage loss distribution during the discharge of a cell with EMD in Leclanché electrolyte; continuous discharge through 4 Ω

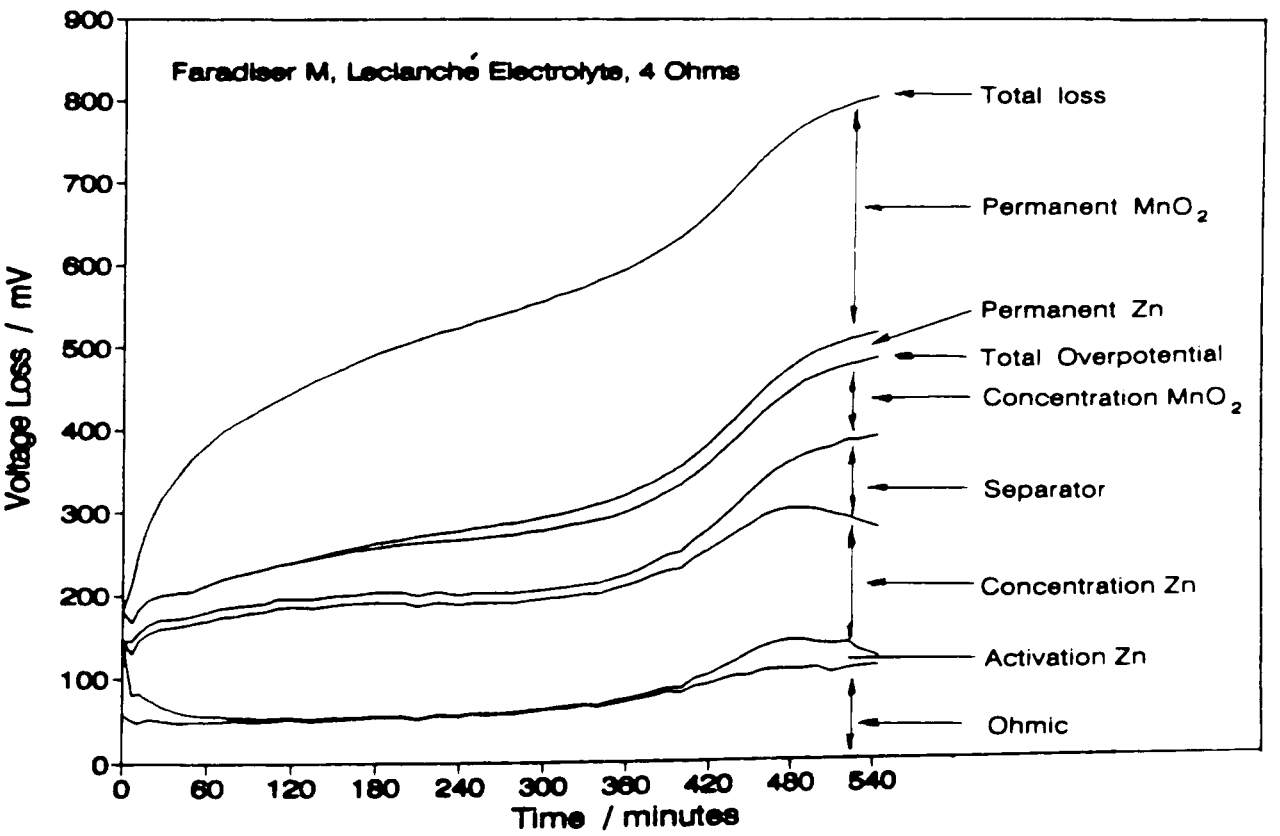

Figure 6.32 : Voltage loss distribution during the discharge of a cell with Faradiser M in Leclanché electrolyte; continuous discharge through 4 Ω

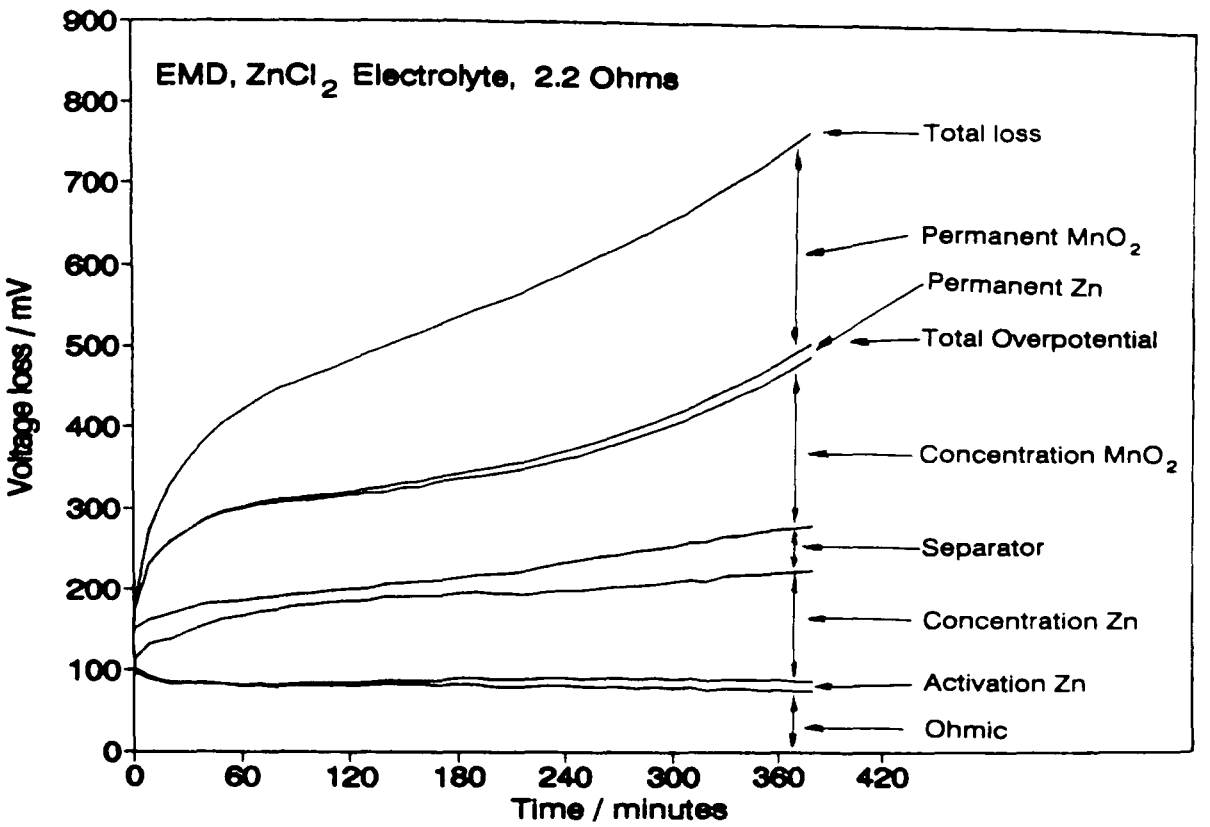

Figure 6.33 : Voltage loss distribution during the discharge of a cell with EMD in $ZnCl_2$ electrolyte; continuous discharge through 2.2 Ω

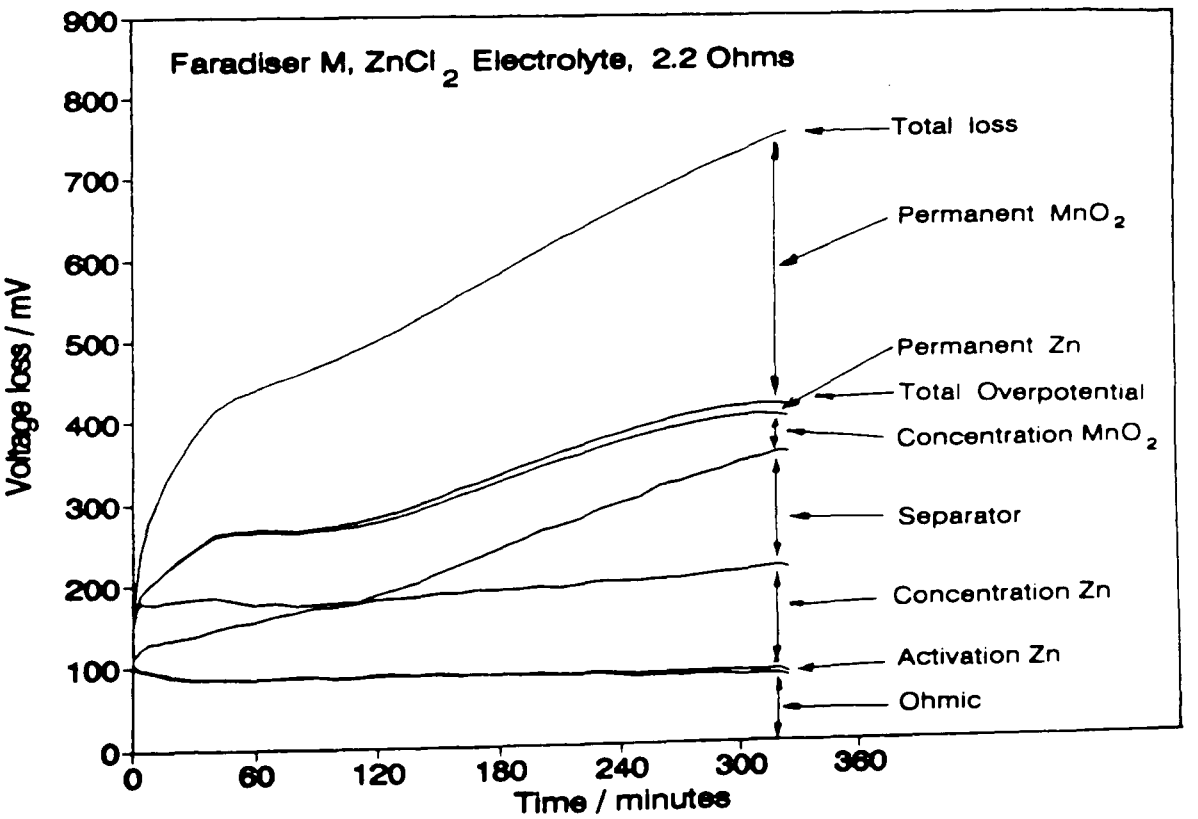

Figure 6.34 : Voltage loss distribution during the discharge of a cell with Faradiser M in $ZnCl_2$ electrolyte; continuous discharge through 2.2 Ω

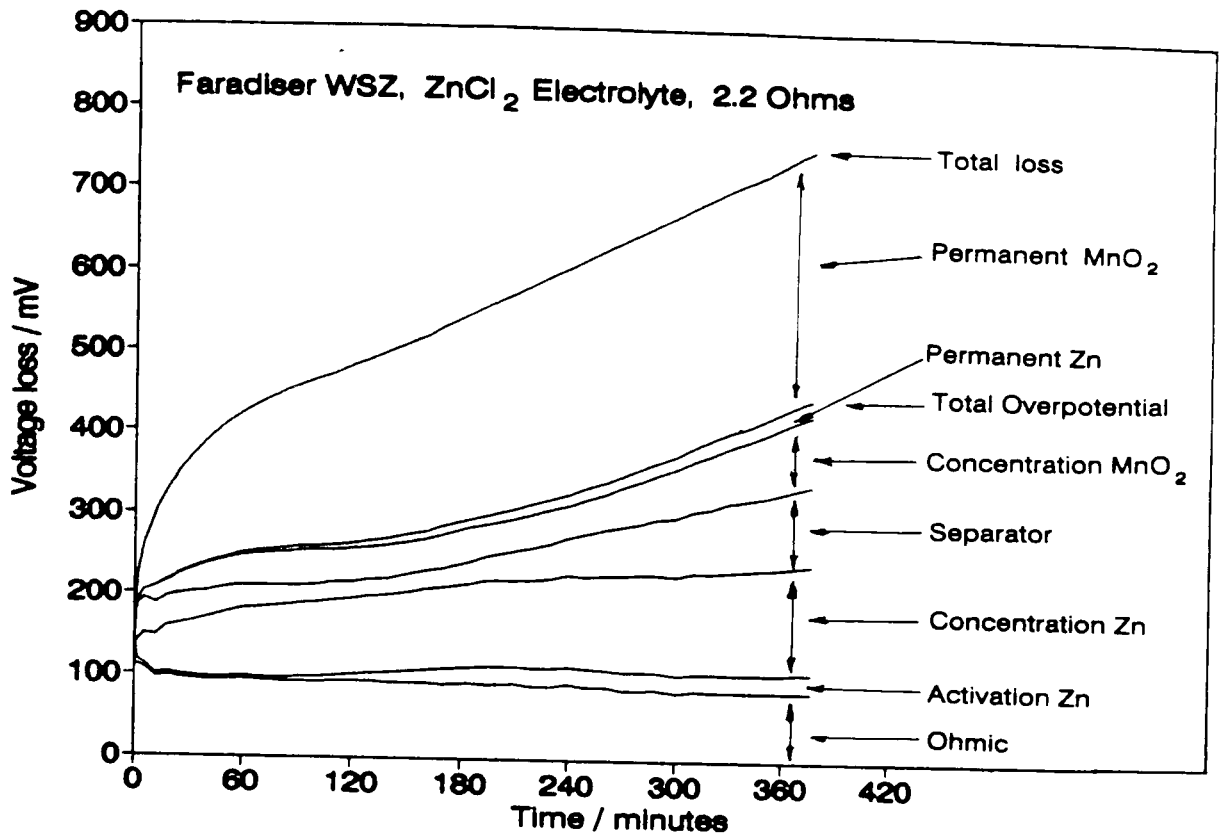

Figure 6.35 : Voltage loss distribution during the discharge of a cell with Faradiser WSZ in $ZnCl_2$ electrolyte (normal formulation); continuous discharge through 2.2 Ω

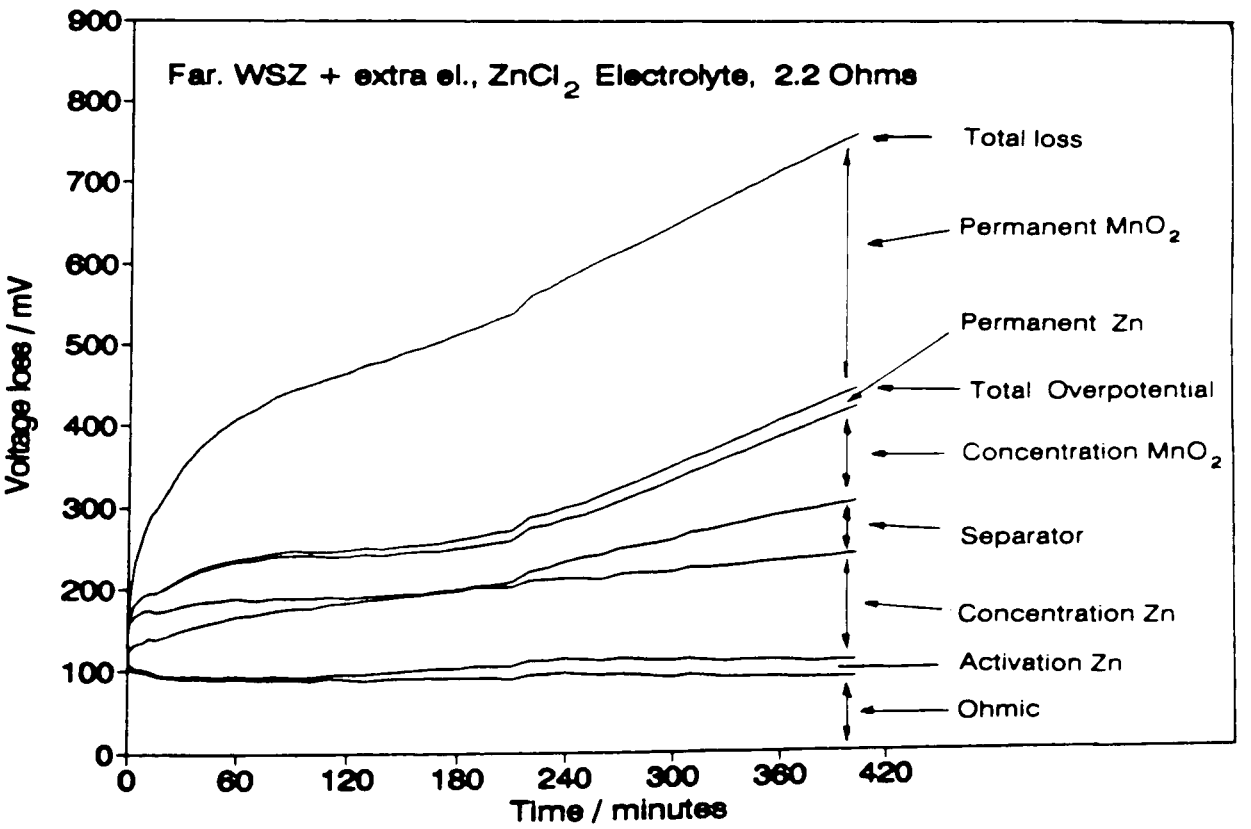

Figure 6.36 : Voltage loss distribution during the discharge of a cell with Faradiser WSZ in $ZnCl_2$ electrolyte (cell with 1 ml of extra electrolyte); continuous discharge through 2.2 Ω

Although the discharge current was higher for the zinc chloride electrolyte cells than for the Leclanché cells, the zinc concentration overpotential was lower in the former type of cells, due to the difference in the zinc transference number in the different electrolytes [80].

6.7 Electrochemical current distribution in the positive electrode

6.7.1 The positive electrode model

Porous electrode models [e.g. 160,163] have been developed using the laws of mass transport in the liquid phase to predict the current distribution within the electrode from the properties of the solid and of the electrolyte phases. The Leclanché cell is a complicated system with many zinc species (chloro-complexes, oxy or oxyhydroxy species) in ill defined proportions plus NH_4Cl and some amino compounds in the conventional mixed electrolyte. During the discharge at heavy drain, the cell is far form equilibrium conditions [103] and the knowledge of the Leclanché electrolyte chemistry (see chapter 3) only provides general guidelines.

The present model has been developed by considering the solid phase only, in order to interpret the measurements made using carbon probes inserted into the positive electrode. The pseudo-homogeneous assumption [160] has been used, i.e. the positive electrode has been considered as a continuous phase having the same physical properties throughout its volume. Its electronic resistivity ρ was therefore considered identical at every point within the electrode.

Due to the electrode's cylindrical symmetry, the current is considered to flow along radial paths exclusively. The calculations are developed for the electrode slice shown in figure (6.37).

In the sector having an external surface area of 1 cm^2 considered in these calculations (figure 6.37), the volume of electrode, dV, in the cylinder of internal radius x and thickness dx is

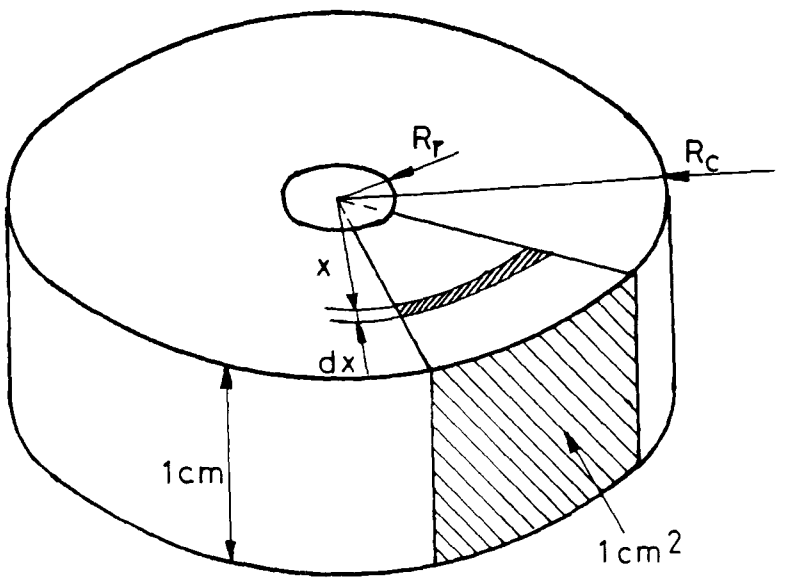

Figure 6.37 : Fraction of the positive electrode considered in the calculations

$$dV = \frac{x\ dx}{R_c} \tag{6.2}$$

The non uniform reduction current distribution or the volumic reduction rate, J (in A cm^{-3}), is approximated by an equation of the form

$$J = a + bx + cx^2 \tag{6.3}$$

in which a, b and c are supposedly known.

The electronic current, dI, generated in the volume dV by the reduction of manganese dioxide is

$$dI = - J\ dV \tag{6.4}$$

where the sign minus shows that the electronic current, I (amperes), through the sector considered in the solid phase increases with decreasing x.

Integrating noting that I=0 at x=R_c gives

$$I = \frac{a}{2}\left(R_c - \frac{x^2}{R_c}\right) + \frac{b}{3}\left(R_c^2 - \frac{x^3}{R_c}\right) + \frac{c}{4}\left(R_c^3 - \frac{x^4}{R_c}\right) \tag{6.5}$$

The ohmic resistance dr across the volume dV is

$$dr = \rho \frac{R_c\, dx}{x} \tag{6.6}$$

Application of Ohm's Law gives the potential difference, U, caused by the electronic current I flowing through the solid phase and integration with the boundary condition $U=0$ at $x=R_r$ gives

$$U = a\rho\left(\frac{R_c^2}{2}\ln\frac{x}{R_r} + \frac{R_r^2-x^2}{4}\right) + b\rho\left(\frac{R_c^3}{3}\ln\frac{x}{R_r} + \frac{R_r^3-x^3}{9}\right) + c\rho\left(\frac{R_c^4}{4}\ln\frac{x}{R_r} + \frac{R_r^4-x^4}{16}\right) \tag{6.7}$$

The ionic current penetrating the electrode slice through 1 cm^2 of lateral surface area is

$$\frac{I_t}{2\pi H R_c} \tag{6.8}$$

where I_t is the total cell discharge current and H the electrode length.

At the current collector interface, all the ionic current has been converted into electronic current by the electrochemical reduction. The electronic current, at the current collector interface, in the portion of the electrode which is considered is given by the expression (6.8). Introducing (6.8) in (6.5) with $x=R_r$ gives

$$\frac{I_t}{2\pi H R_c} = \frac{a}{2}\left(R_c - \frac{R_r^2}{R_c}\right) + \frac{b}{3}\left(R_c^2 - \frac{R_r^3}{R_c}\right) + \frac{c}{4}\left(R_c^3 - \frac{R_r^4}{R_c}\right) \tag{6.9}$$

It was shown in section (5.2.4) that electronic probes (carbon probes) in electronic contact with a mixed conductor (the wet electrode mix) detect only electronic potential differences, that is to say the ohmic drop caused across the carbon black by the passage of the electronic current and given by equation (6.7). It is therefore possible to solve equations (6.7) and (6.9) for the electrochemical current distribution parameters a, b and c (in equation 6.3) and for the mix

resistivity ρ at a given moment of the discharge if three values of U are known for different values of x together with the total discharge current.

The discharge current was known from the CCV and the constant resistance load and the three different U values from the potential differences between the current collector and the carbon probes.

6.7.2 Discharge results

Figures (6.38) and (6.39) show the potential differences measured in cells containing EMD, between the carbon probes and the current collector on 4 Ω in the mixed Leclanché electrolyte and on 2.2 Ω in the $ZnCl_2$ electrolyte, respectively. Similar curves were recorded for Faradiser M (4 and 2.2 Ω in Leclanché electrolyte and 2.2 Ω in $ZnCl_2$ electrolyte) and for Faradiser WSZ (on 2.2 Ω in $ZnCl_2$ electrolyte). The trend to lower potential differences with increasing discharge time was related to the simultaneous decrease of the discharge current. Despite a higher discharge current on the 2.2 Ω load, the potential differences were lower in the zinc chloride electrolyte (2.2 Ω) than in the conventional Leclanché electrolyte (4 Ω). This has been interpreted in terms of electrode mix conductivity being better in the former than in the latter cells due to higher content of electronic conductor (see tables 2.1 and 2.2).

6.7.3 Electrochemical current distribution profiles

The electrochemical current distribution (volumic reduction rate) profiles were calculated at different stages of the discharge (beginning, middle and end) for the different formulations. The results are shown in figures (6.40) to (6.45) as the electrochemical current generated per cubic centimetre of positive electrode as a function of the distance (in cm) from the cell centre. In all cases, the electrode reduction was non uniform with some regions showing a negative (recharge) current density, either at the electrode edges (4 Ω discharges) or in its middle (2.2 Ω discharges). Negative current densities were also observed by Brodd [159] during his work on specially built MnO_2 electrodes. The change of the discharge current had a dramatic effect on the current distribution as shown in figures (6.41)

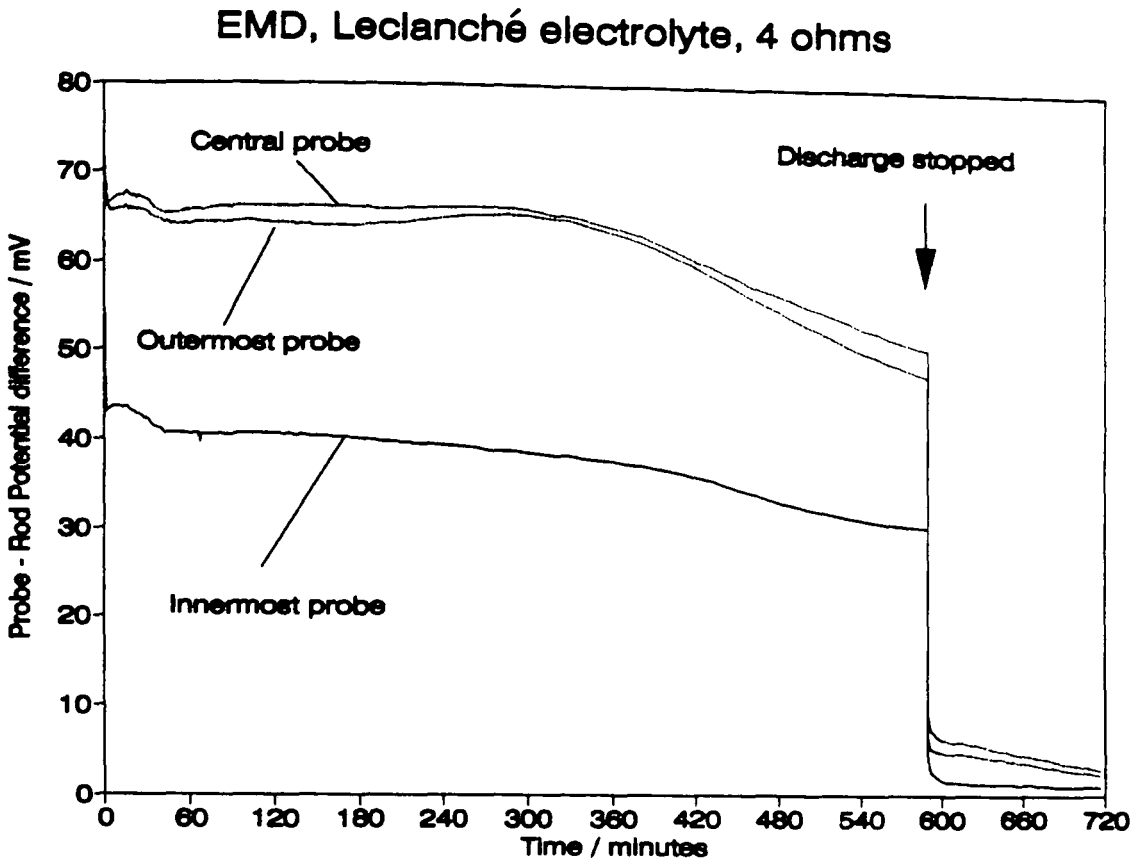

Figure 6.38 : Current collector - carbon probes potential differences; EMD in Leclanché electrolyte; continuous discharge through 4 Ω

and (6.45). The change of the position of the minimum of the distribution with changing discharge current is in contradiction with the findings of Daniel-Bek [153, 154], but agrees with the Newman and Tobias's model [160].

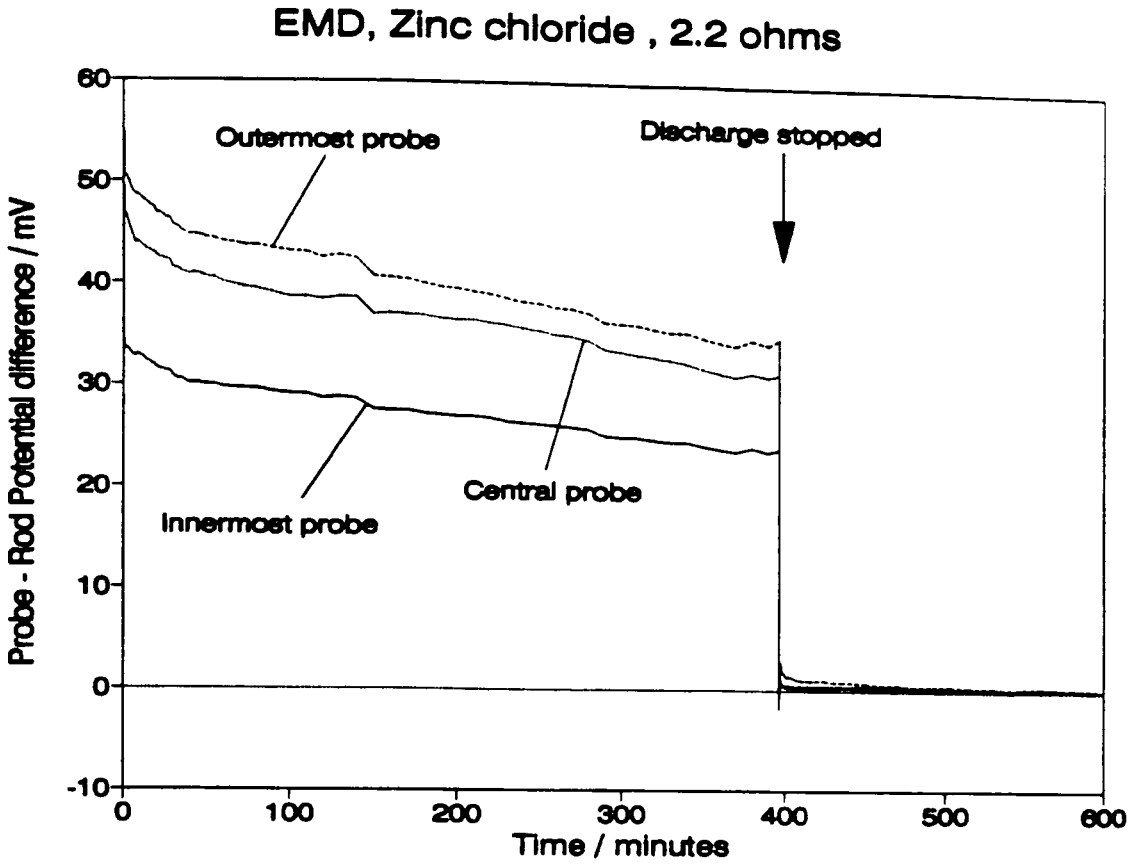

Figure 6.39 : Current collector - carbon probes potential differences; EMD in $ZnCl_2$ electrolyte; continuous discharge through 2.2 Ω

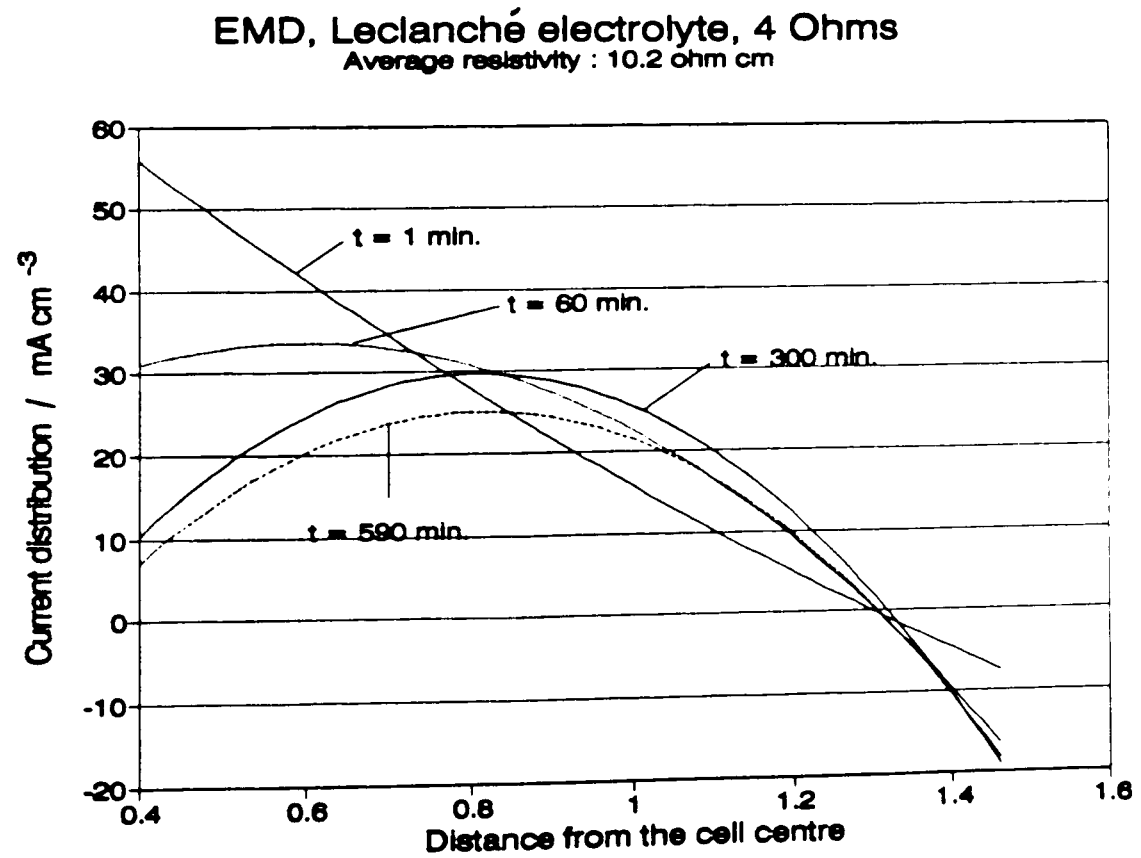

Figure 6.40 : Electrochemical current distribution profiles; EMD in Leclanché electrolyte; continuous discharge through 4 Ω

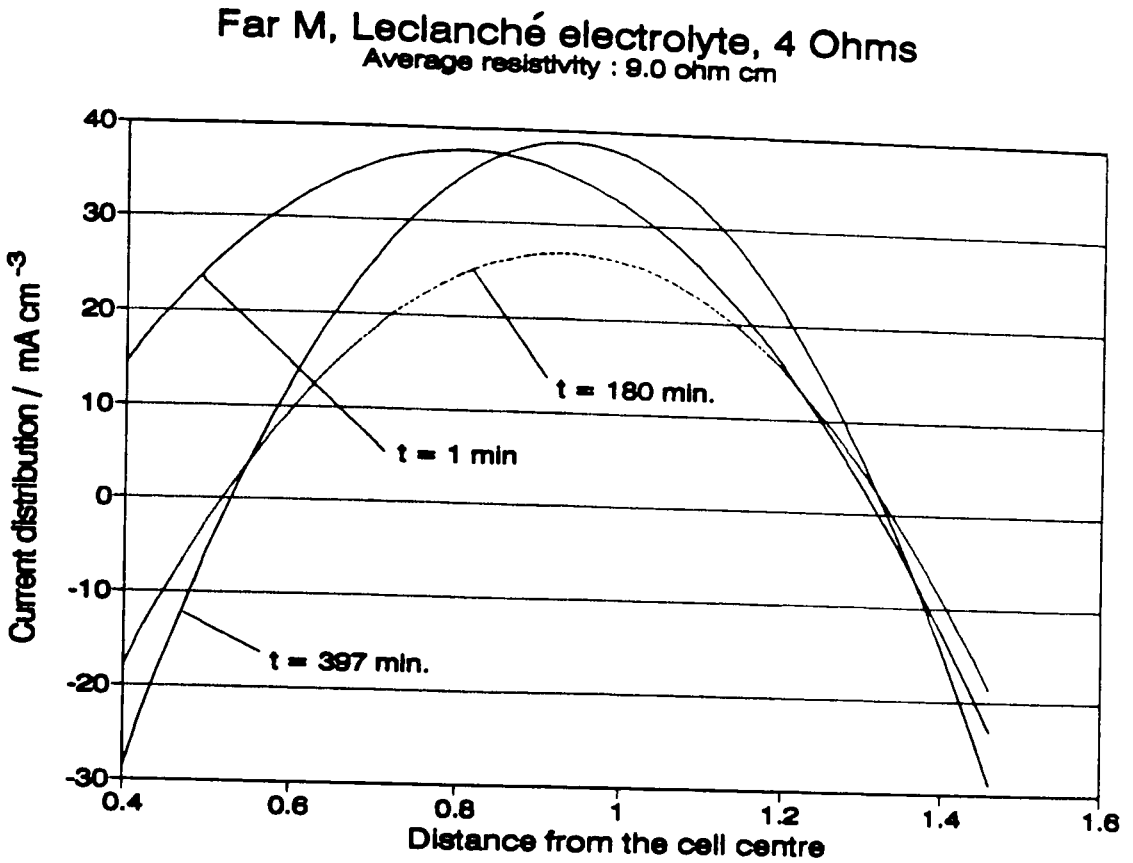

Figure 6.41 : Electrochemical current distribution profiles; Faradiser M in Leclanché electrolyte; continuous discharge through 4 Ω

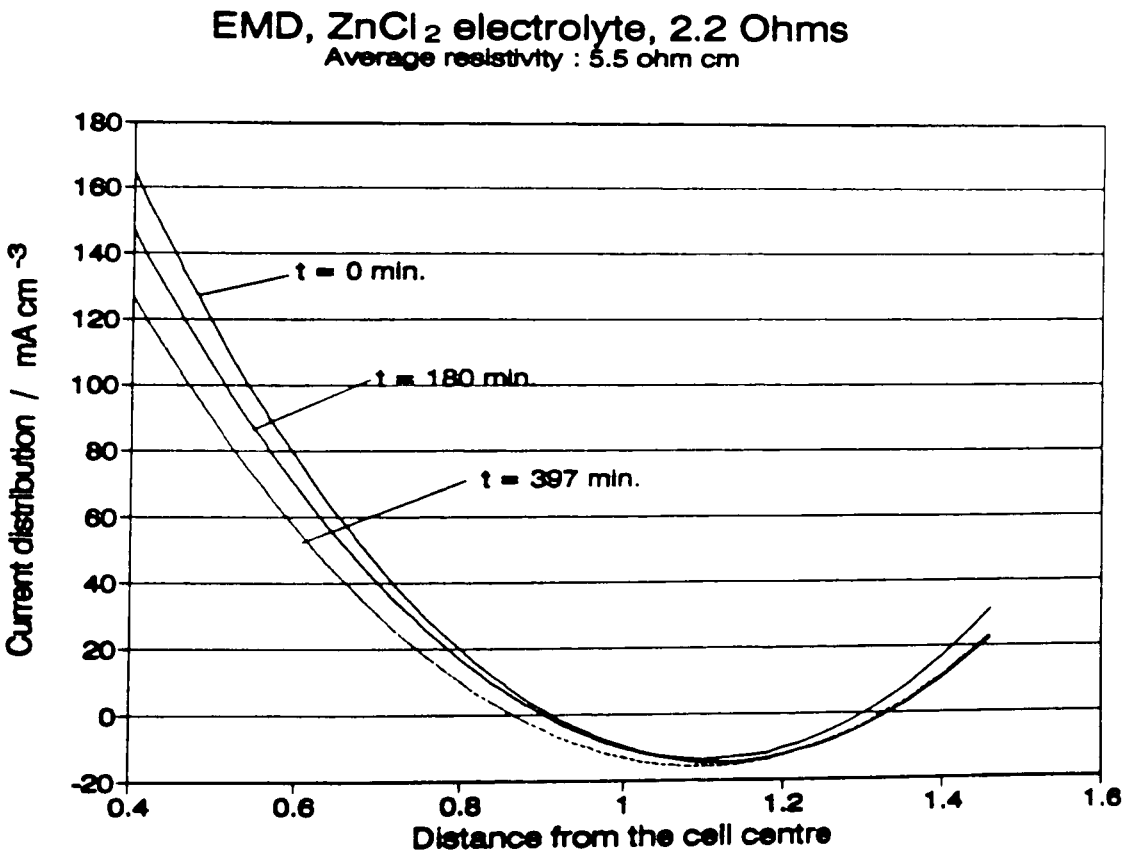

Figure 6.42 : Electrochemical current distribution profiles; EMD in $ZnCl_2$ electrolyte; continuous discharge through 2.2 Ω

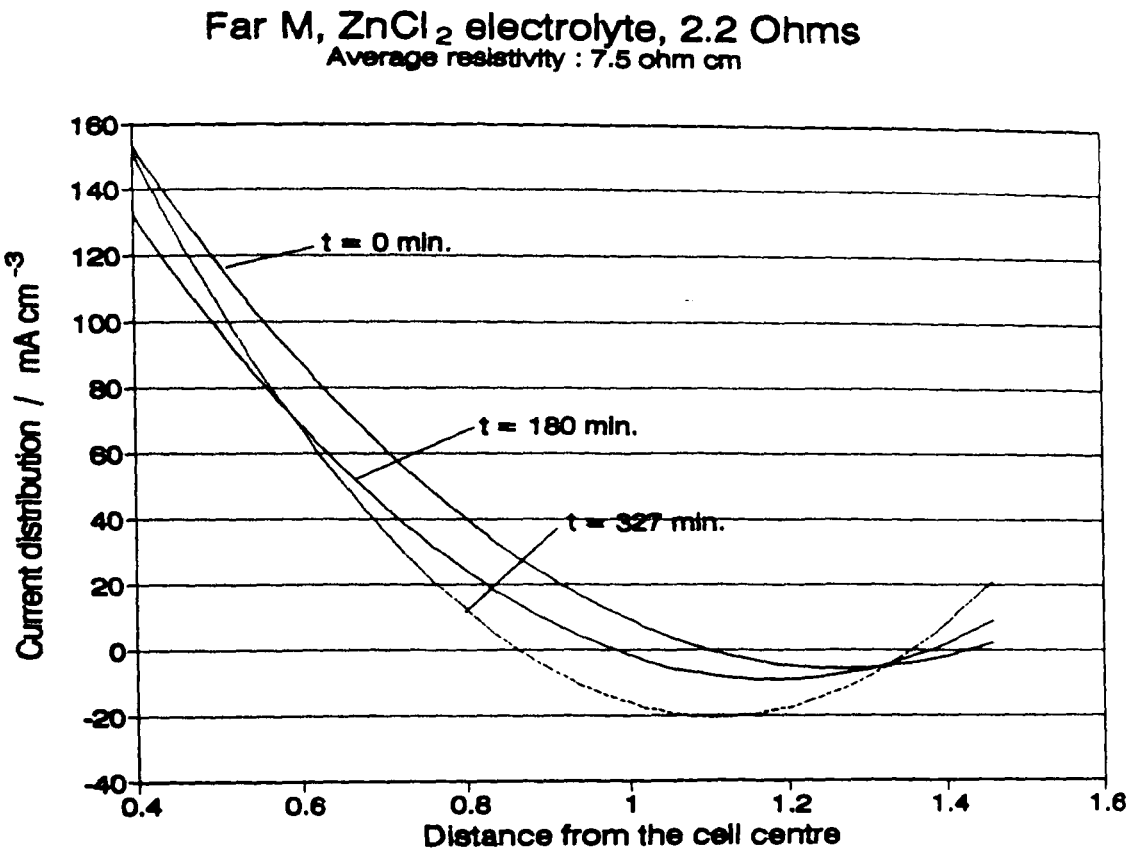

Figure 6.43 : Electrochemical current distribution profiles; Faradiser M in $ZnCl_2$ electrolyte; continuous discharge through 2.2 Ω

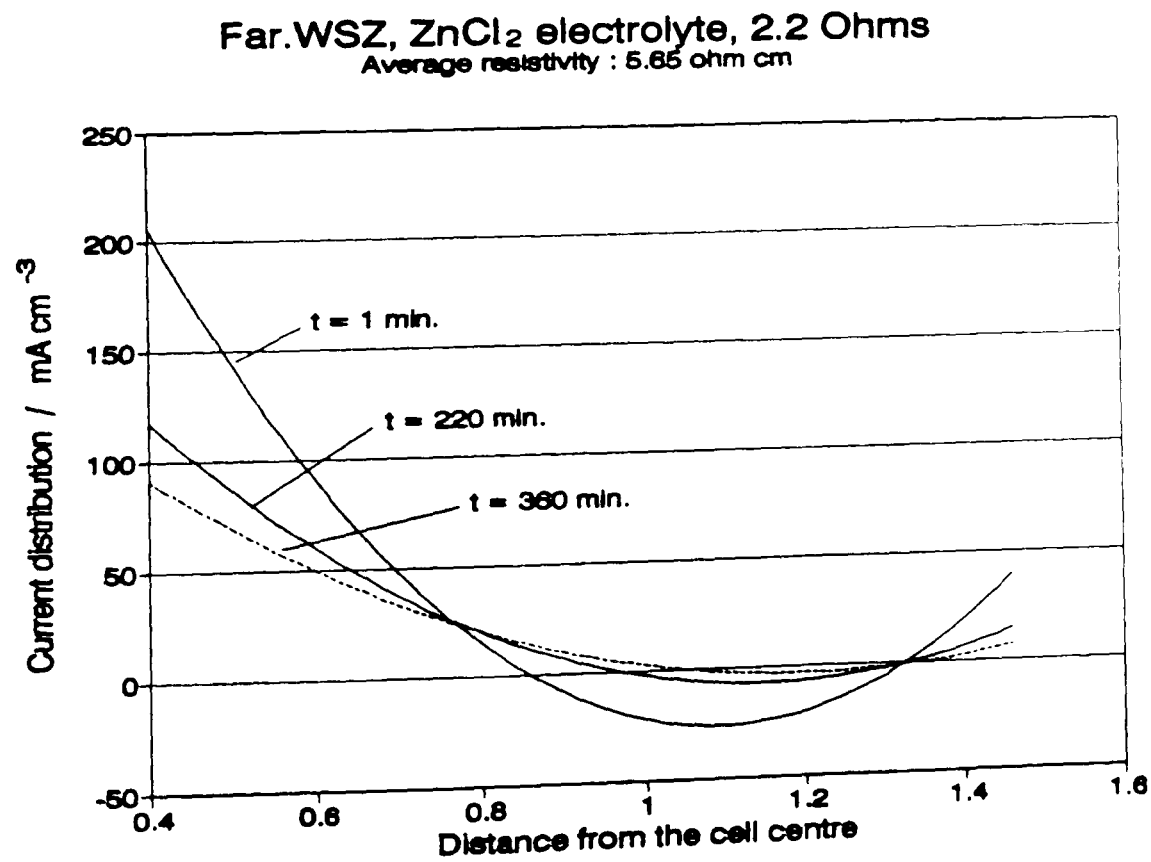

Figure 6.44 : Electrochemical current distribution profiles; Faradiser WSZ in $ZnCl_2$ electrolyte; continuous discharge through 2.2 Ω

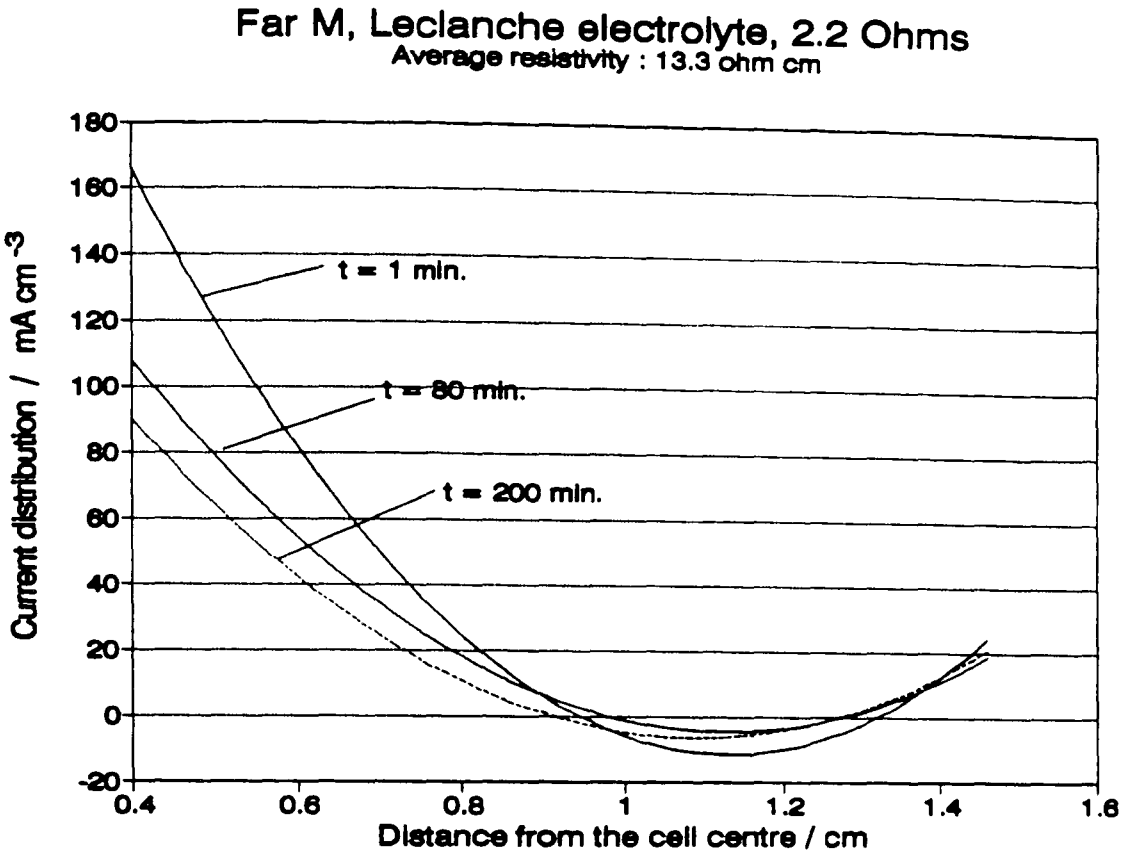

Figure 6.45 : Electrochemical current distribution profiles; Faradiser M in Leclanché electrolyte; continuous discharge through 2.2 Ω

All the cells discharged on 2.2 Ω exhibited the highest reduction rate (electrochemical current density) close to the current collector. This position of the maximum suggests that the resistivity of the solid phase was higher than the resistivity of the electrolyte phase, both in $ZnCl_2$ and in mixed Leclanché electrolyte.

The maximum of the current distribution in the middle of the electrode thickness calculated for the 4 Ω discharges does not fit with any reported model as they all predict one single minimum of the current distribution, at either side of the electrode or in its middle [e.g., 160]. The discrepancy may originate in the disturbance of the electrode structure by the probe insertion [226] or by the large size of the probes compared to the electrode thickness (2.4 mm in a 11 mm thick electrode) making the choice of a distance between the probe and the cell centre somewhat arbitrary. In this work, the distance between the innermost point of the probe and the cell centre has been taken as x (in equation 6.7). The much lower resistivity of the carbon probe material than of the electrode mix (and therefore negligible ohmic potential difference between the different points of the probe)

has guided this choice; any other distance, for example from the probe centre to the current collector, gave inconsistent results. The polynomial form of the current distribution equation (equation 6.3) may also be disputed although such an equation must provide a good approximation of the profile over the small range of distances encountered within the electrode (electrode radius/current collector radius < 4). The validity of the assumptions used in the derivation of the models based on the laws of mass transport in the electrolyte may also be questioned for such a complex system and therefore the applicability of these results to the Leclanché positive electrode may be unreliable.

Apart from the current density profiles, the electrode model also gives the resistivity of the cathode mix.

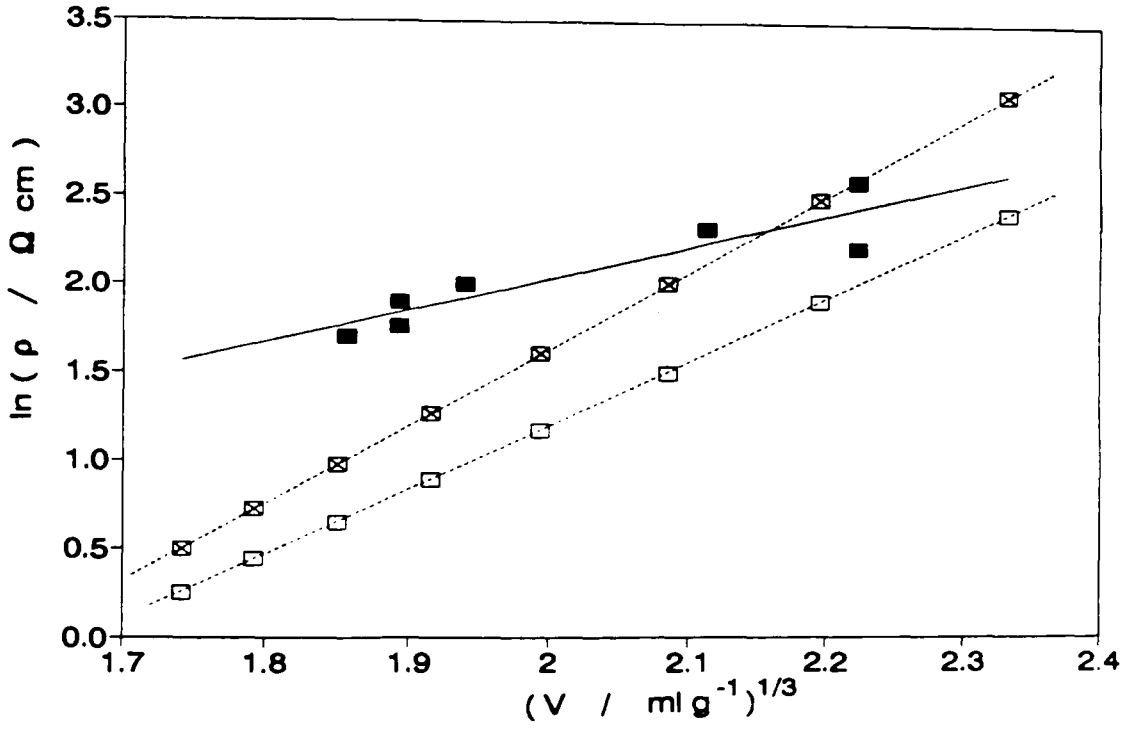

Figure 6.46 : ■ calculated mix conductivity; Caudle *et al.* data (□, fig.4; ⊠ fig.5 [227]); ---- best equation (6.11); V is the volume containing 1 g of carbon black.

The results of the calculations are shown in figure (6.43) as a function of the acetylene black content of the cell (from tables 2.1 and 2.2). As all the cells were made with the same positive electrode volume (31.7 cm^3), this content is proportional to the volume fraction of carbon black in the mix. No report of the electronic conductivity of the wet electrode mix has been found and therefore the

results are compared with the values given by Caudle *et al.* [227] for two different carbon blacks mixed with manganese dioxide (dry mixes). They found that the resistivity (ρ) of the dry mix was related to the volume of mix containing one gram of carbon black (V) by an equation of the form

$$\ln \rho = a + b V^{\frac{1}{3}} \tag{6.10}$$

where a and b are two constants depending on the carbon black origin, ρ is in Ω cm and V in $cm^3\ g^{-1}$. The least square line drawn in figure (6.46) corresponds to the equation

$$\ln \rho = -1.6 + 1.816 V^{\frac{1}{3}} \tag{6.11}$$

The calculated mix resistivities are in good agreement with the data of Caudle *et al.* [227] at low carbon content (large V) but become significantly higher as the carbon content increases. The different slope of the resistivity-carbon concentration relationship for dry and wet mixes may be explained by the partial destruction of the acetylene black structure that occurred during the preparation of the electrode mass [228].

6.8. Conclusions

6.8.1 Discharges in Leclanché electrolyte

The performance of cells with Faradiser M in the Leclanché electrolyte on the 4 ohm continuous discharge test was lower than those with EMD when expressed in terms of duration to 0.9 V on closed circuit or in terms of the coulombs delivered by the cell down to this cut-off voltage. The average performances were equivalent when expressed as current delivered per unit mass of manganese dioxide. The voltage, after a given time on load, of the cell containing Faradiser M was lower throughout the discharge than the voltage of the cell with EMD. This was due to a lower positive electrode potential for the former material than for the latter. Although the final reduction levels and the electrolyte pH were similar for both cells, the electrode potential of Faradiser M after recovery was

also significantly lower than the electrode potential of EMD, due, at a given reduction degree, to a lower MnO_2 potential. The concentration overpotential of the manganese dioxides were very similar for both materials, suggesting that the products of the electrochemically active surface area and the proton/electron diffusion coefficient were similar for CMD and EMD.

The very steep increase of the zinc electrode overpotential during the first hour on test reveals that the decrease of the NH_4Cl concentration and the accumulation of the zinc ions at the electrode, reported by Agopsowicz *et al.* in a study of the simulated separator region [80], also occur in actual cells. The regular decrease, down to a practically constant small value, of the zinc electrode charge transfer overpotential at the beginning of the discharge and the change of the rate of increase of the concentration overpotential which occurred when the activation overpotential became constant, show, for the first time in actual cells, the effect of the moving boundary phenomenon reported by Agopsowicz *et al.* [80].

The internal resistance of the cells with EMD increased at an almost constant rate throughout the discharge. This showed that no significant blockage of the separator occurred during the test. The internal resistance of the cells with Faradiser M also increased during the discharge, but its rate increased after about 5 to 6 hours, indicating some clogging of the separator porosity.

Towards the end of the test, a large diffusion potential built-up across the separator region and was responsible for a voltage loss of about 0.1 V by the end of the discharge. This phenomenon is a new finding. It caused the fast decay of the closed circuit voltage of the cell that was observed at the end of the discharge.

6.8.2 Discharges in zinc chloride electrolyte

For the cells made with the same apparent wetness of the positive electrode mix, the performance on the 2.2 Ω continuous discharge test was better for EMD than for the CMDs, both in terms of discharge duration down to 0.9 V CCV and

in terms of coulombs delivered by the cells. Cells with EMD lasted longer than cells with Faradiser WSZ (+5 %) but both materials showed the same specific capacity (about 0.44 F mol^{-1} or about 465 C g^{-1}). The specific capacity of Faradiser M was lower than the other two with about 0.43 F mol^{-1} or 450 C g^{-1}. The addition of one milli-litre of extra electrolyte into the cells with Faradiser WSZ increased their performance which became the best, both in terms of duration (+6 % compared with EMD) and specific performance (12 % more than EMD).

The zinc electrode activation overpotential did not exhibit the same high values at the beginning of the discharges in $ZnCl_2$ than in Leclanché electrolyte in agreement with the findings of Baugh and White [61] concerning the effect of NH_4Cl on the charge transfer overpotential. The increase of this overpotential towards the end of the discharge, also observed in the Leclanché electrolyte, is not understood. It seemed to be related to the zinc chloride concentration at the electrode surface, the higher the concentration (and thus the temporary equilibrium potential), the higher was the charge transfer overpotential.

The zinc chloride concentrations at the negative electrode surface, calculated from the measured temporary equilibrium potential, showed a fair agreement with the equation derived by Dewhurst [65] for constant current electrolysis between about 5 and 60 minutes on load. This confirms, in actual cells, the results obtained by Agopsowicz *et al.* [80] in a simulated separator region.

The potential of the manganese dioxide electrodes versus SCE after one week of recovery when corrected for the pH differences were very similar for all the materials, in contrast to the observation in Leclanché electrolyte where the potential of EMD was higher than the potential of Faradiser M.
The on-load MnO_2 electrode potentials against a reference electrode connected to the electrolyte inside the electrode mass, were very similar for Faradiser WSZ and EMD, and slightly lower for Faradiser M than for the other two materials, the difference being much less than were found in Leclanché electrolyte.

The most significant difference between the different formulations was found in the voltage loss in the separator region. This voltage loss increased in the order EMD < Far WSZ < Far M and by the end of the discharge, it was responsible for about 20 % of the total polarisation of the cells with Faradiser M. The addition of more electrolyte into the cell decreased significantly the magnitude of this loss and delayed the appearance of its final build-up.

The internal cell resistance increased at a practically constant rate throughout the discharge showing no evidence of separator clogging. The origin of the increase of the voltage loss in the separator region must therefore be related to another phenomenon which is dependent on the amount of electrolyte present into the cell. A possible explanation is as follows. The accumulation of zinc species at the electrode surface dramatically decreased the water activity [25,32] in the negative electrode compartment. The consequent water activity gradient produced a flow of electrolyte from the positive electrode mass to the negative electrode compartment [34] (the excess of electrolyte then moved to the air chamber at the top of the cell, see figure 2.3). The rapid change of the voltage loss across the separator suggests a change in the electrolyte flow rate from the cathode to the anode, probably caused by the drying of the cathode mass. The delayed build-up of the voltage loss on addition of extra electrolyte supports this interpretation. Due to the high dependence of the zinc electrode potential on the water activity (see section 3.3), the reduction of the water input in the negative electrode compartment caused a rapid increase of the electrode potential and of the zinc activity difference across the separator. For Faradiser M in Leclanché electrolyte, the situation was worsened by some clogging of the separator porosity.

6.8.3 Reduction rate distribution in the positive electrode

A pseudo-homogeneous model of the positive electrode has been derived by application of Ohm's Law to the solid phase electronic resistivity using a presumed electrochemical current (reduction rate) distribution function. This model does not make use of any of the assumptions concerning the mass transport or the electrode overpotential usually required by the electrolyte-based models

previously proposed. The use of a presumed electrochemical current distribution function in order to derive the potential distribution equations is an original way of tackling the problem.

The calculated electrochemical current distribution revealed the very non-uniform reduction rate of the different parts of the positive electrode with either a maximum of the reaction rate about mid-way between the current collector and the edge of the electrode (on 4 Ω continuous discharges) or close to the current collector (on 2.2 Ω continuous drain). The maximum electrochemical current density close to the current collector showed that the solid phase resistivity was higher than the electrolyte phase resistivity. The finding of a maximum of the reaction rate in the middle of the electrode thickness cannot be explained by the previously proposed models of porous electrodes. Although this casts some doubts on the validity of the present model, the applicability of the previously proposed models to the very complicated Leclanché system may also be questioned.

The agreement between the calculated electronic conductivity of the electrode mass and the data available for the dry mix was very good when the carbon content of the cell was low, but there was some discrepancy with higher acetylene black contents. The dependence of the electronic resistivity on the electronic conductor concentration seemed to follow the same relationship as for the dry mixes but with a lower decrease of the resistivity on increasing the carbon black content. This difference may be explained by a destruction of the acetylene black chain structure caused by wet mixing of the electrode constituents.

Investigations of the rate of reduction in actual cells [78,155] by analysis of electrode layers after a discharge gave time averaged reduction rates, while the electronic probe technique used in this work gave electrochemical current density profiles at different stages of the discharges. The only other studies of the reaction rate distribution in actual cells were from Daniel-Bek [153] and Coleman [81] who both used Kirchhoff's law and the dubious assumption of constant electrolyte conductivity.

Chapter 7. Chemical reduction of manganese dioxides.

The objective of this part of the study was to investigate the potential-composition relationship of the manganese dioxides in absence of complications (hetaerolite formation, appearance of new phases) which are unavoidable in a battery environment. The materials (EMD, Faradiser M, Faradiser WSZ and MnO_2 TR) have been chemically reduced and their potentials measured with respect to a saturated calomel electrode. MnO_2 TR is an intermediate, before the chemical oxidation stage, in the production of Faradiser M [229].

7.1. Reductions in acetone

The samples were left in contact with acetone for 5 minutes to 4 weeks (see section 2.6.1). Table (7.1) shows the reduction degrees obtained after 1 hour and 2 weeks of contact between the manganese dioxides and acetone.

Table 7.1 : Reduction of MnO_2 by acetone, for 1 hour and for 2 weeks, results given as r in $MnOOH_r$

Sample	Starting material	for 1 hour	for 2 weeks
EMD	0.082	0.172	0.390
Far M	0.104	0.240	0.346
Far WSZ	0.104	0.204	0.388
MnO_2 TR	0.118	0.264	0.338

The degree of reduction achieved during the first hour of contact was very dependent on the material and seems to be related to the specific surface area of the dioxide, the larger the surface area, the greater the reduction. By contrast, the reduction achieved after 2 weeks of reaction was very similar for all the materials.

After filtration, drying and outgassing, the samples had a strong smell of acetic acid suggesting that the reduction occurred by the following reaction

$$8MnO_2 + CH_3COCH_3 + 3H_2O \longrightarrow 8MnOOH + CH_3COOH + CO_2 \qquad (7.1)$$

or, if some formic acid was also formed

$$6MnO_2 + CH_3COCH_3 + 3H_2O \longrightarrow 6MnOOH + CH_3COOH + HCOOH \quad (7.2)$$

In both cases, the reaction required some water. In the conditions of the reaction, the source of water was either the acetone (less than 0.2 % [202] or 0.07 g) or the manganese dioxides (about 5 % of total water or 1.5 g) and the reduction could therefore have been limited by the amount of available water. This hypothesis was tested for Faradiser M by adding 0.5, 1 and 1.5 ml of water to the suspension of MnO_2 in acetone. The results are given in table (7.2) after 2 weeks of reaction.

Table 7.2 : Effect of added water on the reduction of Faradiser M in acetone, results after 2 weeks of contact.

Sample	r in MnOOH
no water added	0.346
0.5 ml added	0.352
1.0 ml added	0.354
1.5 ml added	0.350

Table (7.2) shows that water addition had no effect. Fatiadi [230] mentioned the role of surface hydroxyl groups in the oxidation reaction mechanism and reported that partial deactivation of active (in chemical oxidations) manganese dioxide by acetone has been observed; Fitzpatrick and Tye [200] confirmed the reaction between MnO_2 and acetone and used it to reduce manganese dioxide in non-aqueous medium, however the reason for the limitation of the reduction remains unclear.

Acetone reduced samples were further reduced by a solution of hydrazine hydrate in propan-2-ol, in hexane suspension (see section 2.6.2). Figure (7.1) shows the X-ray powder diffraction pattern of EMD, Faradiser M and Faradiser WSZ reduced to about $MnOOH_{0.98}$ (by acetone and hydrazine hydrate) in the region of the main manganite peak [231]. The low intensity of this peak shows that the samples were devoid of other phases than the solid solution (manganite is the new phase normally produced by heterogeneous reduction). When the reduction by the hydrazine hydrate solution (following the reaction with acetone)

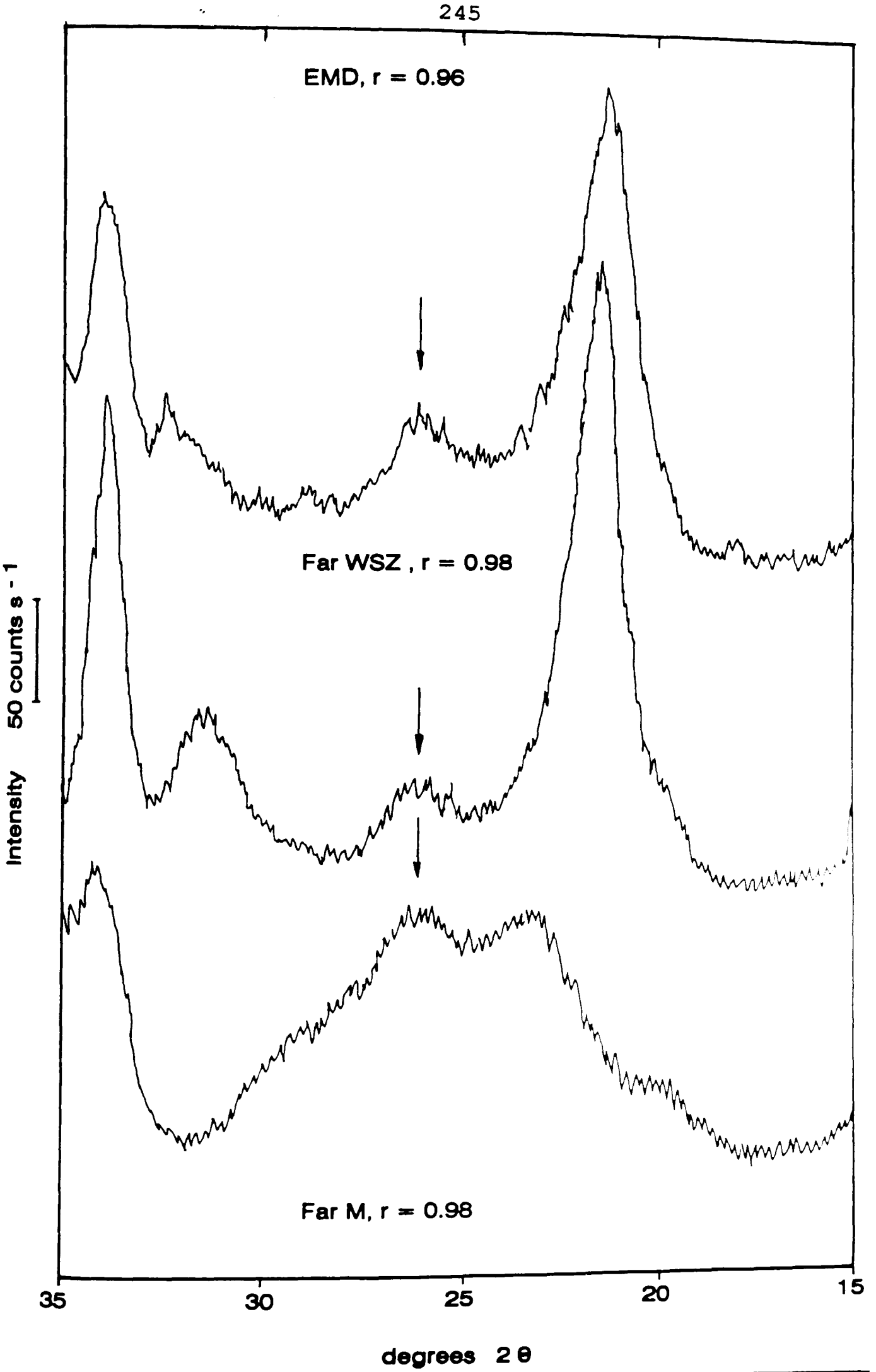

Figure 7.1 : X-ray diffraction pattern of dioxides reduced by acetone and then by $N_2H_4.H_2O$ to about $MnOOH_{0.98}$, the arrows show the main manganite peak position [231]

was carried out at a temperature below 10 °C (ice bath), i.e. in conditions which reduced the solubility of the Mn^{2+}, the main manganite peak was completely absent in the X-ray pattern of the sample, supporting the interpretation given by Fitzpatrick and Tye [200] of the role of Mn^{2+} in the formation of manganite (one sample of each material was reduced by this low temperature procedure).

7.2. Reductions by $N_2H_4.H_2O$ of MnO_2 suspended in Hexane

Table (7.3) shows the results of the addition to the samples of enough hydrazine hydrate solution (see section 2.6.4) to reduce them by 0.02 in r (in $MnOOH_r$). The reaction time was one hour.

Table 7.3 : reduction by $N_2H_4.H_2O$ in hexane suspension, results r in $MnOOH_r$ for expected reduction by 0.02 in r value

Sample	starting material	reduced sample	change
EMD	0.082	0.136	0.054
Far M	0.104	0.218	0.104
Far WSZ	0.104	0.184	0.080
MnO_2 TR	0.118	0.332	0.214

The reduction was significantly larger than calculated from the stoichiometry of the hydrazine hydrate reaction which occurred following the equation

$$4\ MnO_2 + N_2H_4.H_2O \longrightarrow 4MnOOH + N_2 + H_2O \qquad (2.15)$$

The difference increased in the same order (EMD < Far WSZ < Far M < MnO_2 TR) as for the extent of reaction with acetone (see table 7.1) suggesting also an effect related to the specific surface area of the sample.

The hydrazine hydrate was in propan-2-ol solution (see section 2.6). One milli-litre of solution contained about 1.1 10^{-2} mole of propan-2-ol. Assuming that the reaction between MnO_2 and propanol was

$$CH_3\text{-}CHOH\text{-}CH_3 + 2MnO_2 \longrightarrow CH_3\text{-}CO\text{-}CH_3 + 2MnOOH \quad (7.3)$$

the samples (30 g) would have been reduced by 0.067 in r value, i.e. much less than the change observed for MnO_2 TR. Thus this material must also have reacted with the acetone formed by reaction (7.3), e.g. according to equation (7.1) or (7.2) or possibly with the hexane. The latter reaction at room temperature was unexpected as hexane is widely used as solvent in oxidation reactions by MnO_2 [230], but is possible; reaction of manganese dioxide with hydrocarbons has been reported by Fitzpatrick and Tye [200].

Because of the reaction between MnO_2, especially the CMDs, with the organic solvents, the samples with low reduction degrees have been prepared by hydrazine hydrate reduction (in water solution, see section 2.6.3) of samples suspended in water (see section 2.6.3).

7.3. Potential of reduced samples versus SCE

The effect of the equilibration of the reduced samples in the KCl solution is shown in figure (7.2) for Faradiser M reduced to $MnOOH_{0.98}$. The development of the manganite peak is clearly apparent, even after one day into the solution. Some manganite was therefore present on the surface of at least the very reduced samples when the potentials were measured.

Figures (7.3) to (7.6) show the potentials with respect to the saturated calomel electrode, calculated at pH 0 using a correction of 0.0592 V pH^{-1} [13], for EMD, Faradiser M, Faradiser WSZ and MnO_2 TR, respectively. The results are for samples reduced by acetone, and then if needed by hydrazine hydrate (see section 2.6.2), or prepared from the starting material without reaction with acetone (see section 2.6.4). In figure (7.3), the results are compared with the potentials measured in specially made cells by Shaw [118] and tabulated by Tye [83].

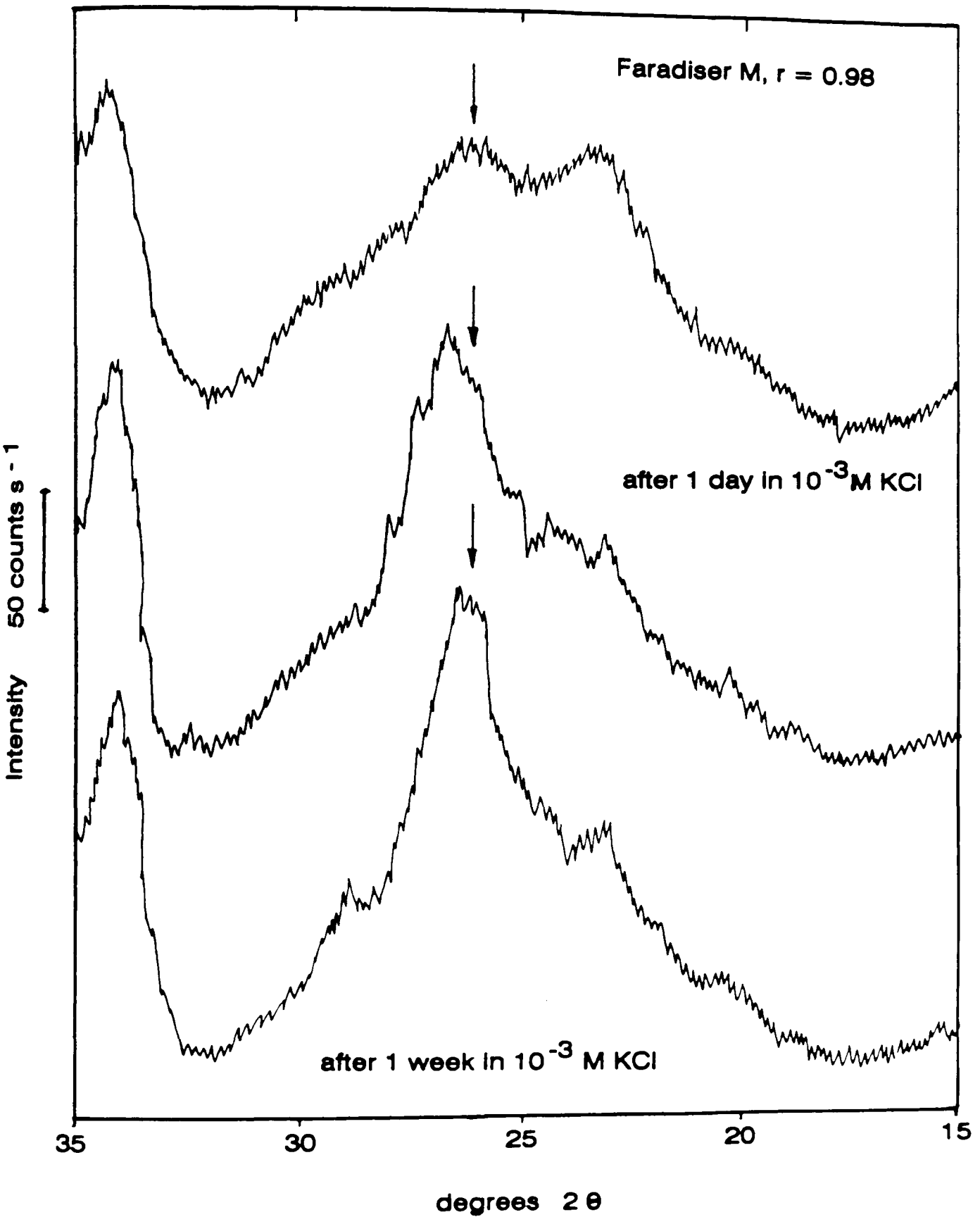

Figure 7.2 : X-ray diffraction pattern of Faradiser M reduced to $MnOOH_{0.98}$ before and after equilibration (1 and 7 days) in 10^{-3} M KCl.

For all the four materials, the spread of the results increased with increasing reduction degree and above the mid-reduction (r=0.5), the results were different for the samples pre-reduced in acetone and those reduced by hydrazine hydrate from the starting material. The samples for which acetone was used gave either

lower (EMD, TR) or higher (Far M, Far WSZ) potentials than the other set of samples.

Figure (7.3) shows that for the acetone reduced samples, the potentials were about 50 mV higher than those measured (on another EMD) by Shaw in Leclanché cells [118] throughout the whole range of reduction. The spread was much larger than for Shaw's results. The reason for the dependence of the manganese dioxide potential on the reduction procedure is not well understood. It shows that acetone and hexane probably affected the surface of manganese dioxide in a different way, possibly through the nature of adsorbed species (acetone reduced samples had a strong smell indicating the presence of some adsorbed acetic acid).

Figures (7.7) and (7.8) show the curves for the pH and the soluble manganese content of the 10^{-3} M KCl solution in which the sample had been equilibrated for 3 days, for EMD reduced with and without the pre-reduction by acetone, respectively. The increase of the solution pH with increasing reduction of the sample may be explained by a decrease in acid strength of the ion-exchangeable protons with increasing reduction of the samples [212] or by the consumption of H^+ by the disproportionation reaction (equation 2.17)

$$MnOOH_r + 2\Delta\ H^+ \rightleftharpoons (1-\Delta)\ MnOOH_{\frac{r-2\Delta}{1-\Delta}} + 2\Delta\ H_2O \qquad (2.17)$$

For low reduction levels, the pH corresponding to the samples reduced in water suspension was significantly higher than the pH corresponding to samples with similar oxidation degree but reduced in hexane suspension. The soluble manganese was also significantly lower for the former samples than for the latter. This was probably also due to a poorly understood surface effect caused by the reduction method.

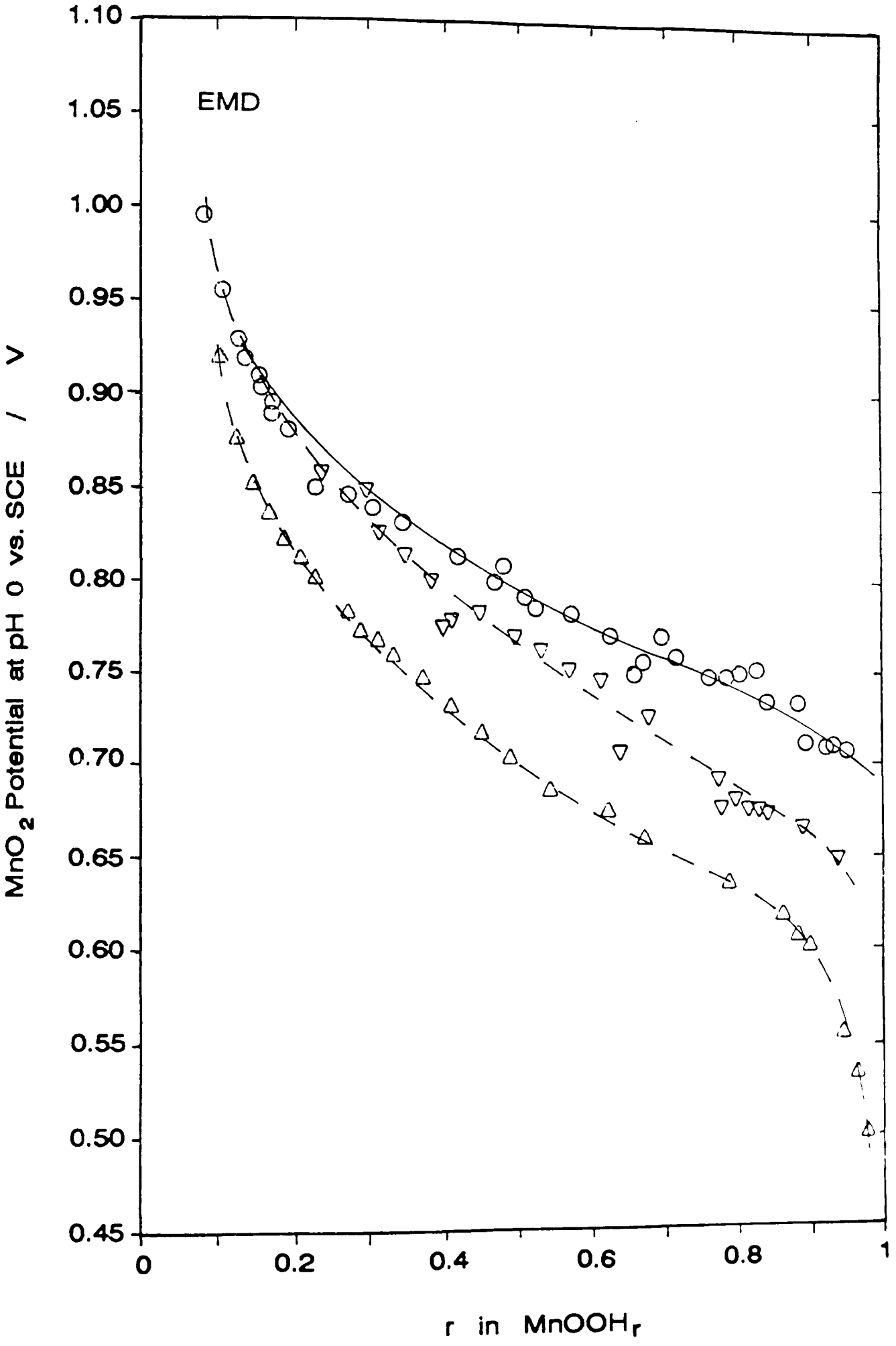

Figure 7.3 : Potential (vs. SCE) of EMD reduced by $N_2H_4.H_2O$; ▽ samples pre-reduced by acetone, ○ reduced from the starting material; △ results from ref. [83]

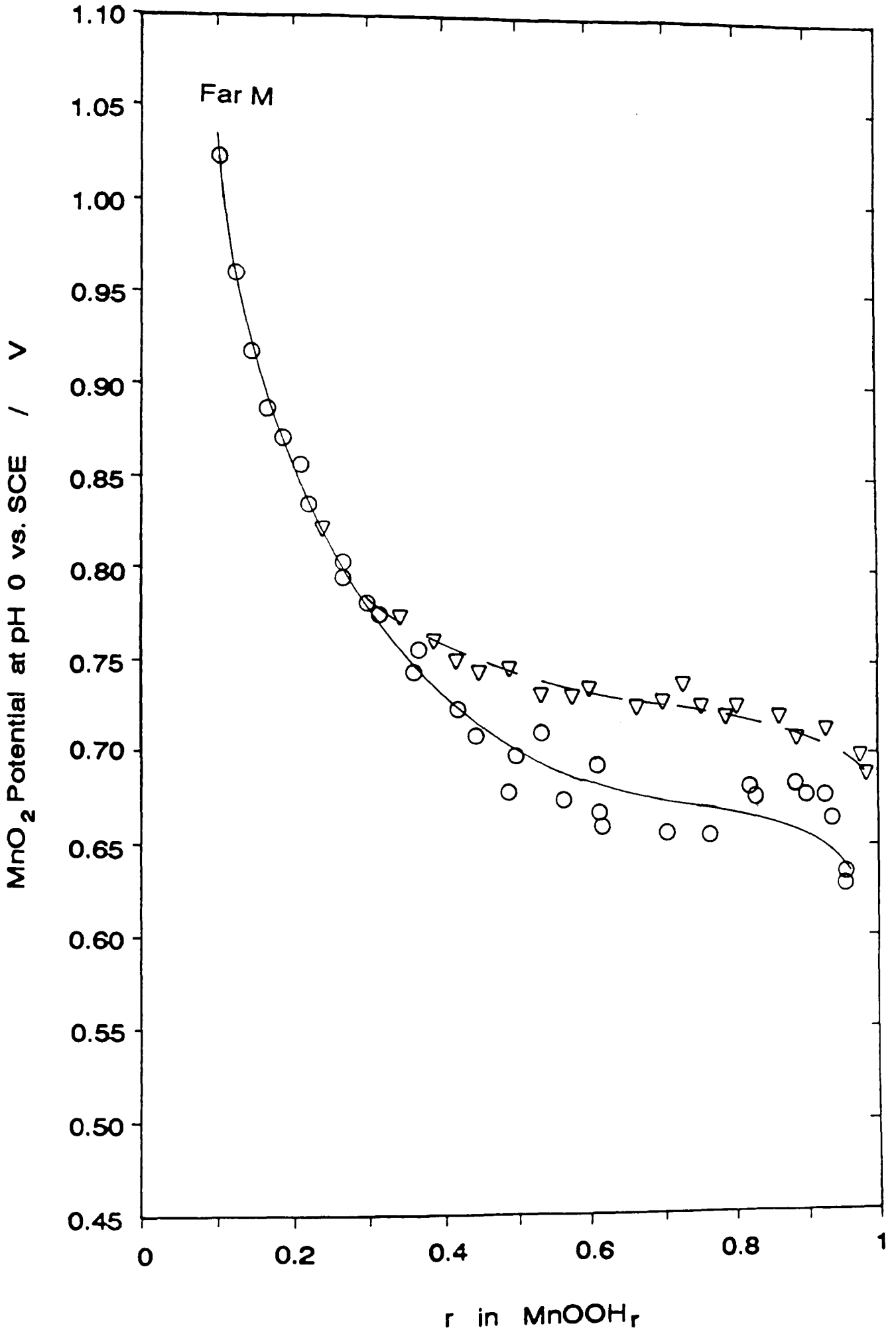

Figure 7.4 : Potential of Faradiser M (vs SCE) reduced by $N_2H_4.H_2O$; ▽ samples pre-reduced by acetone, ○ reduced from the starting material

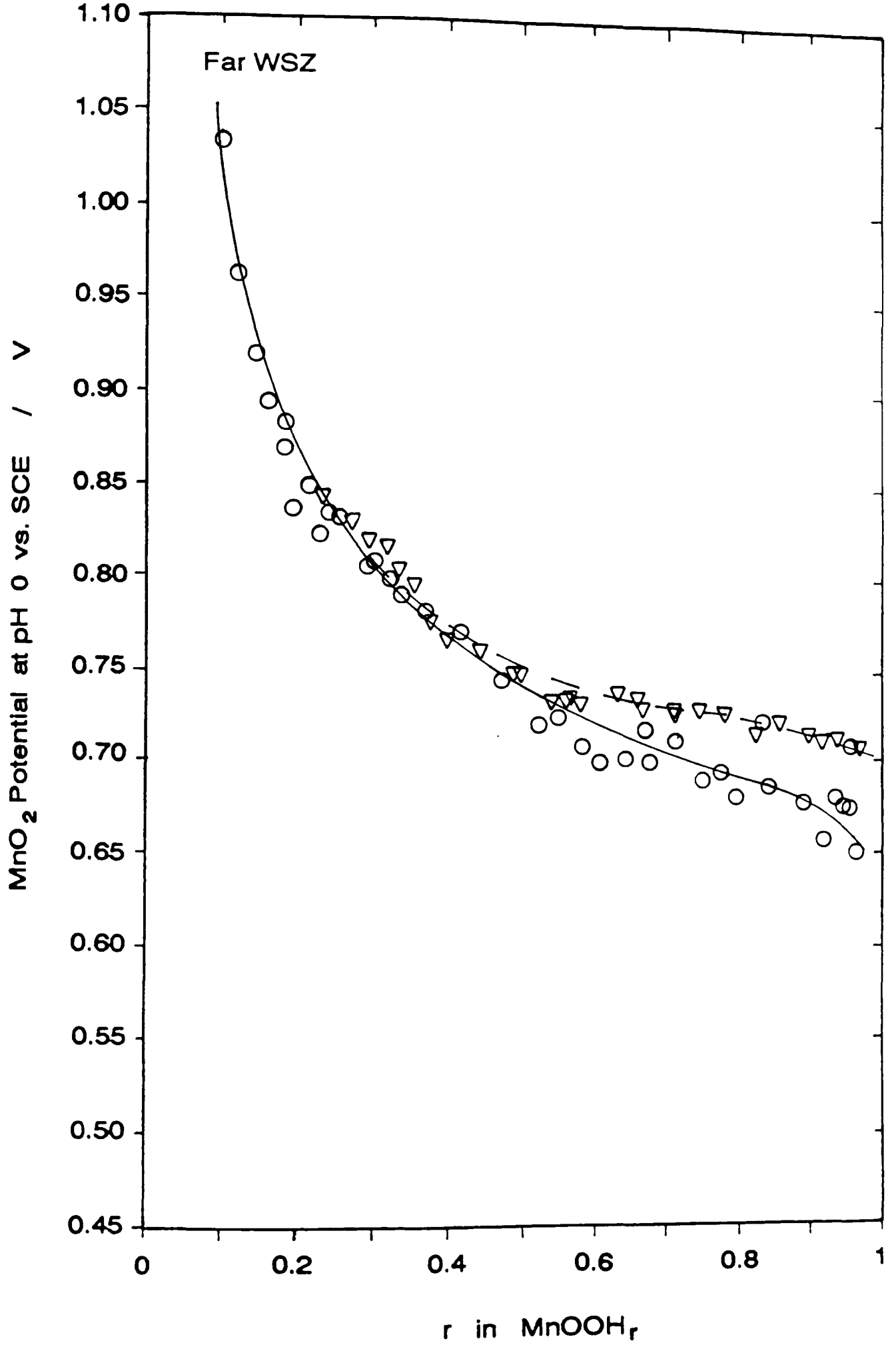

Figure 7.5 : Potential (vs SCE) of Faradiser WSZ reduced by $N_2H_4.H_2O$; ▽ samples pre-reduced by acetone, ○ reduced from the starting material

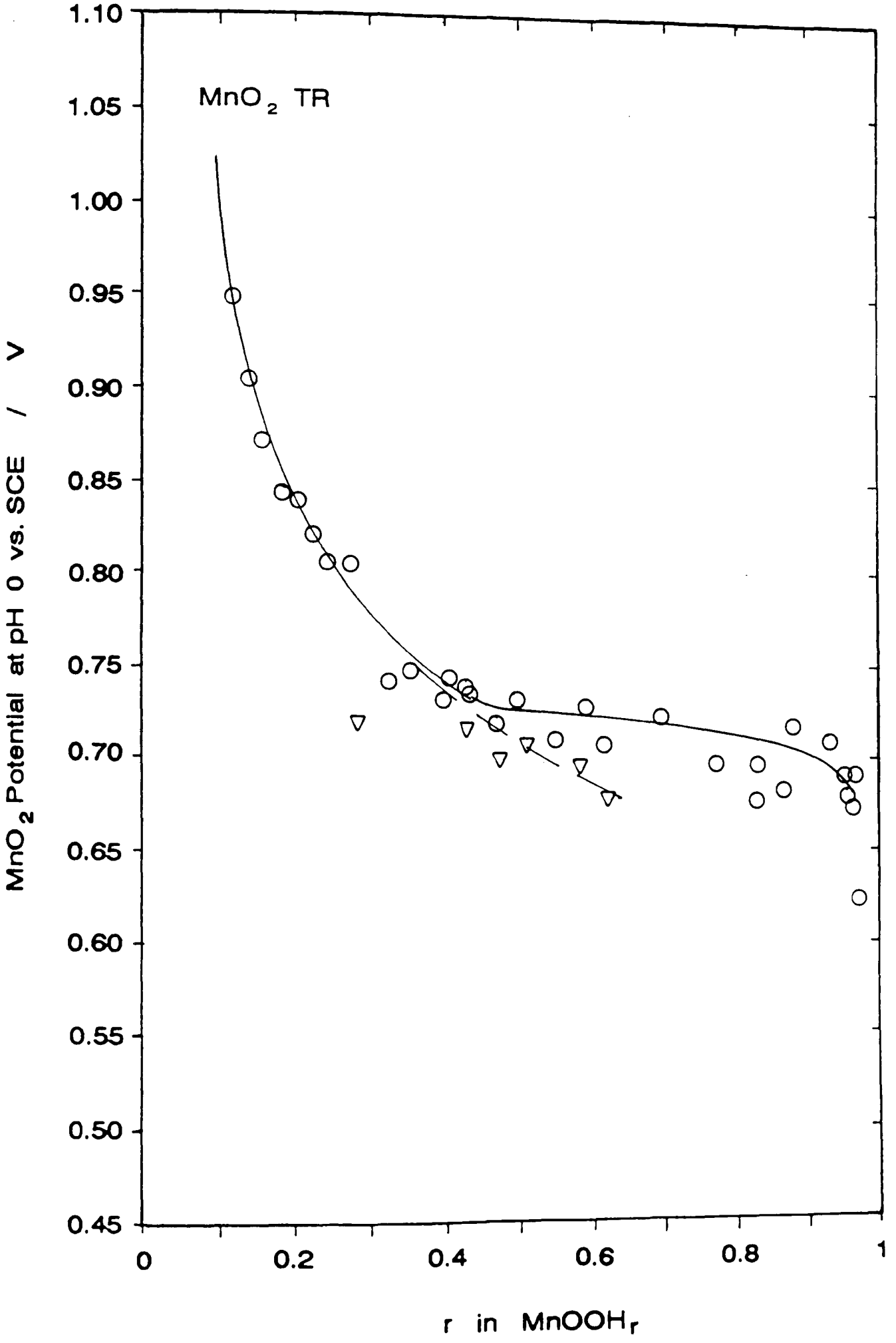

Figure 7.6 : Potential (vs SCE) of MnO_2 TR reduced by $N_2H_4.H_2O$; ▽ samples pre-reduced by acetone, ○ reduced from the starting material

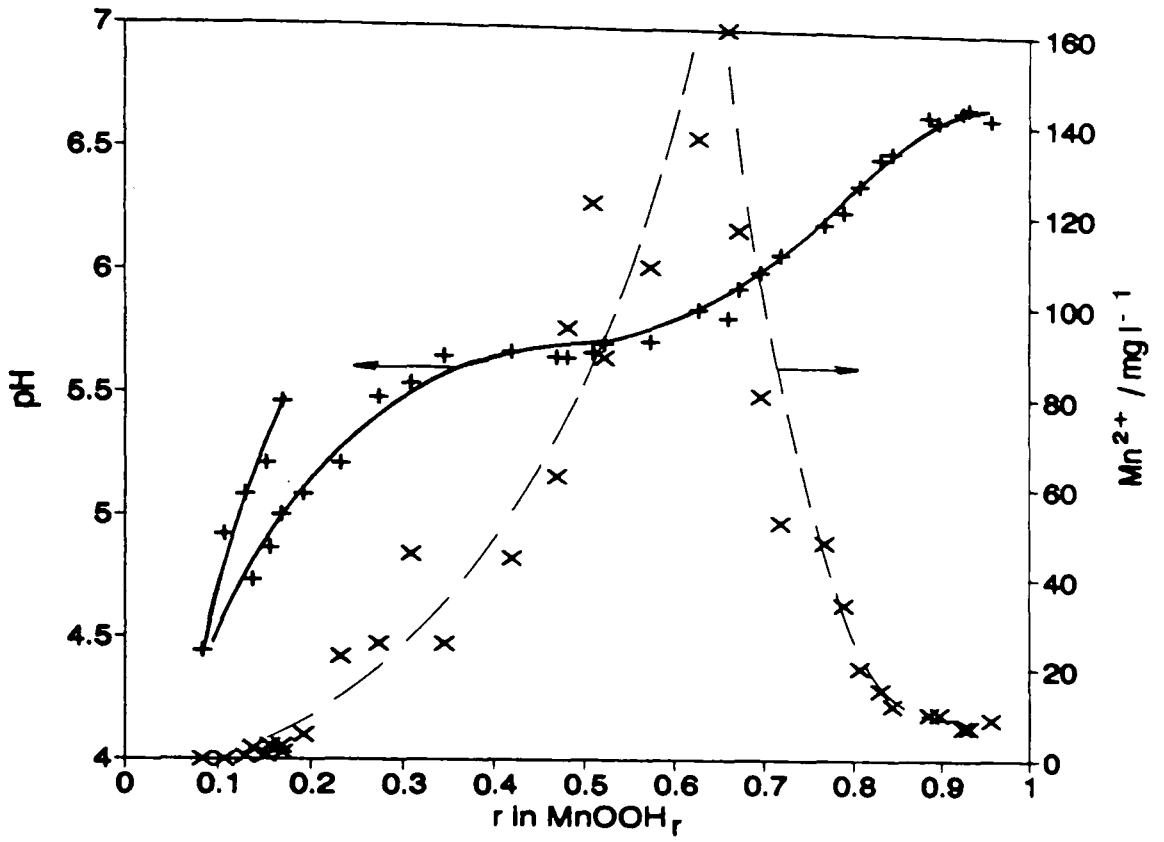

Figure 7.7 : + pH and × soluble manganese in the KCl solution after equilibration of EMD samples reduced without acetone pre-reduction.

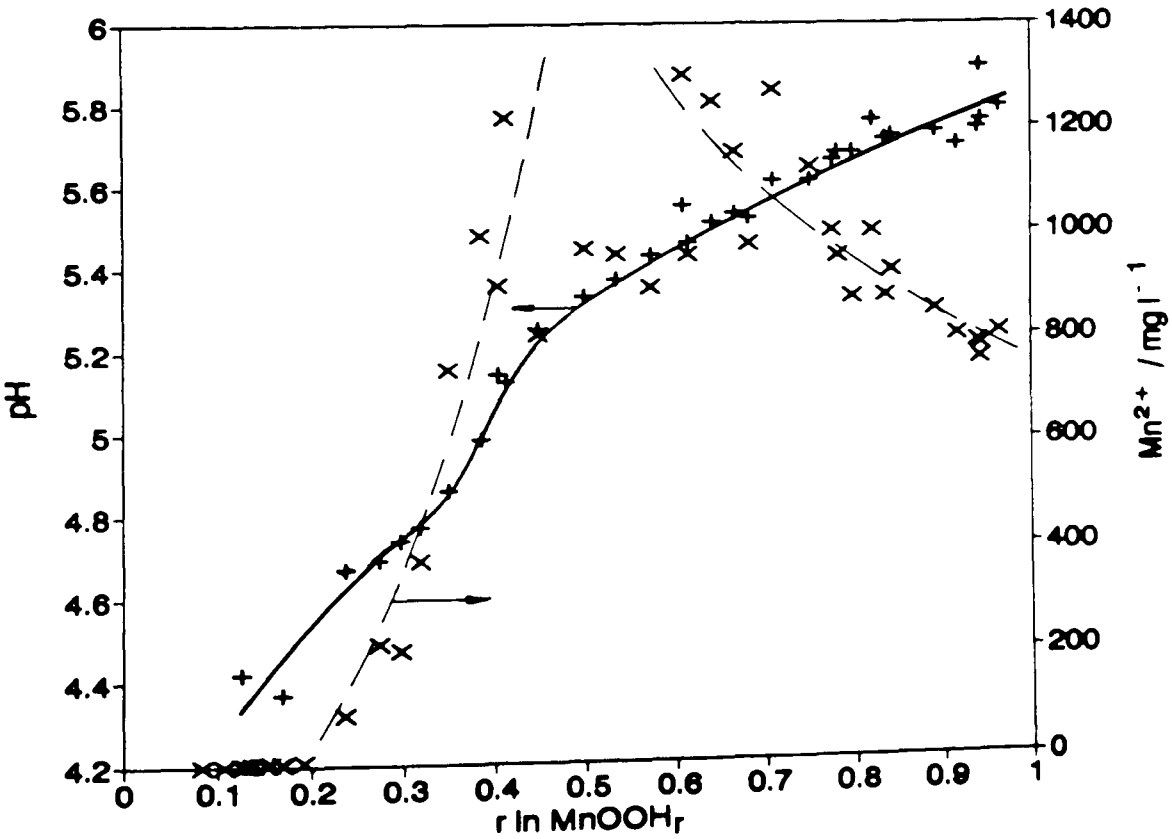

Figure 7.8 : + pH and × soluble manganese in the KCl solution after equilibration with EMD pre-reduced by acetone

The initial increase of the soluble manganese with increasing reduction of the sample shows that the more reduced was the sample, the more it disproportionated, in agreement with the results reported by Shaw [118]. The sharp decrease of the soluble manganese which occurred for all the materials in the second half of the reduction cannot be explained by the same effect but seems to have been related to the pH of the solution. For all the materials, it happened for a solution pH of about 5.5 - 6. The solubility product of manganese hydroxide is 4 10^{-14} [191]. A simple calculation reveals that even at a pH of 7, the manganese solubility is about 200 g l^{-1}, well above the levels measured in the KCl solutions. On the other hand, dissolved oxygen may cause the oxidation of Mn^{2+} into solid MnOOH at pH lower than the $Mn(OH)_2$ precipitation pH [232]. The formation of a brown deposit on the wall of the flasks containing the very reduced samples supports this explanation of fall of the soluble Mn^{2+} concentration. As a consequence of this precipitation, the measured soluble manganese concentration did not represent the total amount of Mn^{2+} formed by the disproportionation of the oxyhydroxide phase and therefore the calculated oxidation degree of the solid phase (equation 2.18) was in error. An important part of the spread in figures (7.3) to (7.6) may be attributed to the uncertainty on the true oxidation stage of the manganese solid solution resulting from the error caused in the correction by MnOOH precipitation. Shaw's results [118] were measured in batteries at constant pH and in the absence of oxygen and were consequently not affected by this phenomenon. For the four materials at high degrees of reduction, the pH of the KCl solution after the sample equilibration was lower for samples reduced in acetone than for the samples reduced without reaction with acetone and consequently, the solution also contained more soluble manganese for the former set of samples than for the latter. The error on the corrected value of the actual oxidation degree of the sample (calculated from the initial sample composition and the measured soluble manganese) was therefore lower for the sets of samples for which acetone was used in the first stage of the reaction. These samples also exhibited smaller manganite peak in their X-ray diffraction diagram. Figures (7.9) to (7.12) show that Faradiser M and Faradiser WSZ behaved similarly to EMD (fig 7.7 and 7.8).

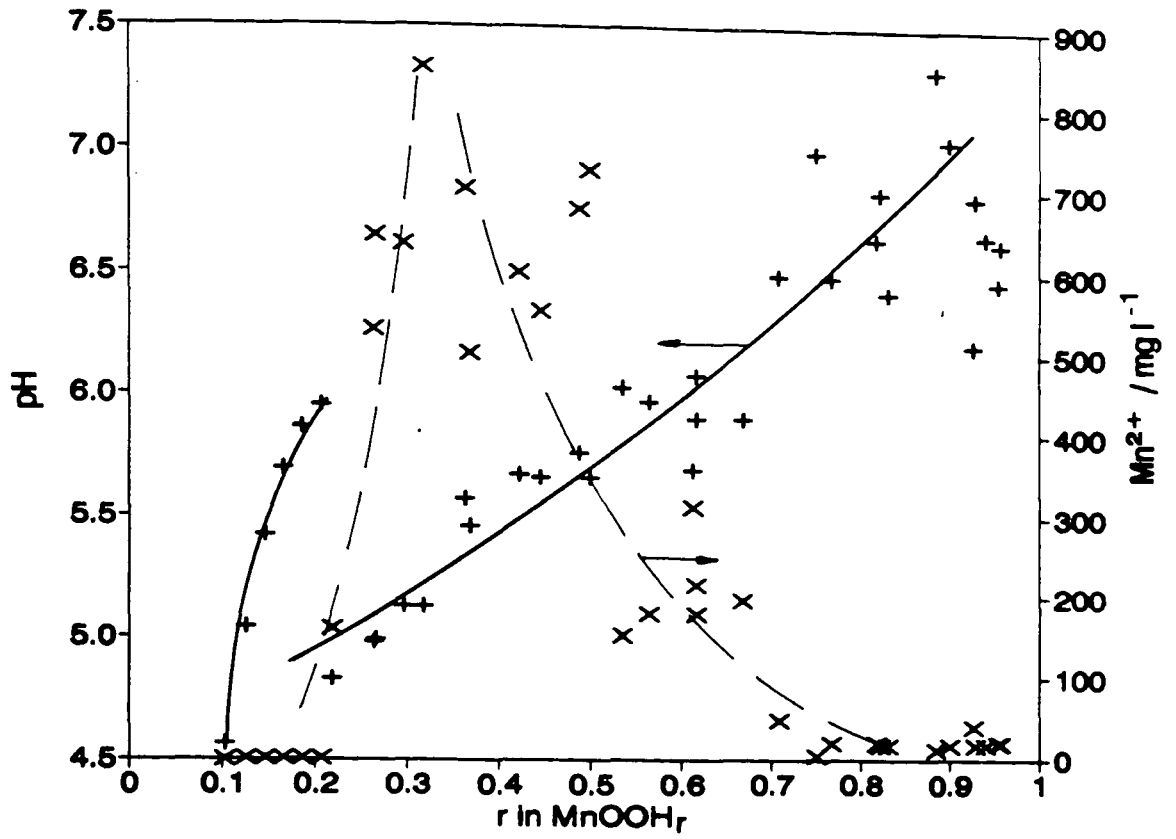

Figure 7.9 : + pH and × soluble manganese in the KCl solution after equilibration of Faradiser M samples reduced without acetone pre-reduction.

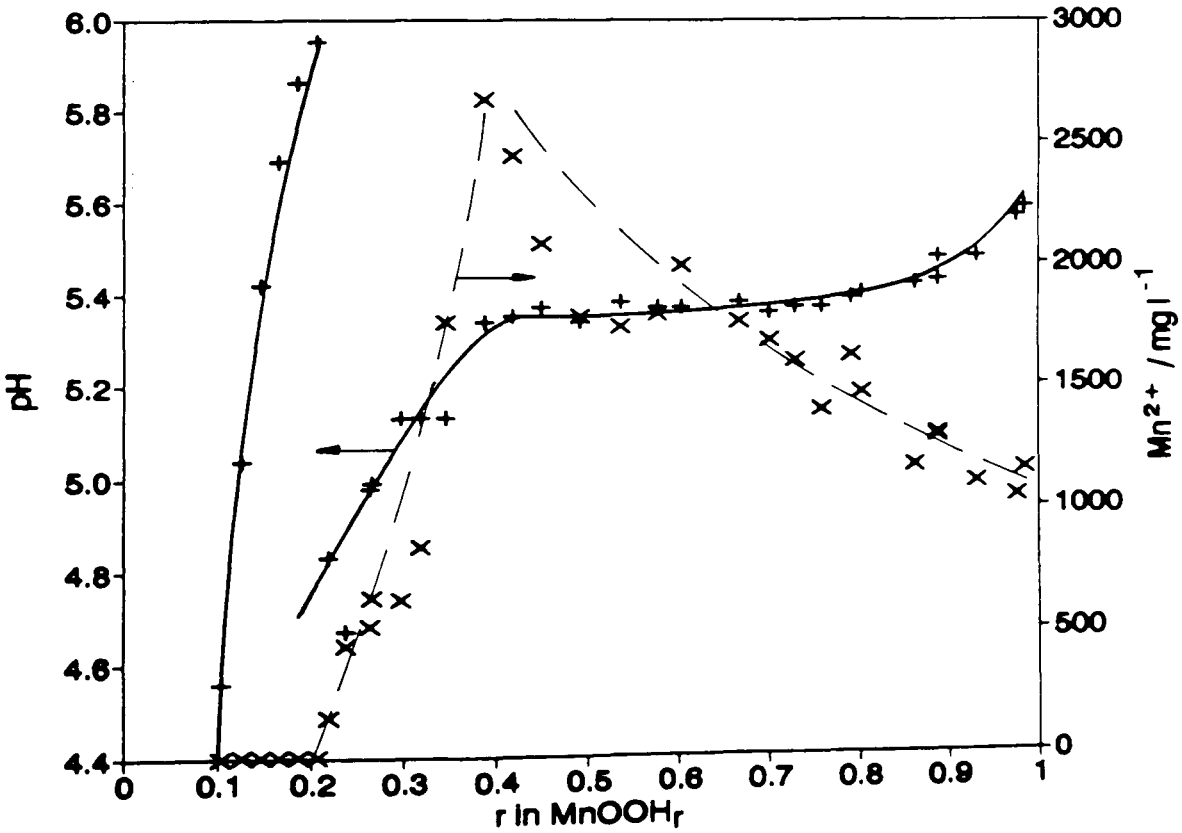

Figure 7.10 : + pH and × soluble manganese in the KCl solution after equilibration with Faradiser M pre-reduced by acetone

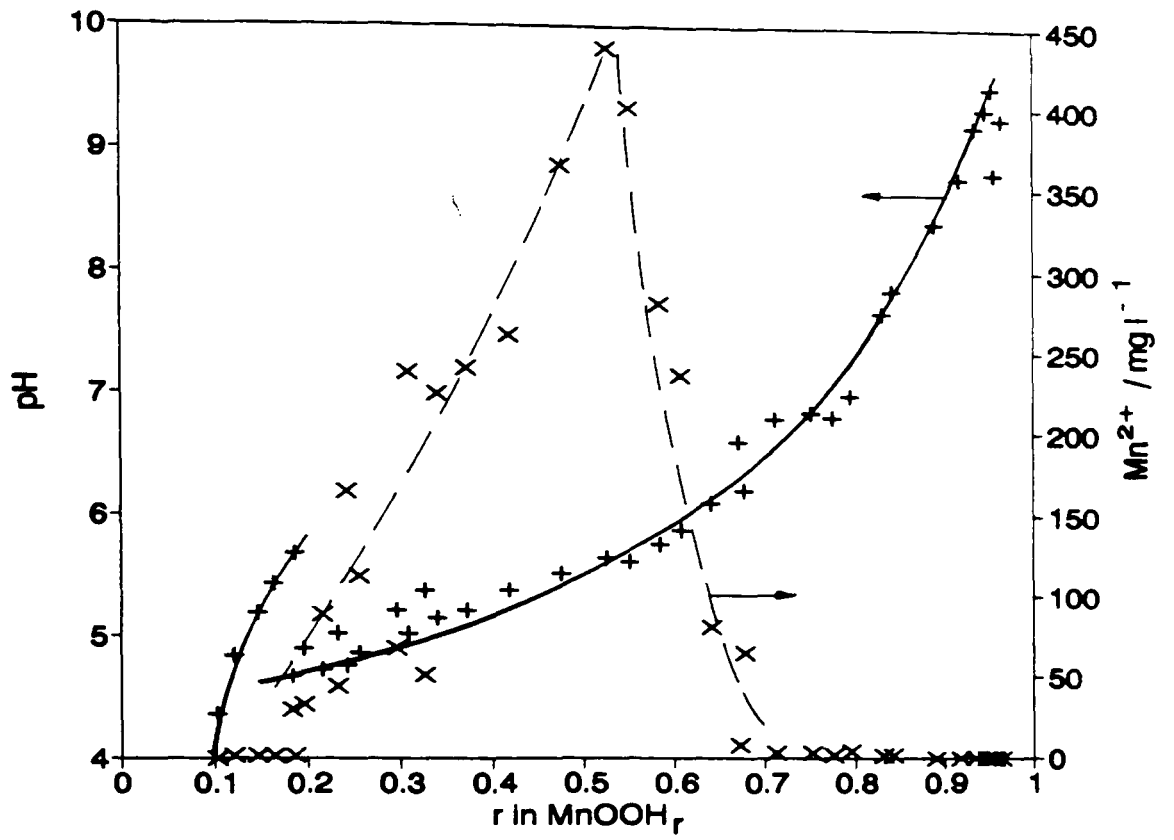

Figure 7.11 : + pH and × soluble manganese in the KCl solution after equilibration of Faradiser WSZ samples reduced without acetone pre-reduction.

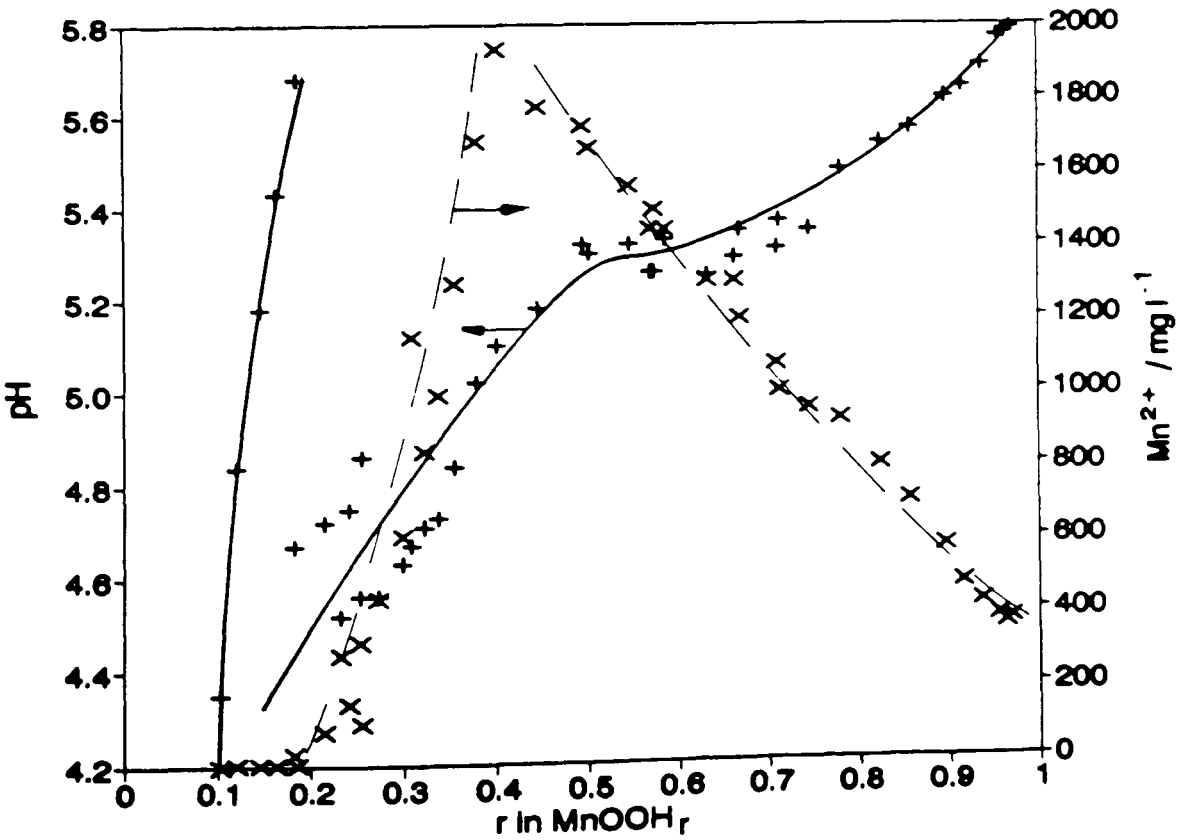

Figure 7.12 : + pH and × soluble manganese in the KCl solution after equilibration with Faradiser WSZ pre-reduced by acetone

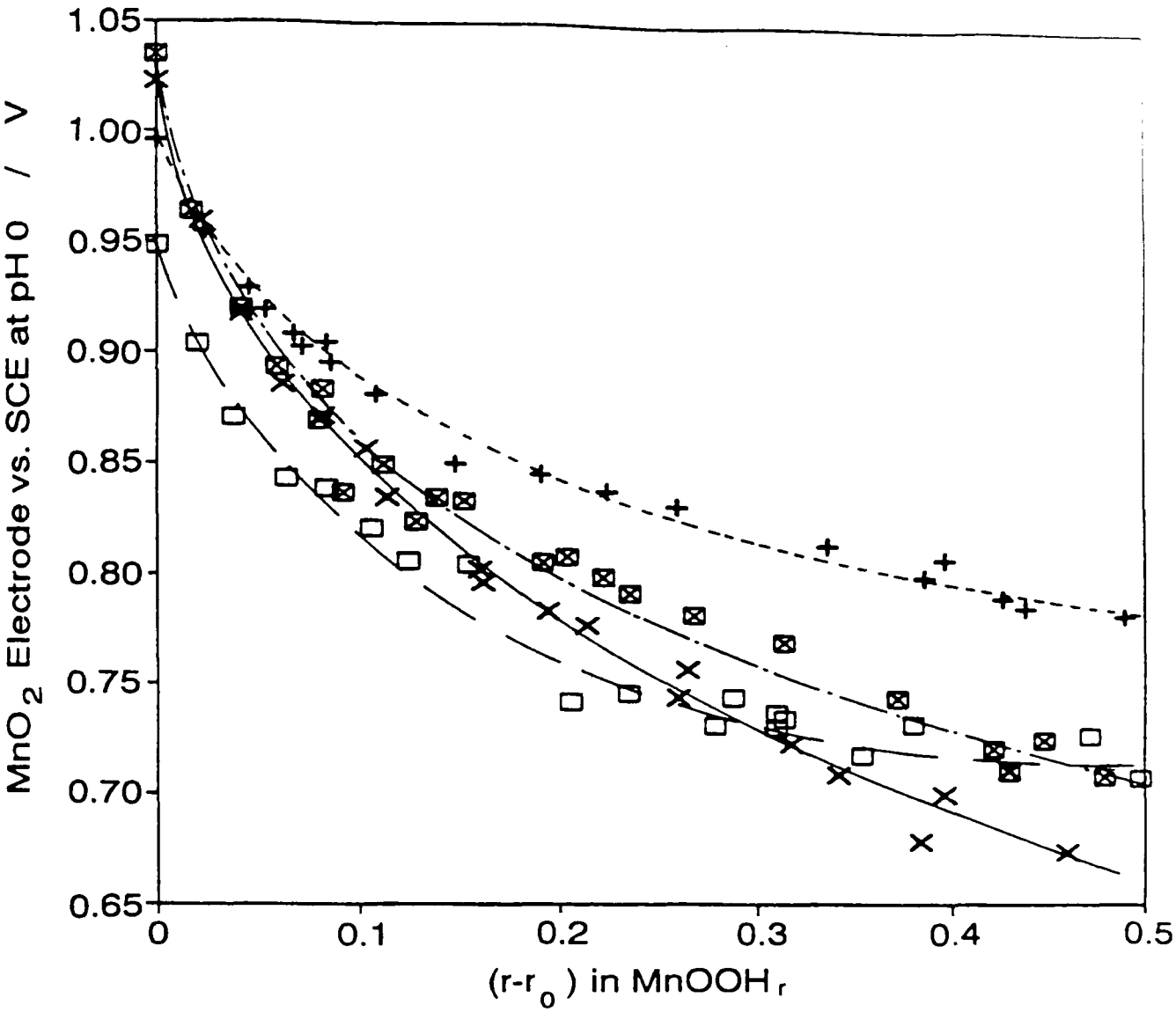

Figure 7.13 : Potential (vs SCE) of reduced samples at pH 0 vs. change of the oxidation degree ($r-r_0$); + EMD, × Faradiser M, ⊠ Faradiser WSZ, □ MnO_2 TR

The true oxidation degree of manganese dioxide after a cell has delivered a given quantity of current (coulombs) is of little interest for the user of a battery who is more concerned by the cell voltage at this stage of the discharge. This has been simulated in figure (7.13) which shows the potential, at pH 0, versus a saturated calomel electrode, of the four materials as a function of the reduction degree expressed in change of r (in $MnOOH_r$). Due to the uncertainty concerning the actual oxidation stage of the very reduced samples (see discussion above), the graph has been limited to the range $0.1 \leq r \leq 0.6$.

Figure (7.13) reveals that the potentials of the un-discharged materials increased in the order

$$MnO_2 \text{ TR} << \text{EMD} < \text{Far M} < \text{Far WSZ}$$

It also shows that the potential of the CMDs decreased faster with reduction than the potential of the EMD. This is in agreement with the observations made during the intermittent discharge tests (see chapter 4). After a reduction to about $MnO_{1.8}$ (0.15 F mol^{-1}), the potential was about 70 mV lower for Faradiser M than for EMD, i.e. the same difference as observed, in Leclanché electrolyte, after continuous discharge and recovery between the two materials (see tables 6.5 and 6.6). The steepest decrease on reduction was exhibited by Faradiser M, with a difference of more than 100 mV compared to EMD, after about 0.5 F mol^{-1}. The curve for MnO_2 TR, although it showed a potential decaying faster on reduction than EMD, is much flatter than the curve for Faradiser M. Faradiser WSZ had a behaviour on reduction intermediate between Faradiser M and MnO_2 TR.

7.4. Potential - composition relationships

The manganese dioxide electrode potential is given by [83]

$$E = E_0 - \frac{2.3RT}{F}pH + \frac{RT}{F}\ln\frac{a_{MnO_2}}{a_{MnOOH}} \qquad (7.4)$$

where E_0 is given by [83]

$$E_0 = \frac{G^0_{MnO_2} - G^0_{MnOOH}}{F} \qquad (7.5)$$

in which G^0 is the free energy of formation of the subscript species, R, T and F have their usual significance.

Johnson and Vosburgh [233] equated the mole fractions of MnO_2 and MnOOH to their activities. Equation (7.4) then becomes [83]

$$E = E_0 - \frac{2.3RT}{F}pH + \frac{RT}{F}\ln\frac{1-r}{r} \qquad (7.6)$$

where r is the H content of the solid solution (r in $MnOOH_r$). Equation (7.6) does not predict a sufficient decrease of the potential with increase in r to match the data obtained for EMD [102].

For the first part of the reduction, Tye [141] considered that the material was a solid solution of $MnOOH_{0.5}$ in the starting material and he derived the equation

$$E = E_0' - \frac{2.3RT}{F}pH + \frac{RT}{F}\ln\frac{(0.5-r')\ (1-r')}{4r'^2} \qquad (7.7)$$

where E_0' corresponds to the formation of $MnOOH_{0.5}$ and r' is defined by

$$r' = \frac{(r-y)}{(1-y)} \qquad (7.8)$$

in which y is the content of inactive Mn(III) in the starting material. For the second half of the reduction, Tye [141] considered a solid solution of MnOOH in the starting material and the potential was expressed by

$$E = E_0 - \frac{2.3RT}{F}pH + 2\frac{RT}{F}\ln\frac{(1-r')}{r'} \qquad (7.9)$$

where r' has the same meaning as in equation (7.7). Equations (7.7) and (7.9) were obtained assuming independent mobilities for the inserted protons and electrons.

Figure (7.14) shows the results obtained for EMD reduced by acetone and then, if necessary by hydrazine hydrate. The fit with equation (7.7) was obtained by assuming $E_0 = 0.845$ V (versus SCE) and the inactive Mn(III), y = 0.068. For the second part of the curve, the fit with equation (7.9) was obtained for the same y as in the first part of the curve and $E_0 = 0.765$ V (versus SCE). Although the spread of the results was rather large, the fit with the equation was very

satisfactory with the exception of the end of the curve where the uncertainty on the actual value of r was maximum.

Figure (7.15) shows a fair agreement between the experimental results (for Faradiser M and acetone reduction) and equation (7.7) for the first part of the reduction (E_0 = 0.80 V vs. SCE, y = 0.100). By contrast with the data in figure (7.14), the measured potentials did not match equation (7.9) at all, the smaller slope suggesting that equation (7.6) would probably apply better. Equation (7.6) was therefore modified to incorporate the inactive Mn(III) and became

$$E = E_0 - \frac{2.3RT}{F}pH + \frac{RT}{F}\ln\frac{(1-r')}{r'} \qquad (7.10)$$

where r' is also given by equation (7.8). Equation (7.10) only differs from equation (7.9) by the coefficient of the logarithm term which reflects the influence of independent (in eq. 7.9) or dependent (in eq. 7.10) mobility of the inserted H^+/e on the electrode potential.

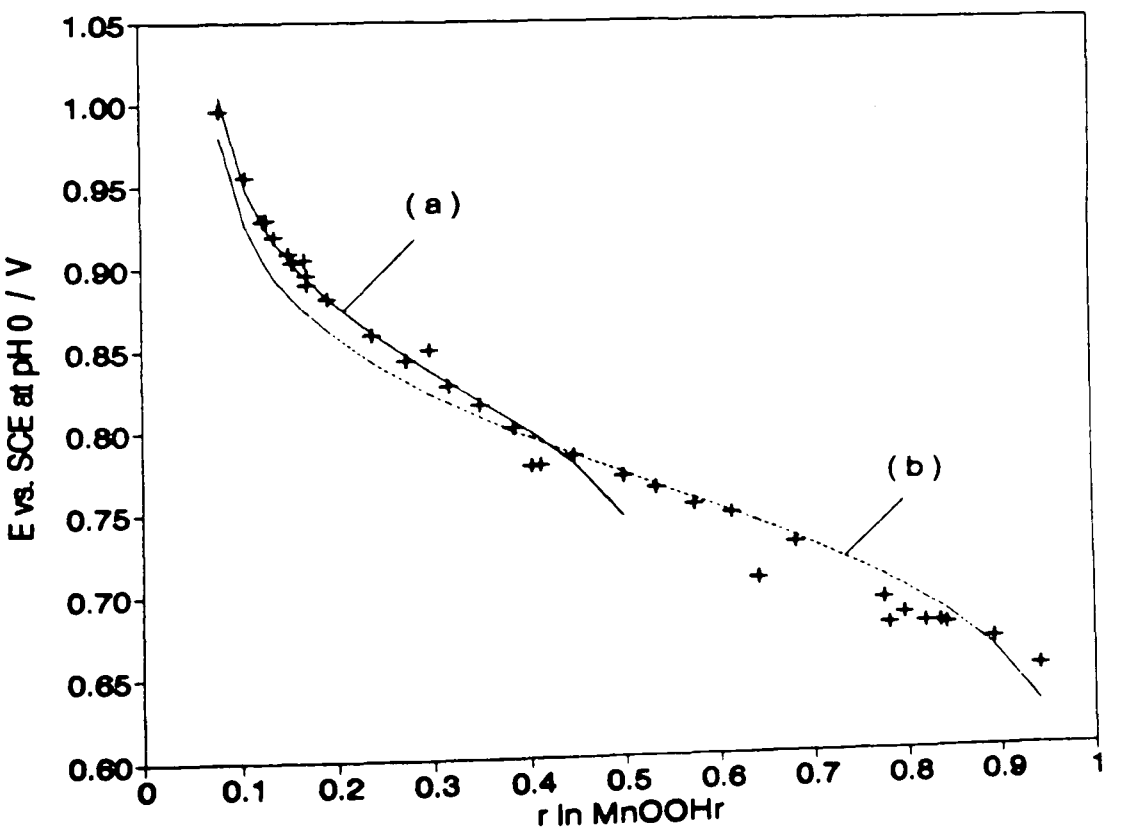

Figure 7.14 : Potential of reduced EMD with acetone pre-reduction; (a) equation 7.7 with E_0'=0.845 V and y=0.068, (b) equation 7.9 with E_0=0.765 V

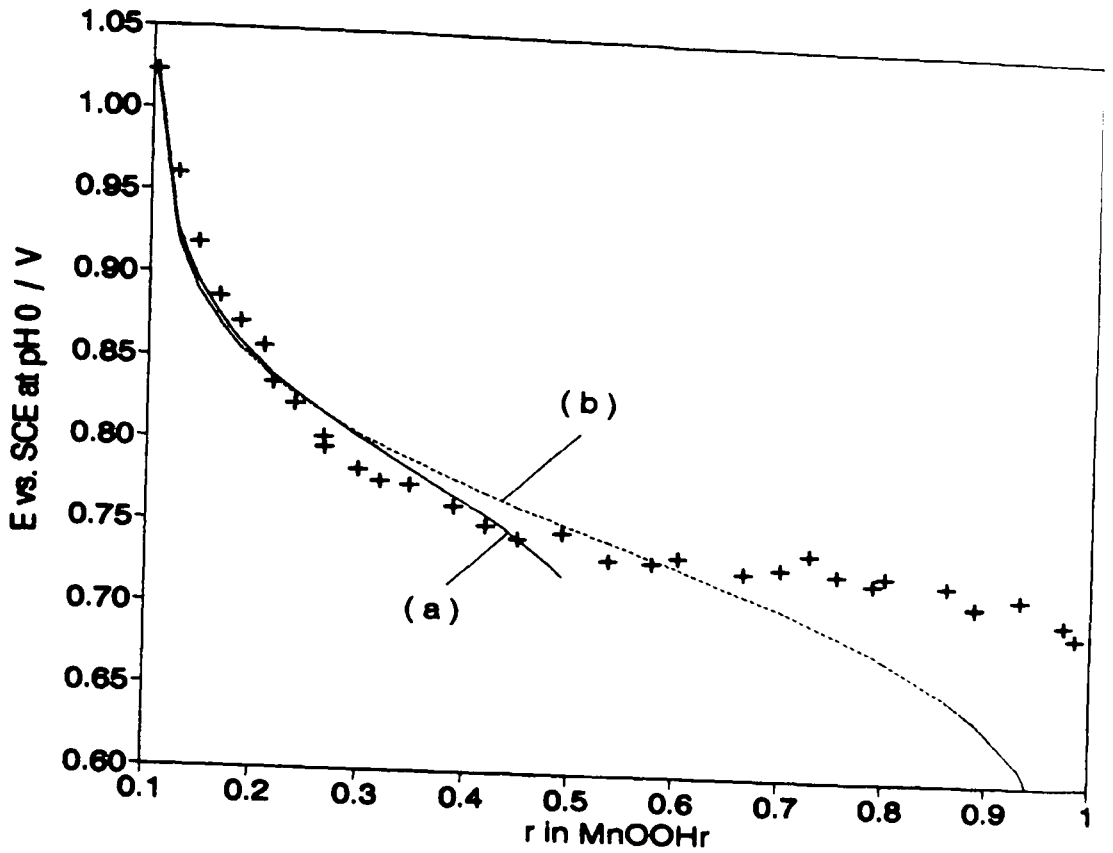

Figure 7.15 : Potential of reduced Far M with acetone pre-reduction; (a) equation 7.7 with E_0'=0.80 V and y=0.100, (b) equation 7.9 with E_0=0.745 V

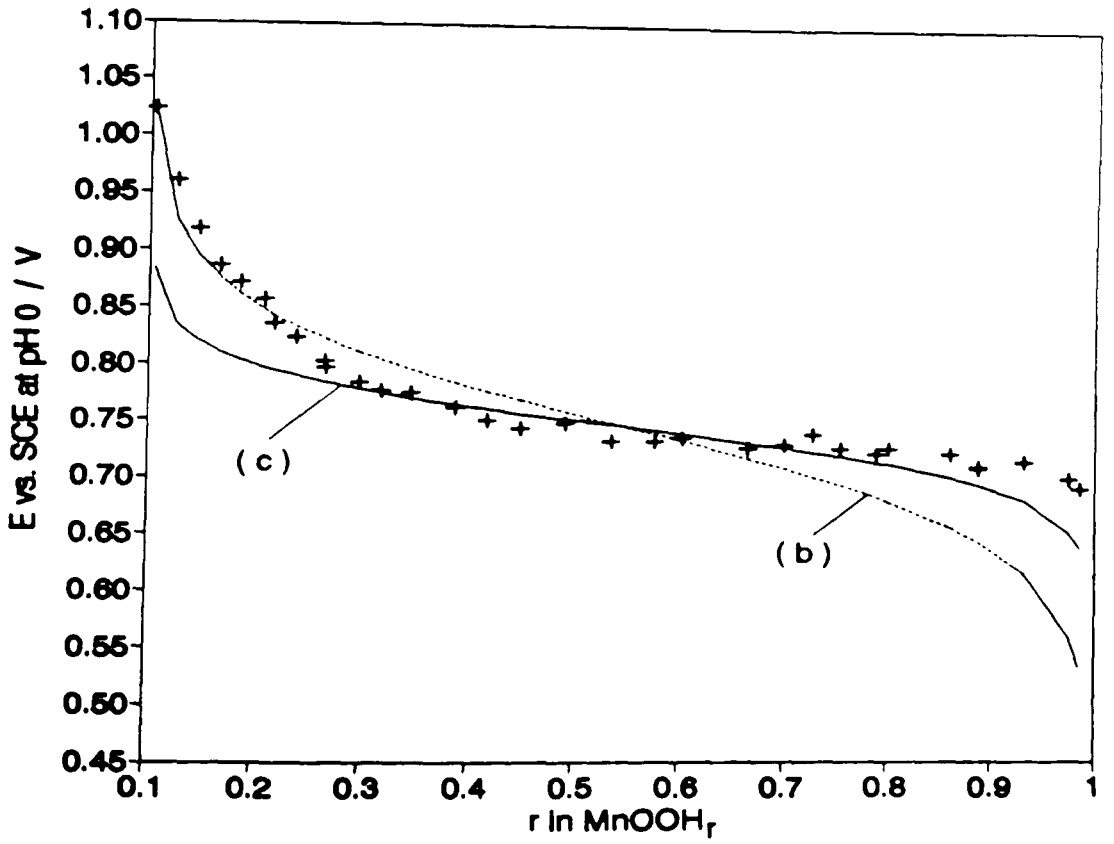

Figure 7.16 : Potential of reduced Far M with acetone pre-reduction; (b) equation 7.9 with E_0'=0.80 V and y=0.100, (c) equation 7.10 with E_0=0.745 V

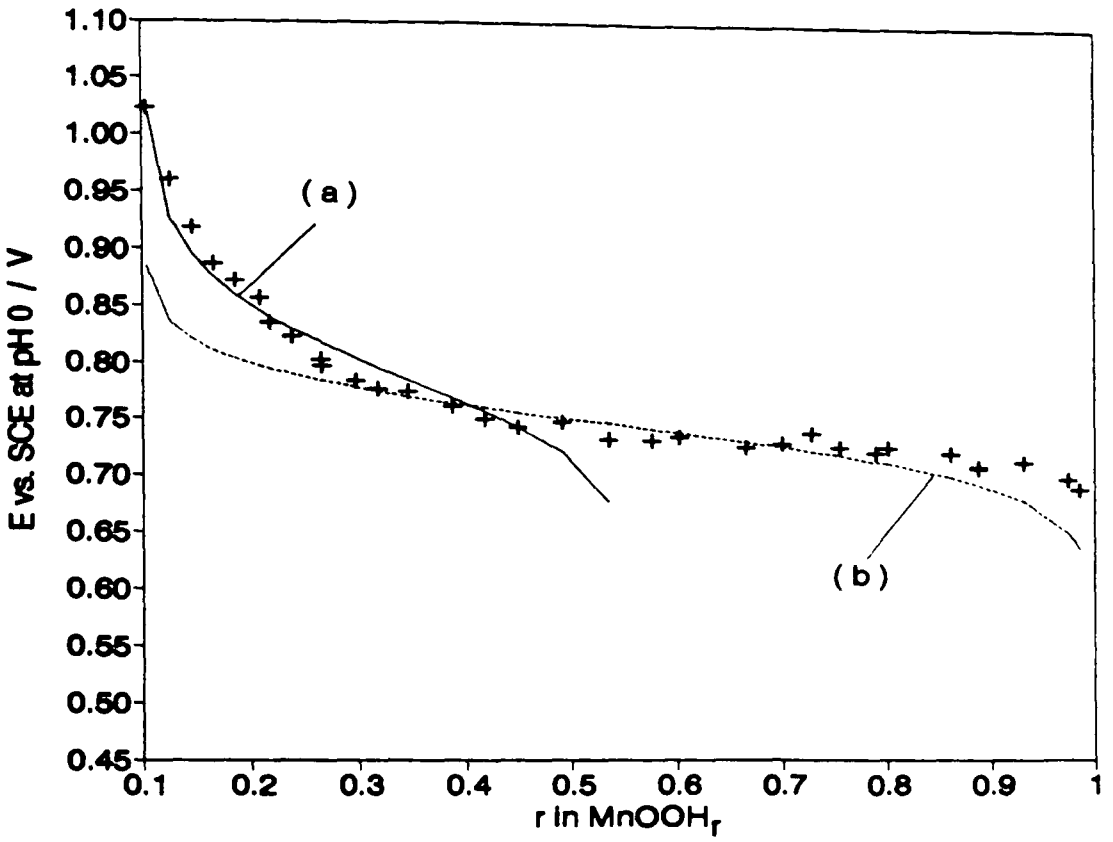

Figure 7.17 : Potential of reduced Far M with acetone pre-reduction; (a) equation 7.7 with E_0'=0.80 V and y=0.100, (b) equation 7.10 with E_0=0.745 V

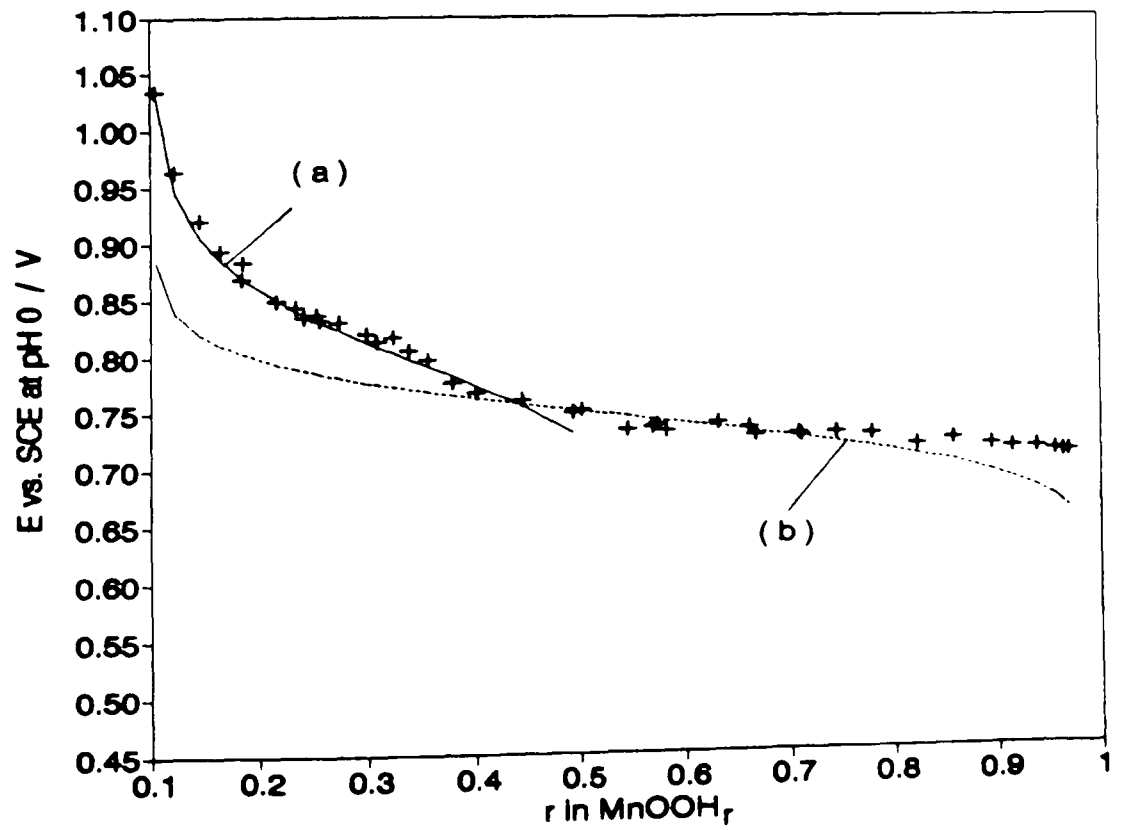

Figure 7.18 : Potential of reduced Far WSZ with acetone pre-reduction; (a) equation 7.7 with E_0'=0.81 V and y=0.100, (b) equation 7.10 with E_0=0.745 V

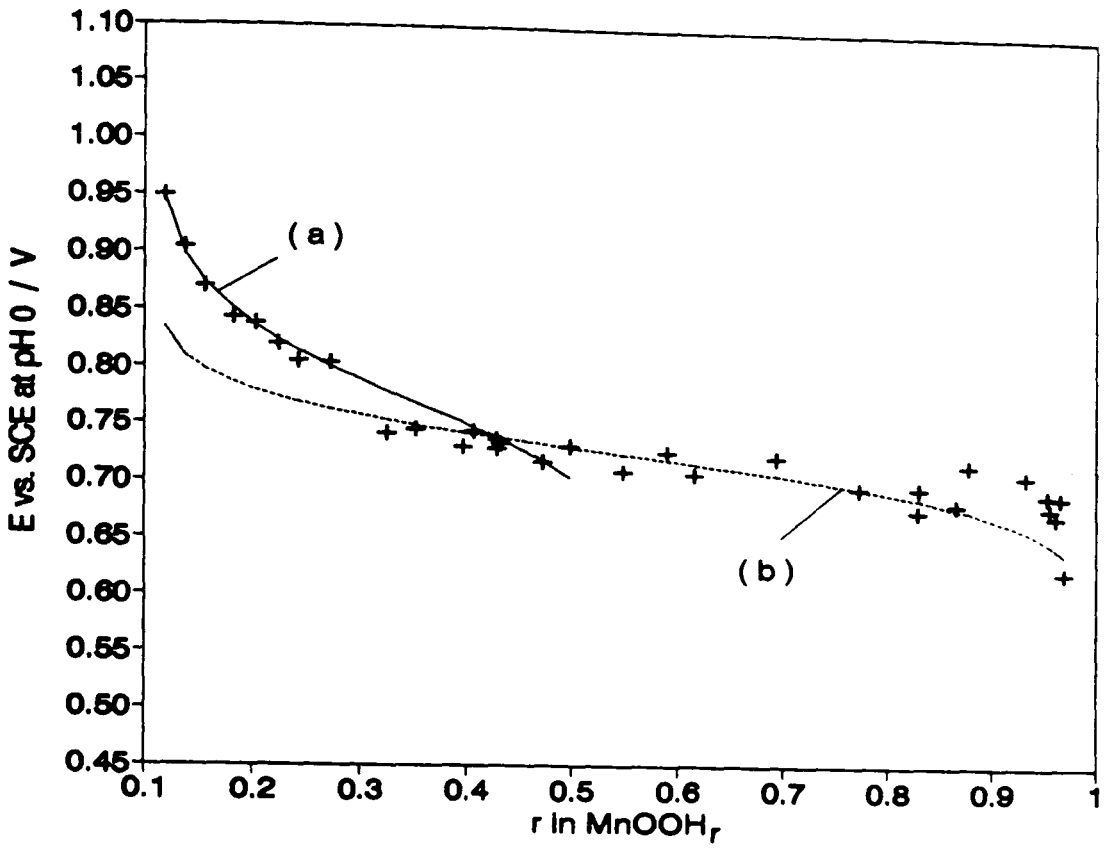

Figure 7.19 : Potential of reduced MnO_2 TR without acetone pre-reduction; (a) equation 7.7 with E_0'=0.785 V and y=0.105, (b) equation 7.10 with E_0=0.725 V

Figure (7.16) shows the comparison of equation (7.9) to equation (7.10), both with E_0 = 0.745 V vs. SCE and y = 0.100. The agreement is much better with equation (7.10) than with equation (7.9), suggesting that in the second half of the reduction, the assumption of independent mobility of the inserted protons and electrons which permitted the derivation of equation (7.9), and which applies to reduced EMD, is not valid for reduced Faradiser M. For the latter material, equation (7.10) is better obeyed suggesting that Faradiser M reduced beyond r=0.4-0.5 may be considered as a solid solution of un-dissociated MnOOH in the starting material. Figure (7.17) shows that the fit to equations (7.7) and (7.10) is satisfactory up to about r = 0.9. The mismatch between the measured potentials and the curve for r larger than about 0.9 was probably due to the uncertainty on the true value of the reduction degree in that range.

Figure (7.18) shows the results for Faradiser WSZ reduced with acetone, with E_0 = 0.81 and 0.745 V vs. SCE for equations (7.7) and (7.10), respectively and y = 0.100.

Figure (7.19) shows the results for MnO_2 TR reduced without acetone (no results could be obtained for the samples reduced by acetone and then hydrazine hydrate). E_0 were taken as 0.785 and 0.725 V vs. SCE for equations (7.7) and (7.10), respectively and y was 0.105. Figures (7.18) and (7.19) show, for Faradiser WSZ and MnO_2 TR, the same fair agreement between the measured potentials and equation (7.10) for samples reduced beyond r=0.4-0.5 as shown in figure (7.17) for Faradiser M, suggesting that, in that range of compositions, the three CMDs formed solid solutions of un-dissociated MnOOH in the starting material.

The parameters used in the curve fitting (E_0 and y) are summarised in table (7.4), for both chemical and electrochemical (intermittent discharge) reductions.

Table 7.4 : Parameters of the potential-composition curve fittings, chemical and electrochemical (see chapter 4) reductions

Material	y	E_0 / V vs. SCE		
		in eq. 7.7	in eq. 7.9	in eq 7.10
Chemical reductions				
EMD	0.068	0.843	0.765	-
Far M	0.100	0.800	-	0.745
Far WSZ	0.100	0.810	-	0.745
MnO_2 TR	0.105	0.785	-	0.725
Leclanché electrolyte				
EMD	0.067	0.780	0.705	-
from ref [83]	0.085	0.774	0.697	-
Zinc chloride electrolyte				
EMD	0.07	0.75	0.68	-
Far M	0.10	0.70	-	0.665
Far WSZ	0.10	0.72	-	0.67

The higher potential for the un-reduced Faradiser M and Faradiser WSZ which were shown in figure (7.9) do not appear in table (7.4). On the contrary, during the first part of the reduction (where the same equation has been used for all the materials), CMDs have lower E_0 than EMD, by about 50 mV and about 40 mV for Faradiser M and WSZ, respectively.

The potentials measured in actual cells were always lower than those measured in dilute KCl solution, by about 60 mV for EMD in Leclanché electrolyte and by about 90 mV for EMD and Faradiser WSZ and 100 mV for Faradiser M in $ZnCl_2$ electrolyte. The largest decrease of E_0 was observed for Faradiser M which also has the largest ion-exchange capacity. The larger decrease of the E_0s in zinc chloride than in Leclanché electrolyte (where NH_4Cl inhibits the zinc adsorption), suggests that the electrode potential was lower in actual cells than in dilute KCl because of a decrease of the free energy of MnO_2 caused by ion-exchange.

7.5. Conclusions

The reaction rate between manganese dioxide and acetone or hexane depended on the type of the manganese dioxide and was strongly correlated with the specific (BET) surface area of the material. This reaction rate decreased very quickly and reached a limit for a reduction degree of about $MnOOH_{0.4}$ in acetone at room temperature. Although the reaction consumed H_2O, addition of water to the acetone did not change the final reduction level of the sample. The reason for the limitation is thus not understood.

Reduction of the dioxides by a reaction in acetone for two weeks at room temperature followed by addition of hydrazine hydrate solution (in propan-2-ol) to the oxide suspended in hexane, gave samples close to the reduction end point ($MnO_{1.5}$ or MnOOH) with very little manganite content, and virtually no manganite at all if the second reduction was carried out at a temperature below 10 °C. The absence of manganite in samples reduced in a solvent of low polarity supports the intervention on Mn^{2+} in the formation of new phases on reduction proposed by Fitzpatrick and Tye [200].

Equilibration of the sample in a 10^{-3} M KCl solution prior to the potential measurement caused partial disproportionation of the sample with corresponding

increase of the soluble manganese concentration and of the solution pH. When the pH of the solution reached a value of about 5.5 to 6, corresponding to about $MnOOH_{0.5}$, oxygen dissolved in the solution caused the oxidation of Mn^{2+} and the precipitation of MnOOH. The calculations, based on the soluble manganese concentration, of the actual oxidation degree of the samples after equilibration were therefore in error and their true composition became somewhat uncertain. The reduction procedure (acetone pre-reduction or not, samples suspended in water or in hexane) affected the pH and the manganese content of the KCl solution used for the potential measurements. It is not clear whether this was due to a surface effect, adsorption of manganous ions or of the product of the solvent oxidation, reduction of different surface sites depending on the reduction reaction, or due to an unknown effect on the bulk of the material. The samples reduced by acetone before the hydrazine hydrate reduction gave apparently more reliable results than those reduced without the acetone pre-reduction. This may be due to a lower pH of the KCl solution after equilibration due to the presence of some acetic acid on the acetone reduced samples.

The reduction occurred in two distinct stages for both CMDs and EMD, although the potential - composition relationships were different for the former than for the latter materials. During the first part of the reduction (up to about $MnOOH_{0.5}$), the electrode potentials of the four manganese dioxides followed the equation derived by Tye [141] for a solid solution of $MnOOH_{0.5}$ in the starting material. Above about $MnOOH_{0.5}$, EMD exhibited the potential-composition relationship derived by Maskell *et al.* [139] for the electrodeposited manganese dioxide that they studied. Both equations were derived using the assumption of independent mobility for the inserted protons and electrons. By contrast, during the second part of the reduction, the three chemically prepared manganese dioxides followed a relationship indicating simultaneous diffusion of the inserted protons and electrons or undissociated MnOOH [215]. The different mechanism for the proton/electron diffusion in EMD and CMD is a new finding.

For all the materials, the presence of some inactive Mn(III) was assumed. The amount of inactive Mn(III) necessary for a good fit between the experimental data

and the equations was larger for the CMDs than for the EMD. The larger concentration of inactive Mn(III) in CMDs than in EMD explained the steeper slope of the potential - composition curve for former materials than for latter.

The electrode potential (against SCE) of both EMD and CMDs were lower after electrochemical reduction in actual cells than after chemical reduction and measurement in dilute KCl solution, due to the decrease of the manganese dioxide free energy caused by the ion-exchange which occurred to a much higher extent in battery electrolyte and especially in zinc chloride electrolyte, than in dilute KCl solution.

The parameters used to describe the electrode potential (E_0) were lower for CMD than for EMD by about 40 to 50 mV, either after chemical or electrochemical reduction.

Chapter 8. Conclusions and further work

8.1. Conclusions

NH_4Cl and $ZnCl_2$ combined in the Leclanché electrolyte to form chloro-zinc complexes. The density of the electrolyte can be explained by the formation of the $(NH_4)ZnCl_3$ complex only. The analysis of the zinc electrode potential (against a saturated calomel electrode) revealed that the latter complex was the predominant species in all solutions except when a large excess of NH_4Cl was present, in which case the predominant species was the $(NH_4)_2ZnCl_4$ complex.

The large deviation from the Nernst's equation observed in concentrated pure $ZnCl_2$ solutions was due to the reduction of the water activity caused by the strong hydration of the zinc species.

After optimisation of its parameters, the zinc complexation model originally developed by Atlung *et al.* [34] permitted the calculation the zinc electrode potential (versus SCE) with an average deviation of less than 4 mV for solutions up to 10 molal in $ZnCl_2$ and at any NH_4Cl concentration. It also gave a good estimate of the water activity in the mixed NH_4Cl - $ZnCl_2$ solutions.

The discharge of a Leclanché cell causes the precipitation of $ZnCl_2.4Zn(OH)_2.H_2O$ when the NH_4Cl concentration is lower than a value that increases with increasing $ZnCl_2$ concentration in the electrolyte; otherwise, the precipitate is $Zn(NH_3)_2Cl_2$. The dependence of the NH_4Cl concentration, corresponding to the transition from the precipitation of $Zn(NH_3)_2Cl_2$ to the formation of $ZnCl_2.4Zn(OH)_2.H_2O$, on the $ZnCl_2$ concentration had not been clearly shown before; it causes the simultaneous precipitation of $Zn(NH_3)_2Cl_2$ and $ZnCl_2.4Zn(OH)_2.H_2O$ during the latest stage of the Leclanché cell discharge.

Electrodeposited and chemically prepared manganese dioxide show different behaviours on intermittent discharge, both in Leclanché and in pure $ZnCl_2$ electrolyte.

In the Leclanché electrolyte, the performance, better for CMD than EMD on intermittent discharge test was due to the formation of hetaerolite in the cells containing the former material. Hetaerolite formation increased the potential of

the positive electrode by increasing the oxidation stage of the solid solution and decreased the potential of the negative electrode by increasing the NH_4Cl concentration due to the dissolution of the $Zn(NH_3)_2Cl_2$ precipitate formed in the early stage of the discharge. No report of experimental study showing NH_4Cl regeneration caused by hetaerolite formation has been found in the literature.

The intermittent discharge of EMD cells in Leclanché electrolyte occurred in the three stages as predicted by Tye [13,18]. The duration of the first two stages can be understood on the basis of the cell formulation, the overall cell reactions and the effect of ion-exchange on manganese dioxide. The electrolyte composition at the end of the discharge test shows that about 20 % of the zinc ions produced by anodic dissolution were precipitated as $Zn(NH_3)_2Cl_2$ during the third stage of the discharge, confirming that both $Zn(NH_3)_2Cl_2$ and $ZnCl_2.4Zn(OH)_2.H_2O$ precipitates were formed during the final stage of the discharge of Leclanché cells; $Zn(NH_3)_2Cl_2$ is probably precipitated by the discharge and subsequently redissolve to precipitate $ZnCl_2.4Zn(OH)_2.H_2O$. The potential of the EMD electrode, corrected for the changes of electrolyte pH, corresponded to the equations proposed by Tye [141] for his solid solution reduction model.

Faradiser M produced much less hetaerolite in pure $ZnCl_2$ than in Leclanché electrolyte and no evidence of hetaerolite formation was found in cells with Faradiser WSZ. Due to hetaerolite formation, cells with Faradiser M exhibited similar specific performance (faraday per mole) to cells containing EMD on intermittent discharge (30 minutes per day through a 4 Ω load) but the performance on this test of both CMDs were lower than for EMD in terms of discharge duration, mainly due to lower quantity of MnO_2 packed into the cells.

The composition of the electrolyte at the end of the intermittent discharge tests of zinc chloride cells suggests that the overall reaction product was not $ZnCl_2.4Zn(OH)_2.H_2O$ as in the final stage of the Leclanché cell discharges, but a product with a formula close to $2ZnCl_2.5Zn(OH)_2.H_2O$, both for EMD and Faradiser WSZ. No mention of the latter compound has been found in the literature.

The anodic dissolution of the zinc electrode at the current densities existing during the 4 Ω or 2.2 Ω discharge test (8-15 mA cm^{-2}) may be considered as unidirectional (negligible cathodic process rate).

The positive electrode potential against a reference electrode connected inside the MnO_2 electrode mass itself, showed no evidence of significant charge transfer overvoltage; the transient overpotential, which does not include the concentration overvoltage, was therefore considered as being purely ohmic.

The NH_4Cl concentration at the zinc electrode surface decreased continuously at the beginning of a continuous discharge in Leclanché electrolyte, causing the charge transfer overpotential to decrease dramatically. When the NH_4Cl concentration reached zero at the electrode interface, the anode behaved as in pure zinc chloride electrolyte, while the region of zero NH_4Cl concentration increased in extent towards the positive electrode. This is the first report in actual cells of the moving boundary phenomenon uncovered by Agpsowicz *et al.* [80] during their investigation of a simulated separator region. The fast decrease of the NH_4Cl concentration at the negative electrode surface caused a correspondingly fast increase of the zinc electrode concentration overpotential due to the disappearance of the beneficial effect of NH_4Cl on the zinc electrode potential.

The $ZnCl_2$ concentration at the negative electrode surface during a 2.2 Ω continuous discharge increased in good agreement with the theory of electrode concentration polarisation until the assumption of semi-infinite diffusion ceased to be valid when the concentration profile reached the positive electrode.

Towards the end of the continuous discharges, a large diffusion potential (about 70-100 mV) built-up in the separator region of both Leclanché and zinc chloride electrolyte cells, causing a fast decrease of the closed circuit voltage. The rapid development of this diffusion potential probably started when the diffusion of water from the positive electrode into the negative electrode compartment began to decrease due to the drying of the manganese dioxide

electrode. The diffusion potential reached a high value because of the unusually strong dependence of the zinc activity on the $ZnCl_2$ concentration.

Throughout all the continuous discharge on 4 Ω in Leclanché electrolyte, the closed circuit voltage and the positive electrode potential were lower for cells with Faradiser M than for those with EMD. Towards the end of the discharge test, the voltage loss in the separator region was also higher for cells with CMD than for cells containing EMD. Although EMD exhibited better performance than CMD in terms of discharge duration, the specific performances, in faraday per mole of MnO_2 were very similar for both materials showing that the disadvantage of Faradiser M was mainly due to the difference in the MnO_2 content of the cells.

In zinc chloride electrolyte, the discharge duration on the 2.2 Ω continuous test also increased with the MnO_2 content of the cells, the specific performances being very similar for EMD and Faradiser WSZ, and slightly lower (about 3-4 %) for Faradiser M than for the other two materials.

During the same discharges, the closed circuit MnO_2 electrode potentials against a reference electrode connected inside the positive electrode mass were very similar for the three materials throughout the test.

The voltage loss in the separator region was the most significant difference between the different materials in zinc chloride electrolyte. It increased in the order

EMD < Faradiser WSZ < Faradiser M, and by the end of the discharge, it amounted to about 20 % of the total voltage loss of the Faradiser M cells. An increase of the cell electrolyte content reduced this diffusion potential significantly and produced only minor changes of the positive and negative electrode potentials.

No report of a large non-ohmic voltage loss in the separator region of a cell undergoing heavy continuous discharge has been found in the literature.

The rate of reduction of the manganese dioxide during the discharge (electrochemical current density) varied with the distance from the current collector, and at a given location with the stage of discharge. On the 4 Ω test in Leclanché electrolyte, the maximum utilisation rate of the manganese dioxide was found in the middle of the electrode thickness. On the 2.2 Ω continuous discharge, a strong maximum of the manganese dioxide reduction rate was found in the region close to the current collector, both in Leclanché and in zinc chloride electrolytes. In all cases, a large part of the positive electrode did not participate to the production of current during the continuous discharge test, consequently, the cells were only used to a fraction of their theoretical capacity.

The decrease of the manganese dioxide electrode potential with degree of oxidation followed the same form of equation, derived assuming independent mobility of the inserted protons and electrons and a solid solution of $MnOOH_{0.5}$ in the starting material [83], for EMD and CMD during the first part of the reduction. For samples more reduced than about $MnOOH_{0.4}$, the potential-composition relationship of EMD conformed to an equation derived for a material in which inserted protons and electrons move independently and for a solid solution of MnOOH in the starting material [141]. Beyond about $MnOOH_{0.4}$, the potential-composition relationship for all the CMDs studied in this work was of the form of the equation derived by Tye [215] for a material in which MnOOH is undissociated, i.e. in which proton and electron diffusions are not independent. This difference between EMD and CMD, which was observed during chemical and electrochemical reduction, has not been reported before.

At a given oxidation stage, the potential, corrected for pH difference, of a given manganese dioxide was lower in battery electrolyte than in dilute KCl solution due to the decrease of the manganese dioxide free energy caused by the ion-exchange phenomenon.

8.2. Further work

8.2.1 Study of the Leclanché electrolyte

At high $ZnCl_2$ concentrations, the calculated densities of the Leclanché electrolyte are overcorrected for the complexation phenomenon. Another treatment of the effect of zinc complexation on the density might avoid this drawback.

Even after optimisation of all its parameters, the model used for the calculation of the zinc electrode potential gives systematic errors, e.g. at low NH_4Cl concentration and fails at $ZnCl_2$ concentrations above about 10 molal. A refinement of the treatment of the zinc hydration might prove profitable.

The results of intermittent discharges revealed that in the pure $ZnCl_2$ electrolyte the precipitate was different from that in the mixed Leclanché electrolyte. This has to be confirmed either by a more extensive study of intermittent discharges, or by simulation of the discharge by ZnO addition to $ZnCl_2$ solutions in order to re-determine the stoichiometry of the precipitate.

8.2.2 Battery discharge

A linear relationship at a given discharge current between the zinc charge transfer overpotential and the NH_4Cl concentration has been suggested in section 6.2.1. This may be checked either by studying constant current discharges or by systematic measurements, e.g. with a rotating disc electrode.

It has been concluded in chapter 5 that the transient overpotential of the manganese dioxide electrode was essentially ohmic. It is possible to verify this conclusion by using the interruption technique to measure the MnO_2 overpotential over a large range of discharge current. A linear relationship between the overpotential and the discharge current would reveal a low charge transfer overpotential.

8.2.3 Manganese dioxide study

The precipitation of the manganous ions produced by the disproportionation of the highly reduced manganese dioxides made the calculation of the true

oxidation stage of the solid solution unreliable. This precipitation was caused by oxidation of the manganous ions; working in absence of oxygen or in a solution buffered at pH $\leq$ 5 would prevent the precipitate being formed and improve the accuracy of the measurement. For Faradiser WSZ which does not form hetaerolite rapidly, it is also possible to perform the measurements during intermittent discharge to a larger extent than has been carried out in this work.

Careful comparison between EMD and CMD of the change of the lattice parameters during reduction may also reveal similar behaviour of both materials at low reduction degree and different behaviour beyond the mid-reduction point.

References

1. G. Leclanché, French Patent 71865, 8th June 1866

2. G. Leclanché, British Patent 1637, 16th June 1866

3. G. Leclanché, French Patent 124108, 26th April 1878

4. N.C. Cahoon, in N.C. Cahoon and G.W. Heise eds., The Primary Battery, Vol.2, Wiley and Son, (1976), 1-147

5. C. Gassner, German Patent 37758, 8th April 1886

6. G. Leclanché, Les Mondes, (Paris), 16, (1868), 532-535

7. G.W. Heise and N.C. Cahoon, J. Electrochem. Soc., 99, (1952), 179C-187C

8. W.L.F. Hellesen, U.S. Patent 439151, 28th October 1890

9. C. Hambuechen, U.S. Patent 1292764, 28th January 1919

10. C.J. Coleman, U.S. Patent 495306, 11th April 1893

11. R.A. Witherspoon and A.F.G. Cadenhad, Trans. Electrochem. Soc., 70, (1936), 49-55

12. M. Bregazzi, Electrochem. Technol., 5, (1967), 507-513

13. F.L. Tye, in T. Tran and M. Skyllas Kazacos eds., Proceedings of the 7th Austalian Electrochemical Conference, The Royal Australian Chemical Institute, (1988), 37-48

14. A. Kozawa, in K. Kordesch ed., Batteries, Vol.1, Manganese Dioxide, Marcel Dekker, (1974), 385-519

15. O.W. Storey, E. Steinhoff and E.R. Hoff, Trans, Electrochem. Soc., 86, (1944), 337-344

16. J.Y. Welsh and D.W. Paterson, J. Metals, 9, (1957), 762-765

17. J.Y. Welsh, U.S. Patent 2956860 (1960)

18. F.L. Tye, in M. Barak ed., Electrochemical Power Sources, Peter Peligrinus, London, (1980), 50-150

19. N.C. Cahoon, Trans. Electrochem. Soc., 92, (1947), 159-172

20. Y. Marcus, Ion solvation, John Wiley and Son, Chichester, (1985)

21. J.E. Desnoyer and C. Jolicoeur, in B.E. Conway, J.O'M. Bockris and E. Yaeger eds., Comprehensive Treatise of Electrochemistry, Vol. 5, Plenum Press, (1983), 1-109

22. W. Bol, G.J.A. Gerrits and C.L. Van Panthaleon, J. Appl. Cryst., 3, (1970), 486-492

23. D.D. Perrin, J.Chem. Soc., (1962), 4500-4502

24. R.H. Stokes, Trans. Faraday Soc., 44, (1948), 137-141

25. R.H. Stokes and R.A. Robinson, J. Am. Chem. Soc., 70,(1948), 1870-1878

26. Lutfullah, H.S. Dunsmore and R. Paterson, J. Chem. Soc. Faraday Trans. 1, 72, (1976), 495-403

27. H. Weingartner, K.J. Muller, H.G. Hertz, A.V.J. Edge and R. Mills, J. Phys. Chem., 88, (1984), 2173-2178

28. D.E. Irish, B. Mc Carroll and T.F. Young, J. Chem. Phys., 39, (1963), 3436-3444

29. N.A. Marley and J.S. Gaffney, Appl. Spectrosc., 44, (1990), 469-476

30. T. Sato and T. Nakamura, Hydrometallurgy, 6, (1980), 3-12

31. W. Boch and J. Goc, Arch. Acoust., 4, (1979), 73-85

32. K. Sasaki and T. Takahashi, Electrochim. Acta, 1, (1959), 261-271

33. E. Skou, T. Jacobsen, W. Van Der Hoeven and S. Atlung, Electrochim. Acta, 22, (1977), 169-174

34. S. Atlung, K. West and T. Jacobsen, in D.H. Collins ed., Power Sources 6, Academic Press, London, (1976), 403-438

35. J.N. Pearce and G.G. Pumplin, J. Am. Chem. Soc., 59, (1937), 1221-1222

36. International Critical Tables, 3, McGraw Hill, New York, (1929), 60

37. P. Novotny and O. Sohnel, J. Chem. Eng. Data, 33, (1988), 49-55

38. International Critical Tables, 3, McGraw Hill, New York, (1929), 64

39. A. Agnew and R. Paterson, J. Chem. Soc. Faraday Trans.1, 74, (1978), 2896-2906

40. J.A. Rard and D.G. Miller, J. Chem. Eng. Data, 29, (1984), 151-156

41. T.M. Herrignton, M.G. Roffey and D.P. Smith, J. Chem. Eng. Data, 31, (1986), 221-225

42. T. Takahashi and K. Sasaki, J. Electrochem. Soc. Japan, 24, (1956), 414-419

43. T.F. Young and M.B. Smith, J. Phys. Chem., 58, (1954), 716-724

44. F.H. Spedding, M.J. Pikal and B.O. Ayers, J. Phys. Chem., 70, (1966), 2440-2449

45. W.C. Root, J. Am. Chem. Soc., 55, (1933), 850-851

46. D.O. Masson, Phil. Mag., 8, (1929), 218-235

47. This work

48. R. Friess, J. Am. Chem. Soc., 52, (1930), 3083-3087

49. A.M. Bredland and M.N. Hull, J. Electrochem. Soc., 123, (1976), 311-315

50. H.F. McMurdie, D.N. Craig and G.W. Vinal, Trans. Electrochem. Soc., 90, (1946), 509-526

51. T. Takahashi ans K. Sasaki, J. Electrochem. Soc. Japan, 25, (1957), 118-122

52. P. Delahay, M. Pourbaix and P. Van Rysselberge, J. Electrochem. Soc., 98, (1951), 101-105

53. L.M. Baugh, F.L. Tye and N.C. White, J. Appl. Electrochem., 13, (1983), 623-635

54. L.M. Baugh and N.C. White, J. Appl. Electrochem., 17, (1987), 1281-1295

55. L.Z. Vorkapic, D.M. Drazic and A.R. Despic, J. Electrochem. Soc., 121, (1974), 1385-1392

56. L.M. Baugh and N.C. White, J. Appl. Electrochem, 17, (1987), 1037-1047

57. T. Takahashi, H. Nakaushi and K. Sasaki, J. Electrochem. Soc. Japan, 22, (1954), 589-592

58. P.A. Meerburg, Z. anorg. Chem., 37, (1903), 199-221

59. M.L. Meeus, G. G. Crocq and C.A. Lemaître, in J. Thompson ed., Power Sources 7, Academic Press, (1979), 463-484

60. D.R. Crow, Principles and Applications of Electrochemistry, Chapman and Hall, London, (1988)

61. L.M. Baugh and N.C. White, in L.J. Pearce ed., Power Sources 11, International Power Sources Committee, (1986), 301-327

62. L.M. Baugh and N.C. White, J. Appl. Electrochem., 17, (1987), 1021-1036

63. L.M. Baugh and A. Higginson, J. Power Sources, 13, (1984), 297-318

64. Ph. Brouillet and F. Jolas, Electrochim. Acta, 6, (1962), 245-251

65. D.J. Dewhurst, Trans. Faraday Soc., 56, (1960), 599-605

66. H.J.S. Sand, Comptes Rendus Acad. Sci., 131, (1900), 992-995

67. A.C. Harris and H.N. Parton, Trans. Faraday Soc., 36, (1940), 1139-1141

68. S.F. Patil, N.G. Adhyapak and P.R. Patil, Int. J. Appl. Radiat. Isotop., 35, (1984), 761-766

69. J. Jorne and W.T. Ho, J. Electrochem. Soc., 129, (1982), 907-912

70. D.G. Leaist, Ber. Bunsenges. phys. Chem., 90, (1986), 797-802

71. D. Loftus, J. Roberts, R. Waever, S. Leach and N. Nanis, J. Electrochem. Soc., 130, (1983), 332-334

72. D.G. Miller, A.W. Ting and J.A. Rard, J. Electrochem. Soc., 135, (1988), 896-904

73. J.A. Lee, W.C. Maskell and F.L. Tye, Separators and Membranes in Electrochemical Power Sources, in P. Meares ed., Membrane Separation Processes, Elsevier, Amsterdam, (1976), 399-476

74. F.L. Tye, J. Power Sources, 9, (1983), 89-100

75. Y. Uetani, H. Sasama and T. Iwamaru, Proceedings Volume 85-4, The Electrochemical Society, Pennington, N.J., (1985), 475-492

76. J.P. Gabano, B. Morignat and J.F. Laurent, Electrochim. Acta, 9, (1964), 1093-1117

77. M. Fukuda, T.Hirai and H. Manabe, J. Electrochem. Soc. Japan, (overseas ed.), 27, (1959), E108-E110

78. N.C. Cahoon and G.W. Heise, J. Electrochem. Soc., 94, (1948), 214-219

79. H. Kahil and J. Guiton, Surface Technol., 20, (1983), 181-192

80. A. Agopsowicz, R. Brett, J.E.A. Shaw and F.L. Tye, in D.H. Collins ed., Power Sources 5, Academic Press, London, (1975), 503-524

81. J.J. Coleman, Trans. Electrochem. Soc., 90, (1946), 545-583

82. R. Huber and J. Bauer, Electrochem. Technol., 5, (1967), 542-548

83. F.L. Tye, Proceedings Volume 85-4, The Electrochemical Society, Pennington, N.J., (1985), 301-341

84. A. Tvarusko, J. Electrochem. Soc., 111, (1964), 125-131

85. E. Preisler, in B. Schumm, H.M. Joseph, and A. Kozawa eds., Manganese Dioxide Symposium, Volume 2, Tokyo, I.C. MnO2 Sample Office, (1980), 184-206

86. J.A. Lee, C.E. Newnham and F.L. Tye, J. Colloid. Interface Sci., 42, (1973), 372-380

87. K. Shimizu and J. Koshiba, Proceedings Volume 85-4, The Electrochemical Society, Pennington, N.J., (1985), 391-402

88. J.P. Gabano, B. Morignat, E. Fialdes, B. Emery and J.F. Laurent, Z. physik. Chem., 46, (1965), 359-372

89. P.C. Picquet and J.Y. Welsh, New Mater. New Process., 2, (1983), 12-18

90. J. Brenet, P. Picquet and J.Y. Welsh, in B. Schumm, H.M. Joseph, and A. Kozawa eds., Manganese Dioxide Symposium, Volume 2, Tokyo, I.C. MnO2 Sample Office, (1980), 214-243

91. J. Muller, F.L. Tye and L.L. Wood, in D.H. Collins ed., Batteries 2, Pergamon Press, (1965), 201-217

92. J.P. Gabano, P. Etienne and J.F. Laurent, Electrochim. Acta, 10, (1965), 947-963

93. A. Kozawa, J. Electrochem. Soc., 106, (1959), 552-556

94. H. Tamura and Nagayama, Progress in Batteries and Solar Cells, 5, (1984), 143-146

95. E. Preisler, J. Appl. Electrochem., 6, (1976), 311-320

96. R.F. Amlie and A. Tvarusko, J. Electrochem. Soc., 111, (1964), 496-501

97. X. Xi, C. Zenhai, Z. Peijiang, Z. Haikui, Z. Hong, S. Fang and L. Hong, in K. Kordesh and A. Kozawa eds., Battery Material Symposium, Volume 2, Graz, IBA Office, (1985), 169-180

98. P. Ruetschi, J. Electrochem. Soc., 131, (1984), 2737-2744

99. A. Kozawa, J. Electrochem. Soc., 106, (1959), 79-82

100. A. Kozawa, Proceedings Volume 85-4, The Electrochemical Society, Pennington, N.J., (1985), 384-390

101. T. Valand, Electrochim. Acta, 19, (1974), 639-643

102. S. Atlung, in A. Kozawa and R.G. Brodd eds.,Manganese Dioxide Symposium, Volume 1, Cleveland, IC MnO_2 Sample Office, (1975), 47-65

103. N.C. Cahoon, R.S. Johnson and M.P. Korver, J. Electrochem. Soc., 105, (1958), 296-298

104. N.C. Cahoon and M.P. Korver, J. Electrochem. Soc., 109, (1962), 1-6

105. S. Yoshizawa, in B. Schumm, H.M. Joseph, and A. Kozawa eds., Manganese Dioxide Symposium, Volume 2, Tokyo, I.C. MnO2 Sample Office, (1980), 1-10

106. Y. Uetani, T. Iwamaru and Y. Ishikawa, in B. Schumm, H.M. Joseph, and A. Kozawa eds.,Manganese Dioxide Symposium, Volume 2, Tokyo, I.C. MnO2 Sample Office, (1980), 505-519

107. J.M. Cowley and A. Walkley, Nature, 161, (1948), 173

108. W.C. Vosburgh, J. Electrochem. Soc., 106, (1959), 839-845

109. A. Kozawa and R.A. Powers, J. Electrochem. Soc., 113, (1966), 870-878

110. W.C. Maskell, J.E.A. Shaw and F.L. Tye, Electrochim. Acta, 26, (1981), 1403-1410

111. E. Divers, Chemical News, 46, (1882). 259-260

112. H.F. McMurdie, Trans. Electrochem. Soc., 86, (1944), 313-326

113. T.D. Ferrell and W.C. Vosburgh, J. Electrochem. Soc., 98, (1951), 334-341

114. N.K. Chaney, in the discussion section of the paper by D.A. MacInnes, Trans. Am. Electrochem. Soc., 29, (1916), 315-321

115. A.M. Chreitzberg, D.R. Allenson and W.C. Vosburgh, J. Electrochem. Soc., 102, (1955), 557-561

116. E.A. Mendzheritskii, Soviet Electrochem., 5, (1969), 815-816

117. W.C. Vosburgh and P.S. Lou, J. Electrochem. Soc., 108, (1961), 485-490

118. J.E.A. Shaw, PhD Thesis, (1982), CNAA

119. V.N. Dam'e and E.A. Mendzeritskii, Soviet Electrochem., 4, (1968), 244-248

120. P.C. Picquet and S. Davis, Proceedings Volume 85-4, The Electrochemical Society, Pennington, N.J., (1985), 247-261

121. H.D. Holler and L.M. Ritchie, Trans. Electrochem. Soc., 37, (1920), 607-616

122. N.C. Cahoon, Trans. Electrochem. Soc., 68, (1935), 177-185

123. K. Sasaki, Memoirs of the Faculty of Engineering, Nagoya University, 3, (1951), 81-101

124. P. Benson, W.B. Price and F.L. Tye, Electrochem. Technol., 5, (1967), 517-523

125. J. Caudle, K.G. Summer and F.L. Tye, J. Chem. Soc. Faraday Trans. I, 69, (1973), 876-884

126. J. Caudle, K.G. Summer and F.L. Tye, J. Chem. Soc. Faraday Trans. I, 69, (1973), 885-893

127. R.S. Johnson and W.C. Vosburgh, J. Electrochem. Soc., 100, (1953), 471-472

128. K.J. Vetter, J. Electrochem. Soc., 110, (1963), 597-605

129. J.P. Gabano, J. Seguret and J.F. Laurent, J. Electrochem. Soc., 117, (1970), 147-151

130. J.F. Laurent and B. Morignat, in D.H. Collins ed., Batteries, Pergamon Press, (1963), 309-328

131. A. Kozawa and R.A Powers, Electrochem. Technol., 5, (1967), 535-542

132. B.D. Desai, R.A.S. Dhume and V.N. Kamat Dalal, J. Appl. Electrochem., 18, (1988), 62-74

133. H. Bode and A. Schmier, in D.H. Collins ed., Batteries, Pergamon Press, (1963), 329-333

134. D.M. Holton, W.C. Maskell and F.L. Tye, in L. Pearce ed., Power Sources 10, The Paul Press, (1985), 247-270

135. G. Coeffier and J. Brenet, Bull. Soc. Chim. France, (1964), 2835-2839

136. W.C. Maskell, J.E.A. Shaw and F.L. Tye, J. Appl. Electrochem., 12, (1982), 101-108

137. W.C. Maskell, J.E.A. Shaw and F.L. Tye, Electrochim. Acta, 27, (1982), 425-428

138. W.C. Maskell, J.E.A. Shaw and F.L. Tye, J. Power Sources, 8, (1982), 113-120

139. W.C. Maskell, J.E.A. Shaw and F.L. Tye, Electrochim. Acta, 28, (1983), 225-230

140. W.C. Maskell, J.E.A. Shaw and F.L. Tye, Electrochim. Acta, 28, (1983), 231-235

141. F.L. Tye, Electrochim. Acta, 30, (1985), 17-23

142. X. Xi, S. Fang and C. Zhen-Hai, Progress in Batteries and Solar Cells, 7, (1988), 231-235

143. Y.P. Chabre, J. Electrochem. Soc., 138, (1991), 329-330

144. K. Takahashi, Electrochim. Acta, 26, (1981), 1467-1476

145. J.J. Laragne and J. Brenet, Bull. Soc. Chim. France, (1970), 2455-2458

146. F. Tedjar and J. Guiton, Surf. Coat. Technol., 35, (1988), 1-10

147. P. Brouillet, A. Grund, F. Jolas and R. Mellet, in D.H. Collins ed., Batteries 2, Pergamon Press, (1965), 189-199

148. A.B. Scott, J. Electrochem. Soc., 107, (1960), 941-944

149. K. Kornfeil, J. Electrochem. Soc., 109, (1962), 349-351

150. A. Era, Z. Takehara and S. Yoshizawa, Electrochim. Acta, 12, (1967), 1199-1212

151. Z. Hong, C. Zhenhai and X. Xi, J. Electrochem. Soc., 136, (1989), 2771-2774

152. J.J. Coleman, J. Electrochem. Soc., 98, (1951), 26-30

153. V.S. Daniel-Bek, J. Phys. Chem. USSR, 22, (1948), 697-710

154. V.S. Daniel-Bek, Soviet Electrochem., 2, (1966), 621-626

155. T. Tsuruoka, S. Okamoto and Y. Amano, J. Electrochem. Soc. Japan, 29, (1954), 582

156. D. Simonsson, J. Electrochem. Soc., 120, (1973), 151-157

157. Y. Yamazaki and N.P. Yao, J. Electrochem. Soc., 128, (1981), 1658-1662

158. S. Szpak and T. Katan, J. Electrochem. Soc., 122, (1975), 1063-1071

159. R.J. Brodd, Electrochim. Acta, 11, (1966), 1107-1117

160. J.S. Newman and C.W. Tobias, J. Electrochem. Soc., 109, (1962), 1183-1191

161. R.J. Brodd, Electrochem. Technol., 6, (1968), 279-294

162. E.A. Grens and C.W. Tobias, Ber. Bunsenges. phys. Chem., 68, (1964), 236-249

163. S.L. Marshal, Proceedings Volume 90-10, The Electrochem. Soc., Pennington, N.J., (1990), 189-210

164. F.A. Posey, J. Electrochem. Soc., 111, (1964), 1173-1181

165. J.S. Dunning, D.N. Bennion and J. Newman, J.Electrochem. Soc., 118, (1971), 1251-1256

166. R. Alkire and B. Place, J. Electrochem. Soc., 119, (1972), 1687-1692

167. D. Simonsson, J. Appl. Electrochem., 3, (1973), 261-270

168. E.C. Dimpault-Darcy, T.V. Nguyen and R.E. White, J. Electrochem. Soc., 135, (1988), 278-285

169. K.J. Euler, J. Appl. Electrochem., 2, (1972), 105-112

170. K.J. Euler and B. Seim, J. Appl. Electrochem., 8, (1978), 49-59

171. K.J. Euler, U. Euler and B. Seim, J. Power Sources, 6, (1981), 25-34

172. G. Leclanché, Comptes Rendus Acad. Sci., 83, (1876), 1236-1238

173. S. Davis, private communication

174. P. Henderson, Z. phys. Chem., 59, (1907), 118-127

175. J. Bagg, Electrochim. Acta, 35, (1990), 361-365

176. J. Bagg, Electrochim. Acta, 35, (1990), 367-370

177. G. Glasstone, J. Chem. Soc., 123, (1923), 2926-2934

178. A. Tvarusko, J. Electrochem. Soc., 109, (1962), 557-560

179. J. Gerard, G. Gerbier and J.P. Gabano, in D.H. Collins ed., Batteries 2, Pergamon Press, (1965), 219-232

180. J.E.B. Randles, Disc. Faraday Soc., 1, (1947), 11-19

181. S. Schuldiner and R.E. White, J. Electrochem. Soc., 97, (1950), 433-447

182. P.C. Milner, J. Electrochem. Soc., 107, (1960), 343-348

183. J.L. Ord, J.C. Clayton and W.P. Wang, J. Electrochem. Soc., 124, (1977), 1671-1677

184. R. Barnard, C.F. Randell and F.L. Tye, J. Appl. Electrochem., 10, (1980), 109-125

185. J.D.E. McIntyre and W.F. Peck, J. Electrochem. Soc., 117, (1970), 747-751

186. A. Ohta, J. Watanabe and R. Furumi, in A. Kozawa and R.J. Brodd eds., Manganese Dioxide Symposium, Volume 1, Cleveland, IC MnO2 Sample Office, (1975), 159-182

187. Y. Uetani, T. Iwamaru and Y. Ishikawa, Electrochim. Acta, 26, (1981), 1411-1416

188. Y. Uetani, T. Togo, T. Iwamaru and I. Toshikubo, in A.Kozawa and R.J. Brodd eds., Manganese Dioxide Symposium, Volume 1, Cleveland, IC MnO2 Sample Office, (1975), 183-201

189. Vogel, Textbook of Quantitative Inorganic Analysis, 4th ed., Longman, (1978)

190. K.J. Vetter and N. Jaeger, Electrochim. Acta, 11, (1966), 401-419

191. R.C. Weast ed., CRC Handbook of Chemistry and Physics, 58th ed., CRC Press, (1978)

192. J. Hendriks, A. Van der Putten, W. Wisscher and E. Barendrecht, Electrochim. Acta, 29, (1984), 81-89

193. R.A. Robinson and R.H. Stokes, Trans Faraday Soc., 36, (1940), 740-748

194. Mitsui Denman (Ireland), EMD Specifications

195. Sedema (Belgium), Technical Specifications

196. T.B. Warner and S. Schuldiner, J. Electrochem. Soc., 114, (1967), 359-360

197. I. Trachtenberg, J. Electrochem. Soc., 111, (1964), 110-113

198. J. Garche, G. Schadlich and K. Wiesner, J. Electroanal. Chem., 180, (1984), 587-597

199. P.E. Lake and E.J. Casey, J. Electrochem. Soc., 106, (1959), 913-919

200. J. Fitzpatrick and F.L. Tye, J. Appl. Electrochem., 21, (1991), 130-135

201. H. Suzuki, N. Nagayama and K. Ishikawa, New Mater. New Process., 2, (1983), 22-27

202. Merck-BDH specifications

203. D.T. Sawyer and J.L. Roberts, Experimental Electrochemistry for Chemists, John Wiley, New York, (1974)

204. JCPDS, (1989), 30-69

205. JCPDS, (1989), 12-304

206. J.J. Borodzinski and Z. Galus, J. Electroanal. Chem., 135, (1982), 227-241

207. G. Senanayake and D.M. Muir, Electrochim. Acta, 33, (1988), 3-9

208. T. Jacobsen ans E. Skou, Electrochim. Acta, 22, (1977), 161-167

209. B.D. Bunday and G.R. Garside, Optimisation Methods in Pacal, Edward Arnold, London, (1987)

210. P. Henrici, Elements of Numerical Analysis, John Wiley, (1964), 87-89

211. N. Katayama, H. Tamura. N. Nagayama and R. Furuichi, Progress in Batteries and Solar Cells, 7, (1988), 44-48

212. H. Bode and A. Schmier, Ber. Busenges. phys. Chem., 68, (1964), 954-959

213. P.R. Everatt and F.L. Tye, Progress in Batteries and Solar Cells, 7, (1988), 128-132

214. Analysis carried out by Sedema

215. F.L. Tye, Electrochim. Acta, 21, (1976), 415-420

216. G. Armstrong and J.A.V. Butler, Trans. Faraday Soc., 29, (1933), 1261-1266

217. H.B. Morley and F.E.W. Wetmore, Can. J. Chem., 34, (1956), 259-363

218. D.C. Grahame, J. Phys. Chem., 57, (1953), 257-261

219. J. Garche, G. Schadlich and K. Wiesner, J. Electroanal. Chem., 180, (1984), 587-597

220. G.J. Dudley and B.C.H. Steele, J. Electrochem. Soc., 125, (1978), 1994-1997

221. G.J. Dudley and B.C.H. Steele, J. Solid State Chem., 31, (1980), 233-247

222. S.R. Narayanan and S. Sathyanarayama, J. Appl. Electrochem., 19, (1989), 495-499

223. J. Crank, The Mathematics of Diffusion, 2d ed., Clarendon Press, Oxford, (1985)

224. A. Kozawa, in K.V. Kordesch and A. Kozawa eds., Battery Material Symposium, Volume 2, Graz, (1985), 3-19

225. B.K. Thomas and D.J. Fray, J. Appl. Electrochem., 12, (1982), 1-5

226. T. Katan, Proceedings Volume 84-8, The Electrochem. Soc., Pennington, N.J., (1984), 418-429

227. J. Caudle, D.B. Ring and F.L. Tye, in D.H. Collins ed., Power Sources 3, Oriel Press, (1971), 593-606

228. S. Davis, F. Nachtergael, J.B. Soupart and K. Van Herk, Progress in Batteries and Solar Cells, 9, (1990), 67-85

229. A. Kozawa and B. Schumm, New Mater. New Processes, 2, (1983), 38-44

230. A.J. Fatiadi, Synthesis, (1976), 65-104 and 139-167

231. J.C.P.D.S., (1989), 18-805

232. J. Brenet and P.C. Picquet, Proceedings Volume 85-4, The Electrochem. Soc., Pennington, N.J., (1985), 3-20

233. R.S. Johnson and W.C. Vosburgh, J. Electrochem. Soc., 99, (1952), 317-322

Appendix 1. Calculation of the zinc electrode potential

The notation used in this appendix is the same as used in chapter 3, section 3.3, namely, m_i, N_i and X_i are the molality, the mole number and the mole fraction of the species i. The subscripts z, n, w, ,Cl, 0, 1, 2, 3 and 4 are used for $ZnCl_2$, NH_4Cl, water, chloride, Zn^{2+}, $ZnCl^+$, $ZnCl_2$ (the dissolved di-chloro complex), $ZnCl_3^-$ and $ZnCl_4^{2-}$, respectively.

A1.1 The total number of moles

In an amount of solution containing 1 kg of water, there are N_w moles of free water, i.e. not bound in any hydration shell, m_n moles of NH_4^+, m_{Cl} moles of free chloride, and m_0, m_1, m_2, m_3 and m_4 moles of the different zinc species. Thus, the total number of mole N_t is

$$N_t = N_w + m_{Cl} + m_n + m_Z \tag{A1.1}$$

since the sum of the molalities of the different zinc species is the total zinc molality m_z.

A1.2 The average zinc hydration number h_0

The zinc hydration equilibrium constant is

$$K = \frac{X_{Zn(H_2O)_{N2}^{2+}} \; X_w^{(N1 \; - \; N2)}}{X_{Zn(H_2O)_{N1}^{2+}}} \tag{3.40}$$

and the average hydration number,h_0, is [208]

$$h_0 = \frac{N1 \; X_{Zn(H_2O)_{N1}^{2+}} + N2 \; X_{Zn(H_2O)_{N2}^{2+}}}{X_{Zn(H_2O)_{N1}^{2+}} \; + \; X_{Zn(H_2O)_{N2}^{2+}}} \tag{A1.2}$$

From (3.40), we have

$$X_{Zn(H_2O)_{N2}^{2+}} = K \; X_{Zn(H_2O)_{N1}^{2+}} \; X_w^{-(N1 \; - \; N2)} \tag{A1.3}$$

Substituting in (A1.2) gives

$$h_0 = \frac{N1\ X_{Zn(H_2O)_{N1}^{2+}} + N2\ K\ X_w^{-(N1\ -\ N2)}\ X_{Zn(H_2O)_{N1}^{2+}}}{X_{Zn(H_2O)_{N1}^{2+}}\ (\ 1\ +\ X_w^{-(N1\ -\ N2)})} \qquad \text{(A1.4)}$$

which becomes

$$h_0 = \frac{N1\ +\ N2\ K\ X_w^{-(N1\ -\ N2)}}{K\ X_w^{-(N1\ -\ N2)}\ +\ 1} \qquad \text{(A1.5)}$$

Equation (A1.5) is equation (8) in reference [33]. Division by the water mole fraction factor gives

$$h_0 = \frac{N1\ X_w^{(N1-N2)} + K\ N2}{X_w^{(N1\ -\ N2)} + K} \qquad \text{(3.40)}$$

N2 is therefore the lower limit of the zinc hydration number and is approached when the water activity vanishes, i.e. in very concentrated solutions. When the water activity tends to 1 (in dilute solutions), the terms containing *K* becomes negligible and the zinc hydration number tends towards *N1*.

A1.3 The water mass balance

In this treatment, the NH_4^+ and Cl^- ions are regarded as non hydrated [33]. Equation (3.44) therefore reads

$$Bal_w = 55.51\ -(N_w\ +h_0m_0\ +h_1m_1\ +h_2m_2\ +h_3m_3\ +h_4m_4) \qquad \text{(A1.6)}$$

in which $h_1 = h_0 - 4$, $h_2 = h_0 - 8$, $h_3 = h_0 - 12$ and $h_4 = h_0 - 16$. If h_4 was negative, h_4 was taken as zero. The same consideration was applied to h_3 when *N2* was allowed to values lower than 12. In both latter cases, the maximum number of water molecules released by complexation from the zinc hydration shell was h_0.

A1.4 The zinc mass balance

Combining (3.36) and (3.43), i.e. replacing in the complex stability constants the mole fractions by the molalities (except for water) reads

$$K_i = \frac{\frac{m_i}{N_t}}{\frac{m_0}{N_t}\left(\frac{m_{Cl}}{N_t}\right)^i} X_w^{\delta h_i} \qquad \text{(A1.7)}$$

which gives the general expression

$$K_i = \frac{m_i\, N_t^i}{m_0\, m_{Cl}^i} X_w^{(h_0 - h_i)} \qquad \text{(A1.8)}$$

The molality m_i of the ist complex is then

$$m_i = m_0\, K_i\, m_{Cl}^i\, N_t^{-i}\, X_w^{-(h_0 - h_i)} \qquad \text{(A1.9)}$$

Introducing (A1.9) in

$$Bal_z = m_z - (m_0 + m_1 + m_2 + m_3 + m_4) \qquad \text{(A1.10)}$$

gives

$$Bal_z = m_z - m_0\left(1 + \sum_{i=1}^{4} K_i\, m_{Cl}^i\, N_t^{-i}\, X_w^{-(h_0 - h_i)}\right) \qquad \text{(A1.11)}$$

A1.5 The chloride mass balance

Inserting (A1.9) in

$$Bal_c = (2\, m_z + m_n) - (m_{Cl} + m_1 + 2\, m_2 + 3\, m_3 + 4\, m_4) \qquad \text{(A1.12)}$$

reads

$$Bal_c = (2m_z + m_n) - \left(m_{Cl} + m_0 \sum_{i=1}^{4} iK_i\, m_{Cl}^i\, N_t^{-i}\, X_w^{-(h_0 - h_i)}\right) \qquad \text{(A1.13)}$$

A1.6 Solving of the simultaneous mass balances

The system of equations was considered as solved when the 3 mass balance equations (A1.6), (A1.11) and (A1.13) gave simultaneously an absolute value lower than 0.0001 for Bal_w, Bal_c and Bal_z, respectively. The program used for these calculations is given in section A1.7.

A1.6.1 Calculation of the balance functions at given m_0, m_{Cl} and N_w

The total number of moles, N_t (equation A1.1), and the mole fractions, X_i, were calculated. Equation (3.41) was solved for h_0 and the hydrations numbers, h_i, were calculated. The molalities of the different zinc complexes could then be determined from equation (A1.9). The balance functions Bal_w, Bal_c and Bal_z were then computed from equations (A1.6), (A1.12) and (A1.10), respectively.

A1.6.2 Calculation of m_0 for given N_w and m_{Cl}

At given N_w and m_{Cl}, equation (A1.1) shows that N_t and therefore X_w have a value independent of m_0. In these conditions, Bal_z (A1.11) is a linear function of m_0 with a value of $Bal_z = m_z$ for $m_0 = 0$. The value of Bal_z was therefore calculated for $m_0 = m_z$ (corresponding to no complexation) and the value for $Bal_z = 0$ interpolated between these two points.

A1.6.3 Calculation of m_{Cl} for given N_w

The expression Bal_c given by equation (A1.13) has the value $(2\ m_z + m_n)$ when m_{Cl} is zero. First, the value of m_{Cl} was supposed to be $m_{Cl} = (2\ m_z + m_n)$, the value of m_0 was calculated to satisfy the zinc mass balance (see section A1.6.2) and Bal_c was calculated from equation (A1.13). An estimate, x, of the free chloride molality m_{Cl} satisfying simultaneously the zinc and chloride balance conditions ($Bal_z = 0$ and $Bal_c = 0$) was calculated by linear interpolation between the first two points. Bal_c was calculated for $m_{Cl} = x$ and x used for either the lower limit (for $Bal_c(x) > 0$) or the upper limit (for $Bal_c(x) < 0$) of the possible m_{Cl}

value for the next interpolation. This procedure, some times referred to as a modified Newton's method [210], was repeated until $-0.0001 < Bal_c < 0.0001$.

At the end of these calculations, both zinc and chloride balance functions had their absolute values lower than 0.0001 (mol kg^{-1}).

A1.6.4 Calculation of the free water mole number N_w

Each time the water balance function, Bal_w, was computed for a given value of the free water mole number, N_w, the free chloride and non complexed zinc molalities were also adjusted to satisfy their respective mass balances (see section A1.6.3).

A first value, $Bal_w(x_1)$, of the water balance function was calculated for $N_w = x_1 = 55.51$. Equation (3.43) shows that, in this case, $Bal_w(x_1) < 0$. A first estimate of the solution was taken as $x_2 = x_1/2$ and $Bal_w(x_2)$ was calculated.
If $Bal_w(x_2) < 0$, the solution was $N_w < x_2$, x_1 was replaced by x_2, divided by 2 and the balance function estimated again for this new value of x_1. This procedure was repeated until $Bal_w(x_2) > 0$, i.e. until the solution, N_w, of the equation was $x_2 < N_w < x_1$. At this stage, an interpolation procedure similar to the procedure described in the previous section, was used. The interpolation step was repeated until the absolute value of Bal_w (and Bal_c and Bal_z) was lower than 0.0001 (mol).

A1.6.5 Calculation of the zinc electrode potential

The mole fraction, X_0, and the hydration number, h_0, of the non-complexed zinc was determined from is molality m_0 and the total number of moles N_t. The electrode potential was then calculated from equation

$$E_{Zn} = E_0 + \frac{RT}{2F}\ln(X_0) - h_0 \frac{RT}{2F}\ln(X_w) \qquad (3.47)$$

where E_0 was chosen to fit the experimentally measured electrode potentials.

A1.6 Program used to solve the mass balance equations

This program was written in Turbo Pascal, version 5.5.

```
 PROGRAM SOLVE;
{============}

{ To solve the system of the 3 mass balance equations }

USES CRT,PRINTER;

{ the different constants used in the model }

CONST E0  =-961.8;
      K1 = 0.89;
      K2 = 1.44;
      K3 = 117000 ;
      K4 = 3056000;
      N1 = 16.48;
      N2 = 11.92;
      K  = 0.0518;

TYPE SETOFCHAR = SET OF CHAR;

VAR MN,MZ,H0,XW,X0 :REAL;
    POT,M0,M1,M2,M3,M4,MCL,NW :REAL;
```

```
 FUNCTION GETCHAR (ENS :SETOFCHAR) : CHAR;
{----------------}
{ returns a character belonging to the set ENS }

VAR OK:BOOLEAN;
    CH :CHAR;

BEGIN
   CH:=' ';
   REPEAT
   CH:=READKEY;
   OK := (CH IN ENS) OR (CH = CHR(13));
   IF NOT OK THEN WRITE(CHR(7));
   UNTIL OK;
   GETCHAR:=CH;
   WRITE(CH);
END; { of GETCHAR }


 FUNCTION POINT :REAL;
{--------------}
{ POINT takes the value of the electrode potential }
{ works with global variables }
```

```
 PROCEDURE COMPUTE (NW,MCL,M0:REAL;VAR BALW,BALC,BALZ:REAL);
{-----------------}

{ return the values of the different balance functions
  when the solution contains NW moles of 'free' water,
  MCL moles of free Cl- and M0 moles of Zn2+ }

VAR NT,XW4,XW6,XD4,XD3,XWD,DH3,DH4,H1,H2,H3,H4:REAL;

BEGIN
  NT:=NW+MZ+MN+MCL; { Total number of moles }
  XW:=NW/NT;IF XW <= 0.001
       THEN BEGIN { XW = water mole fraction }
            XW:=0.001;NW:=NT*XW;
            END;
  XW4:=XW*XW*XW*XW;
  XWD:=EXP((N1-N2)*LN(XW));
  H0:=(N1*XWD+N2*K)/(XWD+K);
  H1:=H0-4;H2:=H0-8;H3:=H0-12;H4:=H0-16;DH4:=16;DH3:=12;
  IF H4<0 THEN BEGIN
               H4:=0;
               DH4:=H0;
               END;
  IF H3<0 THEN BEGIN
               H3:=0;
               DH3:=H0;
               END;
  XD4:=EXP(DH4*LN(XW));
  XD3:=EXP(DH3*LN(XW));
    {the different species molalities}

  M1:=(K1*M0*MCL)/(XW4*NT);
  M2:=(K2*M0*MCL*MCL)/(XW4*XW4*NT*NT);
  M3:=(K3*M0*MCL*MCL*MCL)/(XD3*NT*NT*NT);
  M4:=(K4*M0*MCL*MCL*MCL*MCL)/(XD4*NT*NT*NT*NT);

{ the different balance functions }

  BALW:=55.51-(NW +H0*M0 +H1*M1 +H2*M2 +H3*M3 +H4*M4);
  BALC:=(2*MZ +MN)-(MCL +M1 +2*M2 +3*M3 +4*M4);
  BALZ:=MZ-(M0 +M1 +M2 +M3 +M4);
  X0:=M0/NT;   { X0 = Zn2+ mole fraction }

END; { OF COMPUTE }


 PROCEDURE ZINC   (NW,MCL:real;VAR M0,BALW,BALC,BALZ:REAL);
{--------------}
{ adjusts the value of M0 to satisfy the zinc mass balance
  for given NW and MCL }


VAR  X,X1,X2,Y,Y1,Y2,A,BW,BC:REAL;
     I:INTEGER;
     OK,FINISH:BOOLEAN;
```

```
BEGIN
  X1:=0; Y1:=MZ;
  X2:=MZ;
  COMPUTE(NW,MCL,X2,BW,BC,Y2);
  FINISH := FALSE;
  REPEAT
    A:=(Y2-Y1)/(X2-X1);X:=X1-Y1/A; { the estimated solution}
    COMPUTE(NW,MCL,X,BW,BC,Y);
    OK:=(ABS(Y) <0.0001);
    { check of the validity of the estimate }

    IF OK THEN FINISH:=TRUE
          ELSE IF Y <0 THEN BEGIN
                            X2:=X;Y2:=Y;
                            END
                       ELSE BEGIN
                            X1:=X;Y1:=Y;
                            END;
  UNTIL FINISH;
  IF NOT OK THEN BEGIN {in the case the estimate was wrong}
                 A:=(Y2-Y1)/(X2-X1);
                 X:=X1-Y1/A;
                 COMPUTE(NW,MCL,X,BW,BC,Y);
                 END;
  M0:=X; BALZ:=Y;BALW:=BW;BALC:=BC;

END; { OF ZINC }
```

```
 PROCEDURE CHLORIDE (NW:EXTENDED;
{------------------}     VAR MCL,M0,BALW,BALC,BALZ :REAL);

{ adjusts the chloride concentration
                  AND keeps the Zn balance  OK }

VAR X,X1,X2,X3,Y,Y1,Y2,Y3,A,BW,BC,BZ,TC:REAL;
               {TC = total chloride, Y = Cl- balance }
    OK,FINISH:BOOLEAN;

BEGIN
  X1:=0; TC:=MN+2*MZ;Y1:=TC;
  X2:=TC;
  ZINC(NW,X2,M0,BW,Y2,BZ);
  FINISH:=FALSE;
  REPEAT
    A:=(Y2-Y1)/(X2-X1); X:=X1-Y1/A;
    ZINC(NW,X,M0,BW,Y,BZ);
    OK:=(ABS(Y) <0.0001);
    IF OK THEN FINISH:=TRUE
          ELSE IF Y <0 THEN BEGIN
                            X2:=X;Y2:=Y;
                            END
                       ELSE BEGIN
                            X1:=X;Y1:=Y;
                            END;
  UNTIL FINISH;
```

```
  IF NOT OK THEN BEGIN { the mass balance is not satisfied }
                  A:=(Y2-Y1)/(X2-X1);
                  X:=X1-Y1/A;
                  COMPUTE(NW,X,M0,BW,Y,BZ);
                  END;
  MCL:=X; BALC:=Y;BALW:=BW;BALZ:=BZ;

END; { OF CHLORIDE }


 PROCEDURE WATER (VAR NW,MCL,M0:EXTENDED);
{---------------}
{ adjusts the water concentration
            AND keeps the Zn and Cl balances OK }

VAR X1,X2,X,Y1,Y2,Y,A,BW,BC,BZ:REAL;
    OK,FINISH:BOOLEAN;

BEGIN
  X2:=NW;CHLORIDE(X2,MCL,M0,Y2,BC,BZ);X1:=X2;
  REPEAT { looks for a positive value of BALW (y) }
  X1:=X1/2;CHLORIDE(X1,MCL,M0,Y1,BC,BZ);
  OK:=ABS(Y1)<0.0001;
  IF Y1 <0 THEN BEGIN X2:=X1;Y2:=Y1; END;
  UNTIL (OK OR (Y1 >0));

  {at this stage, Y2 <0 and Y1 >0 or the process is finished}
  IF OK THEN BEGIN X:=X1;FINISH:=TRUE;END
        ELSE FINISH:=FALSE;

  WHILE NOT FINISH DO
    BEGIN
    A:=(Y2-Y1)/(X2-X1); X:=X1-Y1/A;
    CHLORIDE(X,MCL,M0,Y,BC,BZ);
    OK:=(ABS(Y) <0.0001);

    IF OK THEN FINISH:=TRUE
          ELSE IF Y < 0 THEN BEGIN
                             X2:=X;Y2:=Y;
                             END
                        ELSE BEGIN
                             X1:=X;Y1:=Y;
                             END;

    END; { WHILE }
END; { OF WATER }

{            main part of POINT                          }
BEGIN;

{ initialisation of the variables at their maximum value }
NW:=55.51;
MCL:=MN+2*MZ;
M0:=MZ;

WATER(NW,MCL,M0);
POINT:=E0+12.8455*LN(X0)-12.8455*H0*LN(XW);
END; { of POINT }
```

```
{                              MAIN PROGRAM                                }
{                              ============                                }
BEGIN
 REPEAT
  CLRSCR;
  WRITE('ZnCl2 molality = ? ');READLN(MZ);
  REPEAT
    REPEAT
    { loop for different samples of the same zinc molality }
     WRITELN;
     WRITE('NH4Cl molality = ? ');READLN(MN);
     WRITE('Is it OK ( Y/N ) ? ');
     UNTIL GETCHAR(['Y','N']) = 'Y';
     WRITELN;

   WRITELN(' .... Computing.... ');
   POT:=POINT;
   WRITELN(LST,'Mz = ',MZ:6:3,' Mn = ',MN:6:3,
                              ' E = ',POT:8:2,' Xw = ',XW:6:4);
   WRITELN('Mz = ',MZ:6:3,' Mn = ',MN:6:3,' E = ',POT:8:2,
                                                ' Xw = ',XW:6:4);
   WRITELN('M0 = ',M0:8:5,' M1 = ',M1:8:5,' M2 = ',M2:8:5,
                              ' M3 = ',M3:7:4,' M4 = ',M4:7:4);
   WRITELN('H0 = ',H0:6:3,' MCL = ',MCL:6:3);
   WRITE('  Xw = ',XW:10:8);
   WRITELN('  E  = ',POT:8:2);WRITELN;
   WRITE('Another with the same ZnCl2 ? ');

   UNTIL GETCHAR(['Y','N'])= 'N';WRITELN;
   { end with this zinc molality }
   WRITE('Another sample ? ');

 UNTIL GETCHAR(['Y','N']) = 'N';{ end of the calculations }

END.
```

Appendix 2. Intermittent discharges, electrolyte composition.

A2.1. Leclanché electrolyte

The ZnO contained in the positive electrode mix may react with NH_4Cl following

$$ZnO + 2NH_4Cl \longrightarrow Zn(NH_3)_2Cl_2 + H_2O \qquad (3.21)$$

or with the protons released by the ion-exchange process, following e.g.

$$ZnO + 2H^+ \longrightarrow Zn^{2+} + H_2O \qquad (A2.1)$$

where Zn^{2+} is used to represent any of the chloro-zinc complexes.

In both cases, one mole (81.37 g) of ZnO produces one mole (18 g) of water which must be added to the water content of the cell (shown in table 2.1).

A2.1.1 First stage of the discharge in cells containing EMD

During the first stage of the discharge, the overall reaction was

$$Zn + 2NH_4Cl_{solid} + 2MnO_2 \longrightarrow Zn(NH_3)_2Cl_2 + 2MnOOH \qquad (1.36)$$

This first stage ended when reaction (1.36) had consumed all the solid NH_4Cl contained in the manganese dioxide electrode mix [13]. Equation (1.36) requires 2 moles of solid NH_4Cl for a discharge of 2 faradays or 53.49 g for 96,487 coulombs. Figures (4.1) and (4.2) show that the first stage of the discharge lasted about 4,000 coulombs, i.e. that the cells contained about 2.2 g of solid NH_4Cl (out of a total of 8.07 g NH_4Cl, see table 2.1).

The water content of the cells was 9.58 g from the electrolyte (table 2.1) and 0.13 g from reactions (3.21) or (A2.1), i.e. 9.71 g. The $ZnCl_2$ concentration (calculated from table (2.1) and the water content) is 2.33 g $ZnCl_2$ in 9.71 g H_2O or 1.76 molal. The solubility of NH_4Cl in this solution is about 29.3 w/w% (see section 3.3) and therefore the electrolyte should contain 17.0 w/w % of $ZnCl_2$. In

these calculations, it was assumed that the ZnO had reacted with 0.78 g NH_4Cl according to equation (3.21). The NH_4Cl contained in the electrolyte is the total NH_4Cl, minus the NH_4Cl necessary to sustain reaction (1.36) for 4,000 coulombs, minus the NH_4Cl bound in the $Zn(NH_3)_2Cl_2$ precipitate i.e.
8.07 - 2.2 - 0.78 = 5.09 g or 29.7 w/w % of the total electrolyte mass.

Table (4.1) shows that the electrolyte contained 17.2 w/w % $ZnCl_2$ and 29.2 w/w % NH_4Cl. This suggests that a little ZnO had been dissolved (to increase the total soluble zinc expressed as $ZnCl_2$) and that some NH_4^+ had been adsorbed on the manganese dioxide.

If some zinc was also adsorbed by the manganese dioxide, the dissolution of more ZnO, and the formation of less $Zn(NH_3)_2Cl_2$, would be required to explain the concentration of zinc in the electrolyte. A larger amount of adsorbed NH_4^+ would also be necessary to explain the length of the first stage of the discharge.

A2.1.2 Second stage of the discharge in cells containing EMD

During the second stage of the discharge, the overall cell reaction is

$$Zn + 2NH_4^+ + 2Cl^- + 2MnO_2 \longrightarrow Zn(NH_3)_2Cl_2 + 2MnOOH \qquad (1.37)$$

Figure (4.1) shows that the second stage of the discharge finished after about 10,500 coulombs. If the increase of the $Zn(NH_3)_2Cl_2$ solubility is not taken into account, reactions (1.36) and (1.37) had consumed 5.93 g NH_4Cl out of the total of 8.07 g, and the electrolyte still contained the 2.33 g of $ZnCl_2$ and the 9.71 g of water. The calculated composition is then 15.1 w/w % NH_4Cl and 16.4 w/w % $ZnCl_2$.

A2.1.3 First stage if the discharge in cells containing Faradiser M

Figure (4.6) shows that the first stage of the discharge lasted about 3,000 coulombs. The cells therefore contained about 1.66 g of solid NH_4Cl (see section A2.1. above). The water content of the cells was (table 2.1) 11.13 g plus 0.11 g formed by the reaction of ZnO with the electrolyte or a total of 11.24 g H_2O.

The electrolyte contained (table 2.1) 2.71 g $ZnCl_2$ and 11.24 g H_2O, i.e. the solution was 1.77 molal in $ZnCl_2$. This corresponded to a solubility of 29.3 w/w % NH_4Cl (see section 3.3).

An electrolyte containing (7.73 - 1.66) g NH_4Cl, 2.71 g $ZnCl_2$ and 11.24 g H_2O would have the composition 30.3 w/w % NH_4Cl and 13.5 w/w % $ZnCl_2$.

If the ZnO contained in the positive electrode mix had dissolved in the electrolyte, the total zinc content expressed as $ZnCl_2$ would have been (2.71 + 0.85) g $ZnCl_2$ or an electrolyte composition with 29.1 w/w % NH_4Cl and 17.1 % $ZnCl_2$. Table (4.2) reveals that the electrolyte of the undischarged cell was too acidic to contain any $Zn(NH_3)_2Cl_2$ precipitate and therefore that all the ZnO had been dissolved. However, the total zinc content of the electrolyte was much lower (15.5 w/w %) than the calculated concentration (17.1 w/w %) suggesting that a significant amount of zinc had been adsorbed on the manganese dioxide. On the other hand, the calculated NH_4Cl concentration is very close to the ammonium chloride solubility showing that very little NH_4^+ had been adsorbed.

A2.2 Zinc chloride electrolyte

If the electrolyte of an undischarged zinc chloride cell is not fully buffered, all the ZnO incorporated into the positive electrode mass has been dissolved, e.g., by reaction (A2.1). This dissolution has increased the soluble zinc content of the electrolyte (1 mole of soluble zinc per mole of ZnO) and the total water content of the cell (one mole of H_2O per mole of ZnO). The calculated composition of the cells are compared in table (A2.1) to the measured $ZnCl_2$ concentrations (from table 4.3). The amount of zinc really present into the electrolyte has been calculated on the basis of the total water and the measured $ZnCl_2$ concentration. The difference between the total zinc and the zinc contained in the electrolyte represents the zinc adsorbed on the manganese dioxide by the ion-exchange phenomenon. It has been expressed in milli-mole of Zn^{2+} per mole of MnO_2. Table (A2.1) also shows the electrolyte composition at the end of the discharge assuming that the overall cell reaction was

$$4Zn + Zn^{2+} + 2Cl^{-} + 8MnO_2 + 9H_2O \longrightarrow ZnCl_2.4Zn(OH)_2.H_2O + 8MnOOH \quad (1.38)$$

or

$$4Zn + Zn^{2+} + 2Cl^{-} + 8MnO_2 + 8H_2O \longrightarrow ZnCl_2.4Zn(OH)_2 + 8MnOOH \quad (A2.2)$$

(equation A2.2 gives the un-hydrated zinc hydroxychloride as the reaction product).

An equation of the form

$$f\ ZnCl_2 + 4Zn + 8MnO_2 + 9H_2O \longrightarrow f\ ZnCl_2.4Zn(OH)_2.H_2O + 8MnOOH \quad (A2.3)$$

where f is a fitting parameter and which corresponds to a precipitate with higher chloride to hydroxyl ratio larger than in equations (1.38) or (A2.2).

Table A2.1 : Comparison between the calculated and the measured electrolyte compositions

Parameter	EMD	Far.M	Far. WSZ
Total water /g	16.74	17.62	16.51
Total zinc /g	6.79	7.04	6.68
undischarged cell			
$ZnCl_2$ w/w %			
calculated	28.86	28.55	28.81
measured	27.0	26.5	26.4
adsorbed zinc / 10^{-3} mol mol^{-1}	16.3	21.2	21.6
discharged cell			
$ZnCl_2$ w/w %			
measured	8.5	16.7	11.7
calculated (1.38)	20.53	22.04	21.66
calculated (A2.2)	19.94	21.55	21.12
(A2.3) with f=1.58	8.56	13.33	11.76

Table (A2.1) shows that the electrolyte composition calculated on the basis of equation (A2.3) with $f = 1.58$ gives a very good approximation of the measured electrolyte compositions after the intermittent discharge, for both EMD and Faradiser WSZ. The precipitate with $f = 1.58$ in equation (A2.3) is very close in composition to $2ZnCl_2.5Zn(OH)_2.H_2O$.